ЖУРНАЛ
ПРИКЛАДНОЙ ХИМИИ

Vol. 31 No. 5

May 1958

JOURNAL OF
APPLIED CHEMISTRY
OF THE USSR

(ZHURNAL PRIKLADNOI KHIMII)

IN ENGLISH TRANSLATION

CONSULTANTS BUREAU, INC.

Vol. 31 No. 5

May 1958

JOURNAL OF
APPLIED CHEMISTRY
OF THE USSR

(ZHURNAL PRIKLADNOI KHIMII)

A publication of the Academy of Sciences of the USSR

IN ENGLISH TRANSLATION

Year and issue of first translation:
vol. 23, no. 1 January 1950

	U. S. and Canada	*Foreign*
Annual subscription	*$60.00*	*$65.00*
Annual subscription for libraries of non-profit academic institutions	*20.00*	*25.00*
Single issue	*7.50*	*7.50*

Printed in the United States

JOURNAL OF APPLIED CHEMISTRY OF THE USSR

Volume 21, Number 5 May 1958

CONTENTS

CONTENTS (continued)

THE THEORY OF THE SODA – SILICA PROCESS FOR THE PRODUCTION OF SODIUM TUNGSTATE FROM SCHEELITE

Ia. E. Vil'nianskii and Z. L. Persits

The S. M. Korov Polytechnic Institute of the Urals

In one of the industrial processes for the chemical conversion of scheelite, the mineral is heated in furnaces with a mixture of sodium carbonate and quartz sand. The cooled melt is leached to give an aqueous solution of sodium tungstate [1]. The function of the silica is to bind the calcium in the form of silicates, which are no more soluble in water than calcium tungstate, in order to prevent or restrict the back reaction under the action of water, with loss of part of the soluble tungstate formed. Since the primary product of the reaction between soda and silica on heating is sodium metasilicate [2], the subsequent process in the furnace may be considered as double decomposition of calcium tungstate and sodium silicate; the possible presence of other components in the native scheelite, and the influence of excess soda may be initially disregarded in considering the theory of the process. The entire process is successful if the double decomposition is fairly complete in the furnace; it is then necessary merely to dissolve the sodium tungstate in water and to separate the insoluble metasilicates from the solution.

The direction and extent of the double decomposition may be estimated, with the aid of the empirical rule formulated by Bergman and Dombrovskaia [3], from the heat of reaction. In this instance (all the substances being in the crystalline state, stable at 25° and 1 atmosphere)

$$CaWO_4 + Na_2SiO_3 = Na_2WO_4 + CaSiO_3. \quad (1)$$

H_{298} (kcal/mole) 392.5 [4] – 364.7 [5] – 395 [4] – 378.6 [4],
and hence H_{298} (Reaction 1) = – 16.4 kcal/mole or – 8.2 kcal/equiv.

This result should indicate the possibility of complete conversion in the desired direction. It is known, however, that there are exceptions to the thermochemical rule with regard both to the direction of the reaction [6], and to the degree of conversion. The latter type of failure of this rule was observed [7] in the formation of double salts, which can, also be formed in the reciprocal system in question. Moreover, the Bergman–Dombrovskaia rule was not tested for systems containing complex chain or ring ions, such as the metasilicate anions in this system. Adequate data for accurate thermodynamic calculations are lacking; this is especially true for calcium tungstate. These facts justify an experimental investigation of the reciprocal system represented by Equation (1).

The system was studied at temperatures not higher than 1200°. This limitation simplified the work, but it also narrowed the scope of the investigation, as it was not possible to plot the liquidus diagram for the system involving high-melting calcium salts. This limitation is largely justified by the fact that for technical reasons complete fusion of the reaction mass is also inadmissible in the industrial rotary furnaces used for the process. In view of this limitation, and the above-mentioned simplification of the composition of the initial mixture, the present investigation must be regarded merely as a first step in the development of a theory of the soda–silica process.

Starting Materials

The 4 substances in Equation (1) were prepared.

Sodium tungstate was prepared by fusion of tungstic anhydride with sodium carbonate, recrystallized, and

and dried. The neutral character of the product was in agreement with literature data [8]. A transparent yellow melt was visible in a quartz crucible at 820°. The cooling curve showed halts at 695° (recrystallization), 592°, and 568° (polymorphic transitions); these values are within the ranges of the corresponding literature values. The slowly-cooled product was white; when viewed under the microscope it was in the form of four-sided isotropic crystals with refractive index $n_D = 1.662 \pm 0.005$; according to the literature [9], the value is 1.678 at 547 mμ. The x-ray patterns showed low lattice symmetry [9], but birefringence could not be detected by the usual methods.

Calcium tungstate was prepared by the mixing of aqueous sodium tungstate and calcium chloride solutions, in the form of a white precipitate which was washed free from chlorides and dried at 300°. It did not melt when heated for 30 minutes at 1200°, and the color did not change; birefringent crystals from 7 to 26μ in size were seen under the microscope.

Sodium metasilicate was obtained by the action of heat on the hexahydrate reagent at 300°. The cooling curve of the melt indicated strong undercooling, with a subsequent rise to 1070°.

Calcium metasilicate was obtained by the action of heat on a stoichiometric mixture of powdered rock crystal containing 99.8% SiO_2 and chemically pure calcium oxide for 2 hours at 1430°. The absence of free base in the product was confirmed by means of phenolphthalein, and no quartz grains could be observed under the microscope. The product consisted of birefringent crystals with the refractive indices of pseudowollastonite.

METHOD

In the first method, finely powdered mixtures of known composition were heated at 1170-1200°, and the cooling curves were then determined. These curves gave a first idea of the phase composition of the cooled melts. however, this idea was not always sufficiently clear, as sometimes the course of crystallization did not correspond to the reversible equilibrium because of incompleteness of the peritectic reaction, and because of undercooling at the start of the appearance of the new phase.

The second method for investigating the phase composition was by examination of thin sections in ordinary or polarized transmitted light. The cooled melts or sinters were polished on an etched glass surface in dry oil, and the thin plates were sealed between glass slides by means of Canada balsam. Only the high-melting calcium salts did not yield firm sinters from which sections could be made.

The third method for identification of the crystalline phases was by measurement of the refractive indices of individual crystals in immersion liquids.

A total of 4 simple salts and 18 mixtures, indicated by circles on the rectangular diagram, was investigated. Some of the typical observations are described below; these may be used in further investigations or for the development of an optical crystalligraphic method for control of the furnace stage of the production process.

EXPERIMENTAL RESULTS

Binary systems. Results for melts of the sodium salts are given in two earlier papers [10, 11]. The respective results differ with regard to the number of liquid phases formed, and therefore with regard to the form of the liquidus line; however, both papers lead to the same conclusion that complete solidification of binary melts leads to the formation of sodium metasilicate crystals and of a binary eutectic consisting of sodium tungstate with a very small amount of metasilicate.

The phase diagram of mixtures of sodium and calcium metasilicates is known [12], but the microscopic appearance of polished sections has not been previously described. A mixture containing 25% $CaSiO_3$ was heated for a long time at 1200°. A polished section was prepared from the monolithic melt; it was seen to contain regions of an isotropic mass of primary $Na_4CaSi_3O_9$ crystals, in agreement with the phase diagram; other regions were occupied by a cellular eutectic, the network of which was formed by birefringent dendrites of sodium metasilicate, and the cells were filled with isotropic double silicate; fibrous bundles, characteristic of sodium metasilicate, were seen at the boundaries between different regions. The section of a melt prepared from a mixture with 43% $CaSiO_3$ contained isometric birefringent primary crystals of $Na_2Ca_2Si_3O_9$, often in twin form.

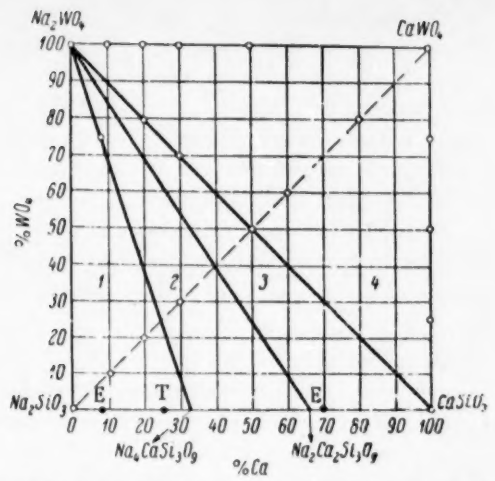

Phase diagram for the system of calcium and sodium tungstates and metasilicates at room temperature. E) Eutectic, T) transition point, C) experimental point. 1,2,3 and 4) phase triangles.

The peritectic transition at 1141°

$$Na_2Ca_2Si_3O_9 + \text{melt} = Na_4CaSi_3O_9 \qquad (2)$$

affected only the outlines of these crystals. The main mass was badly differentiated, and consisted mainly of optically isotropic substance. These results provided the basis for studies of many melts of the system in question (the x-ray pattern of the metasilicate $Na_4CaSi_3O_9$ reveals low lattice symmetry [13]), but the birefringence is evidently so weak that it cannot be detected under the polarization microscope).

All four binary melts along the upper edge of the square (see diagram) contained the same structural components, in different proportions. The upper layer contained sodium tungstate with all its distinguishing characteristics. It was seen in the section in the form of rectangular crystal cross sections and a weakly translucent isotropic mass. The low transparency of the basic field of the melt may be attributed to multiple reflection and absorption of light in the mass of very fine crystals formed in the polymorphic transitions of sodium tungstate. The bottom of the crucible contained the high-melting and heavier calcium tungstate in the form of small crystals, which differed from the original substance by their strong luster and larger size (approximately 10-fold).

It follows from these observations that at the temperatures of the industrial process calcium tungstate does not dissolve in sodium tungstate to an extent which might appreciably affect the specific properties of the latter. However, the noticeable recrystallization of the calcium tungstate itself shows that it must be at least slightly soluble in melted sodium tungstate.

Like the above system, the binary system of calcium tungstate and metasilicate had not been previously studied. Investigations of 3 mixtures showed that these salts do not interact when heated together at 1200°, and retain their individual properties.

Binary mixtures along the stable diagonal. Thermochemical calculations show that the ternary system under consideration must be irreversibly-reciprocal, in Bergman and Dombrovskaia's terminology, and the diagonal joining the points for the products of double decomposition according to Equation (1) in the rectangular diagram must be stable if the system conforms to the thermochemical rule.

Three mixtures of calcium metasilicate and sodium tungstate were prepared. At 1200°, the crucibles contained melted sodium tungstate, with the less fusible and lighter calcium metasilicate floating in it in the form of individual particles or lumps. Calcium metasilicate was not found to be soluble to any extent in sodium tungstate by any of the methods used. Only the fact that very fine crystals of pseudowollastonite were converted into larger wollastonite crystals might suggest that even slight solubility plays a part in the process. With regard to the sodium tungstate, which was seen in the form of an isotropic mass of low transparency in the solidified melt, it is possible that in reality this was a eutectic, which contained so little silicate as a structural component that it could not be detected.

Investigations of the three mixtures showed that the diagonal of the square on which they lie is stable, and the salts connected by this diagonal on the diagram form a binary system. The distinction from the binary systems on the sides of the square lies in the fact that the binary system on the diagonal does not contain salts with a common ion, and its stability consists of absence of ion exchange.

Binary mixtures along the metastable diagonal. Mixtures were made from calcium tungstate and sodium metasilicate, roughly simulating production charges.

Mixtures containing excess sodium metasilicate gave melts the phase composition of which in general corresponded to the position of the points relative to the phase triangles on the square diagram. The primary formations visible were crystals of double metasilicates; these were followed by a binary silicate eutectic. The last to crystallize was sodium tungstate, which filled the interstices between the silicate crystals, and the bottom layer of the melt. The properties of the ternary system suggest that the tungstate phase is in reality a triple eutectic in which the silicates cannot be distinguished because of the great predominance of largely opaque highly disperse crystalline mass of sodium tungstate. The presence in the melt with coordinates (20,20) of primary $Na_2Ca_2Si_3O_9$ formations was contrary to the general rule; the isotropic edges of these birefringent crystals showed that the peritectic Reaction (2) affected only the surface of these crystals. Calcium tungstate was almost completely converted into sodium tungstate, not according to Equation (1), but according to the equations

$$CaWO_4 + 3Na_2SiO_3 = Na_2WO_4 + Na_4CaSi_3O_9, \quad (3)$$

$$2CaWO_4 + 3Na_2SiO_3 = 2Na_2WO_4 + Na_2Ca_2Si_3O_9. \quad (4)$$

The mixture corresponding to the center of the square was heated for 1 hour at 1200° and cooled slowly. The cooled melt contained unchanged calcium tungstate crystals in addition to the newly-formed sodium tungstate and wollastonite. Only 80% of the tungsten was extracted by leaching. The result of this experiment confirms the conclusion concerning the direction of the reaction; the incompleteness of the conversion is readily accounted for by lack of excess reagent in the original mixture. In the industrial process the charge contains excess soda [1]; our calculations and experiments showed that this soda can also enter into double decomposition with scheelite at high temperatures. Ths risk of retrogradation during leaching as the result of interaction of dissolved sodium tungstate with calcium carbonate or hydroxide is avoided in presence of enough silica in the charge, because calcium metasilicate is less soluble in water than the carbonate or hydroxide. The presence of excess soda and other salts in industrial charges should make it possible to lower the temperature of the furnace process.

The microscopic picture of melts containing excess calcium tungstate is in full agreement with the position of the points in Phase Triangle 4; in addition to unchanged calcium tungstate crystals, newly-formed lustrous wollastonite crystals and a crystalline mass of sodium tungstate can be seen.

Studies of the melts corresponding to the metastable diagonal confirmed that the reciprocal system in question conforms to the Bergman–Dombrovskaia rule.

Ternary mixture. The mixture represented on the diagram by the point with coordinates 8, 74.7 was prepared from sodium tungstate and the simple metasilicates. The microscopic picture was similar to that of the (20,20) melt, the sole difference being that the area occupied by sodium tungstate in the section of the ternary melt was considerably greater. Neither of the simple silicates could be detected under the microscope. The phase composition of the melt did not quite correspond to the position of the point on the boundary between Triangles 1 and 2 because equilibrium was not reached in the peritectic transition, but the system conformed to the thermochemical rule in this melt also.

SUMMARY

1. The ternary system consisting of calcium and sodium tungstates and metasilicates is irreversibly-reciprocal, in accordance with the Bergman–Dombrovskaia thermochemical rule.

2. The products of double decomposition of calcium tungstate and sodium metasilicate may be: a) wollastonite and double metasilicates of sodium and calcium, separately or jointly according to the proportions of the starting materials, the heating temperature, and the cooling rate; b) sodium tungstate.

3. Calcium tungstate, wollastonite, and double metasilicates of calcium and sodium are very slightly soluble in melted sodium tungstate at the temperatures of the furnace stage in the industrial process.

4. Calcium tungstate and calcium metasilicate do not interact when heated together at 1200°.

LITERATURE CITED

[1] G. A. Meerson and A. N. Zelikman, Metallurgy of the Rare Metals (Metallurgy Press, 1955), p. 72.*

[2] A. G. Repa, J. Appl. Chem. 25, 5, 744 (1952).**

*In Russian.

**Original Russian pagination. See C. B. translation.

[3] A. G. Bergman and N. S. Dombrovskaia, J. Russ. Phys.-Chem. Soc. 61, 1460 (1929).

[4] F. D. Rossini, D. D. Wagman, W. H. Evans, S. Levine and I. Jaffe, Selected values of chemical thermodynamic properties, National Bureau of Standards, Washington (1952).

[5] N. W. McCready, J. Phys. Coll. Chem. 52, 1277 (1948).

[6] A. G. Bergman, Progr. Chem. 5, 1070 (1936).

[7] E. I. Banashek and A. G. Bergman, Proc. Acad. Sci. USSR 56, 485 (1947).

[8] W. Quist and A. Lund, Z.allg. anorg. Ch., 205, 89, 91 (1932).

[9] R. W. Goranson and F. C. Kracke, J. Chem. Phys. 3, 87 (1935).

[10] H. S. van Klooster, Z. allg. anorg. Ch., 69, 135 (1910/11).

[11] A. G. Bergman, A. K. Nesterova and N. A. Bychkova, Proc. Acad. Sci. USSR 101, 485 (1955).

[12] G. W. Morey and N. L. Bowen, J. Glass Techn., 9, 226 (1925).

[13] C. Kroger and J. Blomer, Z. anorg. allg. Ch., 280, 63 (1955).

Received September 17, 1956

THE INTERACTION OF ALITE AND BELITE WITH QUARTZ IN AUTOCLAVE TREATMENT

A. A. Maier and N. S. Manuilova

The interaction of Portland cement with sand in conditions of autoclave treatment is a matter of interest. The interaction of quartz with Portland cement, and with its most important minerals – alite and belite – has been studied previously [1, 2].

The purpose of the present investigation was to study, under the microscope, the reactions of alite and belite with water and quartz during autoclave treatment for 8 hours under excess pressures of 8 atmos (174.5°) and 16 atmos (203°). The petrographic data was augmented by the results of differential thermal analysis (DTA) and certain chemical and x-ray* data.

In order to ensure comparable results, the starting materials – alite, belite, and quartz – were ground to approximately equal specific surfaces of the order of 3000 cm^2/g.

Interaction of Alite with Quartz

Hydrolysis of alite during autoclave treatment commences at the grain surfaces. Water penetrates along the cleavage cracks, and results in the formation of narrow bands of $Ca(OH)_2$ within the alite grains. As a result, the alite crystals disintegrate into numerous individual grains with rounded edges (Fig. 1), cemented together by

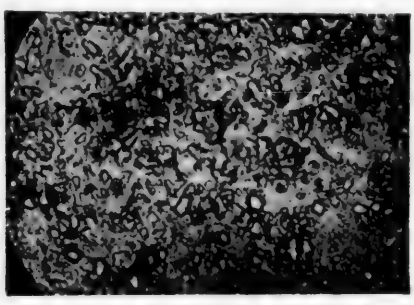

Fig. 1. Microstructure of alite specimen steamed at 8 atmospheres for 8 hours. Without analyzer.

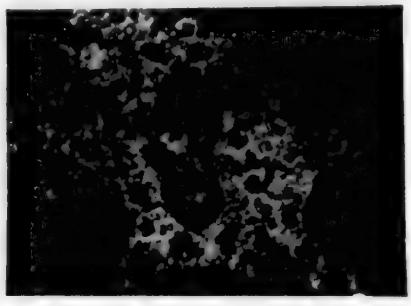

Fig. 2. Crystallization of $Ca(OH)_2$ in the autoclave treatment of alite. With analyzer.

calcium hydroxide liberated during hydrolysis. It is interesting to note the similar optical orientation of the calcium hydroxide crystals, observed over fairly large regions (up to 120μ) (Fig. 2). These $Ca(OH)_2$ crystals resemble a sponge under crossed nicols, and give gray and yellowish-white polarization colors of the first order. An interesting fact is that such crystallization of $Ca(OH)_2$ is never found in systems containing considerable amounts of $Ca(OH)_2$ in the original state; such as lime–sand mixtures hardened in autoclaves. This type of crystallization is evidently associated with gradual liberation of $Ca(OH)_2$ from the mineral, and it is therefore a characteristic feature of hydrated alite. This hypothesis is confirmed by the fact that $Ca(OH)_2$ liberated in the

*The x-ray analysis was performed by D. M. Kheiker at the Scientific Research Institute for Asbestos Cement, with the aid of the URS-504 apparatus.

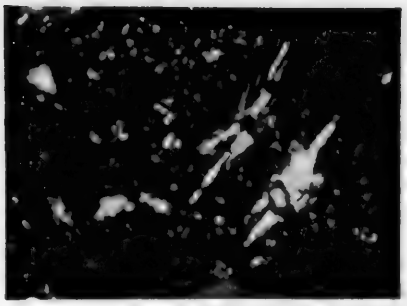

Fig. 3. Formation of $C_2SH(A)$ crystals in a sample of the following composition (%): 70 alite + 30 quartz (16 atmos, 8 hours). With analyzer.

hydration of other minerals, such as C_4AF, also forms relatively large crystals, although of different configuration.

In addition to the regions filled with a polarizing mass of calcium hydroxide, there are some almost entirely isotropic region of a colorless granular mass. This mass is evidently a mixture of various calcium hydrosilicates.

The presence of lines of $C_2SH(A)$ (3.53, 3.27A) and C_3SH_2 (2.90, 2.815, 2.46, 2.08, 1.88 A), the formation of which was formerly regarded possible only at temperatures above 200° [3], was found by x-ray analysis.

Moreover, the possibility must be taken into account that the monobasic hydrosilicate may be formed during the first stages of autoclave treatment of alite [4].

After alite has been steamed at 8 atmos, the product has an irregular granular structure, due to the presence of individual alite crystals, hydrated very little or not at all, against a background of finer grains of the mineral. Increase of the pressure to 16 atmos accelerates alite hydrolysis, the mass becomes more uniformly granular, and the amount of interstitial substance increases.

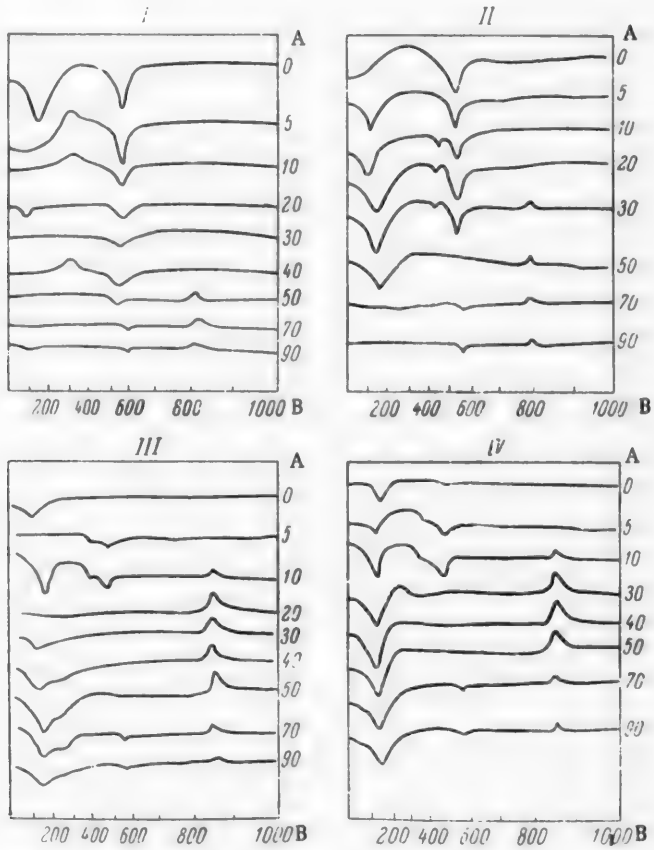

Fig. 4. DTA curves for mixtures of alite and belite with quartz after autoclave treatment for 8 hours at 8 or 16 atmos. A) Quartz content of the reaction mixture (%), B) temperature°. I and II) mixtures of alite and quartz, III and IV) mixtures of belite and quartz. Pressure (atmos) and temperature°: I and III) 8 and 174.5, II and IV) 16 and 203.

The hydrolysis of alite is intensified in presence of quartz. The $Ca(OH)_2$ liberated in hydrolysis reacts with quartz to form more or less differentiated sheaflike bundles of acicular crystals of $C_2SH(A)$ (Fig. 3), which corresponds to the endothermic effect at 450-470° on the DTA curves (Fig. 4). These bundles are characterized by a high relief, direct extinction, and positive elongation; they generally grow from the quartz grains. In mixtures steamed at 8 atmos individual needles appear at quartz contents of 10% and over; the greatest numbers are found with 20% quartz, and they disappear at 40% quartz. When the pressure is raised to 16 atmos, the quartz reacts more vigorously, and needles of $C_2SH(A)$ are distinctly visible even with 5% quartz. They disappear only at 50% quartz, as the more intensive hydrolysis of alite enables more quartz to combine as dicalcium hydrosilicate. Thus, the formation range of acicular $C_2SH(A)$ crystals is wider at 16 atmos than at 8.

It is interesting to note that in some compositions (for example, C_3S + 20% SiO_2 steamed at 16 atmos) acicular crystals with negative elongation were formed. Their birefringence was less than that of crystals with positive elongation. The crystal habit also changed – the bases of the needles coalesced into plates with corroded edges, while the ends appeared to detach and vanish. Such crystals often grow from a common center with $C_2SH(A)$ crystals having positive elongation, and are perpendicular to the latter. This suggests that they constitute a modification of dicalcium hydrosilicate.

The quartz grains are generally very much modified by autoclave treatment. Their periphery has decreased birefringence, and an anisotropic border with fairly high relief is formed around them. This probably consists of dicalcium hydrosilicate, as in some cases it was seen to split into bundles of acicular crystals with positive elongation.

The amount of free lime falls continuously with increasing quartz content. It becomes negligible at 50% quartz, while at 70% quartz calcium hydroxide is found only in samples steamed at 8 atmos. This is in good agreement with chemical and thermographic data. The amount of isotropic finely-granular mass increases at the same time, while samples containing 40% of quartz and numerous fine crystals appear, which polarize yellow or orange colors of the 1st order. They are probably a variety of monocalcium hydrosilicate. This is confirmed by an exothermic effect at 840° in the thermograms, corresponding to CSH(B).

Increase of the autoclaving temperature accelerates the formation of monocalcium hydrosilicate – at 8 atmos its effect on the DTA curves is found at quartz contents up to 50%, while at 16 atmos it is already found at 30%. Hence the formation of monocalcium hydrosilicate, desirable from the strength aspect, can be induced either by increase of the reacting quartz surface (by increase of its relative content, or by finer grinding), or by increase of the autoclaving temperature, when the available quartz reacts more actively. Thus, increase of pressure and increase of the reacting quartz surface both shift the process in the same direction.

It should be noted that when alite is treated with quartz in the autoclave the results are analogous to the reaction of quartz with lime under the same conditions [5]. Hydrosilicates of basicity close to unity are formed only if the lime reacts almost completely, and hydrosilicates of basicity close to two are formed when a considerable amount of unreacted $Ca(OH)_2$ is present.

Interaction of Belite with Quartz

When belite is treated in the autoclave, even at 16 atmos, a considerable amount of unreacted belite grains remains in the samples. It seems likely that the reaction of H_2O with β-C_2S proceeds mainly by direct addition of H_2O to β-C_2S rather than by hydrolysis. This reaction results in the formation of a colorless amorphous mass of low relief, filling all the spaces between the belite grains, and individual bundles of $C_2SH(A)$ needles embedded in this mass. Sometimes these grow directly from the belite grains. Increase of the pressure of 16 atmos intensifies belite hydration and results in the formation, around its grains, of anisotropic borders about 5μ wide, consisting of fibrous crystals with positive elongation, growing in a direction away from the belite grains (Fig. 5).

No thermal effects could be detected on the DTA curve of belite steamed at 8 atmospheres; increase of the pressure to 16 atmos produced a weak $C_2SH(A)$ effect. Determinations with a more sensitive thermograph showed that these $C_2SH(A)$ effects are also found at 8 atmos, but they are very weak; they increase considerably after steam treatment at 16 atmos. In both cases there are also endothermic effects, at their maximum at 620, 695 and 935°; these are evidently to be ascribed to other hydrosilicates. The presence of $C_2SH(A)$ in samples steamed at 8 atmos could not be detected by x-ray analysis. This probably means that most of the hydration products of belite formed at 8 atmos consisted not of $C_2SH(A)$, but of some other hydrosilicate, less stable than $C_2SH(A)$ under these conditions.

Fig. 5. Border of crystals of dicalcium (?) hydrosilicate around belite grains after autoclave treatment at 16 atmos for 8 hours. Without analyzer.

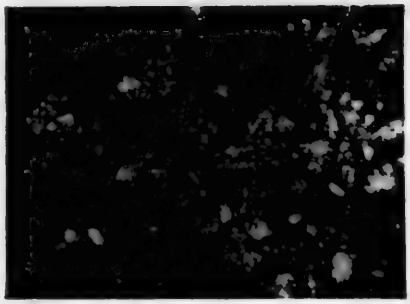

Fig. 6. Bundles of acicular crystals of $C_2SH(A)$ in a sample of belite with quartz after autoclave treatment for 8 hours at 16 atmos. Without analyzer.

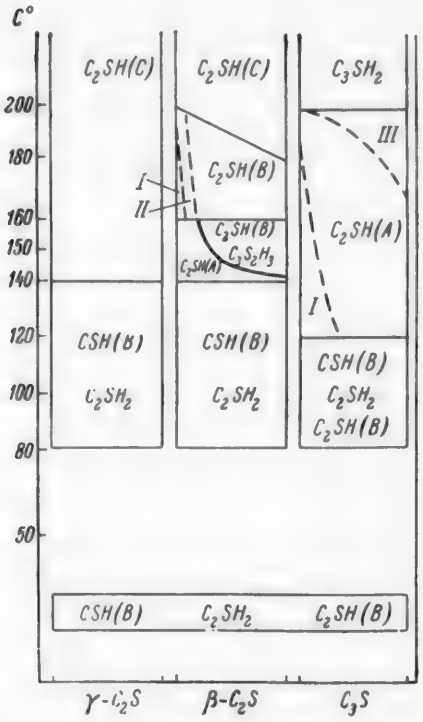

Fig. 7. Hydration products of certain clinker minerals, formed during autoclave treatment. The treatment time is conventionally shown from left to right. The dash lines represent the proposed changes in the phase diagram. I) Formation of unstable compounds, II) crystallization of $C_2SH(A)$, III) formation of C_3SH_2.

It should be noted that in a number of cases when belite was hydrated at 8 atmos for 8 hours there was appreciable crystallization of $C_2SH(A)$, which gave the corresponding lines on the x-ray diagrams. This difference in the character of crystallization was probably due to various impurities and (or) some peculiarities in the firing procedure during the synthesis of the belite.

The hydrolysis of belite both at 8 and at 16 atmos proceeds to only a very slight extent, as shown by the the almost total absence of free lime. The presence of quartz intensifies hydrolysis of belite. In presence of about 2-4% of quartz the face lime content increases; because of the small amount of quartz present, this lime does not have time to react with it. The amount of sheaflike bundles of $C_2SH(A)$ crystals increases with further increase of the quartz content. The greatest amounts are found in samples containing 10% quartz. samples steamed at 16 atmos contain considerably more clearly differentiated (Fig. 6). The interstitial substance in such samples contains $Ca(OH)_2$ crystals. Crystals of dicalcium hydrosilicate grow both out of the belite grains (being formed by hydration of the latter), and out of the quartz grains, owing to interaction of the quartz with the $Ca(OH)_2$ formed by hydrolysis of belite. The quartz is strongly corroded, especially in samples steamed at 16 atmos, and surrounded by a border, also probably consisting of dicalcium hydrosilicate. Increase of the pressure in autoclave treatment always intensifies sharply the hydration of belite. The presence of an endothermic effect at 360° on the DTA curves suggests that, in presence of 5-10% quartz, afwillite $C_3S_2H_3$ is formed in addition to $C_2SH(A)$, but the x-ray pattern did not contain the lines of this compound.

The amount of acicular crystals decreases rapidly with increase of the quartz content above 10%, and with 30-40% quartz they are virtually absent. Simultaneously, isotropic grains of higher relief than in quartz appear on the surface of the quartz grains, similar to those observed by Astreeva [4] and reported by her as calcium hydrosilicate. Numerous belite grains become isotropic in the course of hydration, and merge in relief with the surrounding colorless fine-grained mass. Incompletely hydrated belite contains (in some instances) fine, thin needles of a mineral with negative elongation and moderate relief.

With ≥ 50% quartz, increase of pressure to 16 atmos results in crystallization of numerous crystallization of numerous crystals with double refraction in yellow colors of the 1st order from the isotropic mass.

These apparently consist of monocalcium hydrosilicate CSH(B); thermographic data indicate that it appears at quartz content of 10% and over.

The diagram representing the formation of hydrosilicates during hydration of γ and β-C_2S and C_3S, based on literature data, is given in Fig. 7. Some of our results are not in agreement with this diagram, and augment the existing data. For example, it is shown that $C_2SH(A)$ is formed in the hydration of belite at 175 and 200°, and C_3SH_2 is formed in the hydration of alite at 175°.

In either case hydrosilicates less stable than $C_2SH(A)$ may be formed; they give way to the latter on prolonged steaming or on addition of quartz, i.e., the quartz shifts the system in the direction of equilibrium. The proposed changes are indicated on the diagram by dash lines.

SUMMARY

1. Autoclave treatment for 8 hours, even at 16 atmos, does not result in complete decomposition of alite or belite ground to a specific surface of 3000 cm^2/g. The $Ca(OH)_2$ formed in the hydrolysis of alite forms relatively large single crystals containing included grains of unreacted alite.

2. When alite is treated in the autoclave for 8 hours at 8 atmos, C_3SH_2 is formed together with $C_2SH(A)$. Autoclave treatment of belite leads to formation of $C_2SH(A)$ and a number of other hydrosilicates. In either case hydrosilicates less stable than $C_2SH(A)$ may be formed; they give way to the latter on prolonged steaming or on addition of quartz, i.e., quartz shifts the system in the direction of equilibrium.

3. Most of the hydrosilicates formed in the hydration of alite and belite are present in gel form. Introduction of quartz accelerates decomposition of these clinker minerals and causes intensive crystallization of $C_2SH(A)$. In samples with alite this occurs at 16 atmos with 5-50% quartz, and at 8 atmos with 10-40% quartz. The most intensive crystallization of $C_2SH(A)$ in samples with alite occurs when the quartz content is 10%.

LITERATURE CITED

[1] P. I. Bozhenov and G. F. Suvorova, Cement, 5, 4 (1955).

[2] Iu. M. Butt, L. N. Rashkovich and S. G. Danilova, Proc. Acad. Sci. 107, 4 (1956).*

[3] Iu. M. Butt and L. N. Rashkovich, Coll. Trans. ROSNIIMS 10 (Industrial Construction Press, 1956).**

[4] S. A. Mironov, O. M. Astreeva and L. A. Malinina, Inform. Communication Sci. Res. Inst. Cement, Ministry of the Building Materials Industry USSR, 26 (1955).**

[5] Iu. M. Butt and A. A. Maier, Coll. Trans. ROSNIIMS 11 (Industrial Construction Press, 1956).**

Received September 27, 1956

*Original Russian pagination. See C. B. translation.

**In Russian.

STABILITY OF AQUEOUS SODIUM CHLORITE SOLUTIONS DURING EVAPORATION

Sh. S. Shchegol'

Sodium chlorite has come into extensive use in the foreign textile industry during recent years as a valuable bleaching agent. Chlorite is usually made industrially by the reduction of chlorine dioxide in an alkaline medium in presence of a not very strong reducing agent. There are numerous reports of the use of the following reducing agents: hydrogen peroxide [1], suspended calcium peroxide [2], sulfur compounds, arsenious compounds, carbonaceous materials such as powdered petroleum coke [3-5], metallic powders [1, 6, 7], sodium amalgams [8-12], lower oxides and hydroxides of variable-valence metals such as Co, Mn, Pb, etc. [13, 14]. Detailed reviews of methods for the production of chlorite were recently published in the Soviet and foreign periodicals [1, 12, 14-16].

In most of these methods chlorite is obtained in the form of an alkaline aqueous solution, which must be evaporated and crystallized to yield the commercial product – anhydrous $NaClO_2$ or $NaClO_2 \cdot 3H_2O$. Taylor, White, and others [17, 18] studied the stability of sodium chlorite solutions and showed that only weakly alkaline solutions containing not more than 1 mole of $NaClO_2$ per liter are stable when boiled under atmospheric pressure. When more highly concentrated solutions are boiled, chlorite decomposes to form chlorate and chloride. It was assumed that this was mainly a disproportionation reaction

$$3NaClO_2 \rightarrow 2NaClO_3 + NaCl. \quad (1)$$

It was also observed that part of the chlorite decomposes with liberation of oxygen

$$NaClO_2 \rightarrow NaCl + O_2. \quad (2)$$

The relatively low stability of chlorite solutions at concentrations above 1 M was also reported by Jackson and Parsons [19], who studied the possible use of aqueous $NaClO_2$ solutions in analytical chemistry. Weakly acidic solutions of $NaClO_2$, which have been studied by a number of workers [20-23], are even less stable. There are also reports of the catalytic effects of platinum, palladium, gold, and powdered nickel on the decomposition of chlorite; the data on the effect of chlorides are contradictory [18, 24]. Because of the low stability of $NaClO_2$ solutions at the boil, in most patents on methods for chlorite production it is stated that the solution must be evaporated under vacuum, but there is no existing basis for the choice of the optimum temperature (and the corresponding degree of vacuum). We found no information in the literature on the decomposition kinetics of sodium chlorite during the evaporation of weakly alkaline solutions.

The purpose of the present investigation was to study the stability of chlorite solutions of various concentrations, when boiled at various temperatures, in order to elucidate the principal technological conditions for the separation of chlorite from solutions.

EXPERIMENTAL

The chlorite solutions were boiled in a round-bottomed flask, 250 ml in capacity, fitted with a fractionating column and a reflux condenser, the top of which was connected, through an intermediate flask, to a vacuum pump. To avoid excessive concentration of the solution by loss of water vapor, the latter was cooled to 2-3° in the reflux condenser by brine continuously circulated through the latter. The degree of vacuum was recorded by means of a mercury gage, and the vapor temperature at the exit from the column was noted during the experiments; every 6 hours the solution was analyzed for $NaClO_2$, NaCl and $NaClO_3$. $NaClO_2$ was determined by White's arsenometric method [25], NaCl was determined mercurimetrically with sodium nitroprusside indicator, and $NaClO_3$

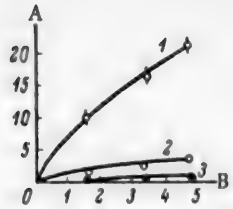

Fig. 1. Effects of concentration and temperature on the degree of decomposition of chlorite. A) Degree of decomposition of $NaClO_2$ in 24 hours (%), B) initial $NaClO_2$ concentration (moles/liter). Temperature (°C): 1) 102-104, 2) 82-83, 3) 53-54.

was determined iodometrically in the sample after titration of $NaClO_2$ and acidification with 6 N sulfuric acid solution. The sodium chlorite used for the experiments was made in the laboratory by reduction of aqueous chlorine dioxide solution either by calcium peroxide [2] or by sodium amalgam [8]. When necessary, purification to remove NaCl and $NaClO_3$ was performed by recrystallization (with the use of the data recently published by Cunningham and Tong San Oey (26) on the systems $NaClO_2-NaCl-H_2O$ and $NaClO_2-NaClO_3-H_2O$), or by dissolution of the chlorite followed by salting-out by means of benzene, and drying [27]. In some of the experiments direct use was made of the reaction solutions obtained after reduction of ClO_2 by sodium amalgam, containing only sodium chloride as an impurity. The pH of the solutions was in the range of 9.2-9.7.*

RESULTS AND DISCUSSION

The curves in Fig. 1, for the decomposition of sodium chloride solutions of various concentrations boiled for 24 hours at normal pressure and under residual pressures of 350 and 98 mm Hg, show that in order to avoid considerable losses of chlorite its solutions should be evaporated under a residual pressure of the order of 100 mm Hg (temperature 52-54°). The decomposition rate increases rapidly with temperature and solution concentration: $NaClO_3$ and NaCl are formed, and their concentration in the solution rapidly increases (Fig. 2a, b, c, d, Curves 1-8). The material balance

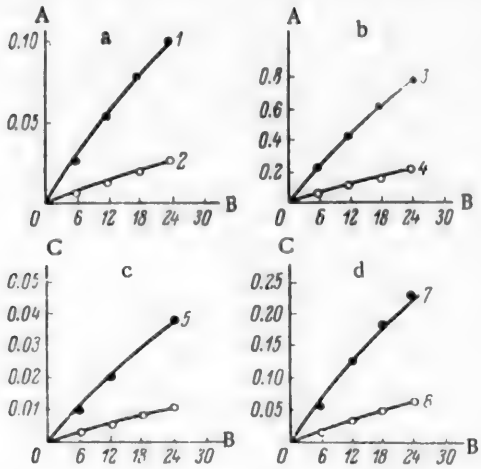

Fig. 2. Accumulation of sodium chloride and chlorate in boiling chlorate solutions at different initial concentrations and temperatures. a) Change of $NaClO_3$ concentration in boiling 1.58 M solution of $NaClO_2$, d) ditto, in 4.7 M solution of $NaClO_2$, c) change of NaCl in boiling 1.58 M solution of $NaClO_2$, d) ditto, in 4.7 M solution of $NaClO_2$. A) Concentration of $NaClO_2$ (moles/liter), B) boiling time (hours) C) concentration of NaCl (moles/liter). Temperature (°C): 1,5-102; 2,6-82; 3,7-104; 4,8-83.

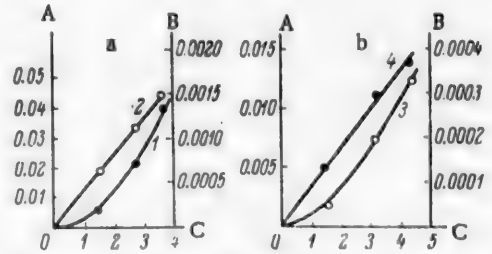

Fig. 3. Kinetics of the decomposition of $NaClO_2$ solutions by Reactions (I) and (II). A) Decomposition rate by Reaction (I) dx_I/dt, B) decomposition rate by Reaction (II) dx_{II}/dt, C) $NaClO_2$ concentration (moles/liter). Reactions: 1, 3) (I); 2, 4) (II). Temperature (°C): a) 103, b) 83.

for chlorite decomposition confirms that the two parallel reactions reported by Taylor, White et al. [17, 18] take place during the decomposition. The amount of chlorate formed is less than should correspond to the amount of chlorite decomposed, while more chloride is formed than should be, according to Equation (I). On the assumption that chlorate can be formed only by Reaction (I), it is possible to calculate the amount of chlorite decomposed by this reaction. The rest of the chlorite decomposed during boiling undergoes disproportionation by Reaction (II). This is confirmed by the good agreement between the actual and calculated amounts of chloride formed. The calculated results for several experiments are given in the table.

*It was found in preliminary experiments that variations of pH in the range of 8-10 have no effect on the decomposition of sodium chlorite in these conditions.

TABLE

Material Balance in Experiments on Decomposition of Boiling Sodium Chlorite Solutions

Concentration of original $NaClO_2$ solution (moles/liter)	Temperature (deg)	Time from start of boiling (hours)	Contents of solution formed (moles/liter)			Formed by reaction (I) (moles/liter)		Formed by reaction (II) (moles/liter)	Calculated amounts of $NaClO_2$ decomposed by reaction			
									I		II	
			$NaClO_3$	NaClO	NaCl	$NaClO_3$	NaCl (calculated)	NaCl (calculated)	moles/liter	relative %	moles/liter	relative %
1.58	102	21	1.43	0.0104	0.036	0.104	0.029	0.01	0.134	90.6	0.016	9.4
3.36	103	21	2.80	0.41	0.133	0.41	0.11	0.018	0.52	94.5	0.03	5.5
1.70	104	21	3.68	0.77	0.21	0.77	0.21	0.026	0.98	95.9	0.04	4.1

It follows from the table that Reactions (I) and (II) are not equivalent. Chlorite disproportionation proceeds mainly by Reaction (I), but the ratio of the amounts of chlorite decomposed by Reactions (I) and (II) respectively varies with the initial chlorite concentration in the solution. This indicates that Reactions (I) and (II) are of different order [28]. Figure 3 shows kinetic curves for the variations of the decomposition rates by Reactions (I) and (II) with the chlorite concentration at any given instant, at various temperatures. The form of these curves indicates that Reaction (II) is of the first $\frac{dx_{II}}{dt} = k_{II}c$, while Reaction (I) is of the second order $\frac{dx_I}{dt} = k_I c^2$

Reaction (I) evidently proceeds in two stages

$$NaClO_2 + NaClO_2 \rightarrow NaClO_3 + NaClO, \quad (I_1)$$

$$NaClO_2 + NaClO \rightarrow NaClO_3 + NaCl. \quad (I_2)$$

It was shown by White et al. [18], Kozlov [21], Holst [14], and Lewin and Avrahami [29] that Reaction (I) is irreversible and proceeds at a high rate, and therefore the rate of the over-all reaction, by the general rule, is determined by the rate of the slower stage – the second-order reaction (I_1).

Typical calculations gave the following rate constants for the reactions: at 103° $k_I = 0.65 \cdot 10^{-6}$ and $k_{II} = 1.2 \cdot 10^{-7}$; at 83° $k_I = 1.6 \cdot 10^{-7}$ and $k_{II} = 0.2 \cdot 10^{-8}$. At 53° the determination of the constants becomes very unreliable, as the changes in the chlorite, chloride, and chlorate concentrations are within the error limits of the analytical determinations of these components.

A significant fact is that all the experiments showed that the rate of the decomposition reaction gradually decreases with time, whereas if chloride had a catalytic effect on chlorite decomposition the process should be autocatalytic and its rate should at first increase with time. Experiments in which sodium chlorite solutions containing up to 1 mole of NaCl per liter were taken also showed that sodium chloride has no catalytic effect.

SUMMARY

In a study of the decomposition kinetics of aqueous sodium chlorite solutions, boiled under atmospheric pressure and under vacuum it was shown that sodium chloride has no catalytic effect on the decomposition of chlorite.

LITERATURE CITED

[1] T. Rogozinski, Przem. chem., 8, 177 (1952).

[2] R. Kirk and D. Othmer, Encyclopedia of Chemical Technology, III, 700, New York (1949).

[3] K. Cederquist and B. Lunden, Swedish Patent 143965; Ch. A., 48, 9026c (1954).

[4] British Patent 687246; Ch. A., 48, 9637c (1954).

[5] French Patent 1025778; Referat. Zhur. Khim. 7859 (1955).

[6] V. V. Shtutser and A. S. Chernyshev, Sci. Res. Trans. Moscow Textile Inst. 13, 112 (1954).

[7] M. Bigorgne, C. r., 225, 527 (1947).

[8] J. Sevon and F. Sundman, Swedish Patent 113609.

[9] Swiss Patent 25884; Z., 1, 906 (1950).

[10] British Patent 628687; Chemistry and Chem. Technology 6, 148 (1951).

[11] R. McMullin, Chem. Eng. Prog., 48, 440 (1950).

[12] St. Lupan, Rev. Chim. 5, 88 (1954).

[13] British Patent 495289; Ch. A., 33, 3083 (5), (1939).

[14] G. Holst, Ind. Eng. Chem., 42, 2359 (1950).

[15] A. S. Chernyshev, V. V. Shtutser and N. G. Semenova, Progr. Chem. 25, 91 (1956).

[16] I. E. Flis, J. Appl. Chem. 2, 633 (1956).

[17] M. Taylor, J. White, G. Vincent and G. Cunningham, Ind. Eng. Chem., 32, 899 (1940).

[18] J. White, M. Taylor and G. Vincent, Ind. Eng. Chem., 34, 782 (1942).

[19] D. Jackson and J. Parsons, Ind. Eng. Chem., 9, 14 (1937).

[20] M. P. Kozlov, Textile Ind. 4, 25 (1945).

[21] M. P. Kozlov, Author's Summary of Doctorate Dissertation (Leningrad Textile Inst., 1951).*

[22] W. Buser and H. Hanisch, Helv. chim. acta, 35, 2547 (1952).

[23] I. E. Flis and T. M. Vasil'eva, J. Gen. Chem. 26, 1272 (1956).** *

[24] Gmelins Handbuch der anorg. Chem., Syst. 6 (1927).

[25] J. White, Am. Dyestuff Reporter, 31, 484 (1942).

[26] G. Cunningham, and Tong San Oey, J. Am. Chem. Soc., 77, 799, 4498 (1955).

[27] R. Weiner, Z. Elektroch., 52, 234 (1948).

[28] A. N. Brodskii, Physical Chemistry, 2 (Goskhimizdat, 1948).*

[29] M. Lewin and M. Avrahami, J. Am. Chem. Soc., 77, 4491 (1955).

Received August 13, 1956

*In Russian.

** Original Russian pagination. See C. B. translation.

THE PRODUCTION OF METALLIC POTASSIUM AND K – Na ALLOY BY THE REACTION KOH + Na = NaOH + K

M. I. Kliashtornyi

In recent years there has been great interest in K–Na alloy, the production of which is increasing rapidly. In the United States of American the 1951 production reached several thousand tons, whereas the 1949 production was only 50 tons [1].

The main use of K–Na alloy is as a heat-transfer medium, and it is also used in organic synthesis.

The Callery Chemical Corporation produces K-Na alloy in a column apparatus (Fig. 1). In this process sodium vapor rises countercurrent to fused potassium chloride, and the following reaction takes place:

$$KCl + Na = NaCl + K$$

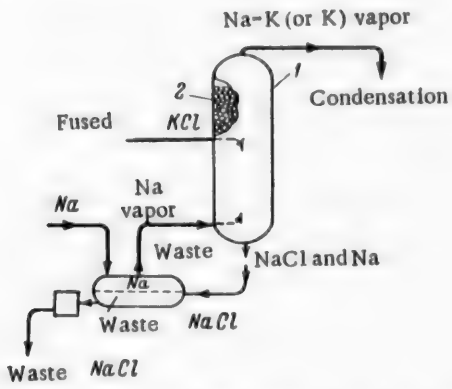

Fig. 1. The Callery Chemical process for the production of K–Na alloy. 1) Column, 2) stainless steel rings.

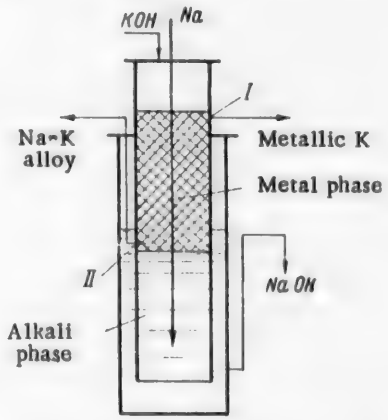

Fig. 2. Schematic diagram of unit with intermediate removal of alloy. I) Cavity I, II) Cavity II.

The K–Na alloy distills in the upper part of the column. The vapor, enriched with potassium, condenses and is collected in a receiver. The metallic sodium entrained by the salt phase leaving the apparatus separates out in the evaporator and is returned to the column.

According to Callery Chemical data, the conversion of potassium chloride reaches 90-95%. This is the real advantage of this method over the exchange process with the use of melted metallic sodium. In the latter case, according to Callery Chemical, only 25% of the original KOH or KCl is converted.

The purpose of the present work was to study the conditions for the production of metallic potassium, with virtually complete conversion of KOH, by the reaction

$$KOH + Na = NaOH + K,$$

with the use of fused metallic sodium.

The desired aim can be achieved by means of intermediate removal of the alloy. The apparatus for this purpose is shown schematically in Fig. 2. The cavitiy for the intermediate removal of the alloy is in the zone of the apparatus where it is filled with the metallic phase.

Because of the increasing demand for K–Na alloy, it is advantageous to produce metallic potassium and K–Na alloy simultaneously. The cost of the original KOH should depend on the difference between the cost prices of KOH and NaOH (somewhat cheaper).

Comparison of the usual countercurrent process and the countercurrent process with intermediate removal of the alloy readily reveals the superiority of the latter process.

The Countercurrent Process

Counterflow is easily achieved because of the density difference between the alkali and metal phases.

We studied the countercurrent process in apparatus of the column type at 400-450°. The apparatus shown schematically in Fig. 3 proved convenient in use. The plates, consisting of sheet nickel disks 200 mm in diameter, were assembled, with the aid of spacing rings 50 mm high, along the tube through which the metallic sodium is fed.

The plates were arranged so that half the overflow orifices at their edges faced in one direction, and the other half, in the other.

The assembled plates were inserted in the body of the apparatus, or in the reaction tube, through the lid of which passed the handle of a stirring device for removal of the deposits accumulating between the plates, and a funnel for the KOH feed.

The metallic sodium entered under the bottom plate and moved upward in a zigzag path, reacting with KOH along its route.

Let us calculate the increase of the metallic potassium content in the metal phase as a function of the molar $\frac{KOH}{Na}$ ratio and of the number of theoretical plates in the countercurrent column, with the use of chemically pure KOH.

We denote by a the content of metallic potassium in the final metal phase in gram-atoms, $M = \frac{KOH}{Na}$, $x_1, x_2, x_3, \ldots\ldots\ldots x_n$ are the amounts of sodium in gram-atoms reacting at the 1st, 2nd, 3rd and n-th plates (the plates are numbered from below).

The equilibrium constant, by Rinck's data [2, 3] is assumed to be 0.5.

Phase Composition on the 1st Plate

Composition of the alkali phase: KOH . . . . . M – a, NaOH . . . . . a. Then

$$0.5 = \frac{(M - a) \cdot (1 - x_1)}{a \cdot x_1}. \qquad (1)$$

This equation is used to find x_1.

Composition of the metal phase: K = x_1, Na = 1 – x_1.

Phase Composition on the 2nd Plate

Composition of the alkali phase: KOH = M – a + x_1, NaOH = a – x_1.

$$0.5 = \frac{(M - a + x_1)\,(1 - x_1 - x_2)}{(a - x_1)\,(x_1 + x_2)}. \qquad (2)$$

This equation is solved to find x_2.

Composition of the metal phase: K = x_1 + x_2, Na = 1 – x_1 – x_2.

Phase Composition on the n-th Plate

Composition of the alkali phase: $KOH = M - a + x_1 \ldots\ldots + x_{n-1}$, $NaOH = a - x - \ldots\ldots - x_{n-1}$,

$$0.5 = \frac{(M - a + x_1 \ldots + x_{n-1})(1 - x_1 \ldots\ldots - x_n)}{(a - x_1 \ldots - x_{n-1})(x_1 + \ldots\ldots + x_n)}. \quad (3)$$

Composition of the metal phase: $K = x_1 + x_2 \ldots\ldots + x_n$, $Na = 1 - x_1 - x_2 \ldots - x_n$.

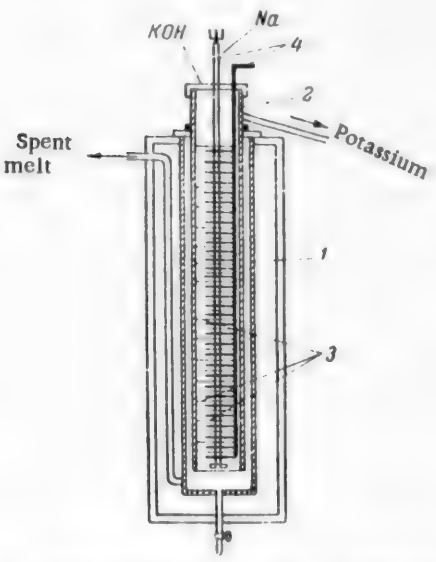

Fig. 3. Column apparatus. 1) Body of apparatus, 2) reaction tube, 3) disks, 4) stirring device.

Fig. 4. Variation of the number of theoretical plates with the KOH/Na ratio. A) KOH/Na ratio, B) number of plates. K content (%): 1) 99, 2) 97, 3) 90.

Figure 4 shows calculated results for 3 different alloy compositions: 99, 97 and 90 atomic % (alloys containing 99-97% of metallic potassium are referred to as "metallic potassium.")

It follows from Fig. 4 that only 3 theoretical plates are required for the production of metallic potassium of 99% content at $\frac{KOH}{Na} = 2.5$. In practice, with $\frac{KOH}{Na} = 2.5$ and with the use of technical caustic potash containing 98.5% KOH, it was necessary to use 30-32 plates in the apparatus, the conversion of KOH being about 35-40%. Because of numerous serious disadvantages, equipment with higher plate efficiency is not used industrially.

Because of the simple construction and small dimensions of the apparatus (with 32 plates, the height of the reaction tube does not exceed 2 meter), it was very effective in use.

The conversion of KOH in the production of the metallic alloy in an apparatus with the same number of plates, at the same $\frac{KOH}{Na}$ ratio, and with the same amount of initial KOH, can be increased considerably by intermediate removal of the alloy. Theoretical calculations and experiments data on the countercurrent process with intermediate removal of the alloy are given below.

Countercurrent Process with Intermediate Removal of the Alloy

Two cases are considered.

Countercurrent process with intermediate removal of the alloy, with removal of equal amounts of metallic potassium and alloy. It is required to obtain metallic potassium with a potassium content (a_1) of 98-99%, and K–Na alloy with a potassium content (a_2) of 70 atomic %.

By the specified conditions, equal molar amounts of metallic potassium and of K–Na alloy containing

TABLE 1

Material Balance for the Apparatus

Substance	Input		Output					
			Cavity I		Cavity II			
	moles	g-atoms	moles	g-atoms	moles	g-atoms	Total	in %
KOH	2.5	—	—	—	—	—	0.81	32.5
Na	—	2	—	0.3	—	0.01	0.31	—
K	—	—	—	0.7	—	0.99	1.69	—
NaOH	—	—	0.7	—	0.99	—	1.69	67.5
Total	4.5				Total		4.5	

70 atomic % of potassium are removed from the apparatus; 2 g-atoms of sodium and not 1 is therefore fed into the apparatus.

We retain in the upper zone of the apparatus the same value $\frac{KOH}{Na} = 2.5$, then in the lower zone we have $\frac{KOH}{Na} = 1.25$. Because of the decrease of the $\frac{KOH}{Na}$ ratio in the lower zone, the conversion of KOH increases, as is clear from the material balance given in Table 1.

The KOH content of the outgoing alkali phase falls to 32 molar % if an equal amount of alloy is removed, whereas without removal of the alloy the KOH content of the outgoing alkali phase is

Countercurrent process with intermediate removal of the alloy, with alloy removed at the optimum ratio. We suppose that the KOH content of the spent alkali phase is to be 2.2%. Let us determine the amount of

TABLE 2

Results of Tests*

Type of process	$\frac{KOH}{Na}$		KOH content of spent alkali phase (molar %)		Potassium content of alloy (atomic %)	
	upper zone	lower zone	experimental	calculated	Cavity I	Cavity II
Without intermediate removal	2.5	2.5	66	60	98	—
Equal amounts removed	2.5	1.25	35	32	97	65
Optimum amounts of alloy removed	2.5	0.78	10	2.2	97	55

metallic sodium which must then be fed into the apparatus. The $\frac{KOH}{Na}$ ratio in the upper zone of the apparatus is 2.5 as before.

The composition of the spent alkali phase in moles is

$$NaOH. \ldots \ldots \ldots .0.978 \cdot 2.5 = 2.44,$$
$$KOH \ldots \ldots \ldots .2.5 - 2.44 = 0.06.$$

*Average results for 6 experiments. Sodium in the metal phase was determined by the zinc uranyl acetate method, and potassium, by the cobaltinitrite method.

Therefore 2.44 g-atoms of metallic potassium was formed in the apparatus; this included 0.99 g-atom of metallic potassium, and 2.44 − 0.99 = 1.45 g-atoms in the form of 70% alloy. The production of the metallic potassium required 1 g-atom of sodium, and of the 70% alloy, $\frac{1.45}{0.7}$ = 2.07 g-atoms of sodium.

Therefore 3.07 g-atoms of sodium per 2.5 moles of KOH must be fed into the apparatus; the $\frac{KOH}{Na}$ ratio in the lower zone of the apparatus is then $\frac{2.5}{3.07}$ = 0.816.

Trials of the countercurrent process with intermediate removal of the alloy were carried out in an experimental unit with 32 plates, shown schematically in Fig. 2. The design and dimensions of the plates and the reaction tube were the same as in the apparatus shown in Fig. 3. The cavity for removal of the alloy was in the region of the 18th plate from the bottom.

It was necessary to find the composition of the alloy obtainable under actual conditions, both at the optimum ratio of the removed alloy, and with equal amounts of removed alloy and metal, for the same ratio $\frac{KOH}{Na}$ = 2.5 in the upper zone of the apparatus. The results of preliminary tests are given in Table 2.

These results show that the KOH concentration of the spent alkali phase did not fall below 10 molar %.

There is reason to believe that in an industrial unit the degree of conversion of KOH can be increased, even at higher values of the $\frac{KOH}{Na}$ ratio in the lower zone of the apparatus.

SUMMARY

In the combined production of metallic potassium and K–Na alloy with intermediate removal of the alloy, up to 90% conversion of KOH can be achieved.

LITERATURE CITED

[1] Chem. Eng. News 33, February 7, 648 (1955).

[2] E. Rinck, Ann. Chem., [10], 18, 390 (1932).

[3] E. Rinck, Ann. Chem., 20, 444 (1945).

Received May 3, 1957

THE INFLUENCE OF Mn, P, AND Si ON THE ACTIVITY OF ALUMINUM IN LIQUID CRUDE (CAST) IRON

V. I. Musikhin, O. A. Esin and B. M. Lepinskikh

Institute of Metallurgy, Ural Branch of the Academy of Sciences

Studies of the properties of aluminum dissolved in liquid ferrous metals are of practical interest, since it is widely used for the deoxidation of steel in modification of cast irons and in the production of iron alloys.

Chipman [1, 2] and his associates [3] determined the activity coefficient of aluminum (γ_{Al}) in iron at 1600°, and the influence of carbon and silicon on it. The equilibrium distribution of aluminum between melted silver and iron was studied for these determinations.

The activity of aluminum in silver (a_{Al}^{Ag}) was assumed to be equal to its mole fraction [1], or was found by extrapolation from results obtained at lower temperatures [2, 3]. The influence of iron and silicon dissolved in the silver was not considered. The values of (a_{Al}^{Ag}) determined in this way can give rise to substantial errors in the calculation of γ_{Al} in iron.

In the present investigation, the activity of aluminum in liquid cast irons with additions of P, Si, and Mn was determined by the electromotive force method, which is free from the defects mentioned.

The cell studied can be represented as

$$Al \mid Al_2O_3 \mid Fe,\ C_{sat.}\ Al,\ Me, \qquad (1)$$

where Me is Mn, P, or Si.

One of the electrodes was liquid aluminum (in the standard state), and the other, its alloy with cast iron. The electrolyte in all cases was solid aluminum oxide (Al_2O_3), from which the cell itself was made.

Galvanic cells with solid electrolytes (various glasses) have been used for determinations of the activities of fusible metals, and gave consistent results [4-7].

From the electromotive forces of the Cell (1), the activity of aluminum (a_{Al}) in cast iron can be calculated by means of the equation

$$E = \frac{RT}{3F} \ln \frac{1}{a_{Al}}, \qquad (2)$$

if it is assumed to be unity in the standard.

For 1250°, this equation assumes the form

$$E = 0.1 \lg \frac{1}{a_{Al}}. \qquad (3)$$

EXPERIMENTAL

The cell for emf measurement (Fig. 1) was molded in the porcelain beaker a from pure Al_2O_3 powder b, containing 5% of refractory clay as a binder. The two compartments c for the metals contained the electrodes, while the partition between them, and the cell itself, served as the electrolyte. With this cell design any possible

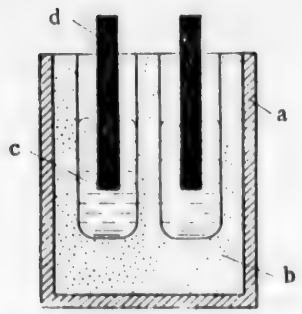

Fig. 1. Cell for emf measurement. Explanation in text.

changes in the electrode and electrolyte compositions were reduced to a minimum, and the results were fairly consistent and reproducible. The emf fluctuations at constant temperature did not exceed 1-3 mv, for measured values of 100-300 mv.

The current leads were graphite rods d. To avoid the formation of aluminum carbides, the temperature was maintained at about 1250° [8]. It was measured by means of a Pt–Pt-Rh thermocouple immersed in the aluminum electrode.

Weighed samples of aluminum were dissolved in the liquid iron (the electrode of variable composition), the emf was measured, samples for chemical analysis were taken, Mn, P or Si was added, and the determinations were repeated.

10-15 determinations were performed for each iron composition in the course of 25-30 minutes, with the aid of a PPTV-1 potentiometer.

The system $Fe-C_{sat}-Al$. The analytical data for the alloys, the emf and the calculated values of a_{Al} and γ_{Al} are given in Table 1.

This system is characterized by negative deviations from ideal solution behavior (Fig. 2, Curve 1). The same diagram contains Curve 2, which represents the variations of log γ_{Al} with its atomic fraction (N_{Al}). The course of the curve changes charply at aluminum contents above 2% ($N_{Al} \cong 0.04$). A similar change of log γ_{Al} apparently occurs at 1600°, although it was not noticed by Chipman [3], probably because of the small number of experimental points for low aluminum contents. However, the available points lie considerably below the straight line corresponding to the aluminum concentrations above 2%, an extrapolation to $N_{Al} = 0$ is hardly justifiable.

TABLE 1

Activity of Aluminum in $Fe-C_{sat}-Al$ Melts at 1250°

N_{Al}	N_C	E (in mV)	a_{Al}	γ_{Al}
0.0036	0.176	320	0.0006	0.18
0.0114	0.172	255	0.0028	0.25
0.0196	0.168	213	0.0074	0.38
0.0255	0.166	182	0.0152	0.59
0.0336	0.163	172	0.0196	0.58
0.0390	0.162	161	0.0246	0.63
0.0562	0.158	140	0.0400	0.71
0.0865	0.152	120	0.0630	0.73
0.1220	0.146	102	0.0955	0.78

TABLE 2

Activity of Aluminum in $Fe-C_{sat}-Al-Mn$ Melts at 1250°

N_{Al}	N_{Mn}	E (in mV)	a_{Al}	γ_{Al}
0.0125	0.004	245	0.0036	0.29
0.0125	0.012	246	0.0035	0.28
0.0125	0.014	247	0.0034	0.27
0.0125	0.023	248	0.0033	0.26

A linear relationship between log γ_{Al} and N_{Al} at low values of N_{Al} follows from the theory of regular solutions. In fact, for the three-component systems $Fe-C_{sat}-Al$

$$RT \ln \gamma_{Al} = B_{Fe,Al} \cdot N_{Al} + B_{Al,C} \cdot N_C - B_{Fe,Al} \cdot N_{Fe} \cdot N_{Al} - B_{Al,C} \cdot N_{Al} \cdot N_C - B_{Fe,C} \cdot N_{Fe} \cdot N_C. \quad (4)$$

Substituting $N_C = 1 - N_{Fe} - N_{Al}$, we have

$$RT \ln \gamma_{Al} = B_{Al,C} \cdot N_{Al}^2 + (B_{Al,C} \cdot N_{Fe} - B_{Fe,Al} \cdot N_{Fe} + B_{Fe,C} \cdot N_{Fe} - 2B_{Al,C}) N_{Al} + (B_{Fe,Al} - B_{Al,C} - B_{Fe,C} + B_{Fe,C} \cdot N_{Fe}) N_{Fe} + B_{Al,C}. \quad (5)$$

At low values of N_{Al} the changes of N_{Fe} are slight, and therefore the expressions in parentheses in Equation (5) may be regarded as constant, while the term in N_{Al}^2 can, in the first approximation, be ignored. We than have the linear equation:

$$\log \gamma_{Al} = AN_{Al} + C. \quad (6)$$

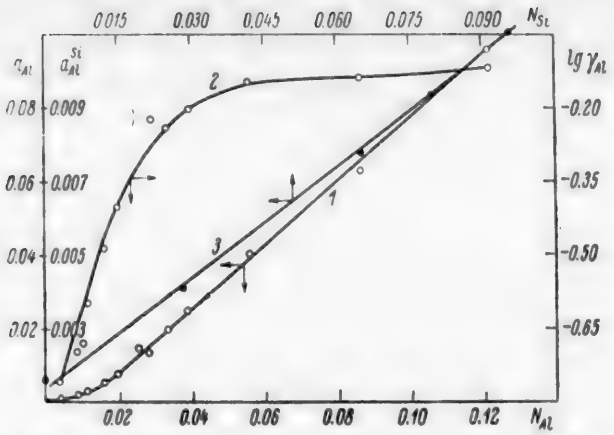

Fig. 2. Activity of aluminum in liquid cast iron at 1250°. Curves in the following coordinates: 1) N_{Al}, a_{Al}; 2) log γ_{Al}, N_{Al}; 3) a_{Al}^{Si}, N_{Si} for $N_{Al} = 0.008$.

Further additions of aluminum to the iron lead to comparable changes of N_{Al} and N_{Fe}, and also of the coefficients in Equation (5), and the relationship is no longer linear.

The system Fe–C_{sat}–Al–Mn. Data on the influence of Mn on a_{Al} are presented in Table 2. Metallic manganese (99.9% Mn) was added to the iron.

The aluminum content of these alloys can be regarded as constant for practical purposes, as the dilution by the small amounts of manganese added (up to 2.7% Mn) is negligible. Although the emf of the cell increased somewhat on introduction of manganese, the increase did not exceed the experimental error. It follows that Mn does not influence a_{Al} in iron in the concentration range studied.

TABLE 3

Activity of Aluminum in Fe–C_{sat}–Al–Si Melts at 1250°

N_{Al}	N_{Si}	E (in mV)	a_{Al}	γ_{Al}
0.008	—	280	0.0016	0.20
0.008	0.028	238	0.0041	0.51
0.008	0.065	211	0.0078	0.97
0.008	0.080	203	0.0094	1.12
0.008	0.096	195	0.0112	1.50

TABLE 4

Activity of Aluminum in Fe–C_{sat}–Al–P Melts at 1250°

N_{Al}	N_P	E (in mV)	a_{Al}	γ_{Al}
0.0071	—	287	0.0014	0.20
0.0068	0.012	278	0.0017	0.24
0.0067	0.026	278	0.0017	0.25
0.0062	0.045	285	0.0014	0.23
0.0054	0.076	275	0.0018	0.33
0.0045	0.118	251	0.0030	0.67
0.0161	—	230	0.0050	0.31
0.0154	0.015	226	0.0055	0.36
0.0144	0.036	231	0.0049	0.34
0.0133	0.059	223	0.0059	0.45
0.0266	—	180	0.0159	0.60
0.0257	0.011	174	0.0182	0.71
0.0250	0.021	162	0.0240	0.96
0.0235	0.039	159	0.0257	1.10
0.0210	0.069	178	0.0166	0.79
0.0180	0.104	182	0.0152	0.85

The probable reason is that a solution of manganese in iron is almost ideal [9] because of the great resemblance between their atoms, while the energy of the Mn–Al bond is not too high. As is known, Al and Mn form two chemical compounds which melt incongruently [10].

The system Fe–C_{sat}–Al–Si. The results for this system are given in Table 3. In distinction to manganese, metallic silicon appreciably increases the activity of aluminum in iron. Line 3 in Fig. 2 represents the variation of a_{Al}^{Si} with the atomic fraction of silicon (N_{Si}) in a melt containing 0.45% Al.

A similar effect for silicon was reported earlier [3] for 1600°, although the presence of considerable amounts of it in the silver makes the results unreliable.

The system Fe–C_{sat}–Al–P. For studies of the effects of phosphorus, ferrophosphorus (20% P) was added to the iron; this diluted the electrode melt considerably and lowered its aluminum content (Table 4). However, despite the increased difference of the Al concentrations at the electrodes, the cell emf remained approximately constant or even decreased somewhat at higher phosphorus concentrations. Therefore phosphorus has a similar effect to that of silicon, i.e., it increases the activity of aluminum in liquid iron.

DISCUSSION OF RESULTS

Aluminum, like silicon and phosphorus, decreases the solubility of carbon in iron [3, 11]. This shows that the Fe–Al bond energy is high in comparison with the Fe–C bond [12]. Qualitatively, this result follows from the theory of regular solutions applied to three-component systems [13].

In the first approximation, the Fe–Al, Fe–Si, Fe–P bond energies in Fe–C_{sat}–Me alloys may be compared by comparison of the heats of formation of chemical compounds of Al [14-16], Si [17] and P [10] with iron, or by the decreases of carbon solubility in Fe–C melts. In the latter case not only Fe–Me bonds are taken into account, but also others, such as Me–C, Fe–C, etc., which characterize more completely the behavior of the element in the cast iron. Such comparison shows that the heats of formation and the amounts of carbon displaced increase in the sequence Al–Si–P [13, 18]. Their bond energies with iron increase in the same sequence. Because of the stronger bonds of Fe with Si and P, aluminum atoms become isolated and the activity of aluminum becomes higher.

This might suggest that the effect of phosphorus should be greater. It is found in practice, however, that the addition of an equal amount of phosphorus produces a somewhat smaller increase of a_{Al} than does silicon.

The explanation is that the bond energy of aluminum and phosphorus is higher. Aluminum does not form chemical compounds with silicon, whereas it gives a whole series of phosphides with phosphorus.

SUMMARY

1. In determinations of the electromotive force of amalgam-type cells at 1250° it was found that concentration cells with solid electrolytes give reproducible results and may be used for determinations of the activities of elements dissolved in ferrous metals.

2. In the concentration ranges studied, silicon and phosphorus increase the activity of aluminum in liquid cast iron, whereas manganese has no effect.

LITERATURE CITED

[1] I. Chipman, Trans. Amer. Soc. Met., 22, 385 (1934).

[2] I. Chipman, Discuss. Farad. Soc., 4, 23 (1948).

[3] I. Chipman and T. P. Floridis, Acta Metall., 3, 5, 456 (1955).

[4] O. Kubaschewski and O. Huchler, Z. Elektroch., 52, 170 (1948).

[5] H. Frauenschill and F. Halla, Z. Elektroch., 53, 144 (1949).

[6] A. L. Vierk, Z. Elektroch., 53, 151 (1949); 54, 436 (1950).

[7] A. F. Alabyshev and A. G. Morachevskii, J. Inorg. Chem. 2, 3, 669 (1957).

[8] M. P. Slavinskii, Physicochemical Properties of the Elements (Moscow, Metallurgy Press, 1952), p. 220.*

[9] F. Korber, Stahl and Eisen, 57, 1349 (1937).

[10] V. P. Eliutin, Iu. A. Pavlov and B. E. Levin, Production of Ferroalloys (Moscow, Metallurgy Press, 1951),* pp. 134, 424.

[11] L. S. Darken, Metals Technology, 7, 2 (1940).

[12] F. D. Richardson, Iron and Steel Inst., 175, 39 (1953).

*In Russian.

[13] N. A. Vatolin and O. A. Eson, J. Gen. Chem. 88, 1543 (1956).*

[14] W. Oelsen and W. Middel, Mitt. KWI Eisenforschung, Dusseld., 19, 1 (1937).

[15] W. Biltz and C. Haase, Z. anorg. allg. chem., 129, 141 (1923).

[16] O. Kubaschewski and W. A. Dench, Acta Metall, 3, 4, 339 (1955).

[17] F. Korber and W. Oelsen, Mitt. KWI Eisenforschung Dusseld., 18, 109 (1936).

[18] E. T. Turkdogan and R. A. Hancock, J. Iron and Steel Inst., 179, 155 (1955).

Received June 19, 1957

*Original Russian pagination. See C.B. translation.

THE RATE OF INTERACTION OF APATITE WITH SULFURIC ACID IN THE COURSE OF MIXING

M. E. Pozin, G. S. Grigor'ev, B. A. Kopylev and A. D. Sokolova

The Lensoviet Technological Institute, Leningrad, The Nevskii Chemical Works

The introduction of continuous mixing in superphosphate production has resulted in a considerable improvement in working conditions, and has made it possible to use sulfuric acid of higher concentrations and therefore to obtain a product with less moisture and a higher P_2O_5 content. It is also considered that the apatite conversion coefficient is increased somewhat and the aging of the superphosphate is accelerated. However, the apatite conversion coefficient remains relatively low in both the chamber and the continuous process, and the raw-material consumption remains high.

One reason for this is the fact that the characteristics of continuous mixing, and the possibilities of this process for accelerating the reaction, have not been studied sufficiently.

The over-all rate of superphosphate formation during aging and curing depends to a considerable extent on the decomposition rate of apatite when mixed with the acid, and on the structure of the calcium sulfate formed at this stage of the process. The higher the degree of decomposition of apatite at the mixing stage, and the larger the crystals of calcium sulfate hemihydrate precipitated, the more rapid is the superphosphate cure.

It is therefore very important to study the rate of the process in its individual stages – during mixing, aging, and cure.

This paper consists of a brief account of the results of a study of the interaction rate of apatite and sulfuric acid during mixing, in relation to the principal factors – acid concentration and ratio.

No detailed data are available in the literature on the rates of the individual stages of superphosphate production under industrial conditions. This is especially true of the initial stage of the process, i.e., mixing. Brutskus and Chepelevetskii [1] studied the kinetics of apatite dissolution in large excess of sulfuric acid at 50, 70 and 90°. Their results show that at each temperature there is a minimum dissolution rate at a definite acid concentration. Analogous results were obtained for the action of mixtures of sulfuric and phosphoric acids on apatite. However, the absolute rates of decomposition are lower with the use of acid mixtures than with sulfuric acid alone.

Later, Chepelevetskii and Iuzhnaia showed that when apatite is dissolved in a large amount of sulfuric acid its maximum decomposition rate is found in the region of low acid concentrations (about 5-7.5% H_2SO_4).

It had been shown earlier [2] that the curve for the variation of the degree of decomposition of apatite in a definite time interval (decomposition isochrone) has two maxima and one minimum.

This influence of the acid concentration on the course of the process can be attributed to two opposing factors – the activity of the acid, which determines the initial reaction rate, and the resistance to the diffusion of acid toward the unreacted apatite particles. The resistance is determined by the thickness and structure of the calcium sulfate layer formed on the particles.

A number of investigations [3, 4] showed that the total rate of phosphate decomposition decreases with increase of the sulfuric acid concentration, but in some instances [2] a maximum decomposition rate is found with

the use of acid containing about 62% H_2SO_4. Under these conditions the absolute degree of decomposition of apatite is lower than with the use of acid containing 40 or 50% H_2SO_4.

The purpose of most investigations of continuous mixing in superphosphate production was to determine the ratio between the amounts of the material fed in, and the volume of the reaction slurry, and also to find conditions for the use of acid of higher concentrations [5-8].

Brutskus and Tsyrlin [9] determined the ranges of the sulfuric–phosphoric acid ratios in the slurry in relation to the sulfuric acid concentration at which the materials enter the mixer.

The values determine the degree of apatite decomposition necessary in the slurry, for the production of superphosphate with satisfactory properties.

Borunov and Sokolova [10] studied the relationship between the degree of decomposition of apatite during continuous mixing, and the acid ratio and temperature. Acid with a constant concentration of about 68% H_2SO_4 was used in their experiments. Their results made it possible to determine the conversion coefficient of apatite in different sections of the mixer, and during aging in the chamber.

For acid ratios in the range from 67.7 to 73 weight parts of monohydrate per 100 wt. parts of apatite, the apatite conversion coefficient in the mixer was 53-63%; the conversion coefficient of den superphosphate under the same conditions varied from 81.2 to 87.2%. In general, increase of the acid ratio by one unit in this range resulted in 1.3-1.4% increase of the apatite conversion coefficient in the course of mixing, and 0.85% increase during aging in the chamber.

It may be seen that the existing data are inadequate for full characterization of the decomposition rate of apatite during mixing, and of its influence on the over-all rate of superphosphate formation.

Investigations of the effects of various factors on the decomposition rate of apatite when mixed when sulfuric acid are necessary in order to reveal the special features of continuous mixing, and to improve the superphosphate process. The results of the first stage of our investigation, in which the rates of decomposition of apatite by sulfuric acid under periodic-mixing conditions were studied, are given below.

EXPERIMENTAL*

Experimental and analytical methods. A known amount of acid of the required concentration was put into a 250 ml porcelain beaker. The acid was heated to 60°, and 100 g of apatite was added over a 1 minute interval, with stirring. The beaker was then placed in a glycerol bath at 105-110° (to simulate the temperature conditions in the industrial mixer), the slurry being stirred continuously. With continued stirring, samples were taken at intervals for determination of the sulfuric–phosphoric acid ratio. The samples were taken 2, 3.5, 5, 6 and 7 minutes from the start of the experiment. The slurry temperature was recorded when the samples were taken.

The temperature was also read, and the consistency of the slurry noted, at the start of the experiment and after the addition of the apatite concentrate.

The degree of decomposition of apatite during mixing, as a function of the mixing time, was determined with acid of 55 to 68% H_2SO_4, at acid ratios from 80 to 150% of the stoichiometric amount.

The starting materials for the experiments were chemically pure sulfuric acid, and apatite concentrate containing 39.42% P_2O_5, 0.12 H_2O and 3.1% F.

The values of the sulfuric–phosphoric acid ratio (A) were used to calculate the degree of decomposition (K) of the apatite in the slurry by means of the formula

$$K = \frac{0.6 \cdot R \cdot 100}{(0.6A + 1) \cdot 1.38\ P_2O_{5\,ap}},$$

where R is the sulfuric acid ratio, i.e., the quantity of H_2SO_4 monohydrate (in g) taken per 100 g of apatite; $P_2O_{5\,ap}$ is the P_2O_5 content of the apatite (%); 1.38 is the factor for conversion of P_2O_5 to H_3PO_4.

*N. A. Petrova, L. Ia. Tereshchenko, and V. S. Bogorad took part in the experimental work.

RESULTS

The table, and Figs. 1 and 2, contain data on the variation of the degree of decomposition with time, with sulfuric acid of different concentrations and at constant acid ratio – 110% of the stoichiometric quantity (70 g of monohydrate per 100 g of apatite concentrate).

TABLE

Variations of the Degree of Decomposition of Apatite Concentrate by Sulfuric Acid, with Time and Acid Concentration (Acid Ratio 70)

Acid concentration (% H_2SO_4)	Degree of decomposition (%) after time (minutes)				
	2	3.5	5	6	7
55	21.0	26.9	44.0	49.4	56.2
58	19.3	25.3	54.0	57.0	62.7
60	24.0	40.1	50.9	55.9	59.2
62	29.6	36.2	37.3	41.9	45.8
65	26.4	29.5	32.0	33.7	34.6
68	22.0	23.0	24.4	28.4	31.2

It is seen that the degree of decomposition of apatite concentrate attained at a given time depends on the concentration of the acid used. With a mixing time of 7 minutes, the degree of decomposition of apatite by acid containing 55-60% H_2SO_4 is 56.2-62.7%, while with acid containing 62-68% H_2SO_4 it is 45.8-31.2%.

The course of the degree of decomposition–time curves, i.e., the increase of the degree of decomposition with mixing time, also varies with the acid concentration. With acid containing 58% H_2SO_4 the degree of decomposition after 2 minutes is 19.3%, after 3.5 minutes, 25.3%; it then increases rapidly, with subsequent retardation (Fig. 1, Curve 2). If the acid concentration is decreased to 55% H_2SO_4, the degree of decomposition during the initial time intervals (2 and 3.5 minutes) is somewhat higher, and during the subsequent time intervals lower, than with 58% acid. With 60% acid the degree of decomposition is higher than with 55 or 58% acid at the start of the process, but the degree of decomposition reached on increase of the mixing time is lower than with acid containing 58% H_2SO_4. If apatite concentrate is mixed with acid containing 62-68% H_2SO_4, the degree of decomposition varies more uniformly with time.

Within the time range studied (2 to 7 minutes), the degree of decomposition increases relatively slowly with the mixing time (Fig. 2). In the case of 62% acid the increase in the degree of decomposition in 5 minutes is 16.2%, whereas for acids of higher concentrations (65 and 68% H_2SO_4) the increase for the same period is

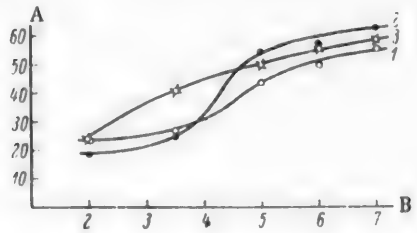

Fig. 1. Variations of the degree of decomposition of apatite by sulfuric acid with time, for acid containing 55, 58 and 60% H_2SO_4. A) Degree of decomposition (%), B) time (minutes). Acid concentration (% H_2SO_4): 1) 55, 2) 58, 3) 60.

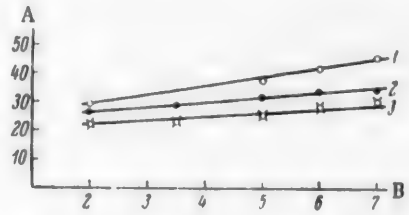

Fig. 2. Variations of the degree of decomposition of apatite by sulfuric acid with time, for acid containing 62, 65 and 86% H_2SO_4. A) Degree of decomposition (%), B) time (minutes). Acid concentration (% H_2SO_4): 1) 62, 2) 65, 3) 68.

8.2-9.2%, or about a half as much. The general character of the kinetic curves in such cases is evidently analogous to that of curves for dissolution retarded by the formation of an acid-permeable film [1]. The curves remain of the same character with change of the acid ratio.

Data on the course of decomposition of apatite by sulfuric acid containing 58 and 60% H_2SO_4, with acid ratios from 90 to 150% of the stoichiometric, are plotted in Figs. 3 and 4. Figure 5 shows the effect of acid concentration on the degree of decomposition of apatite during mixing with sulfuric acid. It is seen that there is an acid concentration ($\sim$ 58% H_2SO_4) corresponding to a maximum degree of apatite decomposition. Evidently, in general this concentration must depend on the acid ratio and the time of stirring; i.e., it is determined by the conditions of mixing. It is clear from Fig. 6 that the acid concentration corresponding to maximum decomposition is shifted toward higher values (60-62% H_2SO_4) with decrease of the stirring time.

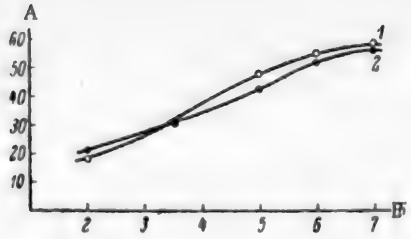

Fig. 3. Effect of acid ratio on the degree of decomposition of apatite by 58% sulfuric acid as a function of time. A) Degree of decomposition (%), B) time (minutes). Acid ratio (% of stoichiometric quantity): 1) 90, 2) 150.

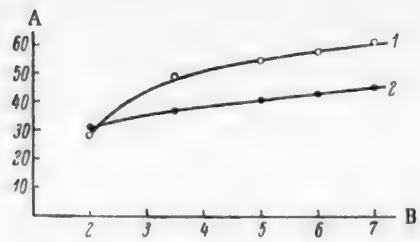

Fig. 4. Effect of acid ratio on the degree of decomposition of apatite by 60% sulfuric acid as a function of time. A) Degree of decomposition (%), B) time (minutes). Acid ratio (% of stoichiometric quantity): 1) 90, 2) 150.

Variations of the degree of decomposition of the apatite with the acid ratio are of considerable interest. With sulfuric acid containing 55 and 68% H_2SO_4, the degree of decomposition increases with increasing acid ratio (Fig. 7). With sulfuric acid containing 60, 62 and 65% H_2SO_4 (in the mixing process), the reverse is true, and the degree of decomposition decreases with increasing acid ratio. With acid containing 58% H_2SO_4, the degree of decomposition increases with increase of the acid ratio in the range from 80 to 110% of the stoichiometric quantity, and decreases in the range from 110 to 150%.

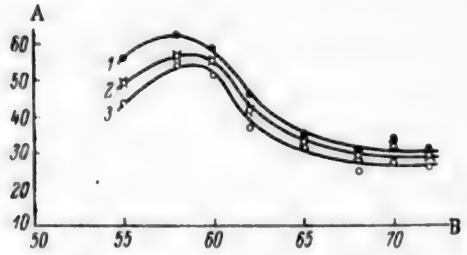

Fig. 5. Variation of the degree of decomposition of apatite with sulfuric acid concentration, at acid ratio 110% of the stoichiometric quantity.
A) Degree of decomposition (%), B) sulfuric acid concentration (% H_2SO_4). Decomposition time (minutes): 1) 7, 2) 6, 3) 5.

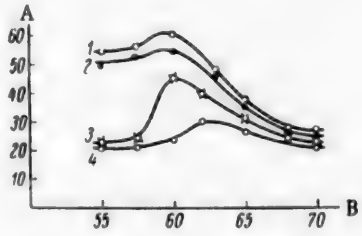

Fig. 6. Variation of the degree of decomposition of apatite with sulfuric acid concentration, at acid ratio 120% of the stoichiometric quantity. A) Degree of decomposition (%), B) sulfuric acid concentration (% H_2SO_4). Decomposition time (minutes): 1) 7, 2) 5, 3) 3.5, 4) 2.

With acid containing 65% H_2SO_4, an appreciable decrease of the degree of decomposition is found only in the transition from 80% to 90% acid ratio. In the acid ratio range from 110% to 150% of the stoichiometric quantity, the degree of decomposition of apatite by 65% H_2SO_4 is almost independent of the acid ratio.

Thus, in the acid concentration ranges studied, variations of the acid ratio have different effects on the degree of decomposition of apatite in the course of mixing with sulfuric acid. The degree of decomposition increases with acid ratio if 55% acid is used, decreases with the use of 60 and 62% H_2SO_4, is virtually constant over a wide range of ratios with 65% acid, and increases with the use of 68% acid.

These data on the decomposition rate of apatite when mixed with sulfuric acid at various concentrations and acid ratios reflect the influence of many processes taking place in the interaction of apatite with the acid. To explain these results it is necessary to take into account the complexity of the process, which is influenced by chemical, diffusional, and crystallochemical factors.

The process may be presumed to comprise the following stages: 1) diffusion of sulfuric acid to the apatite surface, 2) chemical reaction between the acid and apatite, 3) diffusion of the reaction products into the liquid phase, 4) crystallization of calcium sulfate hemihydrate from the liquid phase, and 5) deposition of calcium sulfate crystals on the surface of unreacted apatite particles.

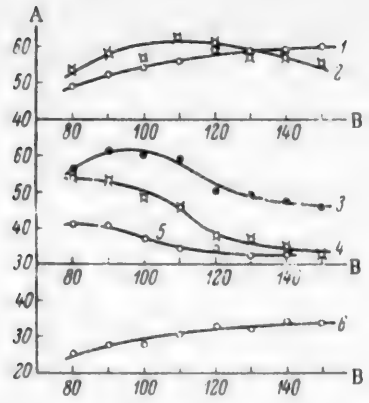

Fig. 7. Effect of sulfuric acid ratio on the degree of decomposition of apatite (decomposition time 7 minutes). A) Degree of decomposition (%), B) acid ratio (% of stoichiometric quantity). Acid concentration (% H_2SO_4): 1) 55, 2) 58, 3) 60, 4) 62, 5) 65, 6) 68.

The slowest of these stages is diffusion of the reaction products into the liquid phase; its rate depends on the solubility of calcium sulfate under the particular conditions. However, the over-all decomposition rate also depends on other factors, in particular on the conditions for the crystallization of calcium sulfate and its deposition on the apatite particles. When calcium sulfate crystallizes rapidly from strongly supersaturated and viscous solutions, fine crystals are formed and are deposited in a dense continuous layer, impermeable to the acid, on the apatite particles. In slow crystallization from solutions of low supersaturation, larger crystals of calcium sulfate are formed, and are not deposited compactly on the apatite particles but leave gaps which serve as channels for the diffusing acid.

As has been noted earlier, the reaction rate of apatite with sulfuric acid depends on the driving force of the process (including the activity of the acid), and the resistance to the diffusion of acid toward the unreacted apatite surface (caused by the layer of calcium sulfate crystals).

The initial rate of reaction is determined mainly by the activity of the acid. At high initial rates of the apatite–acid reaction, the solution is considerably supersaturated with the forming calcium sulfate at the very start of the process. This leads to rapid crystallization of calcium sulfate in the form of fine crystals, giving rise to a dense layer on the apatite particles, so that the subsequent reaction is hindered. However, the degree of supersaturation of the solution with calcium sulfate, the crystallization rate, and the size of the crystals formed, depend also on the volume of the liquid phase, i.e., the acid ratio (for a given acid concentration). Therefore the over-all rate of decomposition of apatite depends both on the concentration and the acid ratio. The over-all rate of the process increases with changes in these until the initial reaction rate begins to increase more rapidly than the resistance. When the increase in the resistance to the diffusion of acid toward the apatite surface with changes of the acid concentration and ratio exceeds the increase of the initial reaction rate, the over-all rate of the process begins to decrease.

These considerations account for the observed variations of the degree of decomposition of apatite with the sulfuric acid concentration and ratio. Thus, the variations of the degree of decomposition with the acid concentration (Fig. 5) are readily explained in the light of the fact that in the concentration range studied the activity of 68% acid is higher than that of 55% acid. With increase of concentration above 55% H_2SO_4, the activity of the acid increases more rapidly than the resistance.*

When the acid concentration is decreased below 68% H_2SO_4, the resistance decreases to a greater extent than the activity of the acid. This effect is also favored by the increase of the liquid volume and the corresponding decrease in the supersaturation of the solution with calcium sulfate. The disproportionate variations of activity and resistance lead to increases of the degree of decomposition both when the acid concentration is increased over 55% H_2SO_4, and when it is decreased to less than 68% H_2SO_4.

Accordingly, the curve for the degree of decomposition as a function of acid concentration has an extremal corresponding to optimum values of acid activity and resistance to diffusion.

The variations of the degree of decomposition with the acid ratio (Fig. 7) can be explained by analogous reasoning.

The degree of decomposition of apatite varies with the acid ratio in conformity to the law of mass action; the degree of supersaturation with calcium sulfate, and the solid-phase crystallization conditions alter

*The lump formation which occurs in the production of superphosphate, especially when apatite is mixed with acid of low concentrations (~55% H_2SO_4 and less), and which leads to a decrease in the degree of decomposition, is evidently also determined by the solid-phase crystallization conditions.

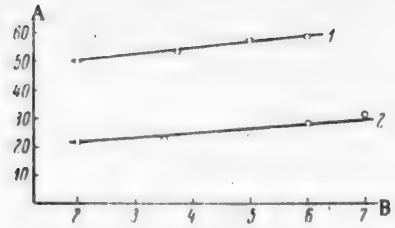

Fig. 8. Variations of the degree of apatite by 68% sulfuric acid with continuous mixing (Curve 1, Nevskii Chemical Works data) and with batch mixing (Curve 2, laboratory data).

simultaneously (because of the changes in the volume of the liquid phase). The degree of decomposition may either increase or decrease with increasing acid ratio, depending on whether the change of the acid ratio has a predominant influence on the initial rate of the process or on the resistance to diffusion. Thus, in the acid concentration range studied, the degree of decomposition increases with the acid ratio if 55 and 68% H_2SO_4 are used. In the former case this is due to an increase of the initial rate of reaction and a relatively small increase, or even a decrease, of the resistance (the volume of the liquid phase being large), and in the second case, to a decrease of the degree of supersaturation with calcium sulfate because of the increased volume of the liquid phase. For acids containing 60-65% H_2SO_4 increase of the acid ratio evidently leads to an increase of the initial rate of reaction to such an extent that the resistance to the diffusing acid is increased sharply. It is significant that, with 58% acid, increase of the acid ratio produces first an increase and then a decrease of the degree of decomposition, whereas with 65% H_2SO_4 the degree of decomposition remains virtually constant over the acid ratio range from 110 to 150% of the stoichiometric quantity.

These results also throw some light on the nature of the interaction between apatite and sulfuric acid at high concentrations when mixed batchwise, and on the causes of retardation of the process.

At the start of the process only part of the apatite reacts, and the actual active mass of the acid is considerably above the selected acid ratio. Subsequently the active mass of the acid decreases. Therefore the decomposition of apatite by acids of 65% H_2SO_4 and higher proceeds at a high rate during the first instant, so that a high resistance to diffusion is created. The resistance increases and the driving force diminishes as the reaction proceeds. The process therefore dies down rapidly.

To ensure a normal course of the process and to obtain superphosphate of satisfactory physical properties, it is necessary to reduce the increased resistance at the start of the process; this is effected when fresh portions of acid are diluted by reacted slurry under conditions of continuous mixing. The conditions are then favorable for the process to take place at a high rate.

Figure 8 shows that the rate of decomposition of apatite by 68% H_2SO_4 is much higher with continuous than with batch mixing. Thus it is possible to obtain a well-reacted slurry with setting properties; the aging of this slurry in the chamber proceeds quite normally.

Therefore the continuous mixing of the reagents, which accelerates the decomposition of apatite in the mixing stage, can be used to accelerate the process of superphosphate production as a whole.

SUMMARY

1. The reaction rate of apatite with sulfuric acid in the course of mixing was studied over a wide range of concentrations (55-68% H_2SO_4) and acid ratios (from 80 to 150% of the stoichiometric quantity); it was found that the variations of the degree of decomposition with time differ for different acid concentrations.

2. With acids containing 55 and 68% H_2SO_4, the degree of decomposition of apatite during mixing increases with increase of acid ratio. With acids containing 60-65% H_2SO_4 the degree of decomposition of apatite (in the mixing stage) decreases with increasing acid ratio.

3. The degree of decomposition of apatite in the course of mixing with sulfuric acid depends on the concentration of the acid used. At acid ratios up to 70 wt. parts of monohydrate per 100 wt. parts of apatite the maximum decomposition rate is obtained with acid containing ~58% H_2SO_4.

4. This justifies the use of acids of decreased concentrations. However, for the production of superphosphate of low moisture content the sulfuric acid fed into the process should be diluted not with water but with partially reacted slurry (i.e., phosphoric acid); this is achieved if the continuous-mixing process is used.

5. One feature of the continuous-mixing process is a higher over-all rate of reaction between the apatite and sulfuric acid than is obtained in batch mixing, as the sulfuric acid is diluted with considerable amounts of the reacted slurry. This also makes it possible to use more highly concentrated sulfuric acid in continuous mixing.

LITERATURE CITED

[1] E. B. Brutskus and M. L. Chepelevetskii, Ann. Sector Phys.-Chem. Analysis Acid. Sci. USSR 20, 383 (1950).

[2] M. E. Pozin, and B. A. Kopylev, Ten Se Den, Trans. Lensoviet Technol. Inst. Leningrad 36, 5 (1956).

[3] M. L. Chepelevetskii, E. B. Brutskus and Z. A. Rodova, J. Chem. Ind. 11 (1941).

[4] G. L. Bridger and E. C. Kapusta, Ind. Eng. Ch., 7 (1952).

[5] M. L. Chepelevetskii, E. B. Brutskus and Z. A. Rodova, Authors' Certif. 33162 (1940); 42227 and 42228 (1941).

[6] N. Kriuchkov and Ia. Przehgodskaia, Scientific Research on Fertilizers, Insectofungicides, and Sulfuric Acid in 1937 (Goskhimizdat, 1940).*

[7] E. B. Brutskus, M. L. Chepelevetskii and Z. A. Rodova, Trans. Sci. Res. Inst. Fertilizers and Insectofungicides (1947).

[8] M. L. Chepelevetskii, E. B. Brutskus and Z. A. Rodova, J. Chem. Ind. 21, 3 (1941).

[9] E. B. Brutskus and D. L. Tsyrlin, J. Chem. Ind. 10, 11 (1951).

[10] I. D. Borunov and A. D. Sokolova, Data on the Exchange of Experience for 1955 (Bureau of Technical Information, Sci. Res. Inst. Fertilizers and Insectofungicides).*

Received December 17, 1956

*In Russian.

EQUILIBRIUM IN THE REACTION $2Br' + Cl_2 \rightleftharpoons Br_2 + 2Cl'$ IN THE PROCESS FOR THE PRODUCTION OF BROMINE FROM NATURAL BRINES

D. S. Stasinevich

The process for the production of bromine from natural brines is based on the oxidation of bromides by chlorine. It is known that the bromine obtained from such brines always contains chlorine, even if a strictly equivalent amount of chlorine or somewhat less was used in the oxidation [1].

Very little information is available in the literature on the equilibrium in the reaction $2Br' + Cl_2 \rightleftharpoons Br_2 + 2Cl'$. In some text books the reaction of chlorine with bromides is considered to proceed to completion with formation of elemental bromine [2], despite the fact that Potylitsyn [3] showed over 70 years ago that the chlorine–bromide reaction is reversible both in aqueous solutions and in melts [3]. This work was rated highly by D. I. Mendeleev [4]. However, there have been very few studies of the chlorine–bromide reaction since. In a number of investigations the equilibrium and rate of the $2Br' + Cl_2 \rightleftharpoons Br_2 + 2Cl'$ reaction in melts has been studied [5-7]. The only available information on equilibrium in solutions is found in the paper by Forbes and Fuoss [8], who measured the potential of a platinum electrode in solutions of bromine in hydrochloric acid and showed that 2.8% of the bromine in a molar solution of bromine in 4 N HCl, and 18.5% in a centimolar solution, interacts with chloride ions, to form BrCl, Cl_2 and Cl'.

The interaction of bromide ions with chlorine may give rise to bromine chloride, BrCl, in addition to elemental bromine. The existence of this compound remained a controversial point for many years, as it could not be detected on the solid-liquid and liquid–vapor equilibrium diagrams for the system Br_2–Cl_2 [9].

The existence of the compound BrCl is now no longer in doubt, and its dissociation constant in the vapor phase and in solution has been determined by several independent methods [5, 6, 10-19] and also found by calculation [20]. The vapor-phase dissociation constant of BrCl varies little with the temperature, and is 0.11-0.12 in the 0-50° range; it follows that bromine chloride is approximately 40% dissociated in the vapor phase. Bromine chloride is more stable in aqueous solutions, including hydrochloric acid. According to Forbes and Fuoss [8], its dissociation constant in 4 N and 6 N HCl is $3.2 \cdot 10^{-4}$, i.e., it is only 1.8% dissociated. The stability of bromine chloride in solutions of chlorides may be attributed to the formation of the complex ion $BrCl_2'$, i.e., $BrCl \cdot Cl'$. It is known that compounds of the type $MeBrCl_2$, where Me is Rb or Cs, are more stable then compounds of the type $MeBr_2Cl$ [21].

Another consequence of complex-ion formation is the higher solubility of bromine chloride in chloride solutions, as compared with bromine and chlorine. This fact is utilized in a number of patents [22], where it is stated that the first portions of halogen mixtures distilled from chlorinated brines contain less chlorine than the subsequent portions; this is possible only if they contain not free chlorine but chlorine in the form of a compound with good solubility in chloride solutions.

The equilibrium constant for the reaction $2Br' + Cl_2 \rightleftharpoons Br_2 + 2Cl'$ can be calculated with great accuracy from the standard potentials of the chlorine and bromine electrodes. However, for calculations relating to the oxidation of bromide by chlorine in real conditions it is necessary to take into account the influence of the dissolved salts on the equilibrium, and also the formation of bromine chloride. The method for studying component distribution between immiscible phases, first used by A. A. Iakovkin for studies of halogen equilibria, can be used in this instance. For calculation of the equilibrium constant, it is convenient to refer the values of the

standard potentials to the same standard state, namely the gaseous state. It is then possible to determine the equilibrium concentrations of bromide and chloride ions in a salt solution from the vapor pressures of bromine and chlorine over the solution, with the use of the same value for the equilibrium constant, valid for any salt composition of the solution. To calculate the equilibrium concentrations of elemental bromine and chlorine in the liquid phase, the distribution coefficients of bromine and chlorine between the given solution and the gas phase must be determined experimentally. The purpose of the present investigation was to determine the distribution coefficients of bromine and chlorine between the gas phase and solution in the system $Br_2-Cl_2-NaCl-H_2O$, and to study equilibrium in solutions of bromine in sodium chloride.

EXPERIMENTAL

The vapor pressures over the solutions were determined by the dynamic method with the aid of an apparatus similar to that used by State Institute of Applied Chemistry [23].

The solutions were prepared as follows. A measured quantity of liquid bromine was dissolved in a sodium chloride solution of known concentration, acidified with hydrochloric acid to pH = 2.5. When all the bromine was dissolved, its concentration was determined by the iodometric method. Gaseous chlorine was then passed immediately through the solution, and total halogens were determined iodometrically after thorough mixing. The solution was immediately put into bubbling flasks, and a measured quantity of air was drawn through it at a low rate (4-5 liters/hour). The air then passed into absorption vessels where the free halogens were absorbed in alkaline sulfite solution. The absorption liquid was neutralized with nitric acid, and its bromine and chlorine contents were determined potentiometrically.

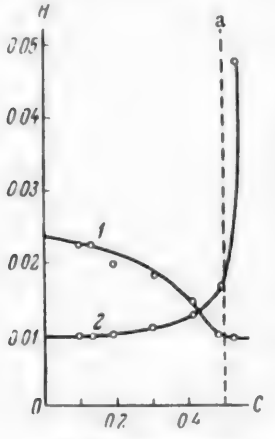

Fig. 1. Distribution coefficients of bromine (1) and chlorine (2) between the gas and liquid phases, for solutions of bromine and chlorine in 4 N sodium chloride at 0°. H) Distribution coefficient, C) $\frac{Cl_2}{Br_2 + Cl_2}$ ratio in the liquid phase, a) composition of the compound BrCl.

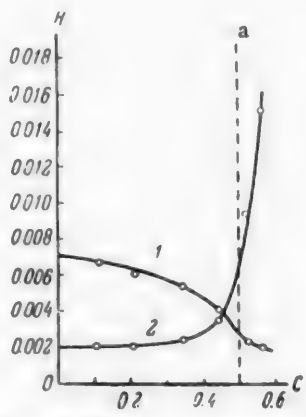

Fig. 2. Distribution coefficients of bromine (1) and chlorine (2) between the gas and liquid phases, for solutions of bromine and chlorine in 4 N sodium chloride at 25°. H) Distribution coefficient, C) $\frac{Cl_2}{Br_2 + Cl_2}$ ratio in the liquid phase, a) composition of the compound BrCl.

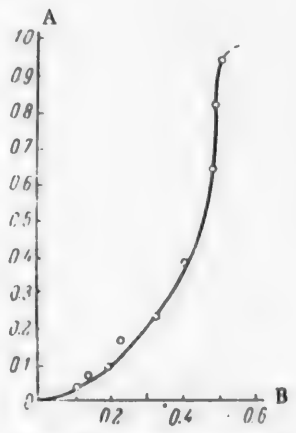

Fig. 3. Ratio of chlorine to total halogens in the equilibrium gas phase as a function of the corresponding ratio in the liquid phase, for solutions of bromine and chlorine in 4 N sodium chloride at 25°. A) $\frac{Cl_2}{Br_2 + Cl_2}$ ratio in the gas phase, B) the ratio in the liquid phase.

In calculations of the liquid phase composition the equilibrium Br^* concentration was calculated from the composition of the equilibrium gas phase and the equilibrium constant. The bromine chloride concentration in

the gas phase was taken into account only in calculations of the equilibrium. The determinations of the distribution coefficients were based on the total contents of elemental bromine and elemental chlorine in the liquid and gas phases (i.e., present both as Br_2 and Cl_2 molecules, and as BrCl).

The bromine and chlorine vapor pressures were determined for their solutions in 4 N sodium chloride at 0 and 25°, for bromine concentrations of 400, 800, and 1600 mg/liter, and for various bromine—chlorine ratios. The vapor pressures of bromine and chlorine were used to calculate their total distribution coefficients between the gas and liquid phases; the results are given in Figs. 1 and 2. The variation of the gas-phase composition with the liquid-phase composition is plotted in Fig. 3.

In addition, the composition of the equilibrium gas phase over solutions of bromine in sodium chloride solutions was studied. The gas phase was found to contain chlorine in every instance; the amount present and the equilibrium constant were used to calculate the equilibrium contents of Br' and Cl_2 in the solution, and the extent of the reverse reaction $Br_2 + 2Cl' \rightleftharpoons 2Br' + Cl_2$.

The results of these determinations are given in the table.

DISCUSSION OF RESULTS

It follows from Figs. 1 and 2 that the total bromine distribution coefficient gradually decreases with increasing chlorine content in the solution because part of the bromine is present as bromine chloride, which has a lower distribution coefficient than bromine. With low chlorine content of the solution, a considerable part of the chlorine is combined with bromine in the form of bromine chloride, and therefore on the left of the diagram the total chlorine distribution coefficient is equal to the distribution coefficient of bromine chloride.

The distribution coefficient of bromine chloride H_{BrCl} and of its dissociation products H_{Br_2} and H_{Cl_2}, and the equilibrium constants K_1 and K_2 for the two phases, are connected by the following relationship:

$$\frac{K_1}{K_2} = \frac{H_{Br_2} \cdot H_{Cl_2}}{H^2_{BrCl}}.$$

Assuming $K_1 = 0.11$ for the gas phase and $K_2 = 3.2 \cdot 10^{-4}$ for the solution, and taking the distribution coefficients of chlorine and bromine between the gas phase and 4 N hydrochloric acid solution as 0.33 and 0.0080 respectively,

TABLE

Composition of Bromine Solutions in Sodium Chloride Solutions, and Composition of the Equilibrium Gas Phase

Chloride concentration in solution (N)	Temperature (deg)	Bromine concentration (millimoles/liter)	Chlorine content (%) of total halogens)	
			in gas phase	in liquid phase
4.0 — NaCl	0	5.0	3.4	10.3
	20	5.0	5.0	14.7
	25	10.0	4.85	10.0
	25	5.0	7.55	12.9
	25	2.5	10.0	18.0
	25	1.0	18.0	22.0
	40	5.0	8.35	18.9
	40	2.5	12.0	24.7
	40	1.0	20.0	27.8
1.0 — NaCl	25	5.0	3.15	8.4
2.0 — NaCl	25	5.0	4.75	10.1
	25	2.5	6.75	14.75
5.2 — NaCl	25	5.0	11.35	16.8
4.0 — HCl	25	10.0	—	18.5
	25	1000	—	2.8
6.0 — HCl *	25	10.0	—	20.0
	25	1000	—	2.4

*Data of Forbes and Fuoss.

we have $H_{BrCl} = 0.0029$ and, consequently, $\frac{H_{BrCl}}{H_{Br_2}} = 0.36$ for this solution. The experimental value for sodium chloride solutions is $\frac{H_{BrCl}}{H_{Br_2}} = 0.30\text{-}0.40$.

With increase of the chlorine content in the system, an increasing proportion of it is present in the free state, and the total chlorine distribution coefficient gradually increases. On the right of the diagram, corresponding to excess chlorine, a considerable amount of the bromine is combined as bromine chloride, and its total distribution coefficient approaches that of bromine chloride. The distribution coefficient of chlorine in this part of the diagram is very much greater than that of bromine. The curves for the total distribution coefficients of chlorine and bromine intersect at a point to the left of the ordinate for the compound BrCl. Thus, the plot of the disbritution coefficient of bromine and chlorine in the system $Br_2-Cl_2-NaCl-H_2O$ fully confirms the formation of the compound BrCl in this system; this compound is more soluble than its components in chloride solutions, and is less dissociated in these solutions than in the gas phase.

The formation of the compound BrCl accounts for the incompleteness of the oxidation of bromide by chlorine. The standard potential of the chlorine electrode is -1.3594 v, and the standard potential of the bromine electrode (for the gaseous state) is -1.0824 v [24]. The equilibrium constant for the oxidation of bromide by chlorine, calculated from these potentials, is $2.2 \cdot 10^9$ at 25°. For this value of the equilibrium constant, the concentration of elemental chlorine needed for almost complete oxidation of bromide in concentrated chloride solutions is roughly 10^{-5} to 10^{-6} mole/liter. However, even such extremely low concentrations of free chlorine can exist in solution together with elemental bromine only in presence of considerable amounts of bromine chloride, which is dissociated to a very slight extent in aqueous chloride solutions. Therefore virtually all the chlorine which does not react with bromide is present in the solution as bromine chloride.

The compositions of the solutions, given in the table, obtained when bromine is dissolved in chloride solutions, correspond at equilibrium to the compositions of bromide solutions to which the stoichiometric quantities of chlorine had been added, and therefore the extent of the oxidation of bromide by chlorine can be determined from the data in the table.

It follows from the data in the table that the degree of oxidation of bromide decreases with increase of chloride concentration, decrease of bromide concentration, and increase of temperature.

SUMMARY

1. The distribution of bromine and chlorine between the gas phase and solution in the system $Br_2-Cl_2-NaCl-H_2O$ was studied, and it was shown that the compound BrCl is formed in this system; this compound is dissociated more in the gas phase than in solution, and is more soluble than chlorine or bromine in chloride solutions.

2. Investigations of equilibrium in the reaction $2Br' + Cl_2 \rightleftharpoons Br_2 + 2Cl'$ in concentrated chloride solutions showed that this reaction does not go to completion owing to the formation of the compound BrCl, and the establishment of equilibrium between Br_2, BrCl, Cl_2, Br' and Cl'.

LITERATURE CITED

[1] M. E. Pozin, Technology of Mineral Salts (Goskhimizdat, 1949).*

[2] F. Ephraim, Inorganic Chemistry, 1 (Goskhimizdat, 1932), p. 178 [Russian translation].

[3] A. L. Potyllitsyn, J. Russ. Phys.-Chem. Soc. 6, 275 (1874); 8, 195 (1876); 11, 413 (1879); 13, 428 (1881); 14, 82 (1882).

[4] D. I. Mendeleev, Principles of Chemistry, 13th edition (Goskhimizdat, 1947), pp. 345, 616.*

[5] K. Jellineck and H. Schutza, Z. anorg. Chem., 227, 52 (1936).

[6] H. Schutza, Z. anorg. Chem., 239, 245 (1938).

[7] V. P. Khromova, Author's summary of Dissertation (Tomsk Univ., 1955).*

[8] G. S. Forbes and R. H. Fuoss, J. Am. Chem. Soc., 49, 142 (1927).*

*In Russian.

[9] B. J. Karsten, Z. anorg. Chem., 53, 367 (1907).

[10] L. T. Gray and J. W. Style, Proc. Roy. Soc., A122, 1910 (1930).

[11] W. Jost, Z. Phys. Ch., B14, 314 (1931).

[12] Ch. M. Blair and D. M. Jost, J. Am. Chem. Soc., 55, 4489 (1933).

[13] H. G. Vesper and G. K. Rollefson, J. Am. Chem. Soc., 56, 620 (1934).

[14] G. Brauer and E. Victor, Z. Elecktroch., 41, 508 (1935).

[15] C. M. Beeson and D. M. Jost, J. Am. Chem. Soc., 61, 1431 (1939).

[16] N. N. Greenwood, Reviews of Pure and Applied Chem., 1, 84 (1951); Progr. Chem. 22, 445 (1953).

[17] S. L. Lilich, J. Gen. Chem. 22, 730 (1952).*

[18] A. J. Popov and J. J. Mannion, J. Am. Chem. Soc., 74, 222 (1952).

[19] H. C. Mattraw, C. F. Pachucki and N. J. Hawkins, J. Chem. Phys., 22, 1117 (1954).

[20] K. V. Butkov, J. Gen. Chem. 23, 232 (1949).*

[21] Gmelins Handbuch der Anorg. Chemie, 7, 279, Brom.

[22] H. M. Dow, U. S. Patent 752331, 752332 (1903).

[23] G. S. Klebanov, E. P. Basova, I. M. Gurevich and E. M. Volnianskaia, Coll. Trans. State Inst, Appl. Chem. 40, 119 (1948). **

[24] Physicochemical Data, Technical Encyclopedia 10.**

Received September 1, 1956

*Original Russian pagination. See C.B. translation.

**In Russian.

CALCULATION OF MASS-TRANSFER PROCESSES

V. V. Kafarov

The searches for the most effective methods for the utilization of diffusion equipment, carried out during recent years, have greatly influenced the origins and development of new concepts of the nature and mechanism of mass-transfer processes, and have assisted in the broadening and deepening of these concepts.

Observations of diffusion processes in intensified conditions confirmed that analysis of continuous diffusion processes in the light of the Lewis–Whitman film theory is not valid.

The following principal theories of mass transfer, characteristic of recent investigations, may be formulated.

Higbie's penetration theory [1], based on the concept of nonequilibrium diffusion into a stationary film. According to Higbie, the penetration time τ of a substance with molecular-diffusion coefficient D and mass-transfer coefficient k are connected by the equation

$$k = \left(\frac{D}{\pi\tau}\right)^{\frac{1}{2}}. \tag{1}$$

For a two-phase system, with diffusion from one phase to the other, it follows from Higbie's theory that

$$k_1 = \left(\frac{D_1}{\pi\tau}\right)^{\frac{1}{2}} \text{and } k_2 = \left(\frac{D_2}{\pi\tau}\right)^{\frac{1}{2}}. \tag{2}$$

It is clear from these equations that the ratio k_1/k_2 is independent of time. By Higbie's theory the concentrations at the interphase boundary are also independent of time, and therefore remain constant throughout the diffusion process.

Modified penetration theory, the Danckwerts theory [2].

In 1951 Danckwerts modified Higbie's theory by introducing the factor of surface renewal. If the average rate of formation of fresh surface per unit contact area is constant, and is equal to f (in $m^2/m^2 \cdot$ second), if the change of a surface element renewed in a given time interval is assumed to be independent of its age, and the rate of absorption into the fresh surface is given by Higbie's equation, then

$$k = \sqrt{D \cdot f}. \tag{3}$$

The fact that k in this equation is proportional to the square root of the diffusion coefficient is a direct consequence of Danckwerts's assumption based on Higbie's theory. We must agree with Potter [3] in his criticism of Equation (3), that Danckwerts did not give an equation or method for determination of the surface-renewal factor f, and this fact invalidates Danckwerts's concepts as a theory of mass transfer. Moreover, Potter correctly points out that f cannot be found without a detailed knowledge of the hydrodynamics of the system, while if the hydrodynamics of the system is known in detail there is no need for the Danckwerts theory.

Kishenevskii's theory [4]. The difference between Kishenevskii's and Danckwerts' theories lies in the fact that instead of the molecular-diffusion coefficient D, the effective diffusion coefficient D' is considered; this is the sum of the molecular-diffusion coefficient D and the turbulent-diffusion coefficient ϵ_d, i.e., $D' = D + \epsilon_d$. This gives the following expression for k:

$$k = \sqrt{D' \cdot f}, \tag{4}$$

Potter's boundary-layer theory [3]. In a recent paper, Potter considers the hydrodynamic state of the boundary layer and the velocity distribution which arises as the result of the relative motion of unidirectional streams. Even under these limited conditions the powers of the Prandtl number (and, correspondingly, of the coefficient of molecular diffusion) do not remain constant out depend on the ratio L/G of the stream velocities, varying between 1/3 and 0.5.

The mass-transfer coefficient depends on the dimensionless ratios $\frac{L}{G}\frac{\gamma_2\mu_2}{\gamma_1\mu_1}$; the consequences of the existence of a two-phase flow are thereby taken more fully into account.

With the relative motion of the streams taken into account, Potter derived an equation of the following form:

$$\frac{kl}{D}=\left(\frac{wl}{\nu}\right)^{0.5}\cdot\left(\frac{\nu}{D}\right)^{n}\psi\left(\frac{L}{G},\ \frac{\mu_2\gamma_2}{\mu_1\gamma_1}\right). \tag{5}$$

Fundamental Principles of Mass Transfer Based on the Concepts of Free Turbulence or Emulsification

For explanation of mass-transfer processes in forced systems, we use the concepts of developed free turbulence or emulsification, the essential meaning of which is as follows.

Free surface. A free surface is taken to be a surface at the boundary between moving phase streams (gas–liquid, vapor–liquid, liquid–liquid). A free surface differs in its nature from a surface at a solid boundary (wall) as the latter causes extinction of turbulent pulsations, whereas a free surface can itself be a source of turbulence. Under definite hydrodynamic conditions a free surface is characterized by intensive renewal.

Turbulence in presence of free surfaces ("free turbulence"). This concept includes turbulence arising in the presence of gas–liquid, vapor–liquid, and liquid–liquid interfaces; the possibility of different hydrodynamic regimes within the limits of each phase is not excluded. The term "free turbulence," as applied to two-phase flow, is consistent in meaning with its classical definition,* since we assume that the nature of an interphase boundary cannot be identified with the nature of a solid fixed boundary restricting the development of turbulence; moreover, the vortices formed are very small.

Developed free turbulence – emulsification. The development of turbulence within each of the phases may result in the interface being drawn into the turbulent pulsations. In such cases the concept of dispersed and continuous phases becomes meaningless, as the phases undergo continuous inversion, becoming either continuous or dispersed and are permeated by innumerable minute vortices, so that the interface is continuously renewed.

A hydrodynamically stable "emulsified" liquid system is formed under these conditions: gas vortices, continuously forming and moving, penetrate into the eddying liquid, in which liquid vortices are also continuously forming and moving. The direction of vortex motion corresponds to the direction of action of the Zhukovskii force. The interphase boundary becomes unstable and continuously changing.

A continuously altering dynamic state of the interface and of the phases themselves is characteristic of the existence of developed free turbulence.

The dynamic surface change factor f can be represented as

$$f=\frac{\Delta p_{g\text{-}l}-\Delta p_g}{\Delta p_g}, \tag{6}$$

where Δp_{g-l} is the pressure drop in a two-phase stream, and Δp_g is the pressure drop in a one-phase stream of the same velocity.

On the basis of an earlier analysis [6], the pressure drop Δp_{g-l} in a two-phase stream can be represented as

$$\Delta p_{g\text{-}l}=\Delta p_g\left[1+A\left(\frac{L}{G}\right)^{m}\cdot\left(\frac{\gamma_g}{\gamma_l}\right)^{n}\cdot\left(\frac{\mu_l}{\mu_g}\right)^{q}\right]. \tag{7}$$

* In classical hydrodynamics [5] free turbulence is taken to mean turbulent flow unrestricted by any walls. In this concept, free turbulence arises in presence of free streams of unidirectional flow.

Substitution of Equation (7) into (6) and transformation gives the following expression for the dynamic surface change factor:

$$f = A\left(\frac{L}{G}\right)^{m}\cdot\left(\frac{\gamma_g}{\gamma_l}\right)^{n}\cdot\left(\frac{\mu_l}{\mu_g}\right)^{q}. \tag{8}$$

The constants A, m, n, and q in Equation (8) can be found from Equations (7) and (8) for given hydrodynamic conditions in the equipment under consideration. The dynamic surface change factor is the factor by which mass transfer is increased in interaction of two-phase streams relative to transfer in a one-phase stream of the same velocity. This increase is the consequence of the development and renewal of the contact surface. Therefore, if transfer in a one-phase stream can be calculated, the factor f can be used to find the transfer in a two-phase stream. Turbulent transfer becomes the predominant transfer mechanism with increase of f.

In view of the fact that the nature of the changes of energy and mass transfer remains the same in conditions of developed free turbulence [7], the factor f is a universal value for quantitative evaluation of diffusion processes.

If the flow has relatively little influence on mass transfer, the following equations are valid:

$$\frac{k_g d_e}{D} = B\left(\frac{w_g d_e}{\nu_g}\right)^{a}\cdot\left(\frac{\nu_g}{D_g}\right)^{b}, \tag{9}$$

$$\frac{k_l d_e}{D_l} = B_1\left(\frac{w_l d_e}{\nu_l}\right)^{a_1}\cdot\left(\frac{\nu_l}{D_l}\right)^{b_1}. \tag{10}$$

At high flow rates, when the influence of hydrodynamic interaction of the streams on transfer cannot be ignored, the dynamic surface change factor f must be introduced into Equations (9) and (10). We then have the following equations

$$\frac{k_g d_e}{D_g} = B_2\left(\frac{w_g d_e}{\nu_g}\right)^{a_2}\cdot\left(\frac{\nu_g}{D_g}\right)^{b_2}\cdot(1+f), \tag{11}$$

$$\frac{k_l d_e}{D_l} = B_3\left(\frac{w_l d_e}{\nu_l}\right)^{a_3}\cdot\left(\frac{\nu_l}{D_l}\right)^{b_3}\cdot(1+f). \tag{12}$$

Putting the value of f from Equation (8) into these equations, we have the mass-transfer equations in general form:

$$\frac{k_g d_e}{D_g} = B_2\left(\frac{w_g d_e}{\nu_g}\right)^{a_2}\cdot\left(\frac{\nu_g}{D_g}\right)^{b_2}\left[1+\left(\frac{L}{G}\right)^{m}\cdot\left(\frac{\gamma_g}{\gamma_l}\right)^{n}\left(\frac{\mu_l}{\mu_g}\right)^{q}\right], \tag{13}$$

$$\frac{k_l d_e}{D_l} = B_3\left(\frac{w_l d_e}{\nu_l}\right)^{a_3}\cdot\left(\frac{\nu_l}{D_l}\right)^{b_3}\left[1+\left(\frac{L}{G}\right)^{m}\cdot\left(\frac{\gamma_g}{\gamma_l}\right)^{n}\left(\frac{\mu_l}{\mu_g}\right)^{q}\right]. \tag{14}$$

Equations of the form of (13) and (14) were derived by us for packed columns [8]. The mass-transfer equations recently obtained by Potter [3] by hydrodynamic analysis of effects at the boundary in unidirectional two-phase streams are analogous to Equations (13) and (14). Since Potter obtained analogous equations under hydrodynamic conditions different from those considered here, it may be assumed that Equations (13) and (14) are fairly general in relation to two-phase streams. The indices a and b may have different values according to the hydrodynamic conditions in the apparatus [7].

In our opinion, the reason why no general equations for calculation of mass-transfer coefficients in relation to diffusion equipment design are available at this time is that mass-transfer coefficients are usually determined without consideration of the factor f, which determines hydrodynamic similarity in two-phase systems. In our view, reliable generalizations can be obtained only for the same values of the constants A, m, n, and q in Equation (8). In this sense, the dynamic surface change factor f may be regarded as the criterion of hydrodynamic similarity of two-phase systems.

Equations (13) and (14) can be simplified for values of f considerably greater than unity, corresponding to developed free turbulence or emulsification. In such cases the ratios in Equation (8) are the determining quantities, and the index of the molecular-viscosity term $q \rightarrow 0$.

Thus, the onset of developed free turbulence in packed columns is characterized by an inversion point at which the dynamic surface change factor is*

$$f = 5.9\left(\frac{L}{G}\right)^{0.337} \cdot \left(\frac{\gamma_g}{\gamma_l}\right)^{0.187} \cdot \left(\frac{\mu_l}{\mu_g}\right)^{0.0375}. \quad (15)$$

Accordingly, Equation (15) can be used for determination of the absorption coefficients of difficultly and easily soluble gases in packed towers at the inversion point.

In diffusion-equipment design calculations, the parameters usually determined are the resultant linear flow velocity $\underline{w}$, from which the cross section of the apparatus, the geometry of which is characterized by the equivalent diameter d_e, is calculated; and the length $\underline{h}$ of the phase-contact zone. These parameters may be included in dimensionless ratios of the following form:

for the velocity, $\frac{w}{\sqrt{gd_e}}$, for the contact zone, h/d_e.

Then, if the influence of the factor $\underline{f}$ is determining, the quantitative characteristics of mass-transfer processes can be found from the relationships:

$$\frac{w}{\sqrt{gd_e}} = \psi\left(\frac{L}{G}, \frac{\gamma_g}{\gamma_l}, \frac{\mu_l}{\mu_g}\right). \quad (16)$$

$$h/de = \psi_0\left(\frac{L}{G}, \frac{\gamma_g}{\gamma_l}, \frac{\mu_l}{\mu_g}\right). \quad (17)$$

Various authors have now evaluated the Relationship (16) for different types of diffusion apparatus operating at maximum rates, corresponding to developed free turbulence. Thus, for packed columns (for absorption, rectification, and extraction) [10, 11], we have

$$\varphi\left(\frac{w^2\sigma}{gF_c^3} \cdot \frac{\gamma_g}{\gamma_l} \cdot \left[\frac{\mu_l}{\mu_w}\right]^{0.16}\right) = A_0 - 1.75\left(\frac{L}{G}\right)^{1/4} \cdot \left(\frac{\gamma_g}{\gamma_l}\right)^{1/8}. \quad (18)$$

The values of A_0 for absorption, rectification, and extraction columns are different. A generalized equation for all types of packed columns has also been derived [12].

For wetted-wall rectification columns [13]

$$\log\left(\frac{w^2}{gd} \cdot \frac{\gamma_v}{\gamma_l} \cdot \mu_l^{0.16}\right) = -0.243 - 1.75\left(\frac{L}{G}\right)^{1/4}\left(\frac{\gamma_v}{\gamma_l}\right)^{1/8} \quad (19)$$

For sieve-plate rectification columns [14]

$$\log\left(\frac{w^2}{gF_c^2 d} \cdot \frac{\gamma_v}{\gamma_l} \cdot \mu_l^{0.20}\right) = -3.23 - 1.75\left(\frac{L}{G}\right)^{1/4}\left(\frac{\gamma_v}{\gamma_l}\right)^{1/8}. \quad (20)$$

In packed absorption, rectification, and extraction columns the maximum separating power is attained under emulsification conditions, with minimum values for the equivalent packing height (HTU), determined, in accordance with Equations (16) and (17), from the relationship [15]

$$\frac{h_e}{d_e} = 24\left(\frac{w}{\sqrt{gd_e}}\right)^{-0.4} \quad (21)$$

SUMMARY

1. General equations have been derived for mass transfer in two-phase streams, with hydrodynamic interaction of the phase streams taken into account.

2. The concepts of developed free turbulence or emulsification were used to introduce the concept of the dynamic surface change factor, which characterizes the similarity of two-phase systems.

*On the basis of an earlier investigation [9], what is generally described as the ratio of the phase-contact area S_p and the geometric area S_g is more correctly regarded as the dynamic surface change factor $\underline{f}$ rather than an area ratio.

3. Experimental data available in the literature were analyzed and it was shown that these considerations are valid in design calculations of diffusion equipment.

LITERATURE CITED

[1] R. Higbie, Tr. Am. Inst. Chem. Eng., 31, 365 (1935).

[2] P. V. Danckwerts, Ind. Eng. Ch., 43, 1460 (1951).

[3] O. E. Potter, Chem. Eng. Sci., 6, 170 (1957).

[4] M. Kh. Kishenevskii, J. Appl. Chem. 22, 1173, 1183 (1948); 24, 413, 542 (1951); 28, 9 (1955).*

[5] H. Schlichting, Boundary Layer Theory (IL, 1956) [Russian translation].

[6] V. V. Kafarov, J. Chem. Ind. 6 (1948).

[7] V. V. Kafarov, J. Appl. Chem. 28, 1234 (1955).*

[8] V. V. Kafarov, Trans. MKhTI. 22, 232 (1956).

[9] V. V. Kafarov and V. I. Trofimov, J. Appl. Chem. 30, 211 (1957).*

[10] W. A. Bain and O. A. Hougen, Tr. Am. Inst. Chem. Eng., 40, 29 (1944).

[11] V. V. Kafarov, J. Chem. Ind. 5 (1953).

[12] V. V. Kafarov and Iu. I. Dytnerskii, J. Appl. Chem. 30, 1698 (1957).*

[13] A. P. Nikolaev, Dissertation, A. I. Mikoian Tech. Inst. Food Ind. (Kiev, 1957).**

[14] M. Cervinka and O. Cerny, Chemicky Prumysl, 6, 232 (1955).

[15] V. V. Kafarov and Iu. I. Dytnerskii, Trans. MKhTI 23, 165 (1956).

Received May 23, 1957

*Original Russian pagination. See C.B. translation.

**In Russian.

MASS TRANSFER IN DISTILLATION IN WETTED-WALL COLUMNS

A. P. Nikolaev

The available data on distillation in single tubes and multitube wetted-wall columns suggest that tubular columns, being very simple in design can in some cases be more effective and convenient in use than other types of distillation equipment, as they are of small dimensions and weight, have low hydraulic resistance, and can be operated at high mass-transfer coefficients with high vapor velocities in the tubes.

Tube columns are convenient for distillation in relation to studies of mass transfer, as the phase contact area in them can be exactly determined. However, although there have been numerous investigations of distillation and rectification in wetted-wall tube columns [1-14], many aspects of these questions require much further study. Some of the most interesting mass-transfer problems, such as the influence of the hydrodynamic conditions of the phase motion on the mass-transfer coefficients, and the applicability of the Lewis–Whitman film theory to wetted-wall rectification processes, were studied most fully in packed columns [15, 16]. There is as yet no agreed view concerning the influence of relative tube length (l/d) on the separation efficiency. The tubes used in experimental studies were mostly not less than 20 mm in diameter, whereas tubes of smaller diameters, and of higher specific surface, are more effective.

Of the equations which have been proposed for calculation of mass-transfer coefficients in film rectification under conditions of turbulent vapor flow, only the Johnson–Pickford and Aksel'rod equations [1, 2] give similar values. These equations differ little from each other, and are represented by straight lines, one being almost a continuation of the other, on the $HTU/d = f(Re_V)$* graph. These equations are valid for Reynolds numbers from 900 to 25,000. Calculations by the Surovis and Furnas equations (Reynolds numbers from 5,000 to 15,000) give much high mass-transfer coefficients than the values given by the Johnson and Aksel'rod equations. One probable reason for this discrepancy is the fact that Surovis used a relatively short tube ($l/d = 11.87$, as compared with $l/d = 60.5$ and 73.0 in Johnson's and Aksel'rods experiments). None of these equations contains a term which takes l/d into account. The reports in the literature that the relative length has no appreciable influence on the separation [12] are probably valid for a restricted range of l/d values, as according to Surovis, Berman [3], and the results of the present investigation l/d often has a considerable influence on mass transfer in tubes, even if the relative tube length is fairly large.

The equations derived analytically by Westhaver [14] and by Maliusov [8] are in good agreement with experimental data, but do not cover the region of laminar vapor flow, where the mass-transfer coefficients are very small.

The equation recommended by Natradze [9] is difficult to apply in practice, as it contains two unknowns, Nu' and S, the number of transfer units (or Nu' and L, the tube length for a given S), and can only be solved by successive approximations.

The paper by Fastovskii and Petrovskii [13] contains experimental data which confirm that the results derived from hydrodynamic similarity are applicable to wetted-wall tube distillation. However, design calculations based on such reasoning are possible only if data are available on the influence of a liquid film present in tubes on the coefficient of friction.

---

*HTU is the height of a transfer unit, d is the internal tube diameter, and Re_V is the Reynolds number for the vapor.

Therefore the existing data on wetted-wall tube distillation are not exhaustive. Further determinations and generalizations are needed.

This paper contains the results obtained in distillation of ethyl alcohol–water mixture in tubes of different diameters and relative lengths, over a wide range of Reynolds numbers and reflux ratios. The possibility of increasing the separation efficiency by the creation of artificial turbulence in the tubes was also investigated.

EXPERIMENTAL

Film distillation. The apparatus used is shown schematically in Fig. 1. The distillation was performed through brass tubes 8, 12, 16 and 20 mm in internal diameter, with l/d ratios of 278, 185, 138, and 111.3 respectively. The lower ends of the tubes were widened (Fig. 1) to prevent entrainment of liquid droplets in the vapor stream. The tubes were fitted with heated insulating jackets. The temperature of the jacket walls was maintained equal to the vapor temperature in the tubes, to prevent reflux at the result of cooling of the outer tube surfaces.

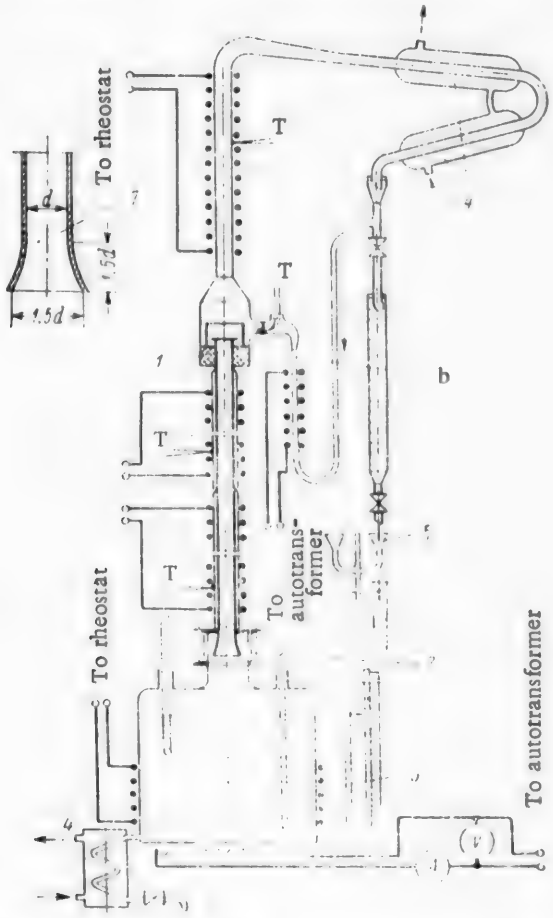

Fig. 1. Experimental unit. 1) Interchangeable tube; 2) inspection head; 3) still; 4) condenser; 5) circulation tube; 6) reflux heater; 7) lower end of tube; T) hot junctions of thermocouples.

The following quantities were determined: the concentration of liquid in the still; of the vapor at the tube exit; the evaporation rate in the still, the amount of distillate; the temperature of the residue; and the pressure in the still. The vapor velocity in the tube and the reflux ratio were found by calculation. The separation efficiency of the tubes was expressed in terms of transfer units determined by graphical integration, or in terms of the Nusselt diffusion criterion Nu'. In analysis of the experimental data the physical parameters of the vapor and liquid in the tubes were based on their concentrations in the median section of the tube.

The distillation results revealed the characteristic variations of mass-transfer efficiency in tubes with changes in the vapor flow conditions, and demonstrated the significant influence of relative tube length on mass transfer. The analogy between mass and energy transfer in flow was confirmed. It was also shown that the tubes may be operated under conditions similar to free-emulsification conditions in packed columns.

The experimental data are plotted in Fig. 2; it is seen that the character of the $HTU/d = f(Re_V)$ curves, and therefore the character of mass transfer, for tubes 8 and 12 mm in internal diameter and with relative lengths $l/d = 278$ and 185, changes sharply as the vapor flow changes from laminar to transitional and from transitional to turbulent. In the laminar region, these curves coincide with the lines given by Maliusov's equation [8], and in the turbulent region, with the line for Aksel'rod's equation [2]. The boundaries between the regions become less distinct with decrease of l/d, probably because of the influence of the conditions of entry. The less the relative length of the tube, the greater is the length to which the disturbances arising at the entry extend into the tube, and the sooner (i.e., at lower values of Re_V) does the transition regime replace the laminar, and turbulence succeed transition. The influence of the entry conditions is naturally most prominent in the laminar and transition regimes. As Aksel'rod used a relatively short tube ($l/d = 73$), as compared with the tubes used in this investigation,

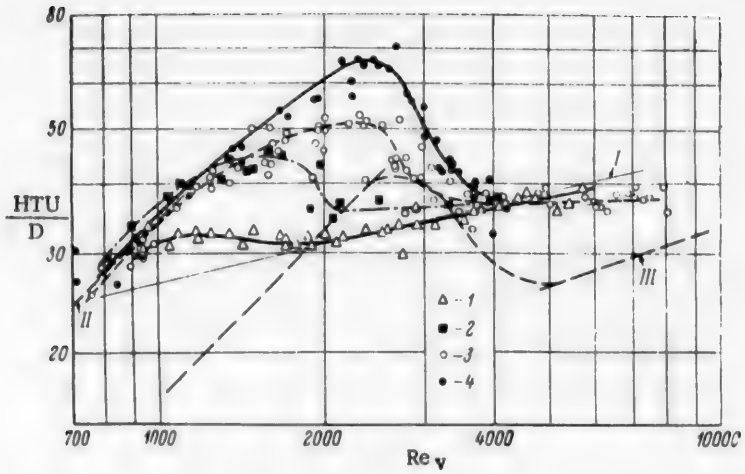

Fig. 2. Variation of HTU/d with Re_V in distillation in tubes under film conditions. Curves corresponding to equations: I) of Aksel'rod, II) of Maliusov, III) $1/\lambda = f(Re)$. Tube diameters (mm): 1) 20; 2) 16; 3) 12; 4) 8.

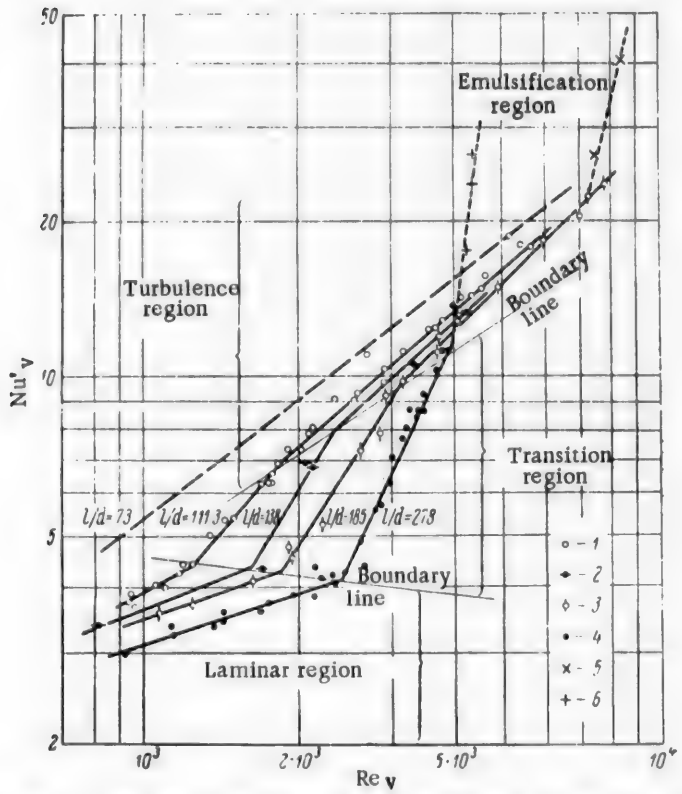

Fig. 3. Variation of Nu'_V with Re_V in distillation in tubes under film and emulsification conditions. Film conditions, tube diameters (mm): 1) 20; 2) 16; 3) 12; 4) 8. Emulsification conditions, tube diameters (mm): 5) 12; 6) 8. The dash line corresponds to Aksel'rod's equation.

he obtained minimum values for HTU/d at low Reynolds numbers. It is likely that with even shorter tubes the HTU/d = f(Re_V) relationship should be represented by straight lines (Fig. 2), which would be situated lower at lower l/d values.

When the experimental results are plotted in Nu' = f(Re_V) coordinates (Fig. 3), the boundaries between the regions representing different conditions of vapor flow in the tubes, and the influence of l/d on the separation efficiency of the tubes, are revealed no less clearly. Berman [3] reported a similar dependence of Nu' on Re_V and l/d in mass transfer in wetted-wall apparatus with vertical canals.

The points of transition between the different regions, for tubes with different l/d ratios, can be found from the equations for the lines joining these points. The boundary line between the laminar and transition region is represented by the equation

$$Nu'_V = 11.78 \cdot Re_V^{-0.135}. \quad (1)$$

The boundary between the transition and turbulence regions is found from the equation

$$Nu'_V = 4.7 \cdot 10^{-2} \cdot Re_V^{0.68}. \quad (2)$$

Because the variations of the Nusselt criterion with Re_V and l/d differ in different conditions of vapor flow, different criterial equations must be used for calculations in these regions:

a) laminar region

$$Nu'_V = 1.503 \cdot Re_V^{0.4} \cdot Pr_V'^{0.33} \cdot (d/l)^{0.324}, \quad (3)$$

b) transition region

$$Nu'_V = 0.692 \cdot 10^{-2} \cdot Re_V^{1.4} \cdot Pr_V'^{0.33} \cdot (d/l)^{0.722}, \quad (4)$$

c) turbulence region

$$Nu'_V = 0.283 \cdot 10^{-2} \cdot Re_V^{0.83} \cdot Pr_V'^{0.63} \cdot (d/l)^{0.1}. \quad (5)$$

In calculations by means of Equations (3-5), the validity of the chosen equation is checked by the values of Nu' found from the boundary-line Equations (1) and (2). For example, the value of Nu'_4 found from Equation (4) for the transition region should lie between the values of Nu'_1 and Nu'_2 found from Equations (1) and (2). If the value of Nu lies outside this range, either Equation (3) or Equation (5) must be used.

It is noteworthy that the curves obtained (Fig. 2) approximate in form to the $1/\lambda = f(Re)$ curve, where λ is the coefficient of friction in the tubes. This resemblance can be explained on considerations of hydrodynamic similarity.

When a liquid or gas moves through a tube, in absence of local resistances, the total thought H is expended to give the kinetic energy ($w^2/2g$) and to overcome the friction in the tube ($\zeta w^2/2g$), i.e.,

$$H = \frac{w^2}{2g} + \zeta \frac{w^2}{2g}.$$

The quantity ζ is usually expressed in the form $\zeta = f(Re)\, l/d$, where $f(Re) = \lambda$, the coefficient of friction, or the fraction of the kinetic energy expended in overcoming friction per unit tube length and per unit reciprocal diameter ($1/d$).

The reciprocal of the coefficient of friction may be written in the form

$$1/\lambda = \frac{l}{\zeta} \cdot \frac{1}{d}. \quad (6)$$

In this equation the ratio l/ζ represents the length of tube in which equal fractions of the total thrust H are expended to overcome friction and to create kinetic energy. If this fraction of the total thrust is taken as unity, the tube length l/ζ may be termed the length equivalent to unit energy transfer (LETU). Hence Equation (6) may be written

$$\frac{1}{\lambda} = \text{LETU}/d$$

This interpretation of the physical meaning of $1/\lambda$ explains the relationship between $1/\lambda$ and LETU/d, and the similarity between the LETU/d = f(Re) and HTU/d = $f(Re_V)$ curves is easily explained, since, by hydrodynamic analogy, an energy-transfer unit in flow should correspond to a definite number of mass-transfer units.

In view of the fact that λ is usually determined for long tubes, where the influence of the entry conditions is weak, the similarity between the curves in question should be most complete when the HTU values are determined in distillation through tubes with high l/d ratios; this is confirmed by comparison of the curves. The curve for the tube 8 mm in diameter (l/d = 278) is nearest in form to the $1/\lambda = f(Re)$ curve.

The fact that the curves coincide in form in the laminar region is not contrary to the fundamental principle of hydrodynamic similarity, as in this case the molecular coefficients of energy (motion) and mass transfer in the vapor stream are quantities of the same order (Pr_V is close to unity).

Distillation in tubes with turbulence baffles. The experimental results showed that distillation with free turbulence in the vapor stream is the most effective with regard to mass transfer. Special inserts in the form of wire and ribbon spirals were fitted into the pipes to increase the turbulence artifically. In contrast to similar inserts used previously in laboratory practice, the spirals were intended to influence only the vapor stream, and were not wetted by the liquid, so that the liquid retention in the tubes remained low, and the critical vapor velocities corresponding to the start of flooding could be kept high.

Ribbon spirals (Fig. 4) proved to be the most effective; with their use the mass-transfer coefficients in the tubes were increased by up to 300% over the coefficients for the empty tubes. The values of HTU ranged from 10 to 20 tube diameters for vapor velocities from 0.5 to 5.5 m/second respectively (Fig. 4).

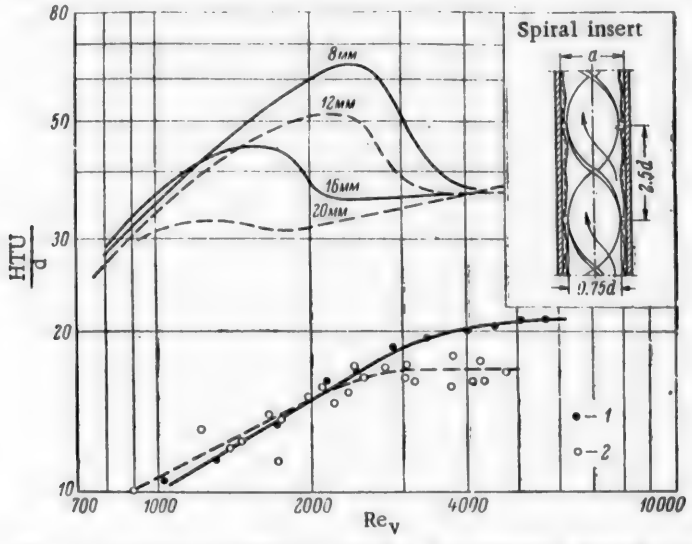

Fig. 4. Variation of HTU/d with Re_V in distillation through tubes with turbulence inserts. Tube diameters (mm): 1) 20; 2) 12.

The resistances to the vapor in the tubes remained very low in the presence of the spirals, although they increased in proportion to the mass-transfer coefficients. The maximum pressure drop per 1 m tube length, for a tube 20 mm in diameter did not exceed 12-15 mm water column, and for tubes 12 mm in diameter did not exceed 15-17 mm water column. In tubes of the same diameter without inserts the pressure drop did not exceed 4-6 mm water column per 1 m tube length.

Distillation under emulsification conditions. It was found by visual observations that distillation through tubes can proceed under emulsification conditions, similar to free emulsification in packed columns. At a definite vapor velocity, somewhat below the flooding velocity, a plug consisting of an emulsion of the vapor in the liquid begins to form in the tube near its lower edge. The emulsion gradually fills the whole tube. The level of the emulsion can be raised to any height of the tube and maintained there as long as required by regulation of the vapor rate.

Stable emulsification could also be maintained in a unit consisting of 3 tubes of 7 mm internal diameter, and in a multitube column of 19 tubes, 12 mm in diameter.

The commencement of the emulsification regime is marked by a sharp increase of the hydraulic resistance of the tubes to the vapor, and an increase of the distillation efficiency. The mass-transfer coefficients in tubes 8 and 12 mm in diameter, operated under emulsification conditions, were 1.5-2 times the values obtained under film conditions in tubes without inserts (Fig. 3). The pressure drop reached 35-55 mm water column per 1 m of tube length.

To determine the vapor velocity at which stable emulsification begins in a tube with a widened opening (Fig. 1), Equation (7) was derived; this is similar to the equations proposed for determination of the phase-inversion point in sprayed tubes and packed columns:

$$\lg\left(\frac{w^2}{Dg}\frac{\gamma_v}{\gamma_l}\mu_l^{0.16}\right) = 0.243 - 1.75\left(\frac{R}{R+1}\right)^{0.25}\left(\frac{\gamma_v}{\gamma_l}\right)^{0.125}. \qquad (7)$$

where w is the average vapor velocity in the tube (m/second); γ_v, γ_l are the vapor and liquid densities (in kg/m^3), μ_l is the viscosity of the liquid (in centipoises), R is the reflux ratio, g is the acceleration due to gravity (in m/second^2), and d is the internal tube diameter (in m).

SUMMARY

1. Film distillation in tubes, for tube l/d ratios exceeding 100, is characterized by three distinct regions of vapor flow: laminar, transitional, and turbulent. The boundaries between the regions become more distinct with increase of l/d.

A different relationship between the mass-transfer coefficient and the Reynolds number is valid in each of these regions.

The l/d ratio influences the positions of the boundaries between the regions, and the mass-transfer coefficients. This influence is especially prominent in the laminar and transitional regions.

Equations (3-5) are recommended for determination of mass-transfer coefficients for Reynolds numbers between 800 and 10,000 and for l/d between 100 and 300.

2. Artificially induced turbulence in the vapor stream, created by means of spiral inserts in the tubes, makes it possible to increase the mass-transfer coefficients 2 to 3-fold above the values for tubes without inserts.

3. Tubes can be operated stably under emulsification conditions, when the efficiency is high. Equation (7) is proposed for determination of stable emulsification conditions.

LITERATURE CITED

[1] L. S. Aksel'rod, Dissertation, MiKhM (Moscow, 1947).*

[2] L. S. Aksel'rod and V. I. Matrosov, J. Chem. Ind. 8 (1952).

[3] L. D. Berman, Heat and Power Engineering 6 (1954).

[4] N. I. Gel'perin and M. S. Khatsenko, Oxygen, 6 (1951).

[5] E. Jackson, Ind. Eng. Chem. 42, 6 (1950).

[6] N. G. Krokhin and N. N. Zelenetskii, Trans. Sci. Res. Inst. Synthetic and Natural Perfumes, 2 (1954).

[7] E. E. Lindsey, Y. M. Kiefer and C. L. Huffine, Ind. Eng. Chem. 44, 1 (1952).

[8] V. A. Maliusov, N. N. Umnik and N. M. Zhavoronkov, Proc. Acad. Sci. USSR 105, 4 (1955).

[9] A. G. Natradze, J. Appl. Chem. 27, 6 (1954).**

[10] A. P. Nikolaev, Dissertation, Kiev Tech. Inst. Food Ind. (Kiev, 1956).*

[11] A. Rose, Ind. Eng. Chem. 28, 10 (1936).

[12] I. P. Usiukin and L. S. Aksel'rod, Oxygen 3 (1952).

*In Russian.

**Original Russian pagination. See C.B. translation.

[13] V. G. Fastovskii and Iu. V. Petrovskii, J. Chem. Ind. 4 (1956).

[14] I. W. Westhaver, Ind. Eng. Chem. 34, 1 (1942).

[15] V. V. Kafarov, Collected Papers on Processes and Equipment in Chemical Technology (Goskhimizdat, 1953).*

[16] V. V. Kafarov, Summary of Papers at the Scientific and Methodological Conference on Mass Transfer (Moscow, 1956).*

Received September 10, 1956

*In Russian.

OVERVOLTAGE IN THE EVOLUTION OF HYDROGEN FROM ALKALINE SOLUTIONS

M. D. Zholudev and V. V. Stender

The Dnepropetrovsk Institute of Chemical Technology

Most investigations of hydrogen overvoltage in alkaline solutions are concerned with a small number of metals: iron [1-8], nickel [9, 10], cobalt [11], mercury [12], palladium (in part) [13], and platinum [14], and they were performed mainly in order to determine the mechanism of hydrogen evolution. We could not find any data in the literature on hydrogen overvoltage in alkaline solutions for a number of metals such as magnesium, zinc, tin, antimony, silver, copper, chromium, manganese, zirconium, tantalum, and others. Such data are necessary for the solution of problems in technical electrolysis of alkaline solutions, for calculations of cell voltages, in consideration of conditions of simultaneous discharge of metal and hydrogen ions, etc. The purpose of the present investigation was to measure the hydrogen overvoltage on the above-named metals, which are of technical importance, in concentrated alkaline solutions at current densities used in practice. The electrolytes used were 6 N and 0.6 N solutions of chemically pure caustic soda. Before the determination of the hydrogen-evolution potentials, these solutions were treated thoroughly with activated charcoal and were then subjected to

TABLE 1

Hydrogen-Evolution Potentials on Iron, Nickel, and Cobalt in Acids and Alkalies, from Data of Different Workers

Metals	Potentials (v) at current densities (amp/m²)						Experimental conditions		Literature source
	50	100	200	500	1000	2000	electrolyte	temperature (deg)	
Iron	—	1.12	—	—	1.32	1.39	KOH 350 g/l	25	[17]
	—	1.17	—	—	1.37	1.43	KOH 350 g/l	25	Our data
	1.159	1.259	1.304	1.372	1.447	—	KOH 150 g/l	20	[5]
	1.14	1.21	1.27	1.35	1.42	—	KOH 150 g/l	20	Our data
	—	1.085	1.122	1.178	1.230	1.284	NaOH 150 g/l	37	[9]
	—	1.11	1.15	1.21	1.26	1.30	NaOH 150 g/l	37	Our data
Nickel	0.37	0.40	0.42	—	0.49	0.51	H_2SO_4 2 g/l	25	[18]
	0.35	0.39	0.42	—	0.50	0.53	H_2SO_4 2 g/l	25	Our data
		1.23		1.33	1.37	1.41	NaOH 16%	20	[19]
		1.25		1.35	1.39	1.43	NaOH 16%	20	Our data
Cobalt	0.39	0.42	0.45	—	0.52	0.56	H_2SO_4 2 g/l	25	[18]
	0.39	0.42	0.45	—	0.52	0.57	H_2SO_4 2 g/l	25	Our data

prolonged action, lasting many days, of a direct current with platinum electrodes at current densities of 2-4 amps/cm². The reference electrodes were: mercury–mercuric oxide alkaline half-cells Hg/HgO, NaOH (6 N), and Hg/HgO, NaOH (0.6 N), the potentials of which, according to Fricke [15], are 0.052 and 0.117 v respectively.

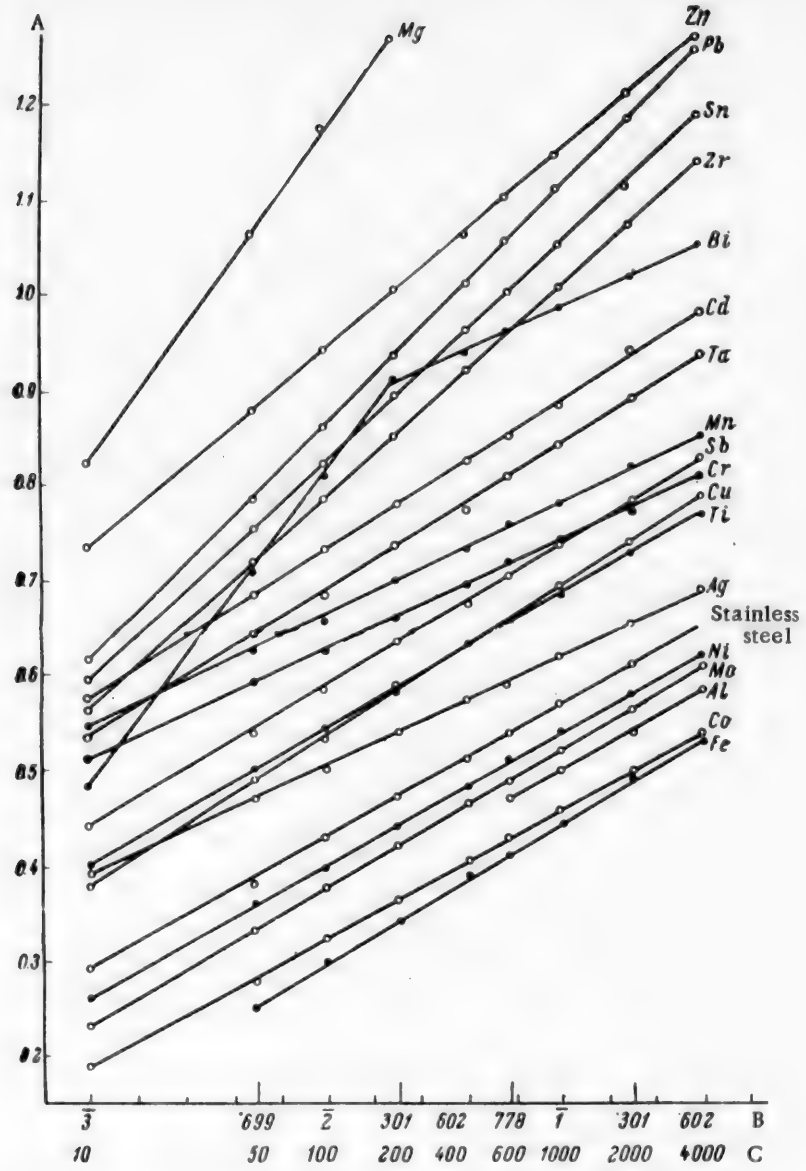

Hydrogen overvoltage (in $\underline{v}$ with a negative sign) at 25° in 6 N caustic soda solution. A) Overvoltage (v); B) log D_C (amps/cm^2); C) current density D_C (amp/m^2).

All the cathode metals were in the form of disks which were fitted closely (without cracks at the edges) into a vinyl plastic frame with a round opening 1 cm^2 in section. The working surfaces of all the cathodes, except lead and zinc, was polished with fine No 000 emery paper and then with dry wool. Before the potential determinations the cathodes were degreased in 6 N caustic soda in a separate cell for 1 hour at a current density of 400 amp/m^2 to remove traces of organic matter (wool fibers), washed in distilled water, and then polarized in the test solution for 1 hour at 400 amp/m^2.

The determinations were performed at 25 ± 0.2°, and in some instances at 50 and 75°, in an open vessel with electrodes 60 mm apart. The use of an open vessel is quite permissible at high current densities [16]. The electrolytic bridge terminated in a very fine tip which was placed on the under side of the cathode and touched it at an angle of 60°.

TABLE 2

Potential Hydrogen Overvoltage at 25° in 6 N Caustic Soda Solution (in v, all data negative)

Current density (amp/m²) and eq. parameters	Mg	Zn	Pb	Sn	Cd	Zr	Mn	Ta	Cr	Bi	Sb	Ti	Ag	Cu	Stain-less steel	Ni	Mo	Al	Co	Fe
10	1.68	1.59	1.47	1.45	1.43	1.42	1.40	1.39	1.37	1.34	1.30	1.26	1.25	1.24	1.15	1.12	1.09	—	1.05	1.01
50	1.93	1.74	1.64	1.61	1.54	1.57	1.48	1.50	1.45	1.57	1.40	1.36	1.33	1.35	1.24	1.22	1.19	—	1.14	1.11
100	2.04	1.80	1.72	1.68	1.59	1.61	1.51	1.51	1.48	1.67	1.44	1.40	1.36	1.39	1.29	1.26	1.24	—	1.18	1.16
200	2.13	1.86	1.79	1.75	1.64	1.71	1.56	1.59	1.52	1.77	1.49	1.44	1.40	1.44	1.33	1.30	1.28	—	1.22	1.20
400	2.25	1.92	1.87	1.82	1.68	1.78	1.59	1.63	1.56	1.80	1.54	1.49	1.43	1.49	1.37	1.34	1.32	—	1.26	1.25
600	2.33	1.96	1.91	1.86	1.71	1.82	1.62	1.67	1.58	1.82	1.56	1.52	1.45	1.51	1.40	1.37	1.35	1.33	1.29	1.27
1000	2.40	2.01	1.97	1.91	1.74	1.86	1.64	1.70	1.60	1.95	1.60	1.55	1.48	1.55	1.43	1.40	1.38	1.36	1.32	1.30
2000	2.51	2.07	2.04	1.97	1.80	1.93	1.68	1.75	1.63	1.88	1.61	1.59	1.51	1.60	1.47	1.43	1.42	1.40	1.36	1.35
4000	2.62	2.13	2.12	2.05	1.84	2.0	1.71	1.81	1.67	1.91	1.69	1.63	1.55	1.65	1.51	1.48	1.47	1.45	1.40	1.39
a	1.95	1.35	1.36	1.23	1.05	1.23	0.90	0.99	0.86	—	0.89	0.83	0.73	0.85	0.71	0.68	0.67	0.64	0.60	0.59
b	0.35	0.21	0.25	0.23	0.16	0.22	0.12	0.15	0.12	—	0.15	0.14	0.12	0.16	0.14	0.14	0.14	0.14	0.14	0.15
i_0 (amp/cm²)	$3 \cdot 10^{-6}$	$4 \cdot 10^{-7}$	$4 \cdot 10^{-6}$	$3 \cdot 10^{-6}$	$4 \cdot 10^{-7}$	$3 \cdot 10^{-7}$	$3 \cdot 10^{-8}$	$3 \cdot 10^{-7}$	10^{-7}	—	10^{-6}	10^{-6}	10^{-6}	$5 \cdot 10^{-6}$	10^{-5}	10^{-5}	10^{-5}	$3 \cdot 10^{-5}$	$5 \cdot 10^{-5}$	10^{-4}
z	0.17	0.28	0.24	0.26	0.37	0.27	0.5	0.4	0.5	—	0.4	0.42	0.5	0.37	0.42	0.42	0.42	0.42	0.42	0.40

Note: To find the overvoltage from the tabulated data, the equilibrium potential (−0.86 v) should be subtracted.

As the potentials changed somewhat with time, they were measured at each current density after a constant electromotive force (± 0.005 v) had become established. The cathodes were made of pure metals such as are met in electrochemical technology. The data on the metals used are given below.

Magnesium – electrolytic, Mg-1 grade. Zinc – electrolytic, Ts-V grade, smooth, coated (on a rotating cathode) with a dense electrolytic deposit of zinc from an alkaline solution containing 6 N NaOH and 30 g of Zn per liter for 10 minutes at 200 amp/m^2. Lead – electrolytic, deposited from an alkaline electrolyte, remelted and cast. The fresh lead surface was exposed by means of a sharp knife. Tin – electrolytic, deposited from a solution containing 50 g Sn, 100 g H_2SO_4, 30 g phenol, and 2 g glue per liter at 25° and 100 amp/m^2. Cadmium – electrolytic, from one of our plants, remelted and cast. Zirconium, tantalum, titanium, and molybdenum – in sheet form, 0.3-0.6 mm thick, made by the powder metal technique. Manganese – electrolytic, from one of our plants. Chromium – electrolytic, deposited from a solution of 150 g CrO_3 and 1.5 g H_2SO_4 per liter at 55° and 5000 amp/m^2. Bismuth – electrolytic, remelted and cast. Antimony – electrolytic, Su-0 grade. Silver – electrolytic, deposited from a solution of 100 g NaCN and 40 g AgCl per liter at 20° and 20 amp/m^2. Copper – electrolytic, microcrystalline, deposited from ordinary pure sulfate solution at 100 amp/m^2. Cobalt – electrolytic, deposited from a solution of 504 g $CoSO_4 \cdot 7H_2O$, 17 g NaCl, and 45 g boric acid per liter at 20° and 400 amp/m^2. Stainless steel – grade 1Kh18N9T. Nickel – electrolytic, deposited from a solution of 150 g $NiSO_4 \cdot 7H_2O$, 100 g $Na_2SO_4 \cdot 10H_2O$, 20 g H_3BO_3, and 15 g NaCl per liter at 20° and 80 amp/m^2. Iron – commercial mild sheet iron, 0.5 mm thick.

As a check of our determinations in acid and alkaline solutions, our results for iron, nickel, and cobalt were compared with literature data (Table 1).

Under similar conditions, the differences between our values, and those of other authors, for iron, nickel, and cobalt are slight, from 0.01 to 0.05 v.

Our results are given in Table 2. It was not our aim to study the mechanism of hydrogen evolution in alkalies; it was merely found that our data for 20 metals (with the exception of bismuth) fit satisfactorily on straight lines plotted in

overvoltage—log current density coordinates, and conform to a general equation of the type $\eta = a - b \log D_c$ (see diagram). The coefficients a and b of this equation (in volts), the exchange current i_0, and the coefficient α, defined as the ratio $\alpha = RT/bF$, are given in Table 2. It is seen that for most metals the value of b is greater than the 0.12 required by the slow-discharge theory. The high values of b are attributed by Kabanov and Rozentsveig [3], Platonova and Levina [2], Murtazaev [11] and others to the presence of oxides and adsorbed oxygen in the metal surface; these are very difficult to remove, not only by prolonged cathodic polarization, but, in the case of such metals as cobalt, even by the action of heat in hydrogen at 400°. In contrast to other metals, the surface of lead and bismuth becomes spongy even after not very long cathodic polarization, and the overvoltate decreases because of the increase in area; the loosening of the surface is probably caused by discharge of sodium ions.

The bend in the curve for hydrogen overvoltage on bismuth is explained, as in the case of iron [3], by the fact that, as the result of increasing polarization the surface becomes free from oxide film, and the slope of the curve decreases and approaches the normal. Aluminum is attacked during cathodic polarization at current densities up to 600 amp/m^2, while at higher current densities cathodic protection occurs. The temperature coefficient of the overvoltage for zinc and antimony is 1.8-2.2 mv per 1° in the 25-75° range. With tenfold decrease of the alkali concentration, the overvoltage on zinc and antimony increases by 50-70 mv. Comparison of our data on hydrogen overvoltage in 6 N caustic soda with the values obtained by Pecherskaia and Stender [18] for hydrogen overvoltage in 2 N sulfuric acid at high current densities shows that the values for antimony, cadmium, copper, molybdenum, and cobalt are very similar, while for zinc, tin, tantalum, and silver the overvoltages are somewhat higher in alkali than in acid, probably because of the state of the surface; the oxide film is more difficult to remove in alkalies than in acids, and the possibility of specific adsorption and accumulation of sodium ions in the electrical double layer is not excluded. this question requires further investigation.

LITERATURE CITED

[1] E. Kalmykova and S. Levina, J. Phys. Chem. 21, 325 (1947).

[2] I. Platonova and S. Levina, J. Phys. Chem. 21, 331 (1947).

[3] S. A. Rozentsveig and B. N. Kabanov, J. Phys. Chem. 22, 513 (1948).

[4] L. L. Kuz'min and V. S. Poroikova, J. Appl. Chem. 22, 572 (1949).

[5] N. N. Voronin and M. A. Shakhova, Bull. Kiev Polytech. Inst. 10, 189 (1950).

[6] M. A. Loshkarev and A. M. Ozerov, J. Appl. Chem. 24, 597 (1951).*

[7] N. E. Buianova and G. A. Tsyganov, Proc. Acad. Sci. Uzbek SSR 1, 23 (1955).

[8] G. A. Tsyganov and N. I. Tugov, Proc. Acad. Sci. USSR 100, 319 (1955).

[9] P. D. Lukovtsev, S. D. Levina and A. N. Frumkin, J. Phys. Chem. 13, 916 (1939); P. D. Lukovtsev and S. D. Levina, J. Phys. Chem. 21, 599 (1947).

[10] A. M. Mirzakarimov and G. A. Tsyganov, Proc. Acad. Sci. Uzbek SSR 7, 31 (1955).

[11] A. Murtazaev, J. Phys. Chem. 23, 1247 (1949).

[12] Z. A. Iofa and Z. B. Pechkovskaia, Proc. Acad. Sci. USSR 59, 265 (1948); O. L. Kaptsan and Z. A. Iofa, J. Phys. Chem. 26, 193, 201 (1952); Z. A. Iofa, J. Phys. Chem. 28, 1163 (1954).

[13] A. N. Frumkin and N. A. Aladzhalova, J. Phys. Chem. 18, 493 (1944).

[14] P. I. Dolin and B. V. Ershler, J. Phys. Chem. 14, 886 (1940); P. I. Dolin, B. E. Ershler and A. N. Frumkin, J. Phys. Chem. 14, 907 (1940).

[15] R. Fricke, Z. Elektroch., 26, 139 (1920).

[16] Hickling and Salt, Trans. Faraday Soc., 36, 1226 (1940); 37, 224,319, 333, 450 (1941).

[17] A. G. Pecherskaia and V. V. Stender, Bull. Acad. Sci. Kazakh SSR, Chem. Ser. 2, 23 (1948).

*In Russian.

[18] A. G. Pecherskaia and V. V. Stender, J. Phys. Chem. 24, 856 (1950).

[19] H. Pfleiderer, Electrolysis of Water (Theoret. Chem. Press, 1935), p. 15 [Russian translation].

Received December 12, 1956

ELECTROLYTIC DEPOSITION OF TIN – NICKEL ALLOY FROM CHLORIDE – FLUORIDE SOLUTIONS

K. M. Tiutina and N. T. Kudriavtsev

The electrodeposition of tin-based alloys is a question of considerable interest in electroplating technology. Coatings of such alloys have a number of valuable properties not found in their constitutent metals. Some of these alloys, such as tin–copper, tin–zinc, and tin–lead, are successfully used in industry as protective and decorative coatings on steel articles.

Electrodeposition of tin–nickel alloy is of great practical importance and theoretical interest. This process has been studied little as yet, but it is receiving much attention in the foreign literature.

The conditions for the electrodeposition of an alloy containing 65% tin and 35% nickel were first worked out in England, where this alloy is used as a substitute for chromium plate when improved decorative properties are required, or instead of tin plate when better mechanical properties (hardness, strength, polishability) are needed. Decorative chrome plating with copper and nickel undercoats can be replaced by coating with tin–nickel alloy with one copper undercoat without intermediate nickel plating.

In appropriate electrolysis conditions, tin–nickel coatings are obtained bright directly from the bath, without subsequent polishing. Such coatings resemble bright nickel or chrome deposits in appearance, but have a pleasant pink tinge.

The composition of the tin–nickel alloy (65% Sn and 35% Ni) corresponds to an intermetallic compound, which cannot be obtained by any method other than electrolysis. This alloy is stable only at temperatures up to 300°. Above 300° it recrystallizes and passes into a stable state with a double structure of Ni_3Sn_2 and Ni_3Sn_4.

The standard potentials of tin and nickel differ by about 0.1 v, the potential of nickel being on the negative side of the potential of tin. Cathodic polarization is more pronounced with nickel than with tin in their deposition from simple salts, and therefore the potential of nickel becomes even more negative during electrolysis. Simultaneous deposition of tin and nickel is therefore possible only in the presence of complex formers which can sharply reduce the activity of tin ions and thereby raise their discharge potential. Of all the complex formers tried, the most effective [1] were found to be fluorides, which largely form complex compounds with tin.

Until now no work has been done in the Soviet Union on the electrolytic production of tin–nickel alloy. Therefore, in addition to considerations of the theoretical aspects of this question, it was desirable to study the conditions of production and the physicochemical properties of this alloy.

The original electrolyte was a solution of tin and nickel chlorides.

The effects of the concentrations of tin and nickel salts and sodium and ammonium fluorides in the electrolyte, organic additives, current density, temperature, and other factors on the composition of the cathode deposit were studied. Fluorides and organic substances were added to an electrolyte containing 300 g $NiCl_2 \cdot 6H_2O$ (~2.5 N) and 50 g $SnCl_2 \cdot 2H_2O$ (~0.5 N) per liter.

It was found that the tin content of the alloy increases with increasing concentrations of sodium or ammonium fluorides; the nature of the cation has little influence on the composition of the deposit.

Sodium and ammonium fluorides differ in their effects on the quality of the deposit: the precipitates are

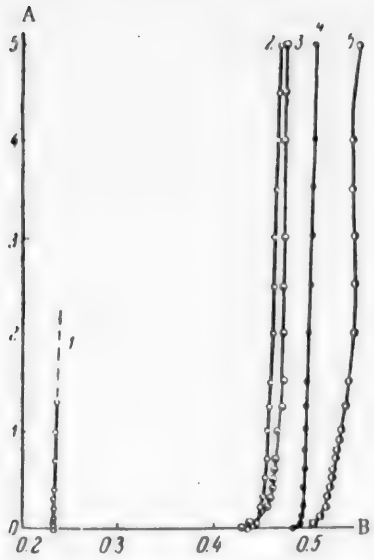

Fig. 1. Effect of fluorides on cathodic polarization in the deposition of tin. Temperature 50°, $SnCl_2 \cdot 2H_2O$ content 50 g/liter. A) Current density D_C (amp/dm^2); B) cathode potential (v). Additions (g/liter): 1) no addition; 2) NaF 40; 3) NH_4F 35; 4) NH_4F 35 and NaF 28; 5) NH_4F 70. The dash line indicates dendrite formation.

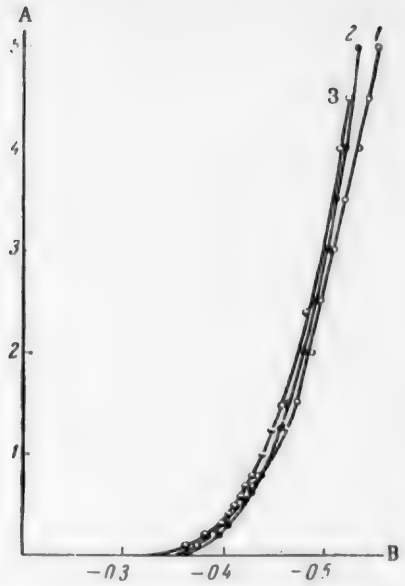

Fig. 2. Effect of fluorides on cathodic polarization in the deposition of nickel. Temperature 50°, $NiCl_2 \cdot 6H_2O$ content 300 g/liter. A) Current density D_C (amp/dm^2); B) cathode potential (v). Additions (g/liter): 1) H_3BO_3 30; 2) NH_4F 40; 3) NaF 20.

dull in presence of sodium fluoride, and bright in presence of ammonium fluoride. However, the alloy obtained from electrolytes with added NH_4F is more brittle; a crackling sound is heard when a plate with the deposit is bent. Metallographic investigation of the Sn–Ni alloy obtained from this electrolyte revealed fine, faint cracks on the surface. The number of these cracks increases with increasing ammonium fluoride concentration and current density.

No such cracks were found in deposits formed in absence of NH_4F. If the electrolyte contains 30 g NaF (0.7 N) and 35-40 g NH_4F (1.0 N) per liter simultaneously, the deposits are bright without visible cracks. Thus, the nature of the fluoride cation has an important influence on the properties of the deposits.

Cathodic polarization was also measured as a function of fluoride concentration, in the simultaneous and separate deposition of tin and nickel. The results of these measurements are given in Figs. 1-3. The polarization curves in Fig. 1 indicate that both sodium fluoride and ammonium fluoride raise the cathode potential of tin considerably (by 200-300 mv), to an increasing extent with increase of fluoride concentration. It follows that tin forms a stable complex compound with fluorides. In electrolytes free from fluorides dendrites form on the cathode at current densities as low as 1.3 amp/dm^2.

Additions of fluorides to nickel chloride solution have no significant effect on the cathode deposition potential of nickel (Fig. 2).

In this case polarization in the simultaneous presence of both fluorides was not studied, because of their restricted solubility in the nickel electrolyte.

In the simultaneous deposition of tin and nickel, fluorides shift the cathode potential sharply (by 150-250 mv) in the negative direction (Fig. 3). Decrease of the relative concentration of either the tin or the nickel salt in the electrolyte lowers the content of the corresponding metal in the cathodic deposit. However, in conditions in which bright deposits are obtained the influence of this factor on the alloy composition is relatively small. It follows from the data in Table 1 that a decrease of nickel chloride concentration from 300 to 50 g/liter, i.e., a sixfold decrease, lowers the nickel content of the alloy by 14%, and a decrease of the tin chloride concentration

from 50 to 10 g/liter (5-fold) lowers the tin content of the alloy by 10%. In both cases the permissible current-density limit below which light-colored or bright deposits are obtainable drops sharply to 0.25-0.5 amp/dm^2.

At current densities above those given in Table 1, the deposits formed are always dull and striped, or with dendrites at the edges.

It follows from these results that a solution of the following composition (in g/liter) is the most suitable for the production of Sn–Ni alloy containing ~65% Sn and ~35% Ni: $NiCl_2 \cdot 6H_2O$ 250-300 (2.1-2.5 N), $SnCl_2 \cdot 2H_2O$ 40-50 (0.4-0.5 N), NaF 28-30 (~0.7 N), NH_4F 35-38 (~1.0 N), pH 4.5-5.0.

The solution has good buffer properties at this pH value. The electrolyte temperature should be 45-55°, cathodic current density 0.5-4.0 amp/dm^2.

The alloy composition varies little in the current-density range from 0.5 to 4 amp/dm^2 at 45-70° (Table 2). In all cases the nickel content of the deposit increases somewhat (by 4-8%) with increasing current density. The nickel content increases appreciably with rise of temperature from 45 to 70° only at low current densities ~0.5 amp/dm^2. At temperatures below 45° the nickel content of the deposit decreases, and is 9% at 25°.

TABLE 1

Effect of Relative Concentrations of the Metals in the Electrolyte on the Alloy Composition at Current Densities Giving Bright Cathodic Deposits. Addition to Electrolyte (g/liter): 28 NaF and 35 NH_4F; pH = 4.0-4.5, t = 50°

Salt concentration (g/liter)		Composition of cathodic deposit (%)		Current density (amp/dm^2)	Current efficiency (%)
$NiCl_2 \cdot 6H_2O$	$SnCl_2 \cdot 2H_2O$	Ni	Sn		
400	50	38.5	61.5	1.0 —4.0	99—100
300	50	35.0	65	1.0 —4.0	96—98
200	50	32.3	67.7	1.0 —3.0	96—98
50	50	21.0	79	0.25—0.5	91
300	40	35.0	65	0.5 —2.0	95—96
300	20	43.0	57	0.25—0.5	57
300	20	43.0	57	1.0 —1.5	85—93
300	10	44.5	55.5	0.25—0.5	57—59

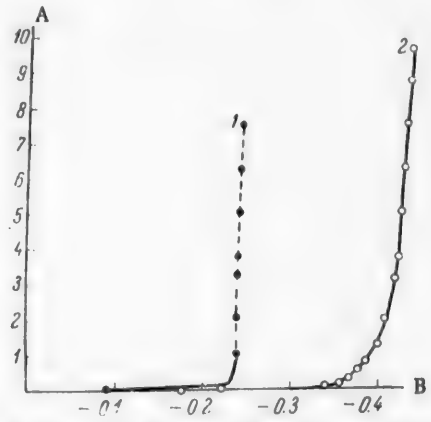

Fig. 3. Effect of fluorides on the cathode potential in the deposition of Sn–Ni alloy. Temperature 50°, electrolyte composition (g/liter): $NiCl_2 \cdot 6H_2O$ 300, $SnCl_2 \cdot 2H_2O$ 50. A) Current density D_c (amp/dm^2); B) cathode potential (v). Additions (g/liter): 1) without addition; 2) NaF 28 and NH_4F 35. The dash line represents the formation of a spongy deposit.

The explanation is that the polarization in the deposition of nickel increases considerably at lower temperatures.

Deposits of Sn–Ni alloy of the same composition can therefore be obtained over wide ranges of temperature and current density. This is one very valuable advantage of this alloy over other electrolytic alloys. As the alloy composition remains constant at different current densities, it is possible to obtain deposits of uniform composition on the surface of relief articles.

Changes of current density from 0.5 to 3.5 amp/dm^2 at 45-65° have little effect on the current efficiency. The average current efficiency is 95-98%, reaching the theoretical value (100%) at 65°.

The temperature and electrolyte pH have an appreciable influence on the external appearance of the alloy deposits (Table 3). Thus, at pH 4.5 the current-density range in which bright deposits are formed becomes narrower with increase of temperature. The widest range of current densities (D_c = 1-4 amp/dm^2) at this pH corresponds to 50°. At 65° dull deposits are obtained at all current densities. At pH 2-2.5 bright deposits can be obtained from this electrolyte in the current-density range from 1 to 4.0 amp/dm^2, between 50 and 70°.

• Light but not lustrous deposits.

TABLE 2

Effects of Current Density and Electrolyte Temperature on the Composition of the Deposit

Current density (amp/dm²)	Nickel content (%) for electrolyte temperature (°C)			
	45	50	65	70
0.5	37.6	38.5	42.7	43.2
1.5	37.0	36.4	38.0	37.6
2.5	35.2	36.0	35.5	37.0
3.5	34.8	35.8	35.0	34.3
4.0	33.1	31.2	34.0	35.0
5.0	—	29.0	29.3	30.5

TABLE 3

Optimum Conditions for the Formation of Bright Alloy Deposits*

Temperature (°C)	D_c range at pH 4.5	D_c range at pH 2.5
45	1.0 – 3.5	1.0 – 3.5
50	1.0 – 4.0	1.0 – 4.0
55	2.5 – 4.0	1.0 – 4.0
65	—	1.0 – 4.5
70	—	1.0 – 4.5

Stirring of the electrolyte raises the permissible current-density limit to 5.5-6 amp/dm² without appreciable effects on the external appearance of the deposit.

Tin and nickel plates or rods should be used as anodes. Studies of the current distribution between anodes of the two metals showed that the current strength on tin is 20 times as high as on nickel at current densities from 0.2 to 5.0 amp per dm² of total anode surface. Accordingly, the tin anode surface should be 1/20 of the nickel anode surface to keep the electrolyte composition constant. The average anodic current density is 0.5-1.0 amp/dm² for the total anode surface.

Investigations of throwing power, by measurements of the metal distribution on an angular cathode [2], showed that the throwing power is somewhat greater in the electrodeposition of tin–nickel alloy from chloride–fluoride solution than in bright nickel plating.

The Sn–Ni alloy coatings (65% Sn + 35% Ni) were tested for porosity, corrosion, internal stresses, and microhardness.

Porosity tests with the aid of potassium ferricyanide solution showed that all the specimens coated with the alloy without a copper undercoat had appreciable porosity, which decreased with increasing thickness of the layer.

Coatings of Sn–Ni alloy 15μ thick, on steel with a copper undercoat 20-30μ thick, were completely nonporous.

The corrosion tests were performed: 1) in a corrosion chamber in which 3% solution of common salt was sprayed 4 times per shift (8 hours) at 30°; 2) in a humidity chamber containing water heated periodically to 50-55° (during 3 hours) and cooled naturally to room temperature (during 21 hours) with dew formation, one cycle per 24 hours; 3) in mineral acid solutions of various concentrations.

The tests in the corrosion chamber (in a mist of 3% NaCl solution) and in the humidity chamber showed that the greatest protective power was found in specimens of polished steel coated with Sn–Ni alloy 15μ thick, over a layer of copper 30μ thick. The first signs of corrosion in the salt chamber appeared after 21 days, while no corrosion occurred in the humidity chamber during 3 months of testing.

The Sn–Ni alloy is relatively resistant to dilute mineral acids. Nitric acid has little action on the alloy, even in concentrated form. It is attacked fairly rapidly in concentrated hydrochloric and sulfuric acids.

The internal stresses were determined from the degree of bending of the cathode during deposition of the alloy on one of its sides. The cathode was a plate 100 × 5 mm, 0.16 mm thick. The anode, consisting of a nickel plate, was placed parallel to the cathode. The reverse side of the cathode was coated with chlorinated vinyl varnish.

When internal stresses form in the deposit, the cathode plate bends during electrolysis, and its free end

* At current densities below 1.0 amp/dm², semibright deposits are formed, while above 3.5 or 4.0 amp/dm² spongy deposits are formed at the cathode edges.

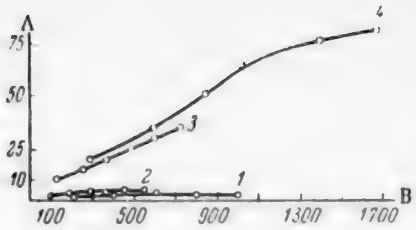

Fig. 4. Effect of fluorides and current density on internal stresses in the deposition of Sn–Ni alloy. A) Deflection in micrometer-eyepiece division; B) quantity of electricity (ma/minute). Additions: 1,2) NaF; 3,4) NH_4F; current density D_c (amp/dm^2): 1,4) 3; 2,3) 1.5.

moves either toward the anode or away from it, according to the nature of the stresses [3]. The deflection of the plate was measured by means of a microscope with a micrometer eyepiece. The electrolysis time was 12 minutes, corresponding to a deposit ~6μ thick at 1.5 amp/dm^2, and ~12μ amp/dm^2. The results of these tests are given in Fig. 4.

It was found that internal stresses causing the cathode to bend away from the anode are present in Sn–Ni alloy deposits; the stresses are considerably greater in presence of amonium fluoride, and increase with the current density. In deposits formed in electrolyte with added sodium fluoride the internal stresses are small, and do not change with current density. In presence of both fluorides together, the internal stresses are similar to those obtained in presence of sodium fluoride.

Microhardness tests on the PMT-3 apparatus showed that Sn–Ni deposits formed from an electrolyte containing both fluorides (NaF and NH_4F) have microhardness of the order of 500-600 kg/mm^2.

The effects of various organic substances which increase cathodic polarization in the deposition of tin were tested in order to obtain deposits with a lower tin content. It was found that p-phenolsulfonic acid is the most effective in this respect. The presence of 0.5 mole of p-phenolsulfonic acid per liter in the chloride–fluoride electrolyte decreases the tin content of the deposit to 53%, and the composition of the deposit remains constant over a wide current-density range, from 0.15 to 4.5 amp/dm^2. However, at 50° bright deposits are obtained in this electrolyte only at current densities up to 0.5 amp/dm^2. It was found [4] that p-phenolsulfonic acid sharply increases the cathodic polarization (by 150-200 mv) in the deposition of tin from chloride–fluoride electrolyte. It has hardly any effect on polarization in the deposition of nickel. Therefore the deposition of tin is retarded considerably in presence of p-phenolsulfonic acid, and the percentage content of tin in the alloy decreases accordingly. At the same time, p-phenolsulfonic acid favors the formation of more elastic deposits of tin–nickel alloy on the cathode, free from cracks even at high contents of ammonium fluoride.

The permissible current-density limit for the formation of bright deposits is raised considerably in presence of p-phenolsulfonic acid (0.5 mole/liter) in electrolytes with a high ammonium fluoride content (60 g NH_4F per liter): at 50°, it is raised to 2 amp/dm^2, and at 70°, to 4.5 amp/dm^2. As in the preceding electrolyte, the tin content of the deposit decreases somewhat (by 3-5%) with increase of temperature from 50 to 70°, and increases at lower temperatures. At 25° the tin content rises to 76%, bright deposits being obtained at current densities up to 2.0 amp/dm^2. These results are fully in agreement with the nature of the cathodic polarization, which decreases much more sharply for the deposition of nickel than of tin with rise of temperature.

The following electrolysis conditions can therefore be recommended for the production of Sn–Ni alloy containing about 50% Sn.

Electrolyte composition (g/liter): $NiCl_2 \cdot 6H_2O$ 300 (~2.5 N), $SnCl_2 \cdot 2H_2O$ 50 (~0.5 N), NH_4F (~1.6 N); p-phenolsulfonic acid 0.5 mole/liter; pH ≈ 4.5; electrolyte temperature 50-70°; cathodic current density 0.5-4.0 amp/dm^2.

SUMMARY

1. The conditions for simultaneous cathodic deposition of tin and nickel from solutions of tin and nickel chlorides containing sodium and ammonium fluorides were studied; it is shown that in presence of sodium or ammonium fluorides the cathode potential of tin is increased considerably, and approaches the potential of nickel deposition in chloride solutions. The nature of the fluoride cation has almost no effect on the composition of the alloy formed on the cathode, but has a strong influence on the physicochemical properties of the deposits.

2. The cathodic deposits formed in the electrolysis of chloride–fluoride solutions without special additives contain about 65% Sn and 35% Ni. The composition of the deposit depends little on the tin and nickel concentrations in the electrolyte, and remains constant over a wide range of current densities, from 0.5 to 4.0 amp/dm^2, and at temperatures from 45 to 70°.

3. Investigation of the current distribution over anodes of the two metals showed that the ratio of nickel to tin anode areas should be 20 to keep the electrolyte composition constant.

4. Alloy coatings 15μ thick, formed with copper undercoats 20 and 30μ thick on polished steel, are nonporous.

Corrosion tests on steel specimens coated with Sn–Ni alloy, in a corrosion chamber with periodic spraying of salt solution, and in a humidity chamber, showed that coatings 15μ thick on copper undercoats 30μ thick have the best protective power.

5. The Sn–Ni alloy is fairly resistant to dilute mineral acids. It is attacked rather rapidly by concentrated hydrochloric and sulfuric acids. Concentrated nitric acid has only a slight action on Sn–Ni alloy.

6. Investigations of the conditions for the formation of alloy deposits with lower tin contents showed that the most effective factor is the presence of 0.5 mole of p-phenolsulfonic acid per liter in the electrolyte. The tin content is then decreased to 50-53%, because of the considerable increase of polarization in the cathodic deposition of tin. The polarization in the deposition of nickel is almost unaffacted by the presence of p-phenolsulfonic acid.

LITERATURE CITED

[1] J. W. Cuthbertson, N. Parkinson and H. P. Rooksby, J. Electrochem. Soc., 100, 3 (1953).

[2] N. T. Kudriavtsev and A. A. Nikiforova, J. Appl. Chem. 22, 4 (1949).

[3] A. T. Vagramian and Z. A. Solov'eva, Methods of Investigation of Metal Electrodeposition (Izd. AN SSSR, 1955).*

[4] N. T. Kudriavtsev, K. M. Tiutina and R. G. Golovchanskaia, Proc. Conf. Acad. Sci. Lithuanian SSR (1957).

Received September 13, 1956

*In Russian.

GAS FORMATION DURING ACID CORROSION OF ZINC

I. I. Zabolotnyi and A. P. Lizogub

The factors determining polydispersion of gas bubbles formed during acid etching of metals have never been submitted to experimental investigation.

The uniformity of the etched metal surfaces, especially in the case of selective corrosion [1], depends, however, on the phenomenon of gas formation. The phenomenon of gas formation during acid corrosion processes allowed one of the authors [2] to determine the porosity and the cracks in the acid resistant layer on the zinc surface. The investigation of the phenomenon of gas formation in the case of acid corrosion of metals is of practical interest in the preparation of metal surfaces, particularly in the preparation of engraving plates.

The theoretical interest of such an investigation becomes clear if one considers the results of the investigation on gas formation during the electrolysis of acid solutions and the explanation of these results by the A. N. Frumkin electro-capillary theory.

A. Cohen and collaborators [3] showed that the size of the bubbles evolved during electrolysis depends on the concentration of the acid, the density of current on the electrodes, and on other factors. According to the Frumkin theory [4] the size of the bubbles at the moment of their separation from the electrode is determined by the vertical force of surface tension at the surface of separation (solution – gas) whose magnitude depends on the angle of contact.

At the same time, Moller [5], and particularly Gorodetskaya and Kabanova [6], showed that the angle of contact of a bubble depends on the electrode potential. Consequently the size of gas bubbles evolved at the electrode depends in the final analysis on the electrode potential.

It would be natural to assume that in the case of electro-chemical corrosion processes there exists a relationship between the size of the bubbles deposited on the corroding metal surface and the potentials of the micro-electrodes of the functioning local elements. If such a relationship did exist it would be of great importance to elucidate it; then one could obtain interesting data on the electrical character of the real galvanic micro-elements and on the mechanism of corrosion processes on the basis of the gas-formation phenomenon.

The method of investigating the functioning of local elements on the basis of gas-formation phenomena during the corrosion processes would probable give more effective results that the investigation method of micro-element models, since the model method, although useful for the explanation of the electrochemical corrosion, is somewhat too simplified.

In view of these considerations we began to investigate the gas formation phenomenon during acid corrosion of metals.

To solve this problem one must take into account the factors which affect the potentials of the micro-elements since the same factors also affect the size of bubbles evolved during acid corrosion. Among these

factors we must consider the nature and the structure of the metal surface, the properties of the corrosive medium, the presence and the concentration of different impurities in the metal and in the corrosive media, etc.

In the first part of our investigation we have limited ourselves to the investigation of gas formation during the corrosion of zinc in aqueous solutions of hydrochloric and sulfuric acids of different concentrations.

EXPERIMENTAL PART

The experiments were performed on little plates (5 × 1.5 mm) cut out of 0.8 mm thick sheets of zinc containing 0.9% Pb, 0.1% Cd and 0.02% Fe. This particular size of the experimental plates was chosen because of its convenience for our investigation of gas formation during acid corrosion. In order to insure constant initial surfaces the samples were polished with chromium oxide of identical dispersion. The state of the polished surface was controlled with a metallographic microscope. All the unpolished sides of the samples were covered with shellac dissolved in alcohol.

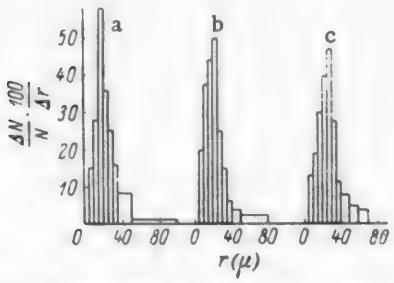

Fig. 1. Distribution of the radii of hydrogen bubbles during corrosion of zinc in a 3% M solution of hydrochloric acid. a) 3 minutes after the beginning of corrosion; b) 8 minutes after the beginning of corrosion; c) 20 minutes after the beginning of corrosion.

Aqueous solutions of hydrochloric and sulfuric acid were used as corrosive media. The corrosion experiments were performed at 18°C.

The size of the hydrogen bubbles evolved during corrosion of the zinc was measured on the micro-photographs of the bubbles, photographed in the solution. We did not use the Gorodetskaya method [7], consisting of taking movies of bubbles moving in the corroding medium, but adopted the following method. The corroding solution was introduced into a tray (40 × 3 × 1.5 cm) with parallel walls. In the middle of the tray was a little glass support upon which was placed the sample. The position of the sample in the middle of the tray favored the renewal of the acid medium at the corroding surface. Since the volume of the corroding medium was large with respect to the surface of the corroding zinc surface, the concentration of the corroding medium remained practically constant during the whole of the experiment. For the same reason the corrosion process only slightly affected the temperature (1-1.5°C) of the solution.

The hydrogen bubbles detaching themselves from the zinc surface during its corrosion were photographed with a camera placed behind the eyepiece of a biological microscope. The bubbles were illuminated by a light passing through the solution.

Every time that the magnification was changed a scale carrying 100μ divisions was placed in the tray and photographed. The diameter of the bubbles was determined by comparing the photographs of the bubbles with

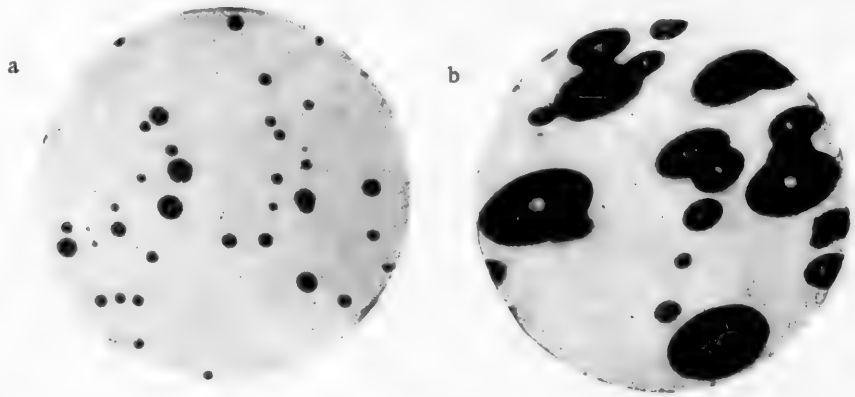

Fig. 2. Microphotographs of the bubbles.

the photographs of the scale, then a bubble size distribution curve was drawn. Three diagrams obtained in a 3% HCl solution are illustrated in Fig. 1; the X axis represents the radius of the bubble (in μ) the Y axis the magnitude of the fraction including all the bubbles whose radius is located between r and $r + \Delta r$. The maximum of the curve represents the most probable radius of the bubble. For each diagram six to twelve pictures were taken over a period of 1 to 1.5 minutes; the exposure for each picture was 1/1250 second.

In connection with the measurement of the radii of bubbles one must note the following: while small bubbles give pictures in the form of circles (Fig. 2,a) the larger bubbles, deformed because of the resistance of the column of liquid, give pictures in the form of flattened ellipsoids (Fig. 2,b). Figure 2 shows that the degree of deformation of the bubbles during their motion in the corroding medium corresponds to the conclusion put forward by Levich [8], who made a detailed investigation of the motion of bubbles in liquids. In order to characterize all the bubbles by the same parameter we measured the radii of small bubbles directly, while the radii of ellipsoidal bubbles were calculated by the formula $r = \sqrt[3]{a^2c}$, where a and c represent the two half-axes of the ellipse. This formula can be derived easily on the basis of the consideration that the volume of the bubbles remains constant and independent of their form. Thus $4/3\pi r^3 = 4/3\pi abc$, and therefore $r = \sqrt[3]{a^2c}$ (in our case the two half-axes of the ellipsoid are equal).

This method of microphotography of the hydrogen bubbles and the determination of their most probable radius allowed us to find the state of bubbles at different heights of the column of the acid solution, the variation of the size of bubbles as a function of the time of the corrosion process and the variation of hydrogen bubble size with the concentration of the HCl and H_2SO_4 solutions.

DISCUSSION OF RESULTS

The pictures of hydrogen bubbles, evolved during acid corrosion and moving in the acid solution, led us to assume that the size of the bubbles is different in different areas of the solution whether at the same or at a different distance from the corroding surface.

The bubbles radii distribution diagrams showed that quite often the most probable radii of the bubbles, photographed in different areas of the solution but at identical distances from the corroding surface, are identical.

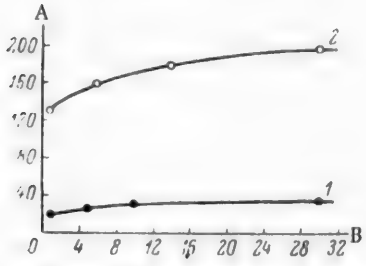

Fig. 3. Variation of the most probable radius of the bubbles as the function of their distance from the corroding surface. A) The most probable radius of the bubble R (in μ); B) Distance of the bubble from the corroding surface (in cm). Concentration of HCl (in %); 1) 2; 2) 8.

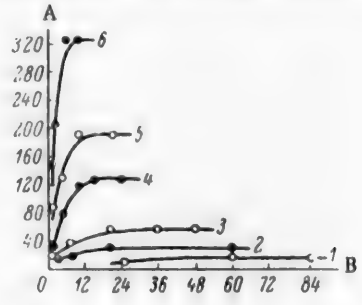

Fig. 4. Variation of the most probable radius of the bubbles as the function of the duration of the corrosion process. A) The most probable radius of the bubbles R (in μ); B) Time (in minutes). Concentration of HCl (in %); 1) 1; 2) 3; 3) 5; 4) 8; 5) 10; 6) 15.

The photographs of the bubbles taken at different heights of the column of the solution revealed that the most probable radius of the bubbles increases with the increase of the distance from the corroding surface; this increase in the radius is probably due to fusion of the initially formed bubbles. This observation led us to photograph the bubbles in the immediate vicinity of the corroding surface at a distance not greater than 1 mm. The curves of Fig. 3 show that the fusion of the bubbles takes place essentially near the corroding surface, where their concentration is the greatest. As one could expect, the rate of fusion of bubbles is greater in more concentrated acid solutions; it decreases however with the increase of the distance from the corroding surface.

The observed polydispersion of the evolved hydrogen bubbles is determined by the difference in the nature and in the areas of the micro-cathodic inclusions of the zinc samples.

Akimov and Klark [9] showed that the potentials of the electrodes of a corroding couple depends, to a great extent, on the ratio of their areas. Thus, for example, in the case of the couple Cu–Zn in a 0.1 N HCl solution the potential of the zinc increases by hundreds of mv toward more positive values when the area of the cathode increases 20 times.

Taking into account these experimental results and also the relationship between the size of the bubbles, evolved on electrodes, and their potential, a relationship which stems from the Frumkin electro-capillary theory, one can assume that the large micro-cathodic inclusions in the zinc samples investigated have more positive potentials and the bubbles formed on them are of larger size. On the contrary the potentials of micro-cathodes of smaller size are more negative; this leads to a decrease of the angle of contact at the surface of separation metal–solution–bubble, and consequently also to a decrease of the size of bubbles evolved at these micro-cathodes.

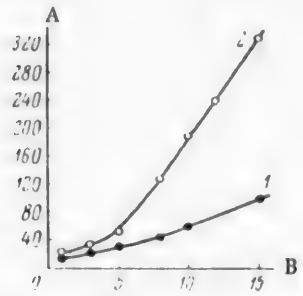

Fig. 5. Size of hydrogen bubbles evolved during corrosion of zinc in (1) sulfuric acid and (2) hydrochloric acid of different concentrations. A) Radius of the bubbles R (in μ); B) concentration of the acid (in %).

The relationship between the electrochemical phenomenon during the corrosion process and the gas formation accompanying this process, is confirmed by experimental data represented in Fig. 4. The curves show that the most probable radius of hydrogen bubbles increases with the duration of the corrosion process but only up to a given limit. The interesting fact is that the character of these curves corresponds to that of the curves of the so-called induction period of corrosion, determined by the different types of corrosion control. It is known that during this period there develops the differentiation between the components of the micro-galvanic elements establishing themselves on the corroding surface. By analogy with this phenomenon the curves of Fig. 4 indicate, in our opinion, an increase of micro-cathodic areas during the development of acid corrosion [10]. The potential of the micro-cathodic areas increases accordingly and this in turn leads to the increase of the size of the bubbles. The size of the bubbles becomes stable at the moment when the area of the micro-cathodes becomes relatively constant.

The decrease of the bubble size with the decrease in the concentration of the acid solutions follows the curves represented in Fig. 5; this decrease is probably due to the concentration polarization, i.e., the rate of flow of hydrogen ions assimilating the electrons on micro-cathodes is too slow. If the concentration of hydrogen ions in the acid solution is low there will be a deficiency of these ions in the layer next to the micro-cathode and, as a consequence, the concentration of the electrons in the double layer will increase. Thus, the negative potential of the micro-cathodes increases, which leads to the decrease of the angle of contact and consequently to the decrease of the size of the bubbles.

The different slopes of the curves of Fig. 5, corresponding to the formation of gas during corrosion of zinc in (1) sulfuric and (2) hydrochloric acid, are due to the difference in the activity of these acids and possibly to some effect of the anions on the stabilization of the size of the hydrogen bubbles formed. This last assumption requires a separate and detailed investigation.

SUMMARY

1. Our method of analysis of the dispersion of hydrogen bubbles, evolved during acid corrosion of zinc, is based on taking micro-photographs of bubbles during their motion in the solution.

2. It was found that there exists a certain regularity in gas formation during the corrosion of zinc in aqueous solutions of sulfuric and hydrochloric acids of different concentrations.

3. The phenomenon of gas formation, observed during acid corrosion of zinc with hydrogen depolarization, is explained on the basis of the A. N. Frumkin theory of electro-capillarity.

LITERATURE CITED

[1] I. I. Zabolotnyii, V. P. Kovtun and B. M. Krimerman, J. Appl. Chem. USSR, 28, 655 (1955).•

•Original Russian pagination. See C.B. translation.

[2] I. I. Zabolotnyii and E. D. Lazebnik, Polygraphic Industry 12, 4 (1950).

[3] A. Cohen, Z. Elektr. Chemie, 29, 1 (1923); A. Cohen and A. Neuman, Z. Physik, 20, 54 (1923).

[4] A. N. Frumkin and A. V. Gorodetskaia, J. Phys. Chem. USSR, 3, 375 (1932); B. N. Kabanov and A. N. Frumkin, J. Phys. Chem. USSR 4, 539 (1933).

[5] W. Moller, Ann. Phys. (4) 27, 665 (1908); Z. Phys. Ch., 65, 226 (1908).

[6] A. V. Gorodetskaia and B. N. Kabanov, J. Phys. Chem. USSR, 4, 529 (1933).

[7] A. V. Gorodetskaia, J. Phys. Chem. USSR 23, 71 (1949).

[8] V. G. Levich, "Physico–Chemical Hydrodynamics" Ac. Sci. USSR, Press Moscow (1952).*

[9] G. V. Kaimov and G. B. Klark, Conference on Corrosion of Metals Acad. Sci. USSR (1939).*

[10] G. V. Akimov, "Theory and Investigation Methods of Corrosion" Acad. Sci. USSR Press, M.-L. (1945).*

Received October 9, 1956

*In Russian.

INVESTIGATION OF THE CORROSION OF ZINC IN ELECTROLYTES COMPOSED OF SULFURIC ACID CARRYING IMPURITIES

A. V. Pomosov, E. E. Krymakova and A. I. Levin

The harmful effect of impurities on electrolytic precipitation of zinc is well known [1]. Thus, for example, the presence of 20 mg/l of Co in an acid zinc sulfate solution decreases the efficiency of electrodeposition of zinc by 15-20%; the presence of 50 mg/l of Ni decreases the amount of electro-deposited zinc virtually to zero [2]. An analogous decrease of the efficiency of deposition and a spoiling of the cathodic precipitate is observed when the solution contains more than 1 mg/l of antimony. The effect of copper ions on the electrolytic process of deposition of zinc is equally harmful; the permissible concentration of copper ions cannot exceed 0.5 mg/l. The concentration of Fe^{3+} and Fe^{2+} ions is permissible up to 70 mg/l but these impurities induce corrosion of zinc, especially in the presence of chlorides. Furthermore, iron, taking part alternately in the cathodic and the anodic processes, leads to a waste of electric current.

All the impurities mentioned, being more electro-positive than zinc, are deposited together with zinc during the electrolysis; they render the cathodic metal impure and form on the zinc surface a great number of micro-elements in which zinc plays the role of the anode.

In order to measure the effect of micro-cells and to find a rational method of protecting the cathode metal against corrosion, it is necessary to understand clearly the mechanism of the functioning of the micro-cells and to determine the factors limiting the corrosion reaction.

To do so we used the well-known method of investigation of corrosion processes based on the drawing of polarization diagrams [3]. This method allows one to determine with sufficient precision the degree to which the corrosion process is slowed down at each consecutive stage of the reaction. In fact, slight polarization of the electrode indicates a freely proceeding electrode process; an important polarization of the electrode indicates on the contrary the slowing down of the electrode process.

Figure 1 shows the diagram of the apparatus used to obtain polarization curves. A model of a corroding microelement was used as the source of the polarization current. The intensity of the polarization current was regulated by varying the external resistance. The current in the circuit was measured with a shunted galvanometer whose sensitivity was $0.66 \cdot 10^{-6}$ ampere; the scale of the galvanometer had 100 divisions.

The cathode and the anode potentials of the cell were measured with respect to a saturated calomel electrode. The electrodes of the cell were plates of electrolytic zinc and plates of the impurity metal under investigation; the ratio of their respective surfaces was equal to 10 : 1.

The experiments were performed at the temperature of 32° ± 1°C; some of the measurements were made at 42° ± 1°C.

The polarization curves were obtained in sulfuric acid solutions of the following composition (in g/l): 1) Zn – 50; 2) Zn – 50, H_2SO_4 – 100; 3) Zn – 50, Mn – 4.

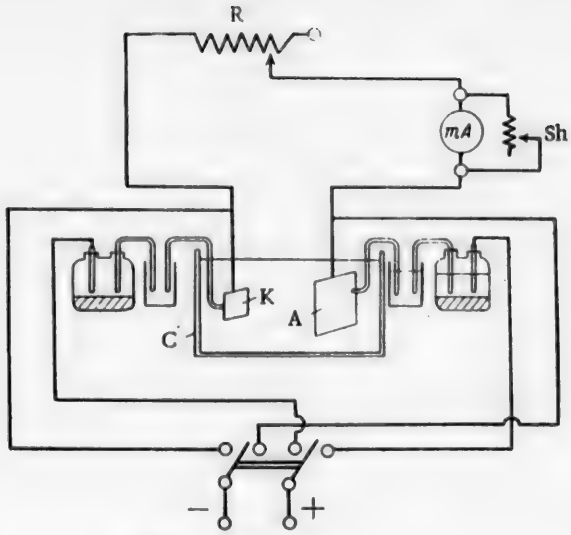

Fig. 1. Diagram of the apparatus used to obtain polarization curves. R) external resistance, mA) Milliamperemeter, Sh) shunt of the milliamperemeter, C) cell, A) Zinc electrode, K) Electrode made of the metallic impurity.

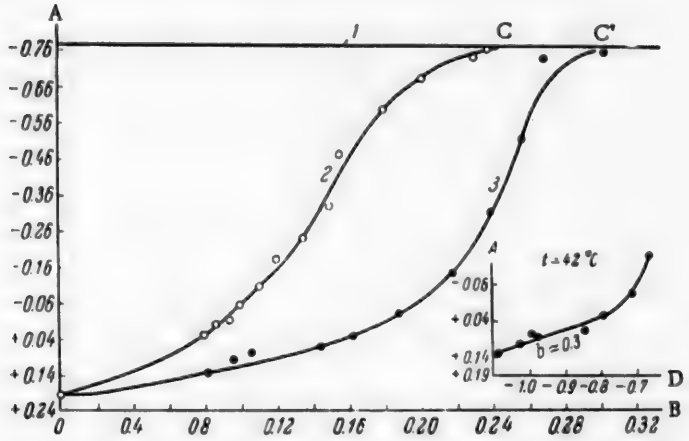

Fig. 2. Polarization curves of the Cu−Zn system in a $ZnSO_4$ solution*. A*) Electrode potential φ; B*) Current intensity I; D) Value of log I. (same for Fig. 3), Curves of the electrodes: 1**) Zn; 2) Cu at 32°C; 3) Cu at 42°C.

The study of polarization in the presence of manganese was of special interest because manganese, oxidized anodically up to the 4 valent or even 8 valent state, is a depolarizer of the cathode. The experiments were performed in a solution of sulfuric acid after it was maintained under a current density of 400 amp/m^2 (oxidation of manganese) for one hour, or in the presence of bi-valent manganese. The electrolyte submitted to preliminary electrolytic treatment became pink.

* In Figs. 2-9 the A coordinate represents the values of the potential φ in volts, the B−coordinate the intensity of current I in m amp.

** In Figs. 2-9 line 1 corresponds to the zinc electrode in $ZnSO_4$ solution.

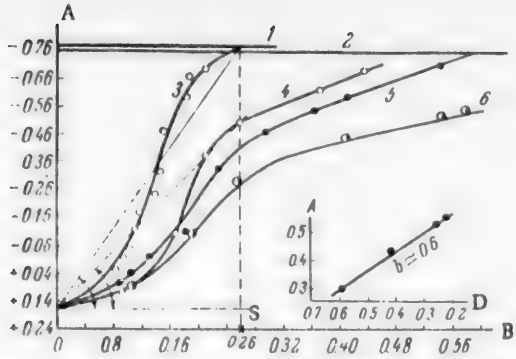

Fig. 3. Polarization curves of the Cu-Zn system in $ZnSO_4$ solution containing H_2SO_4. Electrode curves: 2) Zn in $ZnSO_4$ + H_2SO_4 solution; 3,4,5,6) Cu in $ZnSO_4$ solution containing respectively 0, 25, 50 and 100 g/l of H_2SO_4. The curve in the A–D coordinates was obtained in a $ZnSO_4$ solution containing 100 g/1 of H_2SO_4.

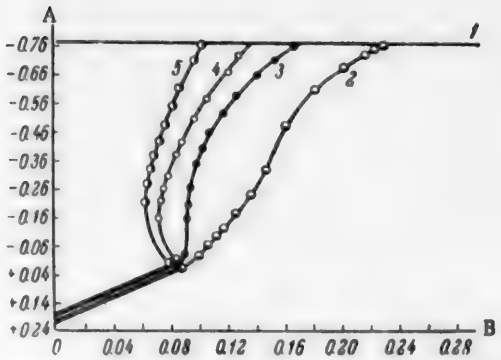

Fig. 4. Polarization curves of the CuZn couple obtained one after the other in the same electrolyte. Electrode curves: 2,3,4,5) Cu.

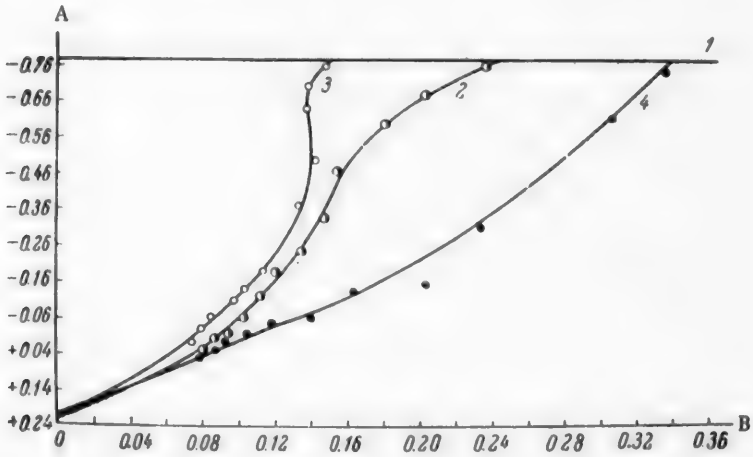

Fig. 5. Effect of manganese on the polarization curves obtained in $ZnSO_4$ solution. Electrode curves: 2) Cu in a solution containing manganese salts, 3) Cu in pure $ZnSO_4$ solution, 4) Cu in a solution containing a salt of manganese of the highest valence.

The results obtained were used to draw polarization curves; the X axis represents the intensity of current in milliamperes, the Y axis the values of potentials (according to the hydrogen scale). The experimental results are represented in Figs. 2-9.

Investigation of Cu – Zn Micro-Cell

The cathode of the micro-cell investigated was made of electrolytic copper M – $O_1$the anode of zinc. Fig. 2 represents the polarization curves of the Cu-Zn system in a zinc sulfate solution (Zn – 50 g/1). Fig. 2 shows that this system is characterized essentially by cathodic polarization. The anode remains practically unpolarized. Consequently one may conclude that in this case the corrosion reaction is slowed down by the cathodic process.

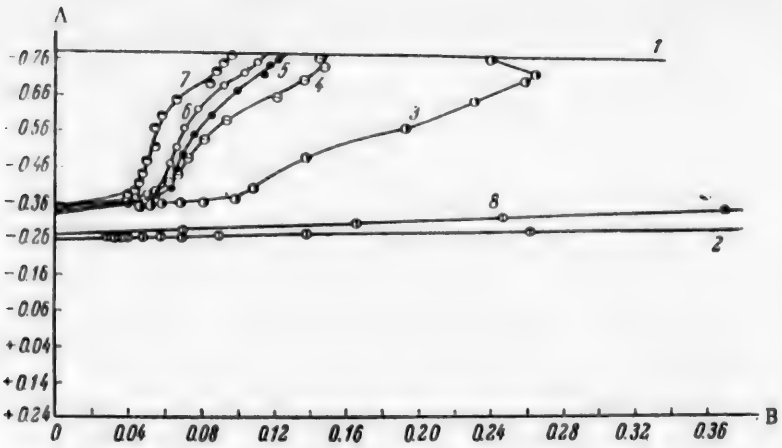

Fig. 6. Polarization curves of the Zn–Cu couples in $ZnSO_4$ obtained one after the other. Electrode curves: 2) Fe in $ZnSO_4$ + 100 g/l H_2SO_4, 3,4,5, 6,7) Fe, obtained consecutively, 8) Fe in a $ZnSO_4$ solution containing a salt of Mn of the highest valence.

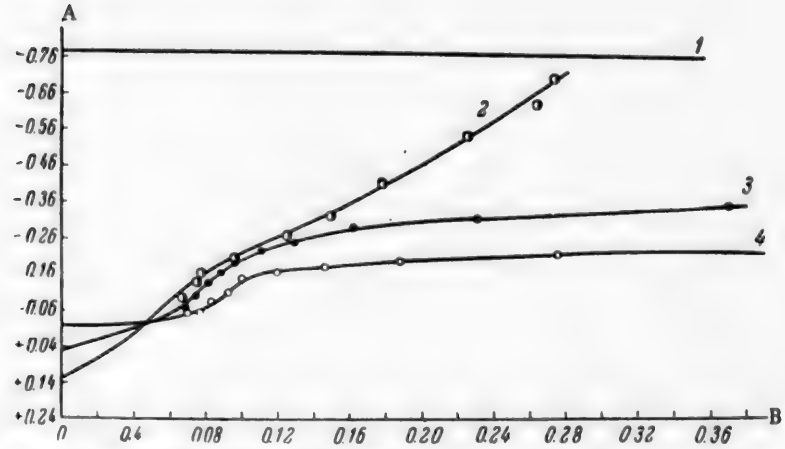

Fig. 7. Polarization curves of the Zn–Ni couple. Electrode curves: 2) Ni in $ZnSO_4$ solution, 3) Ni in $ZnSO_4$ solution containing Manganese salt, 4) Ni in $ZnSO_4$ solution containing 100 g/l of H_2SO_4.

Polarization curves corresponding to zinc sulfate solutions containing sulfuric acid (Fig. 3) show that in this case, too, the reaction is essentially under cathodic control. The anode polarization is again very small but the reaction is slowed to a lesser degree by the cathodic process.

The character of the cathode polarization curves (Figs. 2 and 3) indicate that the electrochemical process taking place on the cathode is very complex. The curve of Fig. 2 drawn in semi-logarithmic coordinates shows that in zinc sulfate solutions the rate of the cathodic process is determined only by oxygen ionization overpotential when the current density is small; when the current density becomes higher the cathodic process depends also on the diffusion rate of oxygen to the cathode. As the temperature increases the oxygen ionization overpotential becomes smaller and the slope of the cathode polarization curve decreases. In the areas of the diffusion current limit one observes, on the contrary, a greater displacement of the cathode potential at 42°C, since under these conditions the solubility of oxygen in the electrolyte is considerably lower. With further increase in the current density one reaches the hydrogen evolution potential and the process of hydrogen depolarization becomes superimposed upon the process of oxygen depolarization. Insofar as the electrodes of the micro-cell are shorted, the process of corrosion of zinc in zinc sulfate solutions (points C and C' in Fig. 2) are determined not only by oxygen depolarization but also by hydrogen overpotential.

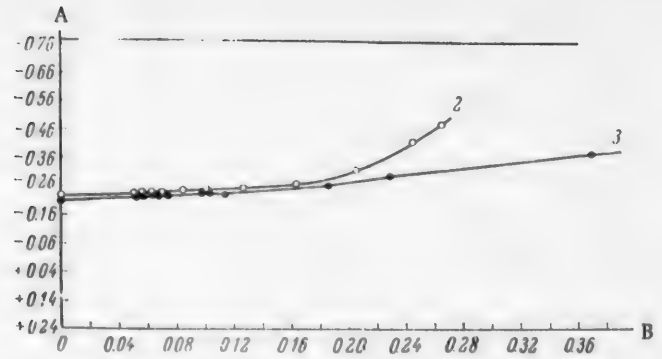

Fig. 8. Polarization curves of the Zn−Co couple. Electrode curves: 2) Co in a $ZnSO_4$ solution, 3) Co in a $ZnSO_4$ solution containing maganese salt.

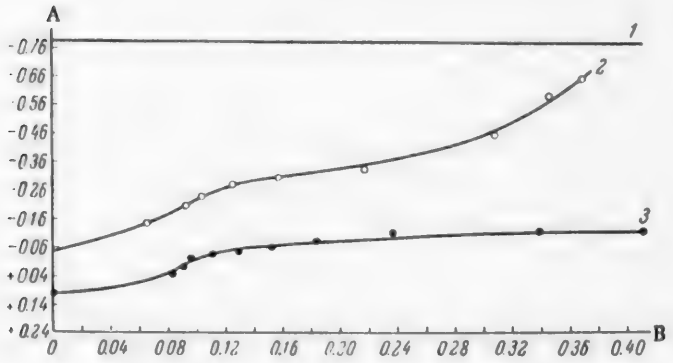

Fig. 9. Polarization curves: 2) Sb in a $ZnSO_4$ solution, 3) Sb in a $ZnSO_4$ solution containing manganese salt.

This situation is represented with particular clarity in Fig. 3 by the polarization curve of the Cu-Zn cell in zinc sulfate solution containing sulfuric acid. In this case, as in the preceeding one, the cathodic process is slowed down by oxygen ionization overpotential as long as the current density is low. As the value of the polarization current becomes larger the cathode polarization increases because of the lesser diffusion rate of oxygen, and the polarization curves become steeper − the diffusion current limit is reached. The curve of Fig. 3, representing the variation of φ as the function of log I in semilogarithmic coordinates, shows that the cathodic process proceeds essentially with hydrogen polarization before the value of hydrogen evolution potential is reached, but the value of the coefficient b is higher than that predicted by the theory for hydrogen overpotential. This discrepancy can be explained by the fact that within the range of the investigated values of current intensity the oxygen diffusion process continues to accompany the hydrogen depolarization process, giving a supplementary displacement of the polarization curves. When the concentration of the acid in the solution increases, the discharge of hydrogen ions is facilitated and the area of the cathodic processes characterized by hydrogen depolarization widens considerably and becomes predominant. As the cathodic polarization decreases the cathodic processes are facilitated and this leads to an increase of the solution rate of zinc.

In fact, in zinc sulfate solutions with I = 0.26 mA, the degree of polarization of the cathode is given by the following relationship:

$$P_C = \frac{\Delta\varphi_C}{I} = \operatorname{tg}\alpha_1 = 3.64\ \frac{V}{\text{ma}};$$

when the concentration of acid in the electrolyte is 25 g/l, it is equal to 2.58 V/ma when the concentration is 50 and 100 g/1, it becomes equal respectively to 2.30 and 1.77 V/ma.

Figure 4 represents polarization curves of the Cu-Zn micro-cell obtained successively in the same electrolyte.

These curves show that the magnitude of cathodic polarization increases with each successive measurement and consequently the corrosion current decreases. This progressive change in polarization is understandable if one takes into account the fact that the solution becomes increasingly richer in zinc ions and poorer in hydrogen ions as the functioning of the cell proceeds, and this leads to the displacement of the cathode potential toward more negative values.

An analogous situation occurs in the case of polarization curves obtained in specially prepared solutions containing different concentrations of zinc ions.

As has been noted before, the presence of manganese compounds in the electrolyte has a considerable effect on the intensity of the reversible solution of zinc cathode. For our purposes, however, the important process is the effect of manganese on the intensity of the functioning of the corrosion micro-cells of the Cu–Zn type and not the role of manganese in the formation of new micro-elements of the MnO_2-Zn type. One can expect that the effect of manganese compounds of different valences will be different.

Figure 5 represents the results illustrating the effect of manganese on the character of the corrosion polarization curves of micro-elements.

The results in Fig. 5 show that the introduction of a bi-valent manganese salt into the electrolyte has no significant effect on cathodic polarization. By contrast, in solutions electrolyzed before the experiment the slopes of the polarization curves are much less steep than the slopes of the polarization curves obtained in solutions free of manganese. It is easy to see that these polarization curves are analogous to the curves obtained in zinc sulfate solutions containing sulfuric acid.

Thus the higher valence manganese compounds are active depolarizers of the cathodic process. It seems that depolarization proceeds according to the following reaction:

$$MnO_4^- + H^+ + e \rightarrow MnO_2 + H_2O.$$

In any case simultaneous presence of copper (or other electropositive metals) and manganese in the electrolyte is undesirable since manganese, being a depolarizer of the cathodic process, greatly intensifies corrosion by micro-cells.

Investigation of the Fe – Zn Micro-Cell

The cathode of the cell was Armco iron, the anode zinc. Figure 6 represents the polarization curves of Fe–Zn micro-cells in zinc sulfate solutions alone or in zinc sulfate solutions containing sulfuric acid. In this case, as in the case of the Cu–Zn micro-cell, the system operates under cathodic control. In zinc sulfate solutions the cathodic process is characterized by oxygen – hydrogen depolarization while in zinc sulfate solutions containing sulfuric acid hydrogen depolarization takes place. The presence of sulfuric acid in the electrolyte leads to a considerable depolarizing action. Polarization curves obtained consecutively in the same electrolyte are displaced to the left and upward, i.e., polarization increases as the electrolyte is being enriched in zinc ions, the total concentration of the sulfates remaining constant.

The introduction of 4 g/*l* of manganese into the acid electrolyte and the preliminary electrolysis of the solution – oxidation of the electrolyte – leads to a decrease of cathodic polarization. The intensity of the depolarizing action of manganese compounds (C_{Mn} = 4 g/*l*) is almost equal to the depolarizing action observed in acid zinc sulfate solutions (in the absence of manganese).

It is extremely difficult to obtain polarization curves in solutions which contain sulfuric acid and 4 g/*l* of manganese because corrosion in these solutions is extremely intense. Thus the consecutively-obtained polarization curves show that the mechanism of the functioning of the Fe–Zn cell is in many respects analogous to that of the Cu–Zn cell, and the intensity of the polarization on the cathodic and anodic areas is of the same order of magnitude.

We are still left with the question of why the presence of copper is infinitely more dangerous than the presence of iron for the electrolysis of zinc. This can be explained by the fact that in the presence of copper, whose potential is more positive ($\varphi^\circ_{Ce/Cu^+} = -0.34$ V) a considerably greater number of micro-cells are formed than in the presence of iron in the solution ($\varphi^\circ_{Fe/Fe^+} = -0.43$ V).

Investigation of the Ni – Zn Micro-Cell

Polarization curves of Ni–Zn micro-cell are represented in Fig. 7.

In a zinc sulfate solution containing sulfuric acid the intensity of the cathodic polarization sharply decreases and consequently the intensity of corrosion of zinc is considerably increased. The addition of manganese compounds to a previously electrolyzed zinc sulfate solution has very little effect on the polarizing action. The general character of the polarization curves of the Ni–Zn system is analogous to that of the Cu–Zn and Fe–Zn systems investigated earlier.

Investigation of the Co – Zn Micro-Cell

The polarization curves of the Co–Zn micro-cell (Fig. 8) are somewhat different from those found for the previously investigated systems.

In zinc sulfate solutions containing sulfuric acid the hydrogen evolution potential on cobalt is displaced toward more positive values. The addition of 4 g/*l* of Mn has practically no effect on the polarization curve; this indicates that the harmful effect of cobalt is so marked that a supplementary addition of manganese is incapable of increasing it. The very gradual slope of the cathode polarization curves during the discharge of hydrogen ions on cobalt indicates that hydrogen overpotential is low. This in turn means that the presence of cobalt in the electrolyte during electrolysis favors the predominance of the discharge of hydrogen ions as opposed to zinc ions, as the Co–Zn micro-cell functions, i.e., cobalt facilitates the cathode stage of the functioning of the micro-cell during the reversible solution of the zinc cathode and thus the intensity of corrosion is increased.

Investigation of the Sb – Zn Micro-Cell

The polarization curves of the Sb–Zn system were obtained either in pure zinc sulfate solution or in zinc sulfate solution containing manganese sulfate. In order to oxidize the Mn^{++} ions to higher valence the solution was submitted to preliminary electrolysis as was mentioned before. No experiments were performed in zinc sulfate solution containing sulfuric acid because in these solutions the zinc electrode dissolves very rapidly.

The polarization curves of the Sb–Zn system are represented in Fig. 9. The cathodic areas were made of antimony, the anodic areas of zinc.

The slopes of the cathode polarization curves of hydrogen discharge on antimony in zinc sulfate are steeper than those relative to hydrogen discharge on a cobalt cathode.

In fact, the polarizability, $P = \frac{\Delta \varphi}{I}$ (with 70 ma, for example) of the Sb–Zn system is equal to 0.0006-0.008 while that of the Co–Zn system varies from 0.001 to 0.0016.

The presence of manganese in the solution of zinc sulfate displaces the cathode potential toward more positive values. Here a noticeable depolarization action of manganese takes place and as the consequence the corrosion intensity of the Sb–Zn micro-cell is increased considerably.

SUMMARY

1. The corrosion of zinc in zinc sulfate solution proceeds with oxygen–hydrogen depolarization, the cathodic process being the limiting corrosion factor. In zinc sulfate solutions containing sulfuric acid zinc corrodes predominantly with hydrogen depolarization.

2. Increase of temperature and particularly the increase of acidity of the electrolyte leads to a greater intensity of the functioning of corrosion micro-elements.

3. Addition of manganese leads to a considerable depolarization of the cathodic process and consequently to an increased rate of the reversible solution of zinc cathode.

4. Of all the impurities investigated, cobalt and antimony are the most dangerous. Antimony becomes dangerous at a concentration above 0.1-0.2 mg/*l*.

LITERATURE CITED

[1] A. N. Gaev and O. A. Esin, "Electrolysis of Zinc" United Sci.-Tech. Press, Sverdlovsk (1937).*

[2] A. G. Pecherskaia and V. V. Stender, J. Phys. Chem USSR, 23, 9 (1950); Non-Ferrous Metals, 4, 45 (1950); V. S. Kolevatova and A. I. Levin, J. Appl. Chem., 27, 456 (1954).* *

[3] G. V. Akimov, "Fundamentals of the Study of Corrosion and Protection of Metals", Metallurgy Press, M. (1946);* N. D. Tomashov, "Corrosion of Metals with Oxygen Depolarization" Ac. Sci. USSR Press, M. (1947).*

Received August 6, 1956

*In Russian.

*Original Russian pagination. See C.B. translation.

INFLUENCE OF TEMPERATURE ON THE EFFECT PRODUCED BY CATHODIC AND ANODIC POLARIZATION OF MA2 ALLOY IN 0.1 N H_2SO_4 + 35 g/*l* NaCl SOLUTION DURING CORROSION CRACKING

V. V. Romanov and V. V. Dobroliubov

We have shown previously that it is possible to prevent either the formation of corrosion cracks or the development of existing corrosion cracks by cathodic polarization; anode polarization, on the contrary, increases this process [1-8].

The effect of cathodic and anodic polarization on the corrosion cracking rate of manganese alloys has been studied by a number of authors.

Mears, Brown, and Dix [5] have found that gradual increase of the cathode current density increases continuously the time interval preceding the cracking of alloys of MA2 type in a solution containing 20 g/*l* of K_2CrO_4 and 35 g/*l* NaCl. For a given current density the alloy became completely protected against corrosion cracking.

Two more investigations were made with a similar alloy. In one of them Zaretskii studied the effect of cathodic and anodic polarization on the corrosion cracking rate in a solution of 0.05 mol NaCl + 0.05 mol $K_2Cr_2O_7$ g/*l* at room temperature, and in the other the effect of cathodic and anodic polarization on the rate of corrosion cracking in a solution containing 35 g/*l* NaCl and 20 g/*l* K_2CrO_4 at 14-15°C was investigated.

Both investigations confirmed the fact that a sufficient cathodic polarization can completely eliminate the tendency of an alloy toward corrosion cracking.

Zaretskii, studying the effect of anodic polarization, found that as the current density increases the time interval preceding the initial cracking becomes smaller, reaches a minimum value, increases somewhat and finally remains constant in spite of the increase of the current density up to 23 ma /cm^2. He explained this result by the relationship between the processes of general corrosion and the processes of destruction along the zones of cracking taking place during corrosion cracking. According to this author the rate of general corrosion first increases with the current density to a lesser extent than the destruction rate along the cracking zones, and this leads to more rapid destruction of the alloy. Further increase in current density increases the rate of general corrosion and renders the surface corrosion process more uniform; consequently the rate of corrosion cracking decreases.

In the second investigation the increase of anodic current density induced a continuous decrease of the time interval preceding cracking up to a certain limit after which the corrosion cracking rate of the alloy remained constant.

In this investigation it was observed that cathodic and anodic polarization affect the character of the developing corrosion cracks in a different way: anodic polarization renders the edges of the cracks relatively sharp and straight while under cathodic polarization the cracks have the tendency to increase in width along the body of grains and partially along the grain boundaries of different grains. The edges of the cracks do not appear as narrow straight cracks.

Since magnesium alloys are used essentially under atmospheric conditions and often in contact with other metals, i.e., under conditions of varying temperature and possible anodic polarization, and since cathodic

protection is used to prevent corrosion cracking, it appears important from the practical as well as theoretical point of view to investigate the influence of temperature on the effect of cathodic and anodic polarization during corrosion cracking of these alloys.

As far as we know such an investigation has not been published.

EXPERIMENTAL

We have chosen for our investigation a 2 mm thick standard sheet MA2 alloy whose chemical analysis is given below:

Composition of the alloy	Al	Zn	Mn	Fe	Si	Ni	Cu	Mg
Amount (in %)	3.4	0.66	0.3	0.007	0.07	0.0003	0.03	remainder

Samples in the form of ordinary Gagarin samples were cut out in the direction of lamination. The surface was prepared in the same way as in our previous experiments [2].

The prepared samples were introduced into a glass container with an opening in the bottom where they were fixed with a rubber cork in which a cut was made.

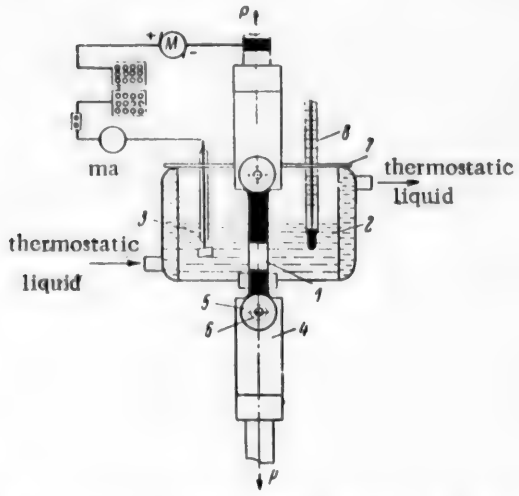

Fig. 1. General diagram of the apparatus for the determination of the influence of temperature on the effect produced by cathodic and anodic polarization during corrosion cracking of metals. 1) Sample; 2) container with the corrosive medium; 3) platinum electrode; 4,5 and 6) clamp and fixing of the sample; 7) cover; 8) thermometer.

The container had closed double walls within which was circulated a thermostatic liquid from an ultra-thermostat. The container with the sample was fixed on an VP-8 motor, which was used to create tension along the axis of the sample. The initial tension was equal to 20 kg/mm^2.

The corrosive medium was a 0.1 N H_2SO_4 + 35 g/l NaCl solution.

Chlorine ions and sulfate ions were used because under atmospheric conditions these ions are the most frequent activators of corrosion processes. The acid medium was chosen to create corrosion processes proceeding essentially with hydrogen depolarization. The volume of the electrolyte was 100 cm^3. The samples were first introduced into a dichloethane polysterol solution up to a certain depth and then dried, to insure the water separation line.

The working surface of the sample was about 3.6 cm^2. The temperatures investigated were: 10, 20, 30, 50 and 70°C. The temperature was regulated with a precision of ± 0.05°C.

During polarization a platinum plate of about 2 cm^2 was used as an auxiliary electrode. The source of current was a direct current generator. The electrical circuit adopted allowed us to chose the required current densities. The general diagram of the apparatus is presented in Fig. 1.

The results presented are averages of five parallel measurements.

The experimental results are represented in Tables 1 and 2 of Fig. 2; they show that in the absence of polarization an increase of temperature induces a constant decrease of the time interval preceding cracking. This relationship, expressed in semi-logarithmic coordinates, has a linear character (Fig. 3). As the temperature increases, the rate of general corrosion of the alloy increases together with the increase of the rate of corrosion cracking; these results, however, have no special interest and therefore are not represented here.

The results represented in Fig. 2, relative to the influence of the temperature on the effect of cathodic

TABLE 1

Influence of Temperature on the Effect of Cathodic Polarization During Corrosion Cracking of the MA2 Alloy in 0.1 N H_2SO_4 + 35 g/l NaCl Solution

Curr. dens. during cath. polarization (ma/cm²)	Time interval preceding cracking at different temperatures (in °C)				
	10	20	30	50	70
1.02	198'40"	102'00"	58'44"	50'04"	16'48"
1.7	166'15"	—	78'08"	—	—
2.55	211'15"	—	77'12"	—	—
3.4	6 hours	98'20"	84'29"	8'18"	—
5.1	→	111'45"	96'39"	—	—
5.95		6 hours	—	—	—
6.8		→	88'45"	50'50"	16'18"
8.5			102'37"	—	—
10.2			115'20"	—	—
11.9			6 hours	51'32"	—
13.6			→	70'20"	—
18.7				6 hours	17'52"
20.4				→	20'28"
28.9					26'00"
30.6					16'30"
32.3					18'40"
34.0					3 2'00"
35.7					6 hours
37.4					→

polarization, show that the cathode curves have a characteristic form. For relatively low current densities one observes observes first a decrease of the time interval preceding the cracking (first region); further increase of current density does not significantly affect the time interval preceding cracking (second region); then a prolonged protection of the alloy against corrosion cracking takes place (third region).

The first region, the largest at a temperature of 10°C, decreases when the temperature is increased and disappears at 70°C. The second region changes in the reverse order, i.e., it is largest at 70°C and disappears at 10°C.

The third region of the cathodic curves, characterizing the magnitude of the protection current,* increases with temperature according to an approximately linear relationship (Fig. 4).

TABLE 2

Influence of Temperature on the Effect of Anodic Polarization During Corrosion Cracking of the MA2 Alloy in 0.1 N H_2SO_4 + 35 g/l NaCl Solution

Curr. dens. during anodic polarization (ma/cm²)	Time interval preceding cracking at different temperatures (in °C)				
	10	20	30	50	70
0	310'	180'24"	84'27"	54'04"	15'11"
3.4	114'47"	148'26"	91'05"	52'44"	15'23"
6.8	79'00"	85'20"	88'53"	51'52"	14'48"
8.5	67'10"	131'39"	89'48"	—	—
10.2	64'54"	127'03"	—	42'56"	—
13.6	64'36"	127'35"	92'51"	43'42"	13'29"

*The current density necessary for the protection of the alloy against cracking was arbitrarily assigned the value for which cracking did not appear after six hours of exposure.

In order to be sure that the increase of the "life span" of the alloy by cathodic polarization is not due to the possible change in the properties of the medium or to protective surface films, in a certain number of experiments the protective current was measured before a six-hour period of exposure. Shortly after the measurement of the current the samples started to disintegrate; the higher the temperature, the sooner the disintegration started.

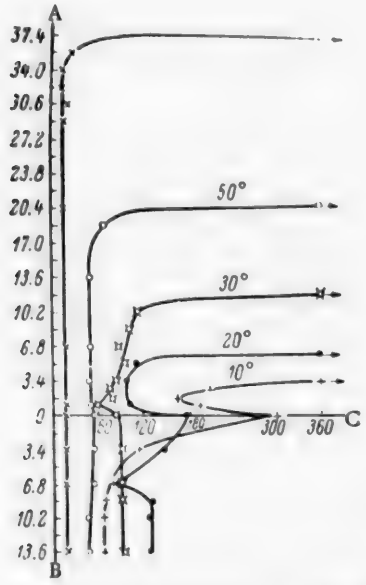

Fig. 2. Influence of temperature on the effect of the cathodic and anodic polarization during corrosion cracking of MA2 alloy in 0.1 N H_2SO_4 + 35 g/l NaCl solution. A) Cathode current density D_k (in ma / cm^2); B) anode current density D_a (in ma./cm^2); C) time interval preceding cracking (in minutes).

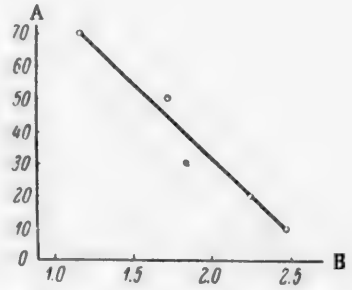

Fig. 3. Effect of temperature on the sensitivity of the MA2 alloy to corrosion cracking in 0.1 N H_2SO_4 + + 35 g/l NaCl solution. A) Temperature (in °C); B) logarithm of the value of the time interval preceding cracking (in minutes)

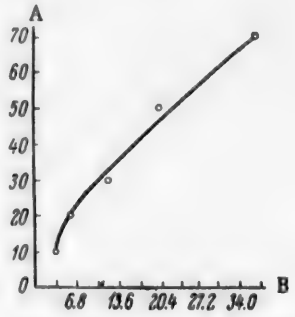

Fig. 4. Effect of temperature on the value of the protective current during corrosion cracking of the MA2 alloy in 0.1 N H_2SO_4 + 35 g/l NaCl solution. A) Temperature (in °C); B) protecting current D_k (mA/cm^2).

The results obtained relative to the influence of temperature on the effect of anodic polarization (Fig. 2) show that this effect occurs only when the temperature is 10 to 20°C; it is absent at higher temperatures. It appears then that at 10°C there occurs a constant and relatively more important decrease of the time interval preceding cracking than at 20°C, i.e., the influence of anodic polarization is more effective at the lower temperature. The shape of the anodic curve at 20°C resembles that described by Zaretskii: as the anodic current density increases the time interval preceding cracking first decreases to a certain minimum, then increases somewhat and finally remains constant.

DISCUSSION OF RESULTS

The increase of the corrosion cracking rate with temperature, in the absence of polarization, can be explained by the increase in working intensity of local cells present at the bottom and edge areas of the developing corrosion cracks. This is apparently related to an increase in the electrical conductivity of the solution and of the diffusion rate with the potential change of the metal, and to the decrease of hydrogen overpotential [9].

The increase of the working intensity of local cells at the bottom and edge areas of the developing corrosion cracks can explain the required increase of the intensity of the protective current with temperature (third region of the cathodic curves). The more intense the work of the cells, the greater must be the applied current intensity to counteract this work.

The initial decrease of the time interval preceding cracking during cathodic polarization observed at 10, 20, and 30°C was also noticed by Evans and Simon when they studied corrosion fatigue of steel [10].

Evans offered the following explanation of this phenomenon: when the intensity of the cathodic current is small and insufficient only isolated potential concentrators become protected; the potential concentrators left either unprotected or insufficiently protected gain the possibility of preferential development and this leads to a more rapid cracking.

Evans and Simon do not develop this hypothesis in any detail. We consider, however, that the protection by low current density may eliminate the mutual effect of the neighboring potential concentrators on the potential distribution at the bottom areas of the crack.

This hypothesis can be used to explain the results obtained (first areas on the cathodic curves). The shrinking of the first region with temperature can be explained again by the increase of the working intensity of local cells situated at the bottom area of the developing corrosion cracks. As the temperature increases, the intensity of the corrosion current generated by the local cells becomes so important that the small cathodic current applied from outside can not affect the functioning of the local micro-cells. The results obtained show that at high temperatures only high current densities are effective; they can provide a quick protection of the alloy against cracking, i.e., a complete suppression of the functioning of local micro-cells located at the bottom and edge areas of the developing cracks.

Up to this point the corrosion cracking rate does not change; it remains close to that observed without polarization.

The form of the anodic curves can be explained by the interaction of two factors — an acceleration, due to the displacement of the potential of the metal toward more positive values [11], and an inhibition, due to the possible change in the character of the corrosion process with the increase of the anodic current density.

Tomaschov, Komissarova, and Timonova [12] have shown clearly that the number of centers (nuclei) of corrosion on magnesium anodes can increase with anodic current density, i.e., an increase of the number of simultaneously appearing potential concentrators takes place; the corrosion process becomes more homogeneous and this of course decreases the corrosion cracking rate.

The effect of the increase in homogeneity of corrosion, (taking place when the anodic current density is increased) on the corrosion cracking rate of the alloy becomes apparent at a given value of current density; in our case this value was close to 8.5ma / cm^2. At 10°C (as well as at 20°C) the accelerating action of anodic polarization stops when this current density is reached; at 20°C one observes even a displacement of the anodic curve back in the direction of greater time intervals preceding cracking. This displacement can be explained by the fact that at 20°C the combined effect of the displacement of the metal's potential and of the increase in the anodic current density is capable of affecting the corrosion cracking rate to a greater extent than at lower temperatures (10°).

SUMMARY

1. The temperature has a significant influence on the effect of the anodic and cathodic polarization during the corrosion cracking of MA2 alloy in a 0.1 N H_2SO_4 35 g/ *l* NaCl solution. The value of the current density necessary to protect the alloy against corrosion cracking increases almost linearly with temperature.

2. When the cathodic current density is low one observes an initial shrinking of the time interval preceding cracking instead of protection. This effect decreases as the temperature increases and disappears completely at 50 and 70°C.

3. The accelerating effect of anodic polarization on the corrosion cracking rate is more effective at 10°C, less effective at 20°C and is absent at 30, 50 and 70°C.

LITERATURE CITED

[1] E. M. Zaretskii, "Corrosion of Metals and Protection Against Corrosion" Defense Press 239 (1955).*

[2] V. V. Romanov, J. Appl. Chem. USSR 29, 8 (1956).**

*In Russian.

**Original Russian pagination. See C.B. translation.

[3] G. Edeleanu, J. Inst. Met., December (1951).

[4] E. A. G. Liddiard and A. Bellew, J. Inst. Met., 82 (9), 426, (1953-1954).

[5] R. B. Mears, R. H. Brown and E. H. Dix, Symposium on Stress Corrosion Cracking of Metals 323 (1944).

[6] V. V. Skorchelletti and V. A. Titova, J. Appl. Chem., 26, 1, (1953).*

[7] C. D. MacDonald and D. T. Weber, "Corrosion of Metals" 436 (1953).

[8] T. R. Hoar and J. G. Hines, J. Iron and Steel Inst., 182, 2, 124-143 (1956).

[9] I. L. Rozenfeld and G. V. Akimov, "Investigation of the Electrochemical and Corrosion Behavior of Metals and Alloys" Moscow 179 (1950).**

[10] U. R. Evans and M. T. Simon, Pr. Roy. Soc. 188 A, 372 (1947).

[11] V. V. Romanov, Bulletin of the Voronezh Division of the D. I. Mendeleev All-Union Chemical Society, 1, 105 (1957).**

[12] N. D. Tomashov, V. S. Komissarova and M. A. Timova, "Investigation of Corrosion in Metals" Bulletin of the Institute of Physical Chemistry, Ac. Sci. USSR, M.-L., 4, 172 (1955).*

*Original Russian pagination. See C.B. translation.

**In Russian.

TABLE 1

Inhibitor Effects of Bases in 12% H_2SO_4 and 15% HCl at Room Temperature

Fraction	12% Solution H_2SO_4				15% Solution HCl	
	base concentrations (%)					
	0.2		0.6		0.2	
	γ	ρ	γ	ρ	γ	ρ
230—240	5.8	$9.8 \cdot 10^{-5}$	7.2	$7.4 \cdot 10^{-5}$	2.03	$3.6 \cdot 10^{-5}$
240—260	4.0	$14.1 \cdot 10^{-5}$	3.9	$14 \cdot 10^{-5}$	2.6	$2.7 \cdot 10^{-5}$
260—280	7.2	$8 \cdot 10^{-4}$	12	$4.5 \cdot 10^{-5}$	7.6	$9.6 \cdot 10^{-6}$
280—300	8.9	$6.4 \cdot 10^{-5}$	27	$2 \cdot 10^{-5}$	7.7	$9.4 \cdot 10^{-6}$
300—320	6.4	$9 \cdot 10^{-5}$	14.5	$3.7 \cdot 10^{-5}$	6.1	$11.7 \cdot 10^{-6}$
320—330	6.3	$9.1 \cdot 10^{-5}$	9.8	$5.5 \cdot 10^{-5}$	5.3	$13.8 \cdot 10^{-6}$
330—345	6.1	$9.3 \cdot 10^{-5}$	5.3	$10.1 \cdot 10^{-5}$	5.2	$13.9 \cdot 10^{-6}$
345—360	3.9	$14.6 \cdot 10^{-5}$	3.6	$14.7 \cdot 10^{-5}$	7.2	$10.1 \cdot 10^{-6}$
330—345 (Without acridine)	7	$8.1 \cdot 10^{-5}$	11	$5 \cdot 10^{-5}$	7	$10.1 \cdot 10^{-6}$
345—360 (Without dehydroacridine)	4	$14 \cdot 10^{-5}$	4.5	$12.8 \cdot 10^{-5}$	7.1	$10.2 \cdot 10^{-6}$
Acridine	1.2	$47 \cdot 10^{-5}$				
Dihydroacridine	1.02	$55 \cdot 10^{-5}$	—	—	—	—
Quinoline	2.6	$21 \cdot 10^{-5}$	—	—	—	—
Quinaldine	3.1	$19 \cdot 10^{-5}$	—	—	—	—
			$\rho_0 = 56 \cdot 10^{-5}$		$\rho_0 = 7.3 \cdot 10^{-5}$	

The bases have approximately the same activities in sulfuric and hydrochloric acids at room temperature, but at 70° the activities in sulfuric acid are much lower.

This cannot be explained in the light of the widely-held theory of specific adsorption. According to this theory, nitrogenous inhibitors interact with the metal surface by means of the electron pairs of the nitrogen atoms. The higher the electron density of nitrogen, the more firmly is the substance adsorbed on the metal, and the better is its inhibiting effect. Therefore the presence of methyl groups in the ortho and para positions to the

TABLE 2

Inhibitor Effects of Bases in 12% H_2SO_4 and 15% HCl at 70 ± 2°

Fraction	12% Solution H_2SO_4				15% Solution HCl			
	base concentrations (%)							
	0.2		0.6		0.2		0.4	
	γ	ρ	γ	ρ	γ	ρ	γ	ρ
230—240	1.8	$60 \cdot 10^{-4}$	1.3	$59 \cdot 10^{-4}$	1.03	$28 \cdot 10^{-3}$	1.8	$21 \cdot 10^{-3}$
240—260	3.0	$26 \cdot 10^{-4}$	0.6	$120 \cdot 10^{-4}$	1.3	$22 \cdot 10^{-3}$	1.5	$19 \cdot 10^{-3}$
260—280	3.5	$2.2 \cdot 10^{-4}$	0.6	$124 \cdot 10^{-4}$	8.3	$3.4 \cdot 10^{-3}$	16.4	$1.7 \cdot 10^{-3}$
280—300	4.3	$1.9 \cdot 10^{-4}$	2.4	$32 \cdot 10^{-4}$	16.5	$1.7 \cdot 10^{-3}$	27.5	$1.0 \cdot 10^{-3}$
300—320	5.2	$15 \cdot 10^{-4}$	2	$39 \cdot 10^{-4}$	10.5	$2.1 \cdot 10^{-3}$	14.1	$2 \cdot 10^{-3}$
320—330	3.9	$20.3 \cdot 10^{-4}$	1.7	$46 \cdot 10^{-4}$	7	$4.1 \cdot 10^{-3}$	7.3	$4 \cdot 10^{-3}$
330—345	5.3	$15 \cdot 10^{-4}$	2.7	$29 \cdot 10^{-4}$	8.1	$3.6 \cdot 10^{-3}$	7.5	$3.9 \cdot 10^{-3}$
345—360	3.7	$21 \cdot 10^{-4}$	1.7	$45 \cdot 10^{-4}$	20	$1.4 \cdot 10^{-3}$	13.3	$2.8 \cdot 10^{-3}$
Acridine	0.67	$116 \cdot 10^{-4}$						
Dihydroacridine	0.5	$156 \cdot 10^{-4}$						
Quinoline	1.5	$51 \cdot 10^{-4}$						
Quinaldine	2.3	$32 \cdot 10^{-4}$						
	$\rho_0 = 78 \cdot 10^{-4}$				$\rho_0 = 29 \cdot 10^{-3}$			

nitrogen increases the inhibitor activity (the ortho effect). The action of inhibitors is represented by the following scheme:

$$\overset{+}{RNH}\ \text{(in solution)} \rightleftharpoons RN + H^+ \rightleftharpoons RN\text{-iron},$$

where RN-iron represents the chemisorbed base.

It is thus postulated by this theory that the onium ions of the bases, present in acid solution, dissociate into hydrogen ions and the free base, which interacts with the metal surface. It follows that inhibitor activity must depend only on the structure of the base and the properties of the metal.

This viewpoint fails to account for the changes in the activities of the same bases with respect to No. 3 steel in sulfuric and hydrochloric acids on increase of temperature.

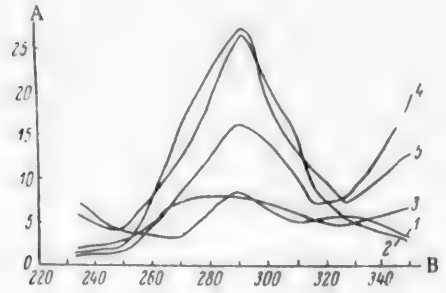

Fig. 1. Variation of inhibitor activity with the boiling point of the bases. A) Inhibitor effect (γ); B) boiling point (in °C). Pickling in 12% H_2SO_4 solution at 20°, with base concentrations (%): 1) 0.2; 2) 0.4; in 15% HCl solution at 20°, with base concentrations (%): 3) 0.2; in 15% HCl solution at 70° and base concentration (%): 4) 0.2; 5) 0.4.

Neither does this theory explain the ortho effect, as increase of the electron density of the nitrogen atom on introduction of the methyl group increases the stability of the onium ion, and probability of its dissociation to form the free base therefore decreases, especially in acid solutions, where a large excess of hydrogen ions is present. It is more likely that the bases react as onium ions with the metals, and the principal role in the formation of a protective film is played by electrical forces rather than by specific adsorption.

The differences in the action of nitrogenous inhibitors in hydrochloric and sulfuric acids are attributed by Iofa [3] and Aiazian [4] to differences in the charge on the metal surface during dissolution in these acids. They showed that in hydrochloric acid the metal surface is negatively charged, whereas in sulfuric acid it carries a weak positive charge, which hinders the adsorption of positive ions on it. Therefore the formation of a protective film by nitrogenous bases in the action of sulfuric acid on steel is caused only by forces of specific adsorption; moreover, these forces are weakened by the opposing action of electrical forces. Nevertheless, at room temperature, when the dissolution rate is 1/12 of the rate at 70°, the protective film is strong enough to retard appreciably the dissolution of the metal. It is also possible that at high temperatures in sulfuric acid the equilibrium potential is shifted in the positive direction, lowering the strength of the protective film.

The explanation of the ortho effect is that the presence of methyl groups increases the strength of the bases, and hence the stability of the onium ion, and decreases the tendency of the latter to hydrolysis; i.e., it increases the onium ion content of the solution. The strongest bases must therefore always be the best inhibitors. Of quinoline, quinaldine, and acridine, the strongest base is quinaldine ($K = 1 \cdot 10^{-9}$), followed by quinoline ($K = 6.3 \cdot 10^{-10}$), and the weakest is acridine ($K = 3 \cdot 10^{-10}$). Their inhibitor activities decrease in the same sequence.

Fractions containing quinoline, quinaldine, and acridine, are more active than the pure substances owing to the presence of their methyl homologs, which are stronger bases.

The foregoing considerations also account for the variations of inhibitor activity with the boiling points of the bases. The first fraction (boiling range 230-240°) contains a certain amount of pyridine homologs with three and four methyl groups (see data on the following page).

These substances are stronger bases than quinoline, and have somewhat higher activity than the quinoline fraction. The subsequent fractions, boiling up to 300°, consist mainly of quinoline homologs, in which the number of methyl groups increases with the boiling point, with corresponding increases of inhibitor activity. Fractions boiling above 300° contain naphthylamines and their homologs, and tricyclic compounds: tetrahydroacridine,

Substance	Boiling point (in °C)	Substance	Boiling point (in °C)
3,5-Xylidine	220-221	2,4,6-Trimethylquinoline	288.0
2,3-Xylidine	223	Hydroacridine	300
2,3,4,5-Tetramethylpyridine	233	1-Naphthylamine	300.8
Quinoline	237.7	2-Naphthylamine	306
Isoquinoline	240	Tetrahydroacridine	328
2-Methylquinoline	246.5	7,8-Benzoquinoline	338
2,8-Dimethylquinoline	255	Acridine	343
6-Methylquinoline	258	Phenanthridine	349
1,3-Dimethylquinoline	262.4	Methylacridine	356
5, -Dimethylquinoline	270.0		

benzoquinoline, acridine, and phenanthridine, which are weaker bases; therefore their inhibitor activity is lower. The last fraction contains their methyl homologs, and the inhibitor activity is greater. In addition to the strength of the bases, the size of the molecule, its cross section, evidently plays a role.

It is probably because of this that the inhibitor effect of bases boiling above 300°, although lower than that of the 280-300° fraction, is higher than that of the low-boiling fraction containing pyridine homologs.

TABLE 3

Effect of KSCN on the Inhibitor Activity of Bases

Fractions	12% Solution H_2SO_4 at 70 ± 2°						15% Solution HCl at 70 ± 2°	
	concentrations of bases and KSCH respectively (%)							
	0.2 & 0.02		0.2 & 0.2		0.4 & 0.4		0.8 & 0.2	
	γ	ρ	γ	ρ	γ	ρ	γ	ρ
230—240	8	$9.7 \cdot 10^{-4}$	—	—	34.4	$16.6 \cdot 10^{-5}$	1.04	$27.9 \cdot 10^{-3}$
240—260	10	$7.8 \cdot 10^{-4}$	14	$5.5 \cdot 10^{-4}$	47.5	$12 \cdot 10^{-5}$	1.7	$15.1 \cdot 10^{-3}$
260—280	16	$4.3 \cdot 10^{-4}$	34	$2.3 \cdot 10^{-4}$	46.7	$12.2 \cdot 10^{-5}$	9.02	$3.2 \cdot 10^{-3}$
280—300	28	$2.18 \cdot 10^{-4}$	37	$2.1 \cdot 10^{-4}$	85	$6.7 \cdot 10^{-5}$	20.7	$1.4 \cdot 10^{-3}$
300—320	25	$3.1 \cdot 10^{-4}$	41	$1.9 \cdot 10^{-4}$	50.5	$11.3 \cdot 10^{-5}$	10.1	$2.8 \cdot 10^{-3}$
320—330	20	$3.9 \cdot 10^{-4}$	31	$2.5 \cdot 10^{-4}$	44	$16.6 \cdot 10^{-5}$	4.7	$6.1 \cdot 10^{-3}$
330—345	18	$4.3 \cdot 10^{-4}$	38	$2.04 \cdot 10^{-4}$	48	$12.0 \cdot 10^{-5}$	3.6	$7.9 \cdot 10^{-3}$
345—360	23	$3.4 \cdot 10^{-4}$	40	$1.94 \cdot 10^{-4}$	62	$9.2 \cdot 10^{-5}$	9.8	$2.9 \cdot 10^{-3}$
		$\rho_0 = 7.8 \cdot 10^{-3}$						$\rho_0 = 29 \cdot 10^{-3}$

Acridine, which has low activity at room temperature, accelerates dissolution at higher temperatures. This is in all probability because it can be reduced to dihydroacridine by the liberated hydrogen. It should therefore be removed from the fractions to be used in pickling.

The results (Table 2) lead to the practical conclusion that, because of their low activity in sulfuric acid on heating, the bases are not suitable as pickling inhibitors.

In the next stage of this investigation we attempted to find means for increasing the inhibitor activity of the bases in sulfuric acid. As acridine forms complex compounds with iron salts and thiocyanates [5], pickling tests were performed in presence of small amounts of KSCN, and it was found that addition of only 0.02% KSCN sharply increases the activity of the bases in sulfuric acid at 70° (Table 3, Fig. 2). In absence of bases the inhibitor activity of KSCN is low (γ = 3-4).

With increased amounts of KSCN and bases it is possible to obtain very high values of the inhibitor effect, up to 85 in some cases. The inhibitor activity varies regularly with the boiling temperatures of the bases in this case also – the highest activity is found in the fraction boiling at 280-300°. The action of KSCN is weaker in hydrochloric acid.

TABLE 4

Pickling Tests on Various Steels in 12% H_2SO_4 at 70° in Presence of 0.2% of the 280-300° Fraction

Steels	Without KSCN		With KSCN 0.02%	
	ρ	γ	ρ	γ
No. 3 steel	$5.46 \cdot 10^{-3}$	1.05	$1.86 \cdot 10^{-4}$	29.6
ShKh-15 steel	$3.04 \cdot 10^{-2}$	2.09	$2.42 \cdot 10^{-3}$	26.2
18-NVA steel	$1.4 \cdot 10^{-1}$	1.06	$3.9 \cdot 10^{-3}$	38.5
Steel of the composition (%)C 0.5, Mn 0.6, Si 1.5	$1.22 \cdot 10^{-1}$	1.5	$8.8 \cdot 10^{-3}$	21.5
No. 40 steel	$15 \cdot 10^{-1}$	1.3	$6.5 \cdot 10^{-3}$	32
30KhSa steel	$8.3 \cdot 10^{-2}$	2.2	$1.3 \cdot 10^{-3}$	14.6
Cast iron	$1.22 \cdot 10^{-1}$	2.6	$1.27 \cdot 10^{-2}$	25.4

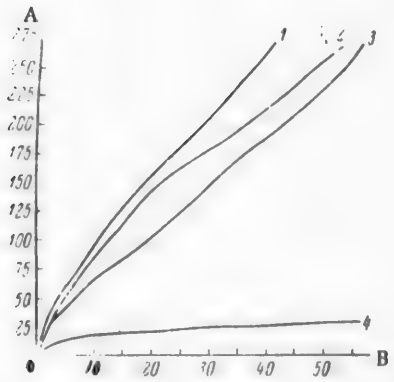

Fig. 2. Effect of additions of KSCN on the inhibitor activity of bases. A) Amount of hydrogen liberated (in ml/100 cc), B) time (minutes). Pickling in presence of (%): 1) without inhibitor, 2) 0.2 of 250-270° fraction, 3) 0.2 of KSCN, 4) 0.2 of KSCN and 0.2 of 250-270° fraction.

The activities of the bases in presence of KSCN were tested for different steels (Table 4).

The bases in presence of KSCN proved to be very active inhibitors for all the steels tested. This mixed additive is more active than the additives used at present: KS,* ChM,* and brewery wastes, which give inhibitor effects (γ) of 10-12.

With the addition of 2 g of bases and 0.2 g of thiocyanates per liter to the pickling liquor, an inhibitor effect (γ) of 25-28 can be obtained for No. 3 steel. Increase of the thiocyanate content to 2 g/liter, with the same base content, increases the activity to γ = 38-41. If the liquor contains bases and 4 g/liter of thiocyanates, the inhibitor activity reaches 85 for some fractions. They also have a number of other advantages: they are completely soluble in the pickling liquor, they do not form a sludge on the metal surface, no additional treatment is required before their use, the pickling can be performed at 70-80°, and a thin transparent film remains after the pickling on the metal surface and protects it for a long time against corrosion; if necessary, this film can be removed by hot water.

It follows from the foregoing that bases, in conjunction with thiocyanates, can be used as effective pickling inhibitors for ferrous metals. The losses of metal in pickling can be very much reduced, and the consumption of acid decreased, with their use.

LITERATURE CITED

[1] Japanese Patent 3607; U.S. Patent 2, 449, 283.

[2] V. A. Kuznetsov and Z. A. Iofa, J. Phys. Chem. 21, 201 (1947); V. S. Samoilov, J. Moscow State Univ. 1, 105 (1946); N. Hackerman and A. C. Marrides, Ind. Eng. Ch., 3, 523 (1954).

[3] Z. A. Iofa, E. I. Liakhovskaia and K. Sharifov, Proc. Acad. Sci. USSR 84, 3, 543 (1952).

[4] E. O. Aiazian, Proc. Acad. Sci. USSR 100, 3, 473 (1955).

[5] A. Albert, The Acridines (E. Arnold, London, 1951).

*Transliteration of Russian – Publisher's note.

Received July 13, 1956

VINYL COMPOUNDS OF SILICON

M. F. Shostakovskii and D. A. Kochkin

There have been great advances in the chemistry of vinyl compounds as the result of outstanding work by Russian and foreign scientists. The researches of A. M. Butlerov, A. E. Favorskii and A. P. El'tekov laid the foundations of the successful development of the chemistry of these compounds.

There has been much interest in recent years in vinyl ethers of the type $CH_2 = CHOAlk$ and $CH_2 = CHOAr$, thiovinyl ether $CH_2 = CHSR$, vinylpyrrolidone $CH_2 = CHN\langle CO, (CH_2)_3 \rangle$, vinylcaprolactam $CH_2 = CHN\langle CO, (CH_2)_5 \rangle$, and vinyl alkyl chlorosilanes $(CH_2 = CH)_nR_mSiCl_{4-n-m}$, i.e., compounds prepared by the method of A. E. Favorskii and M. F. Shostakovskii, based on reactions of acetylene with alcohols (1), mercaptans (2), pyrrolidone and caprolactam (5), dialkyl halosilanes (7) (see the vinylation reactions below).

Vinylation reactions

$$CH{\equiv}CH + ROH \longrightarrow CH_2{=}CHOR, \quad (1)$$

$$CH{\equiv}CH + RSH \longrightarrow CH_2{=}CHSR, \quad (2)$$

$$CH{\equiv}CH + OH(CH_2)_nOH \longrightarrow CH_2{=}CHO(CH_2)_nOCH{=}CH_2, \quad (3)$$

$$CH{\equiv}CH + OHCH_2CH_2NH_2 \longrightarrow CH_2{=}CHOCH_2CH_2NH_2, \quad (4)$$

$$CH{\equiv}CH + NH\langle CO, (CH_2)_n \rangle \longrightarrow CH_2{=}CH{-}N\langle CO, (CH_2)_n \rangle, \quad (5)$$

$$CH{\equiv}CH + HOCOR \longrightarrow CH_2{=}CH{-}OCOR, \quad (6)$$

$$CH{\equiv}CH + RSiHX_2 \longrightarrow CH_2{=}CHSiRX_2, \quad (7)$$

where X=Cl, Br etc.

$$CH{\equiv}CH + R_3SiH \longrightarrow CH_2{=}CHSiR_3, \quad (8)$$

$$CH{\equiv}CH + HO(CH_2)_nSiR_3 \longrightarrow CH_2{=}CHO(CH_2)_nSiR_3. \quad (9)$$

Vinyl compounds and their derivatives are used for the production of compounds of high molecular weight, which are valuable for practical purposes. These substances include the medicinal preparation "Shostakovskii's balsam," polyvinylpyrrolidone (PVP) used as a blood plasma substitute, the insectofungicide M-74, etc.

Vinyl compounds of silicon form a class of polymerizing organosilicon compounds which have been studied little, but are highly promising. They have the structure $(CH_2 = CH)_nSiR_{4-n}$, where $n < 4$, and R is an alkyl or aryl group, halogen, NH_2, OH, etc.

This paper contains the results obtained by the present authors, and certain literature data on the methods of preparation and the properties of a number of vinyl compounds of silicon.

Methods of preparation of vinyl silanes. In 1937, Ushakov and Itenberg [1] synthesized, for the first time, vinyltriethylsilane; this did not polymerize in presence of benzoyl peroxide even on prolonged heating. In 1945, Hurd developed a method for the preparation of allyl chlorosilanes, by the passage of allyl chloride over a contact

mass of silicon and copper (90 : 10) [2]. When vinyl chloride was used, vinyl chlorosilanes were obtained in very low yields.

We studied the reaction of vinyl chloride with silicon–copper (50 : 50) or silicon–nickel (85 : 15) alloys [3]. It was found that this method gives more satisfactory results. It must be noted that the yields of vinyltrichlorosilane (11) and divinyldichlorosilane (11) are low, and do not exceed 20–35% of the theoretical. However, in our opinion the direct synthesis of vinyl halosilanes is the most promising method, and requires further development.

The products in the synthesis of vinyl chlorosilanes also contain ethyltrichlorosilane (14) and ethyldichlorosilane (15), the formation of which may be attributed to hydrogenation of the corresponding vinyl silanes. Hydrogen is formed as the result of pyrolysis of the reaction products and the original vinyl chloride. The considerable content of ethyltrichlorosilane indicates extensive pyrolysis of the original vinyl chloride and of the reaction products.

$$2CH_2{=}CHCl + Si \longrightarrow (CH_2{=}CH)_2SiCl_2, \quad (10)$$

$$3CH_2{=}CHCl + Si \longrightarrow CH_2{=}CHSiCl_3 + 4C + 3H_2, \quad (11)$$

$$3CH_2{=}CHCl + 2Si \longrightarrow CH_2{=}CHSiHCl_2 + CH_2{=}CHSiH_2Cl + 2C, \quad (12)$$

$$4CH_2{=}CHCl + Si \longrightarrow SiCl_4 + 8C + 6H_2, \quad (13)$$

$$CH_2{=}CHSiCl_3 + H_2 \longrightarrow CH_3CH_2SiCl_3, \quad (14)$$

$$CH_2{=}CHSiHCl_2 + H_2 \longrightarrow CH_3CH_2SiHCl_2. \quad (15)$$

Other methods for the preparation of vinyl compounds include: 1) synthesis of unsaturated silicon compounds based on the reactions of organic magnesium compounds [2,4-6], or on interactions of vinyl chloride with alkyl (aryl) halosilanes in presence of metallic sodium [7, 8] etc.; 2) dehydrochlorination of chloroalkyl silanes.

This last method was used for the first preparation of vinyltriethylsilane [1]

$$(C_2H_5)_3SiCHClCH_3 \xrightarrow[\text{Alcoholic alkali}]{-HCl} (C_2H_5)_3SiCH{=}CH_2, \quad (16)$$

and for the preparation of vinyltrichlorosilane [2, 9]

$$CH_2ClCH_2SiCl_3 \xrightarrow[\substack{\text{quinoline}\\ AlCl_3\text{ etc.}}]{-HCl} CH_2{=}CHSiCl_3. \quad (17)$$

We shall not describe these methods in detail, but merely note that they have various important disadvantages which make them unsuitable for the preparation of such compounds as vinylmethyldichlorosilane, etc.

A very promising method for the synthesis of vinyl compounds is vinylation of hydrogen-containing alkyl (aryl) halosilanes or alkyl (aryl) silanes, effected by interaction of these compounds with acetylene [10-15] and its derivatives.

The literature data on this reaction have until now been very scanty. Burkhard and Krieble [10] reported that acetylene and its homologs can be added on to trichlorosilane in presence of peroxide catalysts. In a recent patent [11] it is noted that acetylene can react with certain hydrogen-containing halosilanes in presence of platinum on carbon. However, the yields, nature of the compounds formed, and reaction conditions are not given.

The present authors found, jointly with Vinogradov, that vinylation is best effected by the interaction of acetylene with the appropriate alkyl(aryl) halosilanes in presence of catalysts of the platinum – palladium groups (the metals, acids, salts) at 130-170° [12-15].

The alkyl dichlorosilanes CH_3SiHCl_2 and $C_2H_5SiHCl_2$ are now quite readily available commercially. They are prepared by the passage of the corresponding alkyl (aryl) halides through silicon [16]. Other hydrogen-containing organosilicon compounds can be recommended as the starting materials, for example, various alkyl (aryl) silanes R_nSiH_{4-n}, siloxanes $R_2Si(H)-O-Si(H)R_2$, silylamines $R_2-Si(H)-NH-Si(H)R_2$ [2], alkoxysilanes [15], and others containing active hydrogen atoms.

The reactions of acetylene with chlorosilanes may be represented by the following equations:

$$RSiHX_2 + CH{\equiv}CH \longrightarrow R(CH{=}CH_2)SiX_2, \quad (18)$$

$$RSiH_2X + 2CH{\equiv}CH \longrightarrow R(CH_2{=}CH)_2SiX, \quad (19)$$

$$SiH_3X + 3CH{\equiv}CH \longrightarrow (CH_2{=}CH)_3SiX, \quad (20)$$

$$HSiX_3 + CH{\equiv}CH \longrightarrow (CH_2{=}CH)SiX_3, \quad (21)$$

$$H_2SiX_2 + 2CH{\equiv}CH \longrightarrow (CH_2{=}CH)_2SiX_2 \quad (22)$$

or by the general equation:

$$H_nSiR_{4-n} + nCH{\equiv}CH \longrightarrow (CH_2{=}CH)_nSiR_{4-n}, \quad (23)$$

where R is alkyl, aryl, or halogen; $n < 4$.

It is thus possible to prepare various organosilicon compounds containing several vinyl groups. In addition to the products indicated, various telomeric compounds are formed, the formation of which can be represented as follows:

$$\begin{array}{l} R{-}SiCl_2{-}CH{=}CH_2 + H{-}SiCl_2{-}R \longrightarrow R{-}SiCl_2{-}CH_2{-}CH_2{-}SiCl_2{-}R, \end{array} \quad (24)$$

$$R{-}SiCl_2{-}CH{=}CH_2 + CH{\equiv}CH \longrightarrow R{-}SiCl_2{-}CH{=}CH{-}CH{=}CH_2, \quad (25)$$

$$R{-}SiCl_2{-}CH{=}CH{-}CH{=}CH_2 + H{-}SiCl_2{-}R \longrightarrow R{-}SiCl_2{-}CH{=}CH{-}CH_2{-}CH_2{-}SiCl_2{-}R \quad (26)$$

or

$$R{-}SiCl_2{-}CH{=}CH{-}CH{=}CH_2 + H{-}SiCl_2{-}R \longrightarrow R{-}SiCl_2{-}CH_2{-}CH{=}CH{-}CH_2{-}SiCl_2{-}R \quad (27)$$

$$R{-}SiCl_2{-}CH_2{-}CH_2{-}CH{=}CH{-}SiCl_2{-}Cl + CH{\equiv}CH \longrightarrow R{-}SiCl_2{-}CH_2{-}CH_2{-}CH{=}C(SiCl_2{-}Cl){-}CH{=}CH_2 \quad (28)$$

(R in the SiCl$_2$ groups)

etc.

The vinylation may be performed by various methods: 1) in an autoclave (under pressure); 2) in a flow system under atmospheric pressure; 3) in a flow system under increased pressures.

Vinylation in an autoclave is a quite suitable method for the preparation of vinyl halosilanes; it is carried out at 20-30 atmos [12-15]. A stainless-steel autoclave, 0.5 liter in capacity, is charged with the alkyl dichlorosilane and palladium catalyst on aluminum oxide (0.5-0.8 % by weight) containing 0.5% palladium; acetylene is then passed in. The autoclave is rotated and heated to 170-200° for 2-3 hours; the reaction is completed in this time. The reaction products are distilled through a rectification column. The reaction mixture contains up to 30-40% vinyl alkyl halosilanes. The disadvantages of the process are its batch character and the necessity of using increased pressures.

Continuous vinylation by the contact method under atmospheric pressure is effected in an electrically heated stainless-steel tube, a mixture of acetylene and halosilanes being passed over the catalyst at 300-360° [13]. The reaction products contain up to 40-50% vinyl halosilanes. One disadvantage of this method is rapid poisoning of the catalyst; its service life is 2-3 hours.

It is probably more efficient to carry out the vinylation of alkyl halosilanes in fluidization equipment or in a continuous unit under slight excess pressure.

Work on the development of a more consistent process is continuing.

Physical properties of vinyl silanes. Vinyl silanes are mobile liquids which distill without decomposition. They fume in the air, are readily hydrolyzed with liberation of hydrogen halides, and are soluble in ether, benzene, and other organic solvents. Vinyl alkoxy or aryloxy silanes are colorless, mobile liquids with an ethereal odor; they distill without decomposition only in vacuum. Vinyl alkyl or aryl halosilanes are colorless liquids with a sharp odor, readily soluble in the common organic solvents.

Chemical properties. Apart from their practical interest, vinyl silanes are of considerable interest in relation to studies of the influence of the silicon atom on the properties of a compound containing a double bond directly linked to silicon in the α position. Such compounds are highly reactive, but in a number of instances they differ in properties from vinyl compounds of carbon. Thus, vinyl chlorosilanes do not polymerize when heated in presence of peroxide catalysts, do not copolymerize with a number of vinyl compounds such as vinylcaprolactam, vinyl butyl ether, etc.

The properties of vinyl compounds of silicon have not been studied sufficiently. Certain reactions of vinyl silanes are given below.

Certain reactions of vinyl compounds of silicon

Alcoholysis [17, 18]

$$CH_2{=}CHSiCl_3 + 3CH_2{=}CHCH_2OH \longrightarrow CH_2{=}CHSi(OCH_2CH{=}CH_2)_3. \quad (29)$$

Halogenation

$$CH_2{=}CHSi(OC_2H_5)_3 + Br_2 \xrightarrow{\text{diethylamine}} CH_2{=}CBrSi(OC_2H_5)_3 + HBr\ [18], \quad (30)$$

$$CH_2{=}CBrSi(OC_2H_5)_3 + Br_2 \longrightarrow CH_2Br{-}CBr_2(OC_2H_5)_3; \quad (31)$$

gas-phase chlorination

$$CH_2{=}CHSiCl_3 + Cl_2 \xrightarrow{100-250^\circ} CH_2Cl{-}CHClSiCl_3, \quad (32)$$

$$CH_2{=}CHSiCl_3 + Cl_2 \xrightarrow{200-350^\circ} CH_2{=}CClSiCl_3 + HCl, \quad (33)$$

$$CH_2{=}CHSiCl_3 + Cl_2 \xrightarrow{300-400^\circ} SiCl_4 + \text{decomposition products}\ [9]. \quad (34)$$

Hydrohalogenation

$$CH_2{=}CHSiCl_3 + HCl \underset{\longleftarrow}{\overset{AlCl_3}{\rightleftharpoons}} CH_2ClCH_2SiCl_3\ [9]. \quad (35)$$

$$CH_2{=}CHSi(CH_3)_3 + HBr(I) \xrightarrow{\text{peroxide}} CH_2Br(I)CH_2Si(CH_3)_3;^{\bullet} \quad (36)$$

but

$$CH_2{=}\underset{\displaystyle CH_3}{\overset{\displaystyle |}{C}}Si(CH_3)_3 + HCl \longrightarrow CH_3{-}\underset{\displaystyle CH_3}{\overset{\displaystyle Cl}{\overset{\displaystyle |}{\underset{\displaystyle |}{C}}}}{-}Si(CH_3)_3\ [19,20],^{\bullet\bullet} \quad (37)$$

$$CH_2{=}CHCH_2CH_2Si(CH_3)_3 + HBr \xrightarrow{\text{peroxide}} CH_2BrCH_2CH_2CH_2Si(CH_3)_3\ [21]^{\bullet} \quad (38)$$

$$\searrow$$

$$CH_3CHBrCH_2CH_2Si(CH_3)_3\ [19].^{\bullet\bullet} \quad (39)$$

Interaction with oxides

$$CH_2{=}CHSiCl_3 + 3CH_2{-}CH_2 \longrightarrow CH_2{=}CHSi(OCH_2CH_2Cl)_3\ [22], \quad (40)$$

$$\diagdown\diagup$$

$$O$$

•Addition contrary to the Markovnikov rule.

••Addition in accordance with the Markovnikov rule.

$$CH_2{=}CHSiCl_3 + 3CH_2{-}CHR \;(\text{O}) \rightarrow \begin{cases} CH_2{=}CHSi(OCH_2CHClR)_3 \\ CH_2{=}CHSi\left(OCH\begin{matrix}CH_2Cl\\CH_3\end{matrix}\right)_3 \end{cases}$$ [23]. (41)

Hydrolysis

$$(CH_2{=}CH)_{4-n}SiX_n + nH_2O \rightarrow (CH_2{=}CH)_{4-n}Si(OH)_n + nHCl, \quad (42)$$

a) $-Si(CH{=}CH_2)_2-O-Si(CH{=}CH_2)_2-O-$, b) $-Si(O)_2-O-Si(O)_2-O-$,

в) $(CH_2{=}CH)_3Si-O-Si(CH{=}CH_2)_3$.

Acidolysis

$$(CH_2{=}CH)_2SiCl_2 \xrightarrow{Ac_2O} (CH_2{=}CH)_2Si(OAc)_2 \xrightarrow{H_2O} (CH_2{=}CH)_2Si(OH)_2$$ [24]. (43)

Ozonolysis [20]

$$CH_2{=}CHSi(CH_3)_3 + O_3 \rightarrow (CH_3)_3SiCH(O_3)-CH_2 \xrightarrow[Zn]{H_2O} \quad (44)$$

$$\rightarrow CH_2O + (CH_3)_3SiCHO \xrightarrow{H_2O} (CH_3)_3SiOH + HCHO.$$

Interaction with aldehydes [20]

$$CH_2{=}CHSi(CH_3)_3 + C_3H_7CHO \xrightarrow{\text{peroxide}} (CH_3)_3SiCH_2CH_2COC_3H_7. \quad (45)$$

Addition of dialkyldithiophosphoric acids [25]

$$CH_2{=}CHSi(C_2H_5)_3 + HSP(S)(OR)_2 \rightarrow (C_2H_5)_3SiCH_2CH_2SP(S)(OR)_2. \quad (46)$$

Acetal formation

$$CH_2{=}CHO(CH_2)_nSiR_3 + R'OH \rightarrow CH_3CH(OR')[O(CH_2)_nSiR_3]$$ [26]. (47)

$$CH_2{=}CHO(CH_2)_nSiR_3 + HO(CH_2)_nSiR_3 \rightarrow CH_3CH[O(CH_2)_nSiR_3]_2$$ [26,27]. (48)

Addition of thiocyanogen [28]

$$CH_2{=}CHSi(C_2H_5)_3 + (CNS)_2 \rightarrow (C_2H_5)_3SiCH(CNS)CH_2(CNS). \quad (49)$$

Friedel–Crafts reaction [9]

$$CH_2{=}CHSiCl_3 + C_6H_6 \xrightarrow{AlCl_3} C_6H_5CH_2CH_2SiCl_3 \quad (50)$$

with formation of a side product

$$CH_2{=}CHSiCl_3 + C_6H_6 \xrightarrow{AlCl_3} (Cl_3SiCH_2CH_2)_2C_6H_4. \quad (51)$$

Diels–Alder reaction (diene synthesis [9]

$$CH_2{=}CHSiCl_3 + CH{=}CH-CH{=}CH_2 \xrightarrow{30-70^\circ} C_6H_9SiCl_3, \quad (52)$$

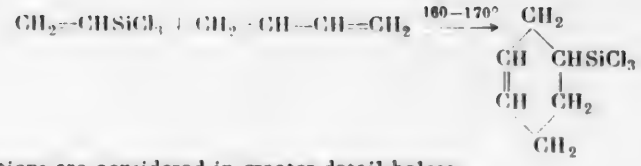

(53)

Some of these reactions are considered in greater detail below.

Reactions with alcohols. Vinyl halosilanes react with alcohols analogously to saturated halosilanes, with formation of the corresponding vinyl alkoxy or aryloxy silanes. The reaction was studied by Nagel and Post [18], and may be a convenient preparative method.

Halogenation of vinyl silanes. Liquid-phase chlorination of vinyltrichlorosilane is readily effected at 30-50° with formation of 1,2-dichloroethyltrichlorosilane [9, 17]. However, the reaction is accompanied by the formation of side products, such as di(trichlorosilyl)-dichlorobutane [9]. The chlorination of vinyltrichlorosilane in silicon tetrachloride is almost quantitative.

The course of the gas-phase chlorination of vinyltrichlorosilane varies with the temperature [9] (32, 33 and 34). At 100-250° chlorine is added on, with formation of 1,2-dichloroethyltrichlorosilane.

When vinyltrichlorosilane is chlorinated attemperatures above 200°, no addition of chlorine takes place, but a hydrogen atom in the vinyl group is replaced by chlorine.

Bromination of vinyltrichlorosilane proceeds very slowly, especially at room temperature [9]. On the other hand, the bromination of triethoxysilane proceeds more rapidly [18]. This fact is used for determinations of the degree of unsaturation of compounds of this type [9].

Hydrohalogenation. Hydrogen chloride is added on to vinyltrichlorosilane at the boiling point in presence of aluminum chloride, with formation of β-chloroethyltrichlorosilane [9]. This reaction is reversible, and does not go to completion. It must be noted that the reverse reaction (dehydrochlorination) can be used as a method for the preparation of vinyltrichlorosilane. Hydrogen bromide adds on to vinyltrimethylsilane in presence of peroxide catalysts almost quantitatively, even at room temperature, with formation of β-bromoethyltrimethylsilane

$$CH_2{=}CHSi(CH_3)_3 + HBr \xrightarrow{\text{peroxide}} CH_2BrCH_2Si(CH_3)_3.$$

Thus, the addition of hydrogen halide to α-vinyl compounds of silicon is contrary to the Markovnikov rule; this shows that the vinyl group at the silicon atom is of a special character. At the same time, it is known that β- and γ-vinyl compounds, and compounds with the double bond in an even more distant position, combine with hydrogen halides in conformity with the rule. It is true that it was recently shown that hydrogen bromide can be added to $(CH_3)_3SiCH_2CH_2CH = CH_2$) both according to [19] and contrary to the Markovnikov rule (in presence of peroxide) [21]. All this shows that the manner of addition of hydrogen halides to vinyl compounds is not finally settled. In our opinion, addition of hydrogen halides to α-vinyl compounds can also proceed in accordance with the Markovnikov rule; this depends on their structure and the reaction conditions.

On the other hand, the addition of hydrogen halides to unsaturated organosilicon compounds is a vivid example of the mutual influence of atoms on the properties of a chemical compound. Thus, the presence of methyl substituents in the molecules of vinyl compounds has a considerable influence on the activity of alkenyl silanes. Isopropenyltrimethylsilane $(CH_3)_3SiC(CH_3) = CH_2$ does not react with gaseous hydrogen chloride at any appreciable rate, while with concentrated hydrochloric acid it reacts according to the Markovnikov rule [20]. Petrov et al. [19, 20] showed that the addition of hydrogen bromide to isopropenyltrimethylsilane also conforms to the rule. Thus, the influence of the α-vinyl group at the silicon atom on the properties of silicon is overcome by the introduction of a substituent α-methyl group. The properties of the compound were greatly changed in this case.

The β effect. Mention must be made in this connection of an interesting effect in silicon chemistry, known as the β effect, or β-elimination. It has been found that compounds containing halogen, carbonyl, and other atoms or groups at the β-carbon atom linked to silicon decompose under the action of dilute alkalies or on gentle heating

$$(CH_3)_3SiCH_2CH_2X \xrightarrow{OH^-} (CH_3)_3SiOH + CH_2{=}CH_2 + X^-.$$

This process is known as the β effect. Several investigations deal with the decomposition of organosilicon β-halides [1, 4, 20, 29].

Ozonolysis. Vinyltrichlorosilane reacts with ozone to form ozonides [20]. The ozonides are unstable and readily decompose with formation of siloxanes. The instability of these ozonides is another example of the decomposition of silicon compounds containing β-carbonyl groups.

Polymerization. The polymerizability of vinyl compounds has been studied very little as yet. There are a few recent brief and disconnected papers, dealing mainly with the polymerization of vinyl alkoxysilanes [9, 30, 31] or unsaturated siliconhydrocarbons [32-34]. However, the available data suggest that the polymerization tendency of vinyl halosilanes and vinyl silanes is low. Uhsakov and Itenberg did not succeed in polymerizing vinyltriethylsilane [1]. In 1954, Petrov, Poliakova, Korshak, et al. [32] polymerized the same compound under a pressure of 5500 atmos in presence of tertiary butyl peroxide at 130° for 6 hours, and obtained substances of low molecular weight (mol. wt. 1109). The compounds $(CH_3)_3SiCH = CHCH_3$ and $(CH_3)_3SiCH = C(CH_3) - CH_3$ do not polymerize even under high pressures. These workers studied the polymerization and copolymerization of various alkenyl silanes under 5000 atmos at 130°. It was found that, in presence of tertiary butyl peroxide, monoalkenyl silanes polymerize to give compounds of low molecular weight (dimers, and even hexamers), which are liquid polymers. Polyalkenyl-3-silanes, tetraallylsilanes, and tetraisobutenylsilanes polymerize under these conditions to give space polymers decomposing above 200°.

Wagner and Bailey in 1953 [9], and Mixer and Bailey in 1955 [30], found that vinyl compounds of the general structure $CH_2 = CHSiR_n(OC_2H_5)_{3-n}$ or $CH_2 = CHSiR_nCl_{3-n}$, where R = CH_3, C_2H_5, and n = 0, 1, 2, 3, either do not polymerize, or form copolymers of relatively low molecular weight. Only vinyltriethoxysilane polymerizes, in presence of di-tert butyl peroxide catalyst, to form transparent colorless liquid polymers of molecular weight 3000-8000. Wagner, Bailey, et al. found that vinyltrichlorosilane polymerizes under moderate pressures to low-molecular products, consisting mainly of tetramers. These polymers can be formed in presence of catalyst, or in its absence at 290°, and contain the structural unit $-CH_2-CH(SiCl_3)-$.

High pressures (about 3000 kg / cm^2) have little effect in increasing the molecular weight of the product. However, the reaction rate is considerably increased, and the temperature required for the formation of the product is lower. Wagner, Bailey et al. showed that polymers of high molecular weight are not formed in presence of peroxides, aluminum chloride, ferrous chloride, zinc chloride, boron tetrachloride or iodine catalyst.

It was recently reported that hydrogen-containing vinyl silanes and vinyl halosilanes can be polymerized by the action of heat in presence of platinum on carbon. Polymers of low molecular weight were obtained [35].

Copolymerization. It was first shown by Hurd and Roedel in 1948 [36] that mixtures of alkenyl siloxanes condensed with alkyl or aryl siloxanes have considerable heat resistance and rapid "hardening" properties. Thus, a silicone rubber containing even a small amount of vinyl groups is hardened (vulcanized) much more rapidly than silicone rubber containing saturated radicals only.

Vinyl silicone rubber is usually made by the addition of methylvinyldichlorosilane and divinyldichlorosilane (1%) to dimethyldichlorosilane. The chlorosilane mixture is then hydrolyzed and condensed to yield a linear polysiloxane of high molecular weight; its vinyl group content reaches 1%. This resinous material is mixed with fillers and vulcanization agents and heated to 150-200°. After being cured for 24 hours at 200°, the rubber has tensile strength up to 46-58 kg/cm^2, elongation up to 40%, and Shore hardness 82 kg/mm [36].

Methylvinyl polysiloxane polymers were also prepared by Hurd and Roedel by the mixing of vinyl monomers and methylvinyl polysiloxanes formed by the hydrolysis of methylvinyldichlorosilane. The polymerization catalysts were benzoyl peroxide or tertiary butyl perbenzoate (0.5-1%). The polymerization was continued for 18-24 hours at 80 and 100° (with tertiary butyl perbenzoate), and for 18-24 hours at 60, 80, and 100° in presence of benzoyl peroxide.

Alkenyl and alkyl siloxanes can copolymerize with vinyl monomers. The methyl methacrylate copolymer

has good electrical insulating properties, and ages rapidly only at 175°. Copolymers of methylvinyl polysiloxanes with diethyl and diallyl phthalates are plastic substances which harden after additional polymerization at 125°. The copolymer formed with butyl methacrylate was colorless, dense, and hard [36]. The same workers showed that copolymerization with acrylonitrile was rapid, and the products were transparent, hard, and brittle. Further heating at 125° led to surface cracking and darkening of the material.

The properties of copolymers of methylvinyl polysiloxanes with styrene or dichlorostyrene greatly depended on the component ratios and the amount of catalyst. In presence of benzoyl peroxide, with a considerable methylvinyl polysiloxane content, the copolymerization products were soft and plastic. If styrene or dichlorostyrene predominated in the mixture, hard and strong thermoplastic materials were formed.

Later, in 1953, Wagner, Bailey et al. [9] also showed that vinyl polysiloxanes obtained by the hydrolysis of vinyltrichlorosilane in ether compolymerize with other vinyl monomers, such as styrene, vinyl acetate, etc. These copolymers have good electrical insulating properties. Vinyl polysiloxanes are also suitable for use as compounds which confer a space structure to polymers in conjunction with alkyl resins [9]. It has been reported that the strength of polyacrylate laminated plastics is increased by treatment of the glass fabric base with vinyl polysiloxanes [9]. In a number of cases it is possible to use siloxane copolymers from the hydrolysis products of vinyltrichlorosilane and other alkyl or aryl trichlorosilanes: phenyl, ethyl, or cyclohexylalkyl trichlorosilanes. Wagner, Bailey, et al. [9] consider that these copolymers have a cyclotrisiloxane or cyclotetrasiloxane structure.

Korshak, Petrov, Matveeva, Mironov, Nikishin, and Sadykh-Zade [33] studied the copolymerization of methyl methacrylate with silicohydrocarbons containing vinyl groups in different positions. It was found that these alkenyl silanes can yield copolymers with methyl methacrylate, soluble in organic solvents. Thus, dimethyldimethallyl- and methyldiallylsilane formed linear polymers. Tributylallylsilane does not copolymerize with methyl methacrylate. Only tetramethallylsilane gave rise to space polymers insoluble in organic solvents. In a subsequent study [34] the copolymerization of mono- and dialkenyl silanes with methyl methacrylate was studied in greater detail, and with a large number of compounds, both at high pressures (5500 atmos) and under atmospheric pressure. It was shown that the copolymerization products formed at high pressure contained small amounts of insoluble cross-linked polymer. The content of this polymer increased with the relative proportion of the silane in the reaction mixture, and with the copolymerization time. The polymers formed at high pressures had higher viscosity than those obtained under atmospheric pressure. These authors confirmed the findings of Wagner and Bailey, for the polymerization of vinyltrichlorosilane, that pressure has a favorable effect on the polymerization rate of alkenyl silanes and on the molecular weight of the polymers formed.

We studied, jointly with F. P. Sidel'kovskaia and V. A. Neterman, the possibility of copolymerization of vinyltrichloro- and vinylalkyldichlorosilanes with monomers such as vinyl butyl ether, vinylcaprolactam, and vinylpyrrolidone in presence of peroxide catalysts and azobisizobutyronitrile. It was found that vinyltrichloro- and vinylalkyldichlorosilanes do not copolymerize with vinyl butyl ether or vinylcaprolactam. Polymers were obtained only with vinylpyrrolidone; these were probably copolymers. Vinyl chlorosilanes act as ionic catalysts in the polymerization of vinyl butyl ether and vinylcaprolactam.

The chemistry of vinyl organosilicon compounds has not been sufficiently studied as yet. These compounds are very promising for the production of various new monomers and polymers with definite properties required for practical purposes.

The vinyl compounds of silicon constitute a new branch of the chemistry of silicon and its organic derivatives.

LITERATURE CITED

[1] S. N. Uhsakov and A. M. Itenberg, J. Gen. Chem. 7, 2495 (1937).

[2] D. T. Hurd, J. Am. Chem. Soc., 67, 1813 (1945).

[3] M. F. Shostakovskii and D. A. Kochkin, Bull. Acad. Sci. USSR, Div. Chem. Sci. 174 (1954);* M. F. Shostakovskii, E. M. Savitskii, D. A. Kochkin and L. V. Musatova, Bull. Acad. Sci. USSR, Div. Chem. Sci. 1493 (1957).*

[4] L. H. Sommer, D. L. Bailey, G. M. Goldberg, C. F. Buck, T. S. Bye, F. I. Evans and F. C. Whitmore, J. Am. Chem. Soc. 6, 1613 (1954); S. D. Rosenberg, I. I. Walburn, T. D. Stankovich et al. J, Org. Chem. 22, 1200 (1957).

*Original Russian pagination. See C.B. translation.

[5] A. D. Petrov and V. F. Mironov, Bull. Acad. Sci. USSR, Div. Chem. Sci. 1491 (1957).*

[6] K. A. Andrianov and M. Kamenskaia, J. Gen. Chem. 8, 969 (1938).

[7] M. Kanazashi, Bull. Chem. Soc. Japan, 26, 493 (1953).

[8] A. D. Petrov, V. F. Mironov and V. G. Glukhovtsev, Bull. Acad. Sci. USSR, Div. Chem. Sci. 461 (1956).*

[9] G. H. Wagner, D. L. Bailey, A. N. Pines, M. L. Dunham and D. B. McIntire, Ind. Eng. Chem. 45, 367 (1953).

[10] C. A. Burkhard and R. H. Krieble, J. Am. Chem. Soc. 69, 2687 (1947); C. A. Burkhard, J. Am. Chem. Soc. 72, 1402 (1950).

[11] G. H. Wagner, U.S. Patent 2, 637, 738 (1953); Chem. Abs. 48, 8254 (1954).

[12] M. F. Shostakovskii and D. A. Kochkin, Proc. Acad. Sci. USSR 109, 113 (1956).*

[13] M. F. Shostakovskii and D. A. Kochkin, Bull. Acad. Sci. USSR, Div. Chem. Sci. 1151 (1956).*

[14] M. F. Shostakovskii, K. A. Andrianov, D. A. Kochkin and V. L. Vinogradov, Authors' Certif. 10540 (1957).

[15] M. F. Shostakovskii, D. A. Kochkin and V. L. Vinogradov, Bull. Acad. Sci. USSR, Div. Chem. Sci. 1452 (1957).*

[16] E. G. Rochow, J. Am. Chem. Soc. 67, 695 (1945); K. A. Andrianov and D. A. Kochkin, Authors' Certif. 9517 (1949); Inventions Bulletin No. 4, 16 (1948); Authors' Certif. 9517 (1949).

[17] C. Tamborski and H. W. Post, J. Org. Chem. 17, 1397 (1952).

[18] R. N. Nagel and H. W. Post, J. Org. Chem. 17, 1382 (1952).

[19] A. D. Petrov and G. I. Nikishin, Bull. Acad. Sci. USSR, Div. Chem. Sci. 6, 1128 (1952).*

[20] L. H. Sommer, D. L. Bailey, G. M. Goldberg, C. E. Buck, J. Am. Chem. Soc. 76, 1613 (1954).

[21] T. Perklev, Svensk. Kem. tidskr, 65, 216 (1953); Referat. Zhur. Khim. 11, 28813 (1954).

[22] M. F. Shostakovskii, D. A. Kochkin and V. L. Vlasov, Bull. Acad. Sci. USSR, Div. Chem. Sci. 1120 (1956).*

[23] M. F. Shostakovskii, M. A. Malinovskii, M. K. Romantsevich and D. A. Kochkin, Bull. Acad. Sci. USSR, Div. Chem. Sci. 632 (1956).*

[24] K. C. Frisch, P. A. Goodwin and K. E. Scott, J. Am. Chem. Soc. 74, 4584 (1952).

[25] A. D. Petrov, V. F. Mironov and V. G. Glukhovtsev, Proc. Acad. Sci. USSR 93, 499 (1953).

[26] M. F. Shostakovskii, I. A. Shikhiev and N. V. Komarov, Proc. Acad. Sci. Azerbaidzhan SSR 11, 757 (1955); Bull. Acad. Sci. USSR, Div. Chem. Sci. 1271 (1956).*

[27] M. F. Shostakovskii, I. A. Shikhiev and N. V. Komarov, Proc. Acad. Sci. Azerbaidhzan SSR 12, 177 (1956).

[28] A. D. Petrov, Iu. P. Egorov, V. F. Mironov, G. I. Nikishin and A. A. Bugorkova, Bull. Acad. Sci. USSR, Div. Chem. Sci. 50 (1956).*

[29] M. I. Batuev, A. D. Petrov, V. A. Ponomarenko and A. D. Matveeva, J. Gen. Chem. 88, 2336 (1956).*

[30] K. V. Mixer and D. L. Bailey, J. Pol. Sci. 108, 573 (1955).

[31] B. R. Thompson, J. Pol. Sci. 109, 373 (1956).

[32] A. D. Petrov, A. M. Poliakova, A. A. Sakharova, V. V. Korshak, V. F. Mironov and G. I. Nikishin, Proc. Acad. Sci. USSR 99, 785 (1954). *

[33] V. V. Korshak, A. D. Petrov, N. G. Matveeva, V. F. Mironov, G. I. Nikishin and S. I. Sadykh-Zade, J. Gen. Chem. 26, 1209 (1956).*

*Original Russian pagination. See C.B. translation.

[34] A. M. Poliakova, V. V. Korshak, A. A. Sakharova, A. D. Petrov, V. F. Mironov and G. I. Nikishin, Bull. Acad. Sci. USSR, Div. Chem. Sci. 979 (1956). •

[35] J. Curry, J. Am. Chem. Soc. 78, 1686 (1956).

[36] D. T. Hurd and G. F. Roedel, Ind. Eng. Chem. 40, 2048 (1948).

Received November 29, 1957

•Original Russian pagination. See C.B. translation.

EMULSION XANTHATION*

S. N. Danilov, N. S. Sidorova-Tikhomirova and O. M. Kulakova

A subject worthy of detailed study is the xanthation of alkali cellulose by means of fine emulsions of carbon disulfide, for acceleration of xanthation and the production of viscose in a single operation (in one apparatus).

Reference is often made to Klein's patent [1] as containing details of emulsion xanthation. Without recommending a separate emulsion of carbon disulfide, Klein describes the emulsification of carbon disulfide during its mixing with alkali cellulose and alkali, and gives a general description of the production of viscose in a single operation from ordinary alkali cellulose, or with the use of cellulose ground in a hollander. Lotarev [2] xanthated alkali cellulose by an emulsion of carbon disulfide obtained by addition of soap, ligroine, or finished viscose. He also proposed the xanthation of cellulose subjected to degradative treatment. Lobering [3] recommended the use of ground cellulose for emulsion xanthation. Lev [4] described experiments on the xanthation of ordinary alkali cellulose by carbon disulfide emulsions. There are reports [5] that in a few foreign factories emulsion xanthation is performed with the use of highly degraded cellulose of low viscosity and concentrated alkali. The production of direct (O/W) and reverse (W/O) emulsion, about which little has been published, is considered in one of our reports [6]. Unstable emulsions of carbon disulfide in water, formed in the presence of spermaceti, pyroxylin, and barium oleate are mentioned in monographs [7].

Various emulsifiers favor the formation of direct (O/W) emulsions of carbon disulfide, whereas W/O emulsions of carbon disulfide, as of other substances, are obtained more readily on addition of electrolytes and emulsifiers. Carbon disulfide does not form an emulsion with water and alkali without the use of emulsifiers; this confirms that a true emulsion is not formed in the process described in Klein's patent [1]. Ultrasonics were used in the experiments described below (performed by Iu. S. Rappe) for the production of carbon disulfide emulsions without emulsifiers. Good direct emulsions are obtained with the use of ultrasonics.

We obtained stable and highly concentrated emulsions with the use of OP-10, which belongs to the group of condensation products of ethylene oxide with alcohols containing aliphatic and alicyclic hydrocarbon radicals, of the composition RO $(CH_2CH_2O)_nCH_2CH_2OH$, by normal stirring and under the action of ultrasonics. Cellulose is readily xanthated at increased rates by means of direct and reverse emulsions of carbon disulfide, with the formation of viscoses of production quality.

The xanthates obtained by emulsion xanthation have a somewhat higher degree of xanthation. Dilute, or preferably concentrated, emulsions may be used.

Xanthation proceeds successfully** with ordinary alkali cellulose with the addition of dilute alkali to a total content of 6.5-7%, as in production viscose. The carbon disulfide first reacts with alkali cellulose containing, as usual, about 15-16% caustic soda, but after some xanthation the reaction continues in presence of 6.5-7% alkali. If the alkali cellulose is held in dilute alkali until a 6.5-7% concentration is obtained throughout the mass, carbon disulfide emulsion does not yield a soluble xanthate. Emulsion xanthation is more complete at low temperatures (5°) than at room or higher temperatures. Conditions for the formation of a readily soluble xanthate have been found; the formation of the xanthate is accompanied by its solution, so that viscose is made in the apparatus used for xanthation of cellulose.

*Communication VII in the series on the chemistry of xanthates and viscose.

**A description of the method was presented to the Main Administration for Synthetic Fibers and the All-Union Scientific Research Institute of Synthetic Fibers of the Ministry of Light Industry, on February 27, 1954.

EXPERIMENTAL

Carbon Disulfide Emulsions

Ultrasonic method (experiments by N. S. Sidorova-Tikhomirova and Iu. S. Rappe). Direct emulsions of carbon disulfide were obtained by the ultrasonic method both in absence and in presence of emulsifier. Because of the mobility of carbon disulfide, the high interfacial tension, and the anomalous increase of surface tension with increase of temperature, emulsions of carbon disulfide in water are not formed by the ordinary method of mixing. Ultrasonic waves make it possible to obtain emulsions of carbon disulfide in pure water, of considerable dispersity, stability, and concentration; these characteristics are closely interrelated. Ultrasonic vibrations may have either an emulsifying or a coagulating effect, according to the power and other characteristics of the ultrasonic field. For the production of more highly concentrated emulsions, and to avoid overheating, it is advisable to add carbon disulfide by small portions or with cooling. The emulsions obtained without emulsifiers had droplets 1-6 μ in diameter with the use of ultrasonic intensity of 0.3-0.7 w/cm^2, the concentration being 0.5-1.2%; the exposure time was 3 minutes.

In presence of emulsifiers (OP-10 or sodium oleate), emulsions of high concentrations (up to 50%) can be obtained by the ultrasonic method; the emulsifier stabilizes the emulsion, but has little effect on the dispersity. The emulsion concentration increases with decrease of temperature. Unstable but concentrated emulsions of carbon disulfide can be obtained by the action of ultrasonics in presence of caustic soda.

Reverse emulsions. To determine whether reverse (W/O) emulsions of carbon disulfide have any advantages for the xanthation of cellulose, such emulsions were prepared as described in the literature [8, 9], with 10% solution of oleic acid in carbon disulfide, and 20% sodium carbonate solution in water (with electrolytes in the aqueous phase, and an emulsifier of good solubility in carbon disulfide). However, in a vessel coated with paraffin wax, and with OP-10 emulsifier, a direct and not a reverse emulsion was obtained [10].

Our reverse emulsions of carbon disulfide with the above-mentioned concentrations of oleic acid and sodium carbonate were of thick consistency, and were stable for about 24 hours. Reverse emulsions with 5% sodium oleate and 10% sodium carbonate are suitable for xanthation, but are less stable than direct emulsions. Reverse emulsions were readily obtained in closed vessels on shaking; this method yielded the same emulsion as the recommended method [11] with the use of a spiral steel stirrer and dropwise addition of sodium carbonate solution from a buret. However, the reverse emulsions were less monodisperse than direct emulsions made with OP-10. Thus, whereas in the direct emulsion (1:1 carbon disulfide in water) nearly all the particles were about 1 μ in size, in the reverse emulsions under the same conditions (water in carbon disulfide, 1:1) the particle size sometimes varied in the range of about 1-7 μ, although emulsions with droplets of 1.0-1.5 were obtained. The reverse emulsions cannot be diluted either by water or by alkali. Their use is therefore restricted, only concentrated reverse emulsions can be used for xanthation, whereas direct emulsions can be diluted without difficulty.

Direct emulsions. The best emulsifier for carbon disulfide is OP-10 in 1-5% aqueous solution; the size of the emulsion droplets is 0.5-0.7-1.0 μ. These emulsions are stable for several days. They can be diluted with water or alkali, but in presence of alkali they gradually break down as the carbon disulfide reacts with caustic soda. However, even on dilution with alkali the emulsions remain stable for 2 hours at low temperatures (5°). An emulsion of 6 parts of carbon disulfide to 1 part of water was of thick consistency and could be kept for over 4 months.

Characteristics of the emulsions. For characterization of the emulsions, the particles were counted statistically under the microscope (up to 2000 particles), and the droplet size distribution curves were plotted, characterizing the emulsion properties (stability at the instant of sampling). A × 90 objective and × 15 eyepiece were used. The size of a square of the micrometer-eyepiece grid was determined, the focusing being performed in presence of an immersion liquid. The emulsion stability was also determined by direct observations of sedimentation, transparency, and the thickness of the liquid layers formed during breakdown of the emulsions. The emulsion type was determined by the usual method – dilution of the emulsion with water and carbon disulfide, application of drops of the emulsion onto glass and paraffin wax, and staining with Sudan III.

Xanthation of Cellulose by Carbon Disulfide Emulsions

Method. The experiments were made on factory alkali cellulose taken after shredding, of the following typical composition (in %): α-cellulose 30-31, NaOH 15.3-15.6. The weight of carbon disulfide was 36% on the

TABLE 1

Degree of Esterification and Distribution of Carbon Disulfide Between Xanthate and By-Products

Viscose	Degree of esterification	Degree of esterification γ (%)	
	γ (%)	xanthate	by-products
Without emulsion	37	68	32
With direct emulsion	48	70	30
With reverse emulsion	50.5	73	27

weight of α-cellulose. A concentrated emulsion of 1 part of carbon disulfide and 1 part of 1% OP-10 solution was prepared separately, and diluted with 4% alkali. The viscoses were analyzed for degree of xanthation of the cellulose, and distribution of carbon disulfide between the main and side reactions (iodine titration by the Geiger method), viscosity, and ripeness (by the NaCl and NH_4Cl tests). The dissolution of the xanthate was checked microscopically (absence of fibers).

The experiments on xanthation and viscose formation were performed in two main versions: 1) separate xanthation and viscose making (two distinct operations); 2) preparation of viscose in the same apparatus, either by consecutive xanthation and dissolution, or in a single step with simultaneous xanthation and dissolution.

In the former case, the xanthation was performed in glass flasks placed in a slowly rotating laboratory "barat"* at room temperature. The xanthate was then dissolved at 5-7° in 4% alkali, taken in an amount such that the viscose contained 8% α-cellulose and 6.5% NaOH. Direct and reverse emulsions of different concentrations were used.

TABLE 2

Experimental Results

Method of viscose preparation	Degree of esterification γ (%)	Distribution of bound carbon disulfide (%)		Viscose ripeness, NH_4Cl test	Viscose viscosity (seconds, ball fall)
		xanthate	by-products	on second day	
Factory viscose	48	66	34	13.1	52.5
Laboratory viscose, without use of emulsion	45	64	36	11.5	170
Laboratory viscose, with use of direct concentrated emulsion	44	84	16	11.0	45
Viscose with use of reverse concentrated emulsion	48	83	17	9.5	65
Viscose with use of direct emulsion diluted with all the alkali	49	80	20	13.0	50

In the latter case, viscose was made by one of three procedures in a laboratory mixer of the Werner–Pfleiderer type, fitted with a cooling jacket, at a shaft speed or 150 revolutions per minute.

In the first procedure, the alkali cellulose was charged into the mixer, cooled to 5-7°, and a direct or reverse concentrated emulsion of carbon disulfide in water was added. The temperature in the mixer was raised

*"Barat" – a rotating iron drum used for the xanthogenation of alkali cellulose in the manufacture of viscose. Transliterated from the Russian – Publisher.

to 25-26° during 1.5 hours. Alkali was then introduced into the mixer in the quantity and concentration required to give viscose of normal composition, and the final dissolution of the xanthate was then carried out for 1.5 hours at 10-12°.

In the second procedure in the mixer experiments, dilute emulsions, i.e., only direct emulsions, were used. Vigorous agitation of the contents of the apparatus is particularly important in this case. A concentrated emulsion was prepared, in the form of a paste consisting of 1 part of carbon disulfide and 1 part of 1% aqueous OP-10 solution. The cooled paste was diluted with 4% caustic soda solution, also cooled to 4-5°, and poured into the mixer containing alkali cellulose cooled to 5°. The temperature was raised to 24-26° over a period of 1.5 hours during xanthation, and then decreased again (by means of a stream of cold water passed through the mixer jacket) to 10-12°, to ensure more rapid dissolution (about 1.5 hours). Control experiments were performed under analogous conditions, but by the ordinary method without the use of emulsions. For comparison of the properties of viscoses obtained with and without emulsifier, water in an amount equivalent to the amount of emulsifier used was added to the viscose in the latter case.

In the third and the most advantageous procedure, a dilute emulsion was made in the cooled mixer (concentrated emulsion paste was added to 4% alkali with stirring), and cooled alkali cellulose was then added.

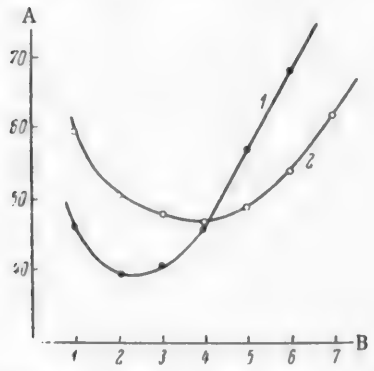

Variations of viscose viscosity with ripening time. A) Viscosity of viscose by ball fall (seconds); B) ripening time (days). Viscose made with 1) diluted; 2) concentrated emulsions.

In the latter two procedures the xanthation of the alkali cellulose was commenced at its initial alkali content (15.5%), and subsequently the xanthation proceeded at lower alkali concentrations as the latter decreased as the result of reactions with the solution. The lower alkali content favors easier dissolution of the xanthate formed.

It was shown in separate experiments that if 4% caustic soda is added to the alkali cellulose, and the mixture is then agitated for several hours to complete equalizations of the alkali concentrations in the cellulose and the solution (6.5%), xanthation is slow after introduction of the carbon disulfide emulsion.

Production and properties of viscose. Experiments on the separate xanthation by means of concentrated direct or reverse emulsions (with 1:2 or 2:1 or 3:1 $CS_2 : H_2O$) followed by dissolution showed that the xanthates formed with the use of carbon disulfide emulsions have somewhat higher degree of substitution, better and more complete solubility, and better distribution of carbon disulfide between the main and side reactions. The best results were obtained with an emulsion of the composition $CS_2 : H_2O = 1:1$. The ripeness values for the viscoses made with and without the use of emulsions were very similar, while the viscosities were lower in the former case than in the latter.

The results are illustrated in Table 1.

Experiments in the same apparatus (Werner–Pfleiderer mixer) gave better xanthates with the use of concentrated emulsions than experiments with the operations performed separately in different laboratory apparatus.

The results of the experiments are given in Table 2.

From the technological aspect, however, the simultaneous xanthation of cellulose and dissolution of the xanthate, with the use of diluted emulsions, is a more interesting process; this definitely requires good mixing (150 revolutions of the stirrer blades per minute). In this case the distribution of carbon disulfide between the main and side reactions is even more favorable (80% and 20% respectively), as is clear from Table 2.

The changes during the ripening of viscoses made with the use of concentrated (2) and diluted (1) emulsions are similar, but the viscosity curve for viscoses made with diluted emulsions is smoother and the viscosity minimum is higher than for viscoses made with concentrated emulsions (see Fig).

It is noteworthy that xanthation by means of diluted emulsions at first occurs only when the alkali content

of the alkali cellulose approaches the normal value (15%). Later, however, as xanthation proceeds, soluble xanthates are formed even at lower alkali concentrations.

SUMMARY

1. Experiments have shown that direct (concentrated or diluted) and reverse (concentrated) emulsions of carbon disulfide can be used for the production of xanthates and viscoses of somewhat higher degrees of xanthation, with better distribution of carbon disulfide between the main and side reactions, of the same stability, but of somewhat lower viscose viscosity, than those obtained in absence of emulsions.

2. When cellulose is xanthated and the xanthate is simultaneously dissolved in the same apparatus, xanthation proceeds at first only when the alkali content of the alkali cellulose corresponds to the normal concentration (about 15%); only later does the xanthation proceed at a lower alkali content, while the xanthate is continuously dissolved.

LITERATURE CITED

[1] F. Klein, British Patent 314504 (1929); O. Faust, Celluloseverbindungen, II, 1903 (1935).

[2] B. M. Lotarev, Soviet Author's Certif. 37802 (1934).

[3] J. Lobering, Koll. Zeitschr. 98, 186 (1942).

[4] E. M. Lev, Report of the All-Union Sci. Res. Inst. For Synthetic Fibers. "Study of the xanthation of cellulose by means of carbon disulfide emulsion" (1946).*

[5] F. Mel'me, Report of Conference on the Production of Chemical Fibers, (State Light Industry Press, 1956), p. 149.*

[6] S. N. Danilov, N. S. Sidorova and O. M. Kulakova, Report of the Institute of High-Molecular Compounds, Acad. Sci. USSR, for 1954. "Emulsion xanthation."*

[7] W. Claytion, Theory of Emulsions and their Technical Treatment (IL, 1950), p. 237 [Russian translation].

[8] L. Ia. Kremnev and N. V. Kuibina, Zh.K.Kh. 14, 15 (1952).

[9] V. G. Ben'kovskii and N. D. Zavorokhin, Zh.K.Kh. 14, 15 (1952).

[10] R. M. Dvoretskaia, Zh.K.Kh. 10, 334 (1948).

[11] L. Ia. Kremnev, Zh.K.Kh. 13, 394 (1951).

Received September 8, 1956

* In Russian.

PREPARATION AND INVESTIGATION OF STYRENE – METHYL ACRYLATE COPOLYMERS

A. Ia. Drinberg, B. M. Fundyler and A. M. Frost

One method of improving the properties of polystyrene is by copolymerization of styrene with various monomers containing highly polar groups. Polar groups in the polymer chain considerably increase the forces of adhesion of these polymers to various surfaces as the result of electrical interaction.

Special interest attaches to copolymers of styrene with various acrylic monomers. Polymers of acrylate esters are highly elastic and have good adhesion to steel, i.e., they have properties lacking in polystyrene.

Compounds with very valuable properties can be obtained by copolymerization of styrene with acrylate and methacrylate esters.

TABLE 1

Characteristics of the Starting Materials

Monomer	Boiling point (in °C)	n_D^{20}	Density (g/cc)	Saponification number (mg KOH)
Styrene	37-40 (P = 7-8 mm	1.5450	0.9049	—
Methyl acrylate	83-85	1.4721	0.9580	646.1

There have been many investigations of the production of copolymers of styrene with acrylate and methacrylate esters. However, the available information on the styrene–methyl acrylate copolymer is confined to data on the copolymerization kinetics [1, 2]. Therefore studies of the influence of various factors on the copolymerization of styrene with methyl acrylate, and tests of the properties of the copolymer in coatings, are of definite interest.

The materials used for the synthesis were styrene and methyl acrylate obtained from the crude products, which were washed to remove inhibitor and redistilled.

The characteristics of the monomers used are given in Table 1.

TABLE 2

Characteristics of Reaction Mixtures

Composition of reaction mixture	Saponification number (mg KOH)	Refractive index n_D^{20}
Styrene–methyl acrylate mixture, 1:1 weight ratio	169	1.4828
Ditto, 1:1.65 ratio	178	1.4781

TABLE 3

Yield of Copolymer as a Function of the Reaction Time

Copolymer	Reaction time (hours)	Weight of product taken (g)	Weight of copolymer isolated (g)	Copolymer yield (%)
Styrene—methyl acrylate copolymer, component ratio 1:1 by weight	8	2.9520	0.2421	16.4
	12	3.1129	0.3517	22.5
	16	2.4884	0.4248	34.1
Ditto, 1:1.65 ratio	8	2.6626	0.3860	29.0
	12	2.4963	0.4395	35.2
	16	2.9303	0.6411	43.7

Styrene and methyl acrylate were copolymerized in sealed glass tubes at 70° by the solution method in 50% toluene solution. Benzoyl peroxide was used as catalyst; the amount added to the reaction mixture was 0.2% on the monomer weight.

The copolymerization was studied at the following weight ratios of styrene to methyl acrylate: 20:1, 4:1, 2:1, 1:1 and 1:1.65. **

TABLE 4

Saponification Numbers of the Copolymers

Copolymer	Reaction time (hours)	Weight of copolymer taken (g)	Amount of KOH* (ml)	Saponification number (mg KOH)
Styrene—methyl acrylate copolymer component ratio 1:1 by weight	8	0.3303	0.1	69.6
	12	0.5880	2.2	108.2
	16	0.2910	1.45	119.9
Ditto, 1:1.65 ratio	8	0.1891	1.3	216
	12	0.2086	1.65	235
	16	0.2061	1.95	250

Copolymerization does not occur at 20:1, 4:1, and 2:1 ratios of styrene to methyl acrylate. Pure polystryene is formed, as shown by the zero values for the saponification number of the products. Copolymers were formed only at 1:1 and 1:1.65 ratios of styrene to methyl acrylate. The characteristics of the reaction mixtures used for the copolymerization are given in Table 2.

As a check on the course of polymerization, samples were taken at definite intervals, and the copolymer yield, saponification number, relative viscosity, and refractive index were determined.

Determination of copolymer yield. For determination of the copolymer yield, a weighed sample of the product was dissolved in toluene and precipitated by methyl alcohol; the precipitate was filtered off, washed with methyl alcohol, and dried at 60-70° to constant weight.

The results are given in Table 3 and Fig. 1.

The copolymer yield increases with increasing content of the more rapidly polymerizing methyl acrylate in the reaction mixture; this is in full agreement with modern views on the mechanism of the copolymerization reaction [3].

The variations of the saponification numbers of the copolymers with the reaction time are given in Table 4 and Fig. 2.

* The titer of the caustic potash solution was 0.0285.

** The 1:1.65 ratio of styrene to methyl acrylate is equimolar.

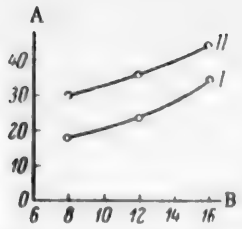

Fig. 1. Variation of copolymer yield with reaction time. A) Copolymer yield (%); B) reaction time (hours). Styrene–methyl acrylate ratio: I) 1:1; II) 1:1.65.

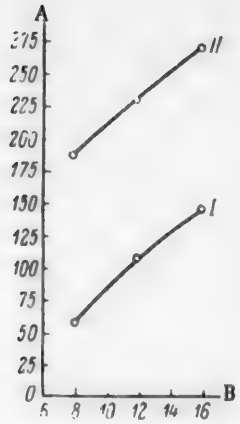

Fig. 2. Variation of saponification number with reaction time. A) Saponification number (mg KOH); B) reaction time (hours). Styrene–methyl acrylate ratio: I) 1:1; II) 1:1.65.

The saponification numbers were used to calculate the approximate composition of the copolymers, i.e., the number of molecules of styrene copolymerized with one molecule of methyl acrylate. The calculation was performed as follows.

The average molecular weight of an elementary unit of styrene–methyl acrylate copolymer can be represented as $86 + 104x$, where 86 and 104 are the molecular weights of methyl acrylate and styrene respectively, and x is the number of styrene molecules in the copolymer combined chemically with one molecule of methyl acrylate. The saponification number of the copolymer can then be expressed as

$$r_0 = \frac{56}{86 + 104x} \cdot 1000 \qquad (1)$$

or, in general form

$$r_0 = \frac{56}{M_1 + M_2 x} \cdot 1000, \qquad (2)$$

where r_0 is the saponification number, determined experimentally.

TABLE 5

Variation of Copolymer Composition with Copolymerization Time

Copolymer	Reaction time	Saponification No. of copolymer (mg KOH)	Molecules of styrene per molecule of methyl acrylate
Styrene–methyl acrylate copolymer, component ratio 1:1	8	58.65	8.4
	12	107.1	4.22
	16	144	2.93
Ditto, 1:1.65 ratio	8	190.1	2.03
	12	235.2	1.51
	16	250.1	1.13

Rearrangement of Equation (2) gives

$$x = \frac{56}{r_0 \cdot M_2} \cdot 1000 - \frac{M_1}{M_2}. \qquad (3)$$

For the copolymerization of styrene with methyl acrylate, Equation (3) takes the form

$$x = \frac{56 \cdot 1000}{r_0 \cdot 104} - 0.827 = \frac{7000}{13 \cdot r_0} - 0.827.$$

The composition of the copolymers, calculated by means of this formula, is given in Table 5.

TABLE 6

Relative Viscosity of Copolymers

Copolymer	Reaction time	Efflux time of copolymer solution (seconds)*	Relative viscosity at 20°
Styrene–methyl acrylate copolymer, component ratio 1:1	8	82.7	1.3603
	12	83.0	1.3719
	16	84.1	1.3818
Ditto 1:1.65 ratio	8	80.5	1.3315
	12	81.7	1.3504
	16	82.9	1.3702

As the reaction proceeds, the number of molecules of styrene per molecule of methyl acrylate in the copolymer gradually decreases, and the copolymer becomes richer in methyl acrylate.

Determination of the relative viscosity of the copolymers. The viscosity of 1% copolymer solutions in toluene was measured. Variations of the relative viscosity of the copolymers during the reaction are given in Table 6.

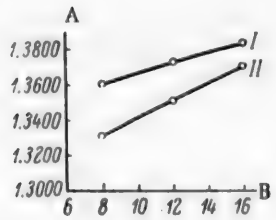

Fig. 3. Variation of the relative viscosity of copolymers with reaction time. A) Relative viscosity; B) reaction time (hours). Styrene–methyl acrylate ratio: I) 1:1; II) 1:1.65.

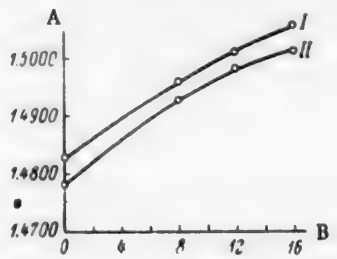

Fig. 4. variation of the refractive index of copolymers with reaction time. A) Refractive index n_D^{20}; B) reaction time (hours). Styrene–methyl acrylate ratio: I) 1:1; II) 1:1.65.

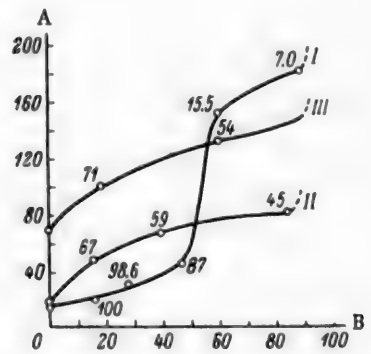

Fig. 5. Curves for the fractional precipitation of copolymers and polymer mixtures. A) Amount of methanol (ml); B) amount of polymer precipitated (%). I) 1:1 mixture of polystyrene and polymethyl acrylate; II) styrene–methyl acrylate copolymer, 1:1 ratio; III) ditto, 1:1.65 ratio. The numbers at the points represent the styrene contents in the precipitates.

The data in Table 6 were used to plot the variations of the relative viscosity of the copolymer with time (Fig. 3). It is clear from this graph that the relative viscosity of the copolymer increases with time. Less-viscous products are obtained with increase of the methyl acrylate content in the original mixture.

The variations of the refractive index of the copolymers with time are plotted in Fig. 4.

It follows from Fig. 4 that copolymerization commences as soon as the heating of the reaction mixture begins. There is no induction period under these reaction conditions.

Fractional precipitation of copolymers. In copolymerization reactions it is very important to determine whether a copolymer is formed in the reaction, or whether the product is a mixture of the polymers of the original components.

*The efflux time of the pure solvent was 60.5 seconds in all cases.

TABLE 7

Fractional Precipitation of Copolymers and Polymer Mixtures

Substance fractionated	Amount of methyl alcohol (ml)	Weight of precipitated fraction (g)	Amount of precipitate obtained (%)	Saponification No. of fraction	Styrene content of precipitated fraction (%)
Artificial 1:1 mixture of polystyrene and polymethyl acrylate	17	Solution turbid			
	20	0.0612	15	0	100
	30	0.1140	28	9.13	98.6
	45	0.1897	46.5	84.5	87
	150	0.2449	60	550	15.5
	180	0.3581	88.9	607	7.0
Styrene–methyl acrylate copolymer, 1:1 monomer ratio	19.5	Solution turbid			
	48	0.0588	15	215	67
	68	0.1533	39	267	59
	82.5	0.3301	84	358	45
Ditto, 1:1.65 ratio	69	Solution turbid			
	100	0.0741	18	188	71
	130	0.2419	59	299	54
	148	0.3671	89.5	377	42

Formation of styrene–methyl acrylate copolymer was determined by the method of fractional precipitation.

An exact amount of 2% solution of the copolymer in toluene was precipitated with methyl alcohol. The methyl alcohol was added dropwise to the copolymer solution until a stable precipitate was formed. The precipitate was collected on a weighed filter and dried to constant weight.

The next portion of methyl alcohol was added to the filtrate to precipitate the next fraction.

TABLE 8

Physical and Mechanical Tests on the Coatings

Coatings	Adhesion	Impact strength (kg/cm)	Bending (mm)	Hardness	Water resistance (days)	Resistance to 3% NaCl solution (days)	Water permeability (hours)
Coatings based on Styrene–methyl acrylate copolymer with 1:1 monomer ratio	Good	50	1	0.68	13	1.5	9
Ditto, 1:1.65 ratio	Good	50	1	0.60	12	1	6
Coatings based on polystyrene	Poor	Fail	Not elastic	0.87	17	5	2.5

The dried precipitates were weighed, their percentage copolymer contents were calculated, and the precipitation curve was plotted. Each fraction was analyzed for its styrene content, which was calculated from the saponification number. Parallel experiments were performed on the fractional precipitation of an artificial mixture of polystyrene and polymethyl acrylate in 1:1 ratio.

The results of these experiments are given in Table 7 and plotted in Fig. 5.

Figure 5 shows that the precipitation curves for the copolymers are smooth. The styrene contents of the fractions decrease gradually. In the case of the artificial mixture of polystyrene and polymethyl acrylate the

precipitation curve shows two distinct fractions. The first corresponds to polystyrene, and the second to polymethyl acrylate.

The amounts of methanol required to precipitate these fractions differ sharply.

Tests of the copolymers in coatings. Lacquers containing 15% of the copolymer in toluene were prepared for the coating tests. The lacquers were applied by pouring on iron and glass plates. Single coats, dried in the cold, with films about 30-35μ thick were tested. The films dried tack-free in 15 minutes, and complete drying was reached in 24 hours.

The results of physical and mechanical tests on the copolymer coatings are given in Table 8; the properties of coatings based on pure polystyrene are given for comparison.

The results showed that introduction of methyl acrylate units into the polystyrene chain increases the adhesion of the coatings, impact strength, and bending strength.

The high hardness, characteristic of polystyrene coatings, is retained.

SUMMARY

1. The copolymerization of styrene with methyl acrylate proceeds either at roughly equimolar ratios of the components, or with excess of methyl acrylate in the reaction mixture.

2. The copolymerization of styrene with methyl acrylate commences immediately as reaction mixture is heated, as shown by the variations of the viscosity and refractive index of the products at the initial reaction stages.

3. The copolymer yield increases with increasing content of methyl acrylate in the original mixture.

4. The polymer becomes richer in the more rapidly polymerizing methyl acrylate as the reaction proceeds; this is shown by the increase of the saponification numbers of the copolymers formed.

5. Coatings bases on styrene–methyl acrylate copolymers have better physical and mechanical properties than coatings based on pure polystyrene.

LITERATURE CITED

[1] C. Walling, J. Am. Chem. Soc. 71, 1930 (1949).

[2] T. Alfrey and E. Merz, Polymer Bull. 1, 86 (1945).

[3] S. N. Ushakov, S. P. Mitsengendler and G. A. Shtraikhman, Progr. Chem. 19, 3 165 (1950).

[4] F. R. Mayo and F. M. Lewis, J. Am. Chem. Soc. 66, 1594 (1944).

Received October 15, 1956

CATALYTIC DECOMPOSITION OF METAMERIC ESTERS – ETHYL BUTYRATE AND BUTYL ACETATE*

B. A. Bolotov, N. A. Baranova and M. V. Bogdanova

It was reported in earlier papers on the catalytic conversion of primary alcohols that the principal products formed in reactions over copper catalysts at 250-275° were esters, and at temperatures above 325°, ketones [1-4].

It was also shown [5] that the esters, isobutyl isobutyrate and isoamyl isovalerate decompose at 300-400° to form aldehydes and alcohols, while at 450-452° they are converted into ketones, with high yields. This leads to the hypothesis that the formation of ketones from esters passes through the stage of decomposition of esters into aldehydes, with subsequent conversion of the latter into ketones.

The reaction products in the catalytic decomposition of ethyl acetate [6] contained, in addition to acetaldehyde and carbon monoxide, considerable amounts of higher ketones: methyl propyl ketone, dipropyl ketone, methyl amyl ketone, etc.; this confirmed the mechsnism of aldol condensation postulated earlier [7, 8].

One may expect that in the catalytic decomposition of the metameric esters, ethyl butyrate and butyl acetate, the products formed should differ both qualitatively and quantitatively and should depend on the direction of the processes taking place. It is clear that in the ketonic decomposition [9] of ethyl butyrate the principal reaction product to be expected is dipropyl ketone, while in the case of butyl acetate it is actone. If these esters decomposed by way of an intermediate stage of aldehyde formation (acetaldenhyde and butyraldehyde), the reaction products should be of the same composition in either case, consisting of three ketones: acetone, methyl propyl ketone, and dipropyl ketone.

Experimental results obtained in studies of the catalytic conversions of ethyl butyrate and butyl acetate over the promoted copper catalyst used previously showed that the reaction products obtained from the two esters contain ketones of similar composition, mixed with ketones formed from an equimolecular mixture of acetaldehyde and butyraldehyde. The composition of the ketones formed remained unchanged if mixtures of the two esters in various proportions were taken for the reaction. The gaseous reaction products contained large amounts of carbon monoxide and hydrogen; this indicates that ester decomposition proceeds through the stage of aldehyde formation, followed by conversion of aldehydes into ketones, in accordance with the aldol condensation mechanism [1, 6, 10].

EXPERIMENTAL

The experiments on the conversion of metameric esters were performed with precipitated copper catalyst No. 5 promoted with thorium oxide. The experiments were carried out in the laboratory unit described earlier [1], in the temperature range of 275-400°, in presence of hydrogen in 1:1 ratio of ester to hydrogen, and space velocity 150-160.

The esters used were: 1) ethyl butyrate, b.p. 120-121.5°, $n_D^{20} = 1.401$, containing 98.5% of the ester; 2) butyl acetate, b.p. 124-125°, n_D^{20} 1.387, containing 98.9% of the ester.

Three series of experiments were performed: 1) a study of the effect of temperature on the yields of ketones from the esters; 2) on the composition of the products obtained from mixtures of these esters, and from

*Communication IX.

TABLE 1

Catalytic Conversion of Metameric Esters

Temperature (deg)	Condensate yield (wt. %)	Yields (in wt. % on the original ester)									Total ketone yield (%)
		acetaldehyde — acetone		butyraldehyde	ethyl acetate	methyl propyl ketone	methyl isobutyl ketone	dipropyl ketone	metameric esters	butyl butyrate	
Ethyl butyrate											
275	81.3	1.0	2.1	1.3	1.8	6.7	2.2	7.4	21.6	13.8	18.4
300	83.0	1.1	1.3	1.8	1.0	16.7	3.0	14.0	9.0	13.7	35.0
325	82.0	1.2	1.2	2.0	0.3	18.5	5.0	26.0	13.0	10.0	50.7
350	85.0	1.0	1.0	1.0	0.8	5.0	1.0	26.0	12.0	11.0	33.0
375	83.0	1.0	0.5	0.7	0.5	4.0	1.0	30.0	5.0	7.0	35.5
Butyl acetate											
300	68.5	0.0	4.0	1.0	0.0	10.3	3.0	15.4	5.0	—	32.7
315	66.0	0.0	3.0	1.0	0.0	15.0	3.5	18.0	1.0	5.0	39.5
340	79.0	0.0	4.6	3.0	0.3	8.0	3.5	16.4	1.0	13.0	32.5
370	82.0	0.0	3.5	7.6	1.0	7.0	3.0	17.0	4.0	10.0	30.5
400	82.0	0.0	4.0	7.0	0.5	3.0	3.0	8.0	3.0	6.0	15.0

mixtures of acetaldehyde and butyraldehyde at 275-375°; 3) on the influence of the relative properties of the original esters on the composition of the reaction products formed at the optimum temperature of ketone formation.

The catalytic conversion of ethyl butyrate and butyl acetate was studied in the 274-400° range. The results are given in Table 1.

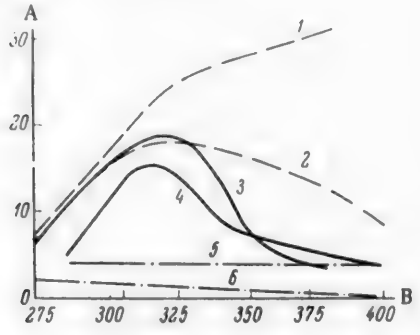

Fig. 1. Effect of temperature on the yields of ketones from ethyl butyrate and butyl acetate. A) Yield of ketone (wt. % on the original ester); B) temperature (in °C). 1,2) Dipropyl ketone; 3,4) methyl propyl ketone; 5,6) acetone. Ketones: 1,3,6) from ethyl butyrate; 2,4,5) from butyl acetate.

The ketone yields as functions of the temperature are plotted in Fig. 1. The conversion of the metameric esters may proceed in the following directions.

1. Ketonic Decomposition

$$2C_2H_5OCOC_3H_7 \rightarrow C_3H_7COC_3H_7 + C_2H_5OH + CO_2 + C_2H_4.$$

$$2C_4H_9OCOCH_3 \rightarrow CH_3COCH_3 + C_4H_9OH + CO_2 + C_4H_8.$$

In the presence of water, which may occur in the reaction products at high temperatures, ester decomposition may proceed in a different direction. In this case olefins should not be present in the reaction products

$$2ROCOR' + H_2O \rightarrow R'COR' + 2ROH + CO_2.$$

The alcohols formed in the ketonic decomposition of esters should also be converted into acetone or dipropyl ketone at 325-350° in presence of copper catalyst.

2. Decomposition into Aldehydes

In this case the metameric esters should yield compounds of the same composition (see following page).

An examination of the results obtained in the decomposition of esters (see Table 1 and Fig. 1) in relation to the following possible reaction schemes, shows that the products obtained from ethyl butyrate contain butyraldehyde and acetaldehyde, ethyl acetate, butyl butyrate, acetone, dipropyl ketone, and methyl propyl ketone. The yield of methyl propyl ketone increases with the temperature, and is 19% at 325°. This ketone can be formed only by the interaction of ethyl and butyl alcohols or the corresponding aldehydes.

Butyl acetate yields the same products as ethyl butyrate. The total ketone yields from both esters increase with temperature, reaching a maximum (40-50%) at 315-325°.

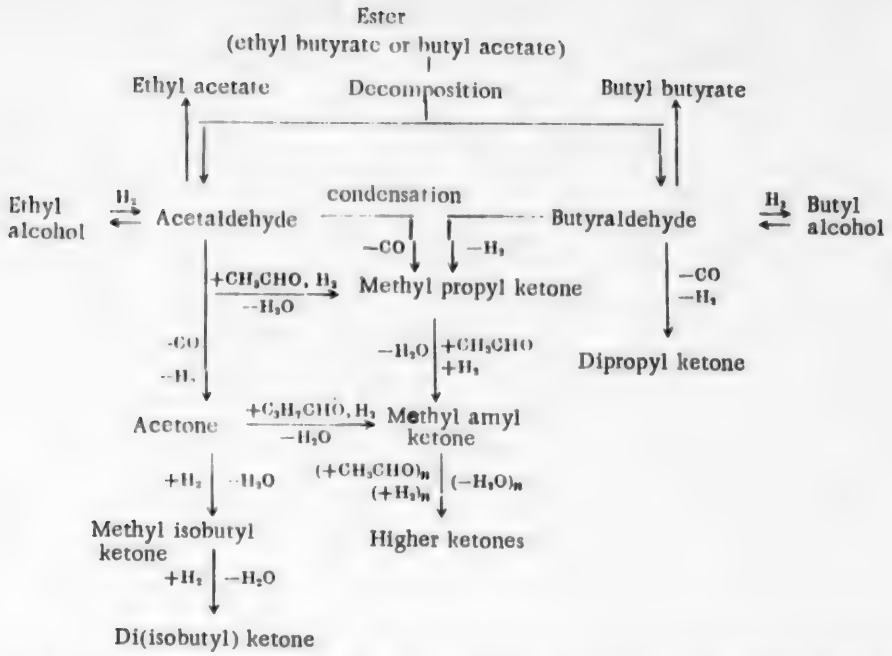

These results lead to the conclusion that the ester conversion proceeds preferentially though the stage of aldehyde formation, with subsequent conversion of aldehydes into ketones by the aldol condensation mechanism.

The gas formed in ester decomposition (Table 2) contains considerable amounts of carbon monoxide and hydrogen, the presence of which may be attributed to aldol condensation reactions.

TABLE 2

Average Composition of Gas in the Catalytic Decomposition of Metameric Esters

Gas composition	Contents (vol. %)								
	ethyl butyrate					butyl acetate			
	temperature (deg)								
	275	300	325	350	375	315	340	370	400
Carbon dioxide	30	32	35	39	40	24	32	34	56
Carbon monoxide	15	20	13	8	13	7	8	12	9
Unsaturated hydrocarbons	2	1	2	7	8	4	3	3	3
Hydrogen	53	47	50	43	39	65	60	51	32

The presence of predominant amounts of carbon in the gas, and the certain degree of preferential formation of dipropyl ketone and acetone from the corresponding esters, also indicate that conversion of carbon monoxide and ketonic decomposition of the esters (first direction) occur.

For more precise determination of the course of ester conversion, experiments were performed under the same conditions, with an equimolecular mixture of ethyl butyrate and butyl acetate, and a similar mixture of acetaldehyde and butyraldehyde. The results of the experiments are given in Table 3. The compositions and yields of the products are the same in both cases. Formation of the unsymmetrical methyl propyl ketone from the esters occurs mainly at 300-325°; this corresponds to the conditions for its formation from mixtures of alcohols [9, 11] or aldehydes (Table 3). Considerable amounts of carbon monoxide are present in the gases formed in the decomposition of the ester mixture, as in the experiments with aldehydes (Table 4). Its greatest content is found at the temperatures of ketone formation. These facts support the earlier suggestion and ketones are formed from esters by an aldol mechanism.

TABLE 3

Catalytic Conversion of Mixtures of Acetaldehyde and Butyraldehyde, and of the Metameric Esters, in 1:1 Molar Ratio

Temperature (deg)	Condensate yield (wt. %)	Yields (in wt. % on the original mixture)											Total ketone yield (%)
		acetaldehyde	acetone	butyraldehyde	ethyl acetate	methyl propyl ketone	methyl isobutyl ketone	dipropyl ketone	metameric esters	butyl butyrate	higher ketones	water	
Ethyl butyrate : butyl acetate = 1:1													
275	76.0	1.0	0.5	1.4	1.7	14.0	—	7.0	14.0	12.6	8.0	—	22
300	84.5	1.5	2.7	2.5	0.3	17.0	—	9.0	7.0	23.0	11.0	—	29
325	81.4	1.4	2.6	3.6	1.0	20.0	—	12.0	2.5	11.0	16.0	—	35
360	84.4	2.5	2.0	3.6	2.0	13.0	—	6.4	8.0	10.0	11.0	—	22
375	84.0	2.5	2.0	4.0	1.2	9.4	—	7.5	2.0	10.0	10.5	—	19
Acetaldehyde : butyraldehyde = 1:1													
290	68.0	0.6	1.3	1.0	0.2	17.0	6.0	12.0	0.1	3.5	9.0	0.5	30
315	74.0	0.1	1.2	2.0	0.5	13.0	2.0	18.0	0.1	4.0	14.0	1.0	32
340	77.5	0.2	1.0	3.0	0.6	9.0	4.0	15.0	0.4	3.0	16.0	3.0	25
370	81.4	0.0	0.2	4.7	0.3	7.5	5.0	12.0	0.3	3.5	30.0	7.5	20

Earlier it had been shown that variations of the alcohol or ester ratios in the original mixtures influenced the composition of the reaction products. The unsymmetrical ketone was formed when the starting substances were present in equimolecular proportions. If the proportion of one of the alcohols or esters was increased, the yield of the corresponding symmetrical ketone rose sharply [10-12].

In the case of different mixtures of ethyl butyrate and butyl acetate, the ketone yields should vary considerably in accordance with the course of the decomposition reactions. If ketonic decomposition of the esters is predominant, the ketone yields should vary sharply with the proportions of the esters taken. If the esters decompose to aldehydes, the ketone yields should not, under equal conditions, vary with changes of the ester ratio, as the proportions of the aldehydes formed should remain constant and equimolecular.

To test this hypothesis, a series of experiments was carried out, with mixtures of esters in different proportions. Experiments with mixtures of ethyl and n-butyl alcohols were carried out for comparison. The experiments were performed under the optimum conditions for ketone formation (temperature 325°, space velocity 150).

It follows from the results (Table 5 and Fig. 2) that the yields of acetone, methyl propyl ketone, and

TABLE 4

Average Gas Composition in the Catalytic Conversion of Mixtures of Metameric Esters, and Acetaldehyde with Butyraldehyde

Gas composition	Contents (vol. %) at ratios							
	$\frac{\text{ethyl butyrate}}{\text{butyl acetate}} = 1:1$ (molar)				$\frac{\text{acetaldehyde}}{\text{butyraldehyde}} = 1:1$ (molar)			
	temperature (deg)							
	300	325	360	375	290	315	340	370
Carbon dioxide	25	30	44	44	28	42	45	56
Carbon monoxide	20	21	8	7	26	20	11	7
Unsaturated hydrocarbons	3	2	3	12	2	2	0	0
Hydrogen	52	47	45	37	44	36	44	37

TABLE 5

Catalytic Conversion of Mixtures of Esters, and of Ethyl and Butyl Alcohols, at 325°

Component ratio	Condensate yield (%)	Yield (wt. % on the original mixture)									Total ketone yield (%)
		acetaldehyde	acetone	butyraldehyde	ethyl acetate	methyl propyl ketone	dipropyl ketone	metameric esters	butyl butyrate	higher ketones	
Ethyl and butyl alcohols											
2 : 1	62.0	2.4	5.0	1.5	0.1	23.6	13.8	1.0	2.0	8.0	42.0
1 : 1	65.0	4.6	3.0	2.0	0.2	20.3	14.1	2.4	3.0	9.5	37.0
1 : 2	70.0	2.0	2.0	3.0	0.2	16.0	25.0	0.4	5.0	10.5	43.0
Ethyl butyrate and butyl acetate											
4 : 1	87.5	2.0	1.0	4.0	0.6	18.0	12.5	12.0	18.9	5.0	31
2 : 1	77.0	2.0	1.0	4.5	1.0	20.0	13.0	3.0	16.0	8.0	34
1 : 1	81.4	1.4	2.6	3.6	1.0	21.0	12.0	2.0	11.0	16.0	34.5
1 : 2	67.0	1.3	3.0	2.0	1.0	18.0	14.0	3.0	7.0	11.0	35
1 : 4	72.0	1.4	4.0	3.0	1.0	16.0	12.0	2.0	12.0	12.0	32

dipropyl ketone vary little for different ester ratios in the mixtures, whereas in the experiments with alcohols there are considerable variations in the yields of the same ketones with changes in the relative contents of the alcohols. With excess of ethyl alcohol in the original mixture, methyl propyl ketone is predominantly formed, whereas excess of butyl alcohol leads to formation of dipropyl ketone.

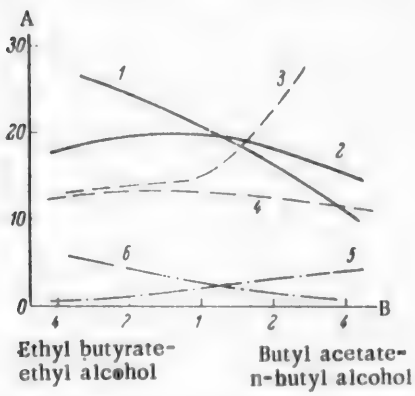

Fig. 2. Effect of component ratio on ketone yields at 325°. A) Ketone yield (wt. % on the original ester; B) molecular ratio of the original substances in the mixture. 1,2) Methyl propyl ketone; 3,4) dipropyl ketone; 5,6) acetone. Ketones: 1,3,6) from alcohol mixtures; 2,4,5) from ester mixtures.

The gaseous products formed in the decomposition of esters (Table 6) have very high carbon monoxide (18-23%) and hydrogen (45-47%) content and a very low olefin content (2-5%).

The gases formed in the conversion of alcohol mixtures have a much higher hydrogen content than the gases formed during ester decomposition. The alcohols evidently liberate additional hydrogen during their conversion into aldehydes, and so alter the relative proportion of hydrogen in the gas.

These results provide further confirmation of the hypothesis that the esters are decomposed to aldehydes, which are then converted into ketones.

Water was present in nearly all the condensates formed in the decomposition of esters and alcohols. Its presence favored a change in the gas composition (increase of the amounts of hydrogen and carbon dioxide) on the one hand, and saponification of the esters on the other. The acid content of condensates obtained from esters did not exceed 1.5-2%, and in the experiments with aldehydes and alcohols it did not exceed 0.5%.

Acetaldehyde, butyraldehyde, acetone, and methyl propyl, methyl isobutyl, methyl amyl, and dipropyl ketones were isolated from the condensates formed in the decomposition of esters. Their derivatives were prepared and the physical constants determined. The characteristics of the products obtained are identical to those published earlier [10, 11], and are not repeated here.

TABLE 6

Average Gas Composition in the Catalytic Conversion of Metameric Ester Mixtures and Mixtures of Ethyl and Butyl Alcohols at 325°

Gas composition	Contents (vol. %) at ratios					
	ethyl butyrate / butyl acetate			ethyl alcohol / n-butyl alcohol		
	2:1	1:1	1:2	2:1	1:1	1:2
Carbon dioxide	23	30	23	11	10	8
Carbon monoxide	18	21	23	10	10	13
Unsaturated hydrocarbons	2	2	5	1	1	1
Hydrogen	57	47	45	78	79	78

SUMMARY

1. The metameric esters, ethyl butyrate and butyl acetate, give rise to similar reaction products when decomposed catalytically over promoted copper catalyst.

2. The optimum temperature of ketone formation is 325°; the total ketone yield is independent of the ester ratio, and reaches 35-40%, calculated on the original ester.

3. The main and predominant direction of the catalytic conversion of esters is decomposition to aldehydes, followed by conversion of the latter into ketones through a stage of aldol condensation. This view is confirmed by the presence of considerable amounts of carbon monoxide in the gas.

LITERATURE CITED

[1] B. N. Dolgov, B. A. Bolotov and L. A. Komissarov, J. Appl. Chem. 28, 1, 71 (1955).•

[2] B. A. Bolotov, P. M. Adrov and L. K. Prokhorova, J. Appl. Chem. 28, 516 (1955).•

[3] B. A. Bolotov, B. N. Dolgov and K. P. Katkova, J. Appl. Chem. 28,1154 (1955).•

[4] B. A. Bolotov, K. P. Katkova and S. B. Izraileva, J. Appl. Chem. 30, 1,131 (1957).•

[5] B. A. Bolotov, B. N. Dolgov and N. P. Usacheva, J. Appl. Chem. 30, 8, 1230 (1957).•

[6] B. A. Bolotov, B. N. Dolgov and K. P. Katkova, J. Appl. Chem. 28, 414 (1955).•

[7] V. I. Komarewsky and I. R. Coley, J. Am. Chem. Soc. 63, 700, 3269 (1941).

[8] I. R. Coley and V. I. Komarewsky, J. Am. Chem. Soc. 68, 716 (1946).

[9] P. Sabatier, and Mailhe, C. r., 152, 669 (1911).

[10] B. A. Bolotov, B. N. Dolgov and P. M; Adrov, J. Appl. Chem. 28, 299 (1955).•

[11] B. A. Bolotov and N. A. Rozenberg-Marshova, J. Appl. Chem. 30, a, 286 (1957).•

[12] B. N. Dolgov and G. V. Golodnikov, J. Gen. Chem. 24, 987, 1167, 1361 (1954).•

Received October 5, 1956

•Original Russian pagination. See C.B. translation.

INVESTIGATION OF THE SAPONIFICATION OF POLYACRYLONITRILE BY SULFURIC ACID

E. A. Sokolova-Vasil'eva, G. I. Kudriavtsev and A. A. Strepikheev

All-Union Scientific Research Institute of Artificial Fibers

The available literature data on the saponification of polyacrylonitrile are largely confined to patents. Only the saponification of polyacrylonitrile to polyacrylic acid is considered in the scientific literature [1].

Studies of the saponification of polyacrylonitrile are of interest, not only in relation to investigations of yet another type of polymer-analog reaction, but also in connection with the growing significance of polyacrylonitrile in synthetic fiber production. The physical properties of polyacrylonitrile fibers include some exceptionally valuable characteristics, but it is generally noted that the moisture regain is inadequate (0.6-0.7% at 65% relative humidity), and the dyeing properties are poor. These characteristics of polyacrylonitrile may be improved by modification of some of the functional groups in the polymer.

It is to be expected that the new functional groups formed in the saponification of polyacrylonitrile should confer increased hygroscopicity and good dyeing properties on the polymer.

Investigation of the saponification of polyacrylonitrile is therefore of considerable interest. It is important to determine the nature of the chemical reaction, the character of the side processes, and the influence of the reaction conditions on the saponification of polyacrylonitrile and on the degree of polymerization of the substance.

These data may serve as the basis for further technological studies of the modification of polyacrylonitrile fiber properties.

In the present investigation, a study was made of the saponification of polyacrylonitrile by sulfuric acid solutions of various concentrations, unheated and at 120°.

EXPERIMENTAL

The following method was used for the saponification of polyacrylonitrile: 5 g of powdered polyacrylonitrile, of molecular weight 45,000, was dissolved in 100 ml of sulfuric acid solution of a given concentration. The time required for this process was 4 hours (unheated).

The saponified polymer was isolated by precipitation by means of anhydrous methyl alcohol. The filtered polymer was extracted with cold methyl alcohol to remove sulfuric acid. For analysis, the saponified product was reprecipitated by alcohol from aqueous solution. Absence of traces of sulfuric acid was confirmed by qualitative tests. The powder was dried in a vacuum drying cabinet under 10-15 mm residual pressure without heating, and then in a desiccator over phosphorus pentoxide.

The polymer saponified by cold sulfuric acid is a white flocculent substance, soluble in water and dilute acid and alkali solutions. The polymer did not dissolve in dimethylformamide.

The saponification of polyacrylonitrile by hot sulfuric acid was carried out by exactly the same method as the cold saponification. The product was isolated from the reaction mixture by precipitation with water. To remove traces of acid, the product was washed thoroughly with water, and then dried in a drying oven at 70-80°, and in a desiccator over phosphorus pentoxide. The saponified polymer was a gray elastic mass, soluble only in dimethylformamide.

The product formed by saponification with 50% sulfuric acid was isolated by addition of the acid solution to excess acetone. The polymer was precipitated as a white gelatinous mass. To remove sulfuric acid, the polymer was dissolved in water and then dialyzed. The aqueous solution, free from traces of sulfuric acid, was evaporated on the water bath. The product was dried at 70-75°, and then in a desiccator over phosphorus pentoxide.

Elementary analysis

Found %: C 49.2; H 5.31; N 0.52. Polyacrylic acid. Calculated %: C 50.0; H 5.55.

Saponification of polyacrylonitrile by sulfuric acid in the cold. The following section contains the results obtained by the saponification of polyacrylonitrile by 75-95% sulfuric acid in the cold. Polyacrylonitrile does not dissolve in cold acid of lower concentrations. As will be shown, the products formed on heating differ in principle from the saponification products obtained in the cold.

It is known from the literature [2] that the hydrolysis of low-molecular nitriles by 50-98% sulfuric acid results predominantly in amide formation, but if the acid concentration is below 50% the hydrolysis product is acid. Therefore it was expected that polyacrylamide would be formed in the saponification of polyacrylonitrile by 75-95% sulfuric acid. Analysis of the saponified products showed that although the nitrogen content of the polymer was close to the theoretical value for polyacrylamide, it did not exactly coincide with it. Whereas the nitrogen content of polyacrylamide is 19.7%, the nitrogen contents of the saponified products varied between 18.65 and 18.85%. The values for total nitrogen and nitrogen determined as ammonia coincide. It follows that all the nitrogen-containing groups in the saponified polymer are saponifiable by alkali. The absence of residual nitrile groups in the saponified polymer was demonstrated by a qualitative reaction [3].

TABLE 1

Saponification of Polyacrylonitrile by Concentrated H_2SO_4 (Unheated)

Experiment No.	Saponification conditions		Nitrogen content, by Kjeldahl (%)	Saponifiable nitrogen (%)	Acid no.	Specific viscosity	Functional units per 100 monomer residues			Moisture regain (%)	Notes
	acid concentration (%)	time (hrs)					amide	imide	carboxyl		
1	95	4	18.65	18.25	0.38	0.71	87.7	12.3	1	18.30	$SO_4^{"}$ ions washed out by cold methyl alcohol
2	85	4	18.85	18.48	0.724	0.85	90	10	1	18.03	
3	75	4	18.73	18.37	0.74	0.78	88.6	11.4	1	—	
4	85	4	16.96	16.58	—	—	67.8	32.2	—	13.4	$SO_4^{"}$ ions washed out by methyl alcohol at 60-70°
5	85	4	16.02	15.71	—	—	56.7	43.3	—	11.5	Dried for 3 hours at 100°

Evidently the lower nitrogen content of the resultant polymer, as compared with polyacrylamide, is the consequence of side reactions. One possibility was that some of the nitrile groups had been saponified to carboxyls. However, the acid number of the polymer was 0.38-0.74, which is virtually negligible.

The saponification of polyacrylonitrile to polyacrylamide is therefore accompanied by reactions involving the formation of nitrogen-containing groups with lower nitrogen content than that of polyacrylamide.

A hypothesis concerning the nature of these groups was advanced on the basis of the existing structural analogy between polyacrylonitrile and low-molecular 1,3-dinitriles. A characteristic of 1,3-dinitriles is the tendency to cyclization in the course of chemical reactions.

Thus, Bogert and Eccles [4] prepared the corresponding imides by the action of sulfuric acid on glutaric and succinic dinitriles at 140-180°. It is reasonable to suppose that analogous reactions take place in the saponification of polyacrylonitrile.

Intramolecular interaction of the amide groups in the polyacrylonitrile saponification product, leading to the formation of cyclic amide groups in the polymer chain may occur as follows:

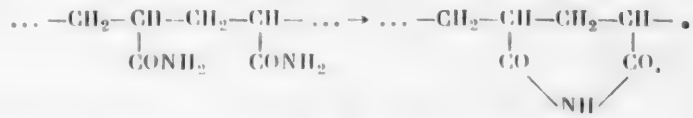

Analytical determination of imide groups in the presence of amide groups in a polymer is impossible. The existence of imide groups in the acrylonitrile saponification product was demonstrated by means of model experiments.

Glutaronitrile was chosen as the model compound for elucidation of the interaction between the functional groups of adjacent units in the polymer.

No data are available in the literature on the saponification of glutaronitrile by unheated sulfuric acid.

The formation of glutarimide on saponification of glutaronitrile would confirm the formation of imide groups in the saponification of polyacrylonitrile.

Glutaronitrile was synthesized from 1,3-propanediol (b.p. 131-132° at 10 mm, $n_D^{22.4} = 1.4364$). Saponification of glutaronitrile under the conditions used for acrylonitrile saponification yielded glutaramide in 62% yield, and glutarimide in 6% yield. The reaction products included 12% of unreacted glutaronitrile. These results suggest that the polymer contains acrylamide residues, and also structural units consisting of glutarimide residues bound into the polymer chain by methylene groups. The contents of the types of units in the polymer were estimated by calculation.

TABLE 2

Viscosities and Nitrogen Contents of Samples

Characteristics	Saponification time (hours)			
	24	48	78	120
Nitrogen content (%)	18.85	18.80	18.86	18.81
Specitific viscosity*	0.894	0.900	0.910	0.898

The results of saponification of polyacrylonitrile by 75-95% H_2SO_4 are given in Table 1.

The effect of the concentration of sulfuric acid in the 75-95% range on the chemical structure and properties of the saponified polymers was studied. It was found that the chemical composition of the polymer remains virtually unchanged over this concentration range (Experiments 1, 2, and 3 in Table 1).

The polymer is extremely sensitive to the action of heat, both in sulfuric acid solutions and during the subsequent treatment. The reaction products in Experiments 1, 2, and 3 (Table 1) were saponified and extracted unheated. These were the samples with the highest nitrogen contents and correspondingly lower amounts of imide residues. The polymer in Experiment 4 was extracted with methyl alcohol at 60-70° to remove sulfuric acid. The nitrogen content of this polymer fell to 16.96%; this corresponds to calculated values of 68 and 32% respectively for the amide and imide residues. Even more extensive imide formation took place in Experiment 5. The nitrogen content of this polymer fell to 16.02%. This polymer has limited solubility in water, because of the imide formation, both intramolecular and intermolecular.

The effect of the saponification time on the polymer composition and viscosity was also studied.

The specific viscosity of the original polyacrylonitrole was 1.659. The viscosities and nitrogen contents of samples saponified for various times are given in Table 2.

These results show that characteristics such as nitrogen content and viscosity do not depend on the saponification time. Evidently, extensive saponification occurs when the polyacrylonitrile is dissolved, and the polymer properties acquired during the chemical changes in the course of dissolution do not change under the further action

*Water was the solvent.

of sulfuric acid. It is noteworthy that the viscosity of the saponified polymer is independent of the time during which the sulfuric acid acts.

Molecular weight determinations on the original polyacrylonitrile and saponified samples showed that the molecular weight falls from 44,500 to 27,400 during saponification. The molecular weight was determined by the osmotic method.

The saponification product of polyacrylonitrile is film-forming. The films obtained from aqueous solutions are transparent and elastic.

When heated to 200° the polymer blackens, and above this temperature (250-260°) it decomposes without melting. The moisture regain of the saponified product reaches 18.3%; the moisture absorption depends on the imide group content. Thus, it falls from 18.3 to 11.5% with increase in the imide-residue content of the polymer from 12.3 to 43.3%.

Saponification of polyacrylonitrile by sulfuric acid on heating. The observed fact that the imide group content of saponified polyacrylonitrile increases on heating was of certain interest, and therefore a systematic study was made of saponification at high temperatures. Sulfuric acid in the 65-95% concentration range was used for the saponification.

TABLE 3

Results of the Saponification of Polyacrylonitrile by Concentrated H_2SO_4 on Heating (t = 90-95°)

Saponification conditions		Nitrogen content, by Kjeldahl (%)	Saponifiable nitrogen (%)	Acid number	Specific viscosity	Functional units per 100 monomer residues			Moisture regain (%)
acid concentration (%)	time (hours)					amide	imide	carboxyl	
95	4	10.48	10.03	144	0.493	15.1	66.4	18.5	—
85	4	10.55	9.96	141	0.468	15.3	66.7	18	9.3
75	4	9.32	9.12	160	0.501	3.8	75.7	20.5	8.8
65 *	5	7.88	—	224	0.362	0	70	30	8.3

The polymer saponified by hot sulfuric acid was a gray elastic mass, soluble only in dimethylformamide. The nitrogen content was only a little more than a half of that of samples saponified unheated (10.55 as compared with 18.8%). The sharp decrease of the nitrogen content in the saponified specimens shows that the imide group formation, which proceeds to a small extent unheated is more extensive on heating.

The saponification of polyacrylonitrile on heating is accompanied by partial saponification of nitrile groups to hydroxyl. The acid number of the polymer rises to 144-244.

The results obtained in the saponification of polyacrylonitrile on heating are given in Table 3.

The chemical composition of the saponified samples was calculated from analytical data.

It follows from these experiments that the polymer obtained by saponification of polyacrylonitrile consists of glutarimide residues as the principal structural units, linked in the polymer chain by methylene groups. In addition to the imide residues, the polymer contains acrylamide and acrylic acid residues.

It is clear from the results of the saponification of polyacrylonitrile by 85, 75 and 65% sulfuric acid that the number of carboxyl groups in the polymer increases with decrease of acid concentration.

When the sulfuric acid concentration was decreased to 50%, and the temperature and saponification time were increased, the reaction product was polyacrylic acid. The results of the saponification of polyacrylonitrile by 50% sulfuric acid are given in Table 4.

*Polyacrylonitrile does not dissolve in cold 65% H_2SO_4.

TABLE 4

Results of the Saponification of Polyacrylonitrile by 50% Sulfuric Acid*

Saponification conditions			Nitrogen content, by Kjeldahl (%)	Saponifiable nitrogen (%)	Acid number
acid concentration (%)	temperature (deg)	reaction time (hours)			
50	125—140	10	0.52	0	722
50	140—150	10	0.32	0	719
50	125—140	120	0.33	0	734

The polyacrylic acid formed by saponification of polyacrylonitrile contains a little nitrogen (up to 0.5%). The nitrogen is found by the Kjeldahl method, but is not found as ammonia in saponification by alkali. Nitrogen-free samples of polyacrylic acid could not be obtained even on increase of the saponification time to 120 hours.

In the light of the results obtained in the saponification of polyacrylonitrile some comments must be made on the existing ideas concerning the action of sulfuric acid on polyacrylonitrile. Rein's patents [5] describe the production of polyacrylonitrile fibers from spinning solutions of the polymer in sulfuric acid. In Rein's opinion, the dissolution of polyacrylonitrile in concentrated sulfuric acid is accompanied by partial saponification. Since no other work had been done on the saponification of polyacrylonitrile, this assertion by Rein was accepted without verification.

The results of our investigation have shown that the dissolution of the polymer in sulfuric acid involves the complete conversion of polyacrylonitrile into polyacrylamide. If it is dissolved in hot sulfuric acid, polyacrylimide, is formed, which is a product of even deeper conversion of polyacrylonitrile.

SUMMARY

1. The saponification of polyacrylonitrile gives products differing in chemical composition, depending on the concentration of the sulfuric acid and the temperature.

2. Saponification of polyacrylonitrile by 75-95% unheated sulfuric acid, yields polyacrylamide with a small content of imide groups. Imide formation predominates on heating, and may result in the formation of polyacrylimide as the principal product. When polyacrylonitrile is saponified by 50% sulfuric acid on heating, the reaction product is polyacrylic acid.

3. The results show that amide groups are converted into imide groups during the saponification of acrylomitrile; this suggests that one possible reaction in the conversion of a polymer containing reactive groups in the 1-3 position intramolecular interaction of the functional groups resulting in ring formation in the polymer chain.

LITERATURE CITED

[1] W. Kern and H. Fernow, Rubber Chemistry and Technology, 17, 356 (1944).

[2] B. S. Rabinovich and C. A. Winkler, Canad. J. of Research, 20B, 73 (1942).

[3] S. Dezani, Atti Acad. Sci. Torino, 52, 826 (1917).

[4] M. T. Bogert and D. C. Eccles, J. Am. Chem. Soc. 24, 20 (1902).

[5] H. Rein, Ang. Ch. 61, 241 (1949).

Received September 30, 1956

* The polymer—acid ratio was 1:50 in all the experiments.

THE EFFECTS OF PLASTICIZERS ON THE PROPERTIES OF POLYVINYL CHLORIDE*

Sh. L. Lel'chuk and V. I. Sedlis

In earlier investigations we determined and discussed the influence of monomeric low-molecular plasticizers on the physical, mechanical and electrical properties, including moisture permeability, of plasticized compositions. The present communication deals with the effects of a polymeric plasticizer, butadiene–acrylonitrile copolymer, known as SKN rubber, on polyvinyl chloride.

Advantages of Polymeric Plasticizers

Three principal properties are required in plasticizers: effectiveness, compatibility, and durability of action. Hardly any monomeric plasticizers conform completely to the third requirement because of their volatility, which results in eventual loss of plasticizer and consequent increase of the hardness and brittleness of the material. Moreover, low-molecular plasticizers have a number of other disadvantages. These include migration of the plasticizer from the inside to the surface layers, and into another material if the plasticized substance is in contact with another, capable of absorbing the plasticizer; this occurs, for example, when plasticized polyvinyl chloride is in contact with polyethylene insulation, with adverse effects on the dielectric properties of the insulation, or when the plasticized material is in contact with cellulose ester coatings, etc. Another defect is the leachability of plasticizers by water or organic liquids, such as gasoline or lubricating oils, with which protective films often come in contact. Such undesirable processes as evaporation and migration of the plasticizer, and leaching, occur especially rapidly in films and similar articles in which the surface area is incomparably greater than the thickness. Moreover, processes which cause premature aging of the article may result in increased moisture permeability, as evaporation or any other loss of liquid plasticizer from the composition results in the formation of micropores which facilitate moisture penetration. This is confirmed by comparisons of the moisture permeability of films of the same composition, but made by different methods: by casting from solution, when micropores are formed during film formation as the result of solvent evaporation, and by hot rolling, when evaporation of the plasticizer is slight or negligible and therefore micropores are not formed. The moisture permeability of rolled films in 120 hours is 2.50 mg/cm^2, and that of cast films is 2.77 mg/cm^2, which is appreciably higher.

Because of their high volatility, certain effective and otherwise completely satisfactory plasticizers cannot be used in a number of compositions and articles, and they have to be replaced by more costly and scarce plasticizers, which are less volatile and have less tendency to migration and leaching; for example, dioctyl phthalate is used in place of dibutyl phthalate. These facts have aroused interest in the use of polymeric plasticizers, the macromolecules of which do not have the mobility of monomeric plasticizers, and which are therefore more resistant to evaporation, migration, and leaching.

One such plasticizer for polyvinyl chloride is nitrile rubber, SKN [1-4], which is a copolymer of butadiene and acrylonitrile. As is known, this material is fairly resistant to the action of gasoline and mineral oils.

Different views have been held concerning PVC–SKN compositions; in particular, it was considered that they are simple mechanical mixtures of two polymers, in which the properties of the rubber predominate, while the PVC acts as filler (some support for this view is provided by the pronounced creep of certain compositions containing polymeric SKN). It was therefore necessary to study the plasticizing action of SKN on PVC, i.e., to study the effectiveness of this plasticizer and its compatibility with PVC.

*Communication III.

EXPERIMENTAL

The plasticization of PVC with a polymeric plasticizer, especially nitrile rubber, presented considerable difficulties. Polymers of this type are usually mixed on rolls at elevated temperatures (150-160°), which have an adverse effect on the properties of the rubber and of the whole composition. Moreover, it is difficult to ensure sufficient uniformity of the composition. For more thorough mixing (homogenization) of polyvinyl chloride with SKN, PVC and SKN latexes were mixed in the required proportions and then coagulated simultaneously.

The product formed by simultaneous coagulation of the two latexes is easily milled, forming a homogeneous elastic translucent film at 130-140°. As is known, nitrile rubber is made in several grades, according to the acrylonitrile group content. The physical and mechanical properties of polyvinyl chloride films plasticized with different amounts of SKN with different nitrile group contents* were studied. The results of these experiments are given in Table 1.

TABLE 1

Physical and Mechanical Properties of PVC Compositions Plasticized with SKN of Different Nitrile Group Contents

SKN type	Nitrile group content (%)	Tensile strength (kg/cm²)					Relative elongation at break (%)				
		SKN content of composition (wt. % relative to PVC)									
		0	25	50	75	100	0	25	50	75	100
I	19.2	553	90	25	8	5	10	15	72	170	240
II	27.1	553	265	168	100	69	10	62	175	225	257
III	35.2	553	405	275	170	110	10	75	224	295	327
IV	39.8	553	420	315	220	138	10	70	203	272	310

The strength of the compositions with a given plasticizer content increases with increase of the nitrile group content of the SKN, and the elongation at break decreases correspondingly. SKN with a low nitrile group content results in the greatest decrease of tensile strength, with the lowest values for the elongation at break. This is accounted for by the heterogeneity of the material due to the poor compatibility of this copolymer with polyvinyl chloride, as confirmed by the external appearance of the films, which are very turbid, heterogeneous in appearance, of low elasticity, and brittle. As will be shown later, the nitrile group content of SKN is very important in relation to the compatibility of polyvinyl chloride with nitrile rubber.

Effectiveness of SKN as a plasticizer for PVC. As for low-molecular plasticizers, the measure of plasticizer effectiveness was the lowering of the glass-transition temperature (T_g) of the plasticized product as compared with T_g for the unplasticized PVC; i.e., the value of ΔT_g.

The plasticizer contents in all the tables and formulas are given relative to the polyvinyl chloride resin, and not to the whole composition. In almost every instance the SKN contents are given in centimoles of plasticizer per monomer mole (62.5) of PVC. For interconversion of weight and molar proportions the following formula should be used:

$$n = \frac{p \cdot 62.5}{54} = 1.157\,p, \qquad (1)$$

where p is the number of weight parts of SKN plasticizer per 100 weight parts of PVC, n is the number of centimoles of SKN per 1 mole of PVC, and 54 is the molecular weight of the monomer unit of the SKN copolymer; this was assumed equal for all types of SKN, in view of the small differences between them (for SKN containing 19.2% nitrile groups, M = 54.2; for SKN with 35.2% nitrile groups, M = 54.5).

The values of ΔT_g for different contents of different types of SKN are given in Table 2.

*For brevity, we refer to the $-CH_2-\underset{\displaystyle CN}{\underset{|}{CH}}-$ group as the nitrile group in this paper.

TABLE 2

Values of ΔT_g for Polyvinyl Chloride Compositions Containing Various Amounts of Different Types of SKN

SKN type	Nitrile group content (%)	ΔT_g (in °C) with content of SKN plasticizer (centimoles)			
		31	62	93	124
I	19.2	83	100	108	117
II	27.1	67	77	87	95
III	35.2	55	67	75	82

TABLE 3

Effectiveness Numbers of Different Types of SKN

SKN type	Nitrile group content (%)	Effectiveness number (in °C)
I	19.2	1.6
II	27.1	1.25
III	35.2	1.08

The lowering of T_g, i.e., ΔT_g, produced by 1 centimole of SKN per 1 mole of PVC, is defined as the effectiveness number E of the plasticizer with respect to PVC.

The effectiveness numbers of 3 different types of SKN are given in Table 3.

As will be shown later, the effectiveness numbers are characteristic constants of SKN as a plasticizer for PVC; there are definite relationships between the effectiveness and a number of the properties of the composition.

Our empirical formula for the decrease of the glass-transition temperature ΔT_g produced by n centimoles of plasticizer, as a function of the effectiveness number E of the plasticizer, is given below.

$$\Delta T_g = (0.25\,n + 45)\,E, \qquad (II)$$

here E is the effectiveness number, and n is the number of centimoles of SKN per mole of PVC.

As T_g for pure polyvinyl chloride, according to our determinations, is 65°, T_g for a composition containing n centimoles of SKN is

$$\Delta T_g = 65 - (0.25\,n + 45)\,E. \qquad (III)$$

Formula (III) is derived on the assumption that the plasticization effect, i.e., ΔT_g, is a linear function of the plasticizer content and the effectiveness number. It follows from Table 4, which contains experimental values of ΔT_g and T_g, and the values calculated from Formulas (II) and (III), that this assumption is justified with a fair degree of accuracy.

TABLE 4

Values of ΔT_g and T_g for Compositions Containing 50% SKN, Calculated From Formulas (II) and (III), and Determined Experimentally

SKN type	Nitrile group content	p = 50% SKN on the wt. of PVC, n = 62 centimoles				p = 75% on the wt. of PVC, n = 93 centimoles			
		calculated		found		calculated		found	
		T_g	ΔT_g	T_g	ΔT_g	T_g	ΔT_g	T_g	ΔT_g
I	19.2	—32	97	—35	100	—44	109	—43	108
II	27.1	—10	75	—12	77	—19	84	—22	87
III	35.2	0	65	— 2	67	— 8	73	—10	75

If the value of T_g is taken as a measure of frost resistance of a composition, Formula (III) can be used to calculate and predict the frost resistance of a polyvinyl chloride mixture of known composition.

The results given by Formulas (II) and (III) are approximate, but are fairly close to the experimental values; the discrepancies are within the limits of experimental error.

It follows from these results that the highest effectiveness with respect to polyvinyl chloride is found in

SKN-19.2, the copolymer with the lowest nitrile group content; its effectiveness number is 1.6; the plasticizer effectiveness decreases with increasing nitrile group content, and the effectiveness number of SKN-35.2 is 1.08. These types of SKN occupy the reverse positions with regard to compatibility with polyvinyl chloride.

Compatibility of SKN with polyvinyl chloride. For a plasticizer to be effective, it must penetrate into the polymer phase and must be retained in it for a long time; i.e., it must be compatible with the polymer. The question of plasticizer–polymer compatibility must be considered from the general viewpoint of polymer solutions. The polymer is regarded as a liquid, and swelling and solution are regarded as processes of liquid mixing.

The problem of the compatibility of substances of high molecular weight is more complex; it has not been studied sufficiently, and few general relationships have been established in relation to it.

The compatibility of polymers has been studied by Barg, [5], Boyer [6], Dobry and Boyer-Kawenaki [7], and Struminskii and Slonimskii [8].

Their results lead to the general conclusion that the compatibility of high polymers is very slight, and incompatibility is more common than compatibility.

In our studies of the compatibility of PVC with SKN, we investigated the behavior of solutions of polyvinyl chloride – nitrile rubber mixtures, with different nitrile group contents in the rubber.

TABLE 5

Behavior of Mixed Solutions of PVC and SKN in Dichloroethane

Components of mixture	Nitrile group content of SKN (%)	Solution concentration (%)	Ratio of solutions	Behavior of solution
SKN III (low molecular weight, Defoe number 50)	34.6	0.5	1 : 1	Does not demix
		1.0	1 : 1	
		1.5	1 : 1	
		2.0	1 : 1	
SKN III (high molecular weight, Defoe number 1900)	35.2	0.5	1 : 1	
		1.0	1 : 1	
SKN II (Defoe number 1400)	27.1	0.5	1 : 1	
		1.0	1 : 1	
		1.5	1 : 1	Demixes
		2.0	1 : 1	
SKN I (Defoe number 1700)	19.2	0.5	1 : 1	
		1.0	1 : 1	
		1.5	1 : 1	
		2.0	1 : 1	

The procedure was as follows. Solutions of polyvinyl chloride and SKN, of different concentrations (0.5, 1.0, 1.5, and 2.0%) were made in dichloroethane. Carefully measured amounts (usually 15 cc) of both polymer solutions were put into a test tube. The liquids were mixed thoroughly and left to stand. The results of the mixing tests are given in Table 5.

It is seen that when PVC solutions are mixed with SKN of different nitrile group contents the behavior of the solutions is different. Mixtures of PVC with SKN containing about 35% nitrile groups do not separate out at any concentrations in the 0-2% range. There is no demixing in mixtures with SKN II in the 0.5-1.0% concentration range. At higher concentrations demixing occurs. Mixtures of PVC solutions with SKN I separate out at all concentrations; this shows convincingly that they are incompatible.

This behavior of the solutions is in harmony with the physical and mechanical properties (Table 1). It follows from Table 1 that, as is to be expected, increase of the nitrile group content in the SKN copolymer produced an increase in the strength of the polyvinyl chloride composition, but the relative elongation at break also increases. As SKN itself becomes harder with increasing nitrile group content, this fact must be attributed to better compatibility of PVC with types of SKN richer in acrylonitrile groups. The data on the mechanical properties of PVC–SKN compositions are in agreement with the results reported by Reznikova, Zaionchkovskii and Voiutskii [9].

TABLE 6

Effect of the Molecular Weight of SKN on the Mechanical Properties of PVC Mixtures (Nitrile Group Content 35%)

Molecular weight	Defoe number	Tensile strength (kg/cm²)					Relative elongation at break (%)				
		SKN content of mixture (wt. % on PVC)									
		0	25	50	75	100	0	25	50	75	100
390000	1900	553	405	275	170	110	10	75	224	295	327
40000	50	553	375	255	172	106	10	91	295	360	380

The low mechanical data for compositions containing SKN I (SKN of the lowest nitrile group content) can be attributed to the poor compatibility of PVC with this type of SKN, and a certain degree of microheterogeneity in the structure of such mixtures. Similar effects, accounted for by microheterogeneity, were observed and described by Komskaia [10] in a study of the physicochemical properties of vulcanizates based on mixtures of different rubbers; it was noted that the mechanical properties of the vulcanizates fell sharply, and the effect was ascribed to microheterogeneities in the mixtures.

Rylov [11] confirmed the possibility of microheterogeneity of polymer mixtures in absence of macromixing.

Studies of the behavior of PVC compositions plasticized with SKN showed that, in addition to the nitrile group content of the SKN, the molecular weight (degree of polymerization) of SKN has a significant influence on compatibility and the plasticization effect. In this connection we used, as plasticizers, two samples of SKN of approximately the same nitrile group content (about 35%), but differing considerably in the degree of polymerization, which was characterized by the viscosity and the Defoe hardness.

One sample had Defoe number 1900, and molecular weight about 390,000, and the other had Defoe number 50 and molecular weight 40,000. The molecular weight was found from the formula $[\eta] = K \cdot M^{\alpha}$; the values of K and α vary with the type of rubber and the solvent. In our experiments, for calculations of the molecular weight of SKN (chloroform as solvent) the values $K = 5.4 \cdot 10^{-4}$ and $\alpha = 0.68$ were used.

TABLE 7

Values of the Moisture-Permeability Constant P of PVC Compositions with Different Contents of SKN of Various Types

SKN type	Nitrile group content (%)	Moisture-permeability constant ($P \cdot 10^8$ g/cm · hour · mm Hg) with SKN contents in compositions (wt. % on PVC)				
		0	25	50	75	100
I	19.2	0.50	2.44	4.13	5.85	7.52
II	27.1	0.50	1.25	2.09	2.70	3.40
III	35.2	0.50	0.85	1.37	1.70	2.12
VI	39.8	0.50	0.80	1.20	1.45	1.75

TABLE 8

Values of ΔT_g, P, D and $\underline{h}$ for PVC Composition Plasticized with SKN of Different Nitrile Group Contents (All compositions contained 25 weight parts SKN per 100 weight parts PVC, or 31 centimoles SKN per 1 mole of PVC)

SKN type	Nitrile group (%)	ΔT_g (°C)	E No. (°C)	$P \cdot 10^8$ (g/cm · hr, mm Hg)	$D \cdot 10^4$ (cm²/sec.)	$h \cdot 10^3$ (g/cc · mm Hg)
I	19.2	83	1.6	4.13	1.50	2.82
II	27.1	67	1.24	2.00	0.66	3.00
III	35.2	55	1.08	1.37	0.40	3.40

Compositions both with the low-molecular and the high-molecular SKN were prepared. The mechanical properties of these samples are given in Table 6.

The tensile strength of specimens containing low-molecular SKN is almost the same as that of compositions with the high-molecular SKN, but the relative elongation of the former is somewhat greater; this should be ascribed to the better compatibility of PVC with low-molecular SKN. The films in the latter case were more homogeneous in appearance, more transparent, and did not whiten on bending. A mixture of polyvinyl chloride

TABLE 9

Moisture-Proof Properties (Values of P) of Different PVC Compositions for Constant T_g of $-28°$

Plasticizer	Centimoles of plasticizer per mole of PVC	Wt. parts of plasticizer per 100 wt. parts of PVC	Moisture-permeability constant $P \cdot 10^8$
Dibutyl phthalate DBP	11	50	3.24
Tricresyl phosphate TCP	12.2	73	2.97
Dioctyl phthalate DOP	8	50	1.98
Dibutyl adipate DBA	7	30	2.20
Dioctyl adipate DOA	5	30	2.33
Dibutyl sebacate DBS	5.6	28	2.10
Dioctyl sebacate DOS	4.6	31	2.07
SKN-35.2	62	50	1.37

with low-molecular SKN is much more easily masticated on rolls. The difference between the mechanical properties of the two samples was most pronounced in studies of film creep with time under constant load (50 kg/cm^2). Tests on the films under prolonged stress showed that films containing the high-molecular SKN were destroyed after 24 hours, whereas films containing low-molecular SKN were destroyed under the same conditions only after a considerably longer time (over 10 days), and their residual deformation after removal of the load was less. This effect can be accounted for by microheterogeneity of the compositions containing high-molecular SKN; this is not visible externally, but becomes apparent if the system PVC–SKN is in the stressed state, with excessive local stresses in individual regions, causing formation of fine cracks and consequent failure of the specimen. This was confirmed by tests on articles made from PVC films plasticized with high-molecular SKN. After a fairly short time fine cracks formed at the regions of greatest stress (at the bends). Articles from compositions containing low-molecular SKN did not show this effect.

Moisture permeability of polyvinyl chloride plasticized with SKN. The method described earlier [12] was used for studies of moisture permeability (coefficient of moisture permeability P, and solubility coefficient h).

The values of P for PVC compositions plasticized with SKN of different nitrile group contents are given in Table 7.

The lowest moisture permeability is found in compositions containing SKN with high nitrile group contents. As in compositions containing low-molecular plasticizers, the moisture permeability increases with the effectiveness of the plasticizer (Table 8).

TABLE 10

Comparison of Moisture-Permeability Coefficients P Calculated from Formula (IV) and Determined Experimentally

SKN type	Nitrile group content (%)	$P \cdot 10^8$ (g/cm · hour · mm Hg)			
		$n = 31$ centimoles		$n = 62$ centimoles	
		calculated	found	calculated	found
I	19.2	2.43	2.44	4.13	4.13
II	27.1	1.30	1.25	2.21	2.09
III	35.2	0.81	0.80	1.19	1.20

It might be thought that the moisture permeability should increase with increasing content of the polar nitrile groups in the plasticizer, because of the increase of water sorption. Water sorption does increase with increasing nitrile group content, but the moisture permeability P decreases owing to decrease of the second factor D in the formula $P = D \cdot h$.

The lowest moisture permeability was found for the film containing SKN of the highest nitrile group content (35-40%), and it also had the highest water sorption. It is known that the content of polar groups such as OH, COOH, COO, CN etc., which form "sites of attraction," is one of the decisive factors in moisture permeability. However, in the PVC–SKN system the moisture permeability decreases with increase of the CN group content, instead of increasing. It is probable that the predominant factor in this case is inter- and intramolecular interaction, which increases with the polar group content. In this case the chains and segments are more rigidly bound and become less mobile; this hinders the formation of temporary channels along which the water molecules migrate, and leads to decreased diffusion and moisture permeability. As Table 8 shows, this is confirmed by the decrease of the diffusion D with increase of sorption h. A similar effect is found with increase of the Cl content in a polymer; an example is chlorinated polyvinyl chloride (perchlorovinyl, Vinifol), the moisture-permeability coefficient of which ($P = 10^{-9}$) is lower than that of polyvinyl chloride ($P = 0.5 \cdot 10^{-8}$). As the nitrile group content of the SKN increases, the polar interaction is intensified and the effectiveness of the plasticizer decreases, but its compatibility with PVC becomes greater and the moisture permeability of the compositions diminishes.

In conclusion, we compare the moisture proof properties of PVC compositions plasticized with different monomeric plasticizers and with SKN (35% nitrile groups) for the same plasticizing effect, i.e., for the same value of ΔT_g, 93°, or the same frost resistance T_g, −28°.

The comparative data are presented in Table 9.

It is seen that, for a given plasticization effect, i.e., for constant T_g, the composition w th SKN-(III) has the lowest moisture-permeability constant; apart from other advantages (absence of migration, little leaching, high resistance to hydrocarbons and oil), this makes this plasticizer useful for the production of moisture proof articles, with low permeability to water vapor, despite its lower effectiveness in comparison with certain low-molecular plasticizers.

The linear relationship, established by us for low-molecular plasticizers, between the moisture-permeability coefficient, the molar content of the plasticizer, and its effectiveness number can be applied to polymeric plasticizers; this gives the following empirical formula for the moisture-permeability coefficient P in terms of the molar content n (centimoles) of the plasticizer in the composition and the effectiveness number E:

$$P = P_0 (0.11n + 1.47)(1.28E - 1.052)\ g \cdot cm^{-1} \cdot hour^{-1} \cdot mm\ Hg^{-1}, \qquad (IV)$$

Table 10 contains values of P calculated from Formula (IV) for different types of SKN with n = 31 and 62 centimoles.

SUMMARY

1. The recent tendency to use polymeric plasticizers is justified in a number of cases; these plasticizers have a number of advantages over low-molecular plasticizers: absence of migration, nonvolatility, and lower leachability. It is shown that butadiene–acrylonitrile copolymer (SKN) is capable of plasticizing PVC. This plasticization is measured in terms of the decrease of the glass-transition temperature (effectiveness number) of the composition, and depends on the nitrile group content of the plasticizer.

2. The compatibility of SKN with PVC increases with increasing nitrile group content in the SKN. The best compatibility and satisfactory effectiveness are found in the butadiene–nitrile copolymer containing 35-40% nitrile groups, with molecular weight about 40,000 (Defoe plasticity about 50). This copolymer yields homogeneous transparent films, of high mechanical strength, low residual deformation, and low permeability to water vapor.

3. The moisture permeability of polyvinyl chloride films containing SKN depends on the nitrile group content of the latter: the moisture permeability decreases with increasing nitrile group content.

4. Formulas are derived for the relationships between certain properties of plasticized compositions (lowering of the glass-transition point, frost resistance, moisture permeability) and plasticizer effectiveness.

LITERATURE CITED

[1] R. A. Emmet, Ind. Eng. Chem. 36, 130 (1944).

[2] M. C. Read, Modern Plastics, 7, 117 (1947).

[3] R. A. Reznikova, Candidate's Dissertation (Moscow, 1952).*

[4] I. E. Pittenger and C. F. Gohm, Modern Plastics, 25, 80 (1947).

[5] E. I. Barg, in the Collection: Plastics, 1, 353 (1935).

[6] R. F. Boyer, J. Appl. Phys. 20, 540 (1949).

[7] A. Dobry and F. Boyer-Kawenaki, J. Pol. Sci. 20, 90 (1947).

[8] G. V. Struminskii and G. L. Slonimskii, J. Phys. Chem. 9, 1941 (1956).

[9] R. A. Reznikova, A. D. Zaionchkovskii and S. S. Voiutskii, Colloid J. 15, 108 (1953).**

[10] N. F. Komskaia, Candidate's Dissertation (Moscow, 1952).*

[11] E. E. Rylov, Candidate's Dissertation (Moscow, 1952).*

[12] Sh. L. Lel'chuk and V. I. Sedlis, J. Appl. Chem. 30, 7, 1041 (1957).**

Received August 23, 1956

*In Russian.

**Original Russian pagination. See C.B. translation.

BRIEF COMMUNICATIONS

INVESTIGATION OF THE RECOVERY OF SELENIUM FROM ALKALINE SOLUTIONS

O. V. Al'tshuler and F. F. Kharakhorin

In view of the scarcity of selenium, and its increasing importance in semiconductor technology, the question of selenium recovery from used and imperfect articles is of some significance. The first step in the recovery is usually dissolution of Se in concentrated alkali. In industrial practice selenium is not subsequently precipitated, by acidification of the alkaline solutions because of the generally-held view that this is inevitably accompanied by the liberation of highly toxic hydrogen selenide (by the reaction $Na_2Se + 2HCl = 2NaCl + H_2Se$ which is cited in general chemistry manuals and in D. M. Iukhtanov's monograph: "Production of Selenium and Tellurium"). This view does not take into account the instability of H_2Se in presence of moisture and oxygen, and especially of moist surfaces. Our experiments with alkaline selenium solutions showed that it is not difficult to find conditions in which, even if H_2Se is formed as a first step, it is decomposed almost at once with liberation of elemental selenium, and selenium does not enter the gas phase either as hydrogen selenide, or in any other form. The liberation of selenium is probably the result of an oxidation reaction which yields elemental selenium and water.

Radioactive Se^{75} in the elemental form was used for the experiments. The active selenium was introduced into fused selenium, which was then dissolved in concentrated alkali. In some experiments Se^{75} was added to previously-prepared alkaline selenium solution.

TABLE

Results of Experiments on Selenium Recovery

Concentration (g/liter)		Activity of alkaline solution (pulses/min)	Activity of absorbent solution (pulses/min)	Selenium as H_2Se (%) of original amount)	Notes
Se	NaOH				
240	600	3370	320	9.4	
180	400	6530	147	2.3	CdSe precipitated
120	300	6400	0.0	0.0	
60	150	6780	0.0	0.0	CdSe not precipitated
30	75	6700	0.0	0.0	

Concentrated hydrochloric acid was added from a dropping funnel into the reaction flask containing the active solution, connected to a series of absorption flasks containing NaOH and $CdSO_4$ solution for absorption of hydrogen selenide. At the end of the precipitation the activity of the absorbent solutions was determined, and the fraction of the selenium which entered the gas phase was calculated. The end of the precipitation was indicated when the formation of a red amorphous precipitate ceased and the solution became decolorized.

The data in the table show that the liberation of hydrogen selenide depends on the degree of dilution of the alkaline selenium solution. The original, most concentrated solution contained 24 g of selenium per 100 ml NaOH (600 g NaOH per liter). In this experiment about 10% of the activity passed into the gas phase. Dilution of the alkaline solution with water suppressed the liberation of H_2Se, and after twofold dilution the absorbent solutions were no longer active. The absence of hydrogen selenide formation under these conditions was also

confirmed visually: when selenium could not be detected radiometrically, the NaOH solution was not colored and cadmium selenide was not precipitated in the absorption flasks. Dilution also ensures that the reaction proceeds smoothly without much evolution of heat or spattering of the solution, with formation of a precipitate which settles and filters well. Moreover, dilution of the original solution prevents precipitation of the sodium chloride formed during neutralization, and makes it easier to wash the sodium chloride out of the precipitated selenium.

Additional experiments showed that liberation of hydrogen selenide depends on the alkali concentration of the original solution, and not on the selenium concentration. Below are given the results of experiments in which the selenium concentration of the solution was kept constant at 20 g/liter, while the alkali concentration was varied from 160 to 640 g/liter. It is seen that hydrogen selenide begins to appear when the NaOH concentration is 480 g/liter, and is evolved at an increasing rate with increase of alkali concentration.

NaOH concentration (g/liter)	Precipitation of CdSe in the absorbent solution
160	No precipitate
320	No precipitate
480	Traces
640	Appreciable

The selenium yield (i.e., the fraction precipitated as elemental selenium) was not less than 95% in absence of losses in the form of hydrogen selenide. The selenium precipitate was filtered off, washed free from chloride, and either dried to constant weight or melted, and weighed.

The results are given below.

Weight of Se taken (g)	Weight of Se precipitated (g)	Yield of Se (%)
5.00	4.86	97
5.00	4.80	96
5.00	5.00	100
9.85	9.55	97

An attempt was made to recover selenium remaining in solution after precipitation by hydrochloric acid. The $BaCl_2$ test showed that such solutions did not contain selenium as selenate. When metallic zinc was introduced into the solution, small amounts of elemental selenium were liberated, indicating the presence of quadrivalent selenium. However, activity determinations on the precipitated selenium showed that only about 10% of the residual activity in the solution after precipitation by hydrochloric acid is associated with selenium; 90% of the activity is evidently due to contamination of the active material by extraneous active impurities.

The small losses of selenium in HCl precipitation are due to partial oxidation of sodium selenide to selenite, which does not liberate selenium on addition of acids.

Our experiments on industrial waste liquors containing selenium showed that selenium can be recovered almost completely from them by hydrochloric acid precipitation; 25-30% dilution is enough to prevent completely the liberation of hydrogen selenide. Thus, a simple method for selenium recovery from alkaline solutions, by the action of hydrochloric acid, may be recommended on the basis of these results.

The dilution of the original concentrated alkaline selenium solutions by water so that the alkali concentration does not exceed 300 g/liter is a necessary condition. The final concentration of hydrochloric acid after precipitation of the selenium should be 2.3-2.5 N.

SUMMARY

1. A method has been developed for the recovery of selenium from alkaline solutions; it is based on precipitation of selenium by the addition of hydrochloric acid. The method was tested with model and industrial solutions.

2. Investigation of the distribution of selenium between the solid, liquid, and gas phases during precipitation showed that a necessary condition for the avoidance of hydrogen selenide liberation is a certain degree of dilution of the concentrated alkaline selenium solutions. The NaOH concentration must not exceed 300 g/liter.

3. The yield of precipitated selenium under these conditions is 95-100%. Slight losses are caused by partial oxidation of selenide to selenite, from which selenium cannot be liberated by the action of acid.

We express our gratitude to D. M. Chizhikov for his constant interest and valuable advice.

Received July 11, 1957

SEPARATION AND ANALYSIS OF MIXTURES OF CHLORINATED METHANE DERIVATIVES BY A CHROMATHERMOGRAPHIC METHOD

D. A. Viakhirev and L. E. Reshetnikova

The commonest method for analysis of industrial mixtures of CH_3Cl, CH_2Cl_2, $CHCl_3$, and CCl_4 is rectification; its defects are its lengthiness and low accuracy. In recent years the use of infrared and mass-spectrum methods [1-3] has been recommended for analysis of these mixtures; however, because of their complexity these methods have not yet been adopted in practice as control methods in the production of chlorinated methanes. Our investigations have shown that the chromathermographic method devised in 1951 by Zhukhovitskii and his associates [4] is a very convenient, rapid, and sufficiently accurate method for this purpose. This method is now used with success for determination of simple hydrocarbons (CH_4, C_2H_4, C_2H_6, C_3H_6, C_3H_8, C_4H_{10} etc) in air, natural gases, and gaseous products formed in cracking and pyrolysis of petroleum [4-9], and is much superior in accuracy and speed to the usual method of low-temperature rectification [10].

EXPERIMENTAL*

The chromathermographic apparatus shown in Fig. 1 was used for experiments carried out in order to determine the optimum separation conditions and to develop an analytical procedure suitable for production control. The apparatus differed from the units described previously [6-9] by the fact that the exit-concentration and temperature curves were recorded automatically by means of the SG-6 recording millivoltmeter connected to a heat-conductivity gas-analysis apparatus GEUK-21 and a Cu–constantan thermocouple.** The analysis was performed as follows. The unknown liquid mixture was introduced into the widened top end of the column by means of a micropipet, and transferred to the adsorbent by application of gentle heat and the passage of a small stream of nitrogen. Gaseous methyl chloride, or samples of production gas, were measured in a gas buret and introduced into the column from the buret.

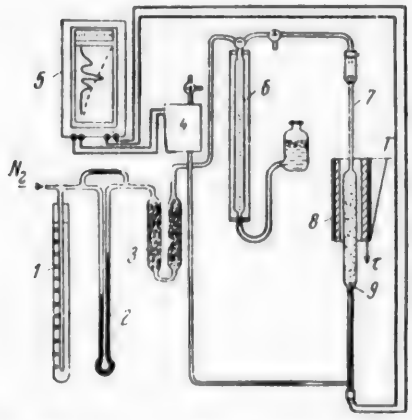

Fig. 1. Semiautomatic chromathermographic gas-analysis apparatus. 1) Manostat; 2) rheometer; 3) $CaCl_2$ tube; 4) GEUK-21 gas-analysis apparatus; 5) recording millivoltmeter; 6) gas buret; 7) chromatographic column; 8) moving furnace; 9) thermocouple.

As soon as the mixture for analysis reached the absorbent, the furnace was moved with its lower end on the thermocouple; the previously regulated current of nitrogen and the driving mechanisms of the furnace and recording instrument were switched on. This instant was taken as the start of the experiment. The ratio of the furnace speed (v) to the velocity of the nitrogen stream (α) was kept constant during each experiment, but could vary for different experiments.

*A. S. Bazarova took part in the experimental work.

**A dual thermocouple was used, with which the temperature could be measured to the nearest ± 1°. The thermocouple was disconnected after the optimum separation conditions had been determined.

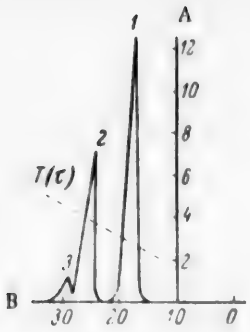

Fig. 2. Vapor chromathermogram of an artificial four-component mixture, obtained on treated MSM silica gel. A) Potential (mv), B) time (minutes). 1) CH_3Cl; 2) $CH_2Cl_2 + CCl_4$; 3) $CHCl_3$. T (τ) represents the temperature curve.

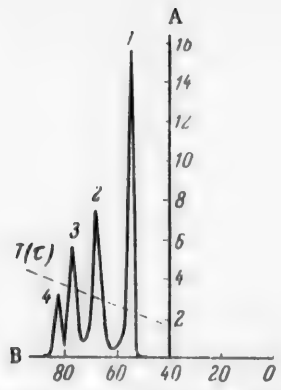

Fig. 3. Vapor chromathermogram of an artificial four-component mixture, obtained on kieselguhr impregnated with vaseline oil. A) Potential (mv), B) time (minutes). 1) CH_3Cl; 2) CH_2Cl_2; 3) $CHCl_3$; 4) CCl_4. T (τ) represents the temperature curve.

The gas leaving the column passed into two compartments of the gas analyzer (by heat conductivity), while the other two compartments were filled with nitrogen. The concentration of the components of the analyzed mixture, desorbed from the column under the influence of two factors – the current of developer (nitrogen), and the moving temperature field of the furnace – was recorded on the moving band of the recording millivoltmeter, connected to the gas analyzer. The temperature curve was simultaneously recorded on the same band; this curve gave the desorption temperatures of the components, so that the sequence of their exit from the column could be established and the optimum separation conditions determined. The quantitative analysis was based on the peak heights as described below.

The sorbents tested were ASK, ASM, and MSM silica gels, and AR-3, AG-2, and KAD active carbons, powdered (d = 0.25-0.5 mm) and dried to constant weight in a thermostat. In addition, on the advice of Prof. A. A. Zhukhovitskii, ASK and MSM silica gels were treated with concentrated HCl, washed with distilled water, and then treated with dilute KOH solution, in order to suppress catalytic reactions. In addition, several sorbents the action of which depends on the principle of vapor-phase partition chromatography [11] were prepared and tested. The sorbent was kieselguhr impregnated with high-boiling liquids: dibutyl phthalate, nitrobenzene, tetralin, sunflower oil, and vaseline oil (medical). Synthetic mixtures of chlorinated methanes, and gases from the methane-chlorination plant, were studied. The substances used for preparation of the synthetic mixtures were thoroughly purified by fractional distillation.

For selection of the optimum separation procedure, the following conditions were varied with each of the

TABLE 1

Check of the Analytical Method with the Use of MSM Silica Gel as Sorbent. Optimum separation conditions: $\alpha' = 200$, $\alpha = 63.7$, $\nu = 0.8$, $\eta = 0.012$

CH_3Cl			$CH_2Cl_2 + CCl_4$			$CHCl_3$		
q_1	q_2	ε	q_1	q_2	ε	q_1	q_2	ε
6.0	6.2	+3.3	6.3	6.4	+1.59	1.46	1.5	+2.7
14.09	14	—0.64	10.5	10.7	—1.9	1.38	1.33	—3.6
10.0	9.9	—1.0	4.33	4.5	+3.9	—	—	—
4.48	4.5	+0.44	4.9	4.96	+1.23	0.76	0.76	0
6.48	6.7	+3.4	3.47	3.5	+0.86	1.54	1.51	—1.95
7.38	7.3	—1.08	3.15	3.2	+1.59	1.4	1.38	—1.43

above-named sorbents: the ratio $\eta = \frac{v}{\alpha}$, the amount of mixture introduced into the column, the maximum furnace temperature, the component ratio in the mixture, etc.

It was found that some degree of separation of four-component chlorinated methane mixtures occurs on many of the sorbents tested. Decomposition of $CHCl_3$ and CCl_4 with liberation of HCl and Cl_2 took place on active carbons. Therefore the use of carbon had to be abandoned. Partial decomposition also took place on untreated MSM, ASM, and ASK silica gels, so that these too could not be used. The separation was satisfactory although not complete on ASK and MSM silica gels treated as described above. CH_3Cl was the first to be desorbed from the column, followed by CH_2Cl_2–CCl_4 mixture, and finally $CHCl_3$.

Figure 2 shows a typical chromathermogram of an artificial four–component mixture, obtained on treated MSM silica gel.

TABLE 2

Check of the Analytical Method with the Use of Kieselguhr, Impregnated with Vaseline Oil, as Sorbent. Optimum separation conditions: $\alpha' = 70$, $\alpha = 22$, $v = 1.3$, $\eta = 0.058$

CH_3Cl			CH_2Cl_2			$CHCl_3$			CCl_4		
q_1	q_2	δ	q_1'	q_2	δ	q_1	q_2	δ	q_1	q_2	δ
4.45	4.5	+1.1	3.8	4.0	+5.2	0.9	0.85	—5.5	0.42	0.39	—7.1
5.3	5.2	—1.8	4.18	4.2	+0.47	1.68	1.6	—4.7	—	—	—
6.0	6.2	+3.3	2.36	2.5	+5.8	0.9	0.9	0.0	0.7	0.68	—2.8
7.05	7.2	+2.1	3.8	4.0	+5.2	2.20	2.10	—5.0	0.42	0.40	—4.7
8.02	8.5	+4.3	4.6	4.4	—4.3	2.78	2.62	—5.7	0.71	0.7	—1.4

Virtually complete separation was effected by the chromathermographic method on kieselguhr impregnated with vaseline oil; this is shown by the chromathermogram in Fig. 3. Similar separation results were obtained by the elution method with the same sorbent; this is in agreement with the results of Purnell and Spencer [12] although they added stearic acid to the vaseline oil. With the use of kiselguhr impregnated with vaseline oil, the desorption sequence was different, namely: 1) CH_3Cl; 2) CH_2Cl_2; 3) $CHCl_3$ and 4) CCl_4 (from the beginning of the experiment).

Owing to the compression effect of the adsorption bands in the chromathermographic column, the heights of the peaks on the chromathermograms are proportional to the contents of the respective components in the mixture [4-6]. Our calibration graphs for the four chlorinated methanes, not given in this paper for reasons of space, were linear, thus confirming the above conclusion. The analytical method was checked by means of these graphs, based on chromathermograms for different samples of a standard artificial mixture, against chromathermograms of known amounts of this mixture. The results of these checks, with the use of MSM silica gel treated with HCl and KOH, and of kieselguhr impregnated with vaseline oil, are given in Tables 1 and 2, the following notation being used: q_1 and q_2 are the respective amounts of a given component taken for analysis, and found from the calibration graph, in milliliters of vapor under normal conditions; δ is the relative error in the determination of the component (%); α' is the volume flow rate of nitrogen (ml/minute); α is the linear nitrogen velocity (cm/minute); v is the furnace velocity (cm/minute). It follows from these data that the arithmetic mean error in the chlorinated methane determinations are, in the first case (%): CH_3Cl 1.64, $CH_2Cl_2 + CCl_4$ 1.84, $CHCl_3$ 1.9, and in the second, CH_3Cl 2.5, CH_2Cl_2 4.2, $CHCl_3$ 4.2, CCl_4 4.0. Since the samples of artificial liquid mixture taken for the check analyses were small (0.005-0.2 ml), these errors may be regarded as quite admissible.

Out method for the chromathermographic analysis of chlorinated methanes is already in use as a control method in one methane-chlorination plant.

SUMMARY

A method of chromathermographic analysis of chlorinated methane mixtures, with the use of MSM silica gel and kiselguhr impregnated with vaseline oil as sorbents, has been developed; its main advantages are speed

(20-40 minutes), the possibility of separate determinations of chlorinated methanes in one small sample (0.005-0.2 ml of liquid or 5-30 ml of vapor), and its objective character, due to automatic recording of the results in the form of chromathermograms.

In conclusion, it is the authors' duty to express their deep gratitude to A. A. Zhukhovitskii for valuable device in the search for optimum separation conditions of the chlorinated methane mixtures, and to Z. S. Smolian, Z. V. Anisimova, Ia. P. Kolesnikov, A. S. Bazarova, and others for their active help in the industrial introduction of this method.

LITERATURE CITED

[1] P. F. Urone and M. L. Druschel, Analyt. Chem. 24, 615 (1952).

[2] R. B. Bernstein, C. P. Cemeluk and B. Arends, Analyt. Chem. 25, 139 (1953).

[3] S. E. Kuprianov, R. V. Dzhagatspanian, V. M. Tikhomirov and N. N. Tunitskii, Factory Labs. 21, 1182 (1955).

[4] A. A. Zhukhovitskii, V. A. Sokolov, O. M. Zolotareva and A. M. Turkel'taub, Proc. Acad. Sci. USSR 77, 433 (1951).

[5] A. A. Zhukhovitskii, A. M. Turkel'taub and T. V. Georgievskaia, Proc. Acad. Sci. USSR 92, 937 (1953).

[6] A. M. Turkel'taub, V. P. Shvartsman, T. V. Georgievskaia, O. V. Zolotareva and A. I. Karymova, J. Phys. Chem. 27, 1827 (1953).

[7] B. V. Aivazov and D. A. Viakhirev, J. Appl. Chem. 26, 505 (1953).*

[8] D. A. Viakhirev, A. I. Bruk and S. A. Guglina, Proc. Acad. Sci. USSR 90, 577 (1953).

[9] D. A. Viakhirev, A. I. Bruk and S. A. Guglina, Factory Labs. 20, 803 (1954).

[10] M. E. Dement'eva, Analysis of Hydrocarbon Gases (State Fuel Tech. Press, Moscow-Leningrad, 1953).**

[11] A. T. James and A. I. P. Martin, Bioch. J. 50, 679 (1952).

[12] J. H. Purnell and M. S. Spencer, Nature, 175, 988 (1955).

Received September 5, 1956

*Original Russian pagination. See C.B. translation.

**In Russian.

CERTAIN AZO DYES OBTAINED FROM 4,4'-DIAMINODIPHENYL-3,3'-DIHYDROXYACETIC ACID AND N-ARYL-3-METHYL-5-AMINOPYRAZOLES

V. I. Mur and I. F. Mikhailova

The K. E. Voroshilov Institute of Organic Intermediates and Dyes

Among the direct azo dyes, those based on 4,4'-diaminodiphenyl-3,3'-dihydroxyacetic acid [1-4] (I) are of interest. When the bisdiazo compound of the latter is coupled with various derivatives of the naphthalene series, blue and gray dyes are obtained [5], characterized by purity of hue and good light fastness after treatment with copper salts. If N-aryl-3-methyl-5-pyrazolones [6] are used as the azoic components, dyes are formed which dye vegetable fibers (after copper-salt treatment) in pure red and ruby shades, but the dyeings are not fast to light. Light exposure leads to considerable deepening of hue; the dyeings fade very little, but acquire hues similar to those given by the copper complexes of dyes made by the coupling of the bisdiazo compound of 4,4'-diamino-3,3'-dihydroxydiphenyl with the same components.

It is known [3] that if the keto group in 1-phenyl-3-methyl-5-pyrazolone is replaced by an imino group, i.e., if aminopyrazole is used instead of pyrazolone, the dyes formed are faster to light and do not change hue after insolation. A patent [7] refers to red dyes, fixed by means of copper salts and made by the coupling of the bisdiazo compound of (I) with N-aryl-3-methyl-5-aminopyrazoles; sulfamide derivatives are not mentioned among the latter.

In view of the fact that sulfamide derivatives are now widely used in dye synthesis, and commercial azo dyes containing sulfamide groups instead of sulfo groups in the molecule are available, it was of interest to synthesize dyes and their copper complexes from (I) and 1-sulfamidophenyl-3-methyl-5-aminopyrazoles, and to study their properties.

Dyes of the following composition were synthesized:

1 molecule of (I) $\rightleftarrows$ 2 molecules of 1-(4'-sulfamidophenyl)-3-methyl-5-aminopyrazole (II),
1 molecule of (I) $\rightleftarrows$ 2 molecules of 1-(3'-sulfamidophenyl)-3-methyl-5-aminopyrazole (III),
1 molecule of (I) $\rightleftarrows$ 2 molecules of 1-(4'-sulfophenyl)-3-methyl-5-aminopyrazole (IV),
1 molecule of (I) $\rightleftarrows$ 2 molecules of 1-phenyl-3-methyl-5-aminopyrazole (V),

their copper complexes were prepared, the absorption spectra of both were determined, and the fastness to light and wet treatments on cotton fibers tested.* It was found the dyes have maximum absorption at very similar wave lengths, with λ_{max} ($m\mu$) of 462 for (II), 463 for (III), 465 for (IV), and 460 for (V). The copper complexes show maximum absorption at longer waves and over wider regions; the values of λ_{max} for the corresponding complexes (in $m\mu$) are 486 for (II), 504 for (III), and 496 for (IV). The absorption spectrum of the (V) copper complex was not determined, as the substance is very difficult to dissolve.

All the dyes give yellow hues on vegetable fibers (the dyeing was carried out under normal direct-dyeing conditions, but with increased amounts of soda), not fast to light or wet treatments; when metallized with copper salts or DTsM the dyeings become red, deeper in dyes containing sulfo and sulfamide groups than in dyes without these groups, and become fast to light (rating 4 on a five-point scale). The fastness to wet treatments after metallizing with DTsM is good for dyes (II), (III), and (V) and satisfactory for (IV).

*The fastness tests were carried out under standard conditions by Colorist Z. A. Gryzlova under the guidance of A. G. Emel'ianov.

It follows that dyes of the above-mentioned types, containing sulfamide groups, are not faster to light than the corresponding dyes containing sulfo groups or without substituents, but are faster to wet treatments than the sulfo derivatives, have deeper hue than the unsubstituted dyes, and are not inferior to the latter in fastness to wet treatments.

EXPERIMENTAL

The azo dyes were prepared by coupling of the bisdiazo compound (I) with the corresponding arylaminopyrazoles in an acid medium; they were purified by recrystallization or reprecipitation by sodium chloride from aqueous alkaline soda solutions; in the latter case the dyes were isolated as the free acids by acidification of aqueous solutions of the sodium salts, and washed with water. The purity of the dyes was tested chromatographically; the sulfamide derivatives were identified by analysis.

1-Phenyl-3-methyl-5-aminopyrazole was prepared as described by Mohr [8], as follows: diacetonitrile $\xrightarrow{\text{phenylhydrazine}}$ cyanoacetonephenyl hydrazone $\xrightarrow{HCl}$ 1-phenyl-3-methyl-5-aminopyrazole; 1-(4'-and 3'-sulfamido and 4'-sulfophenyl)-3-methyl-5-aminopyrazoles were prepared analogously, and also without isolation of the cyanoacetonearylhydrazone, the two processes being combined in a single stage; diacetonitrile was made by condensation of acetonitrile by means of metallic sodium by Holtzwart's method [9]; aryl hydrazines were usually prepared by reduction of the diazo compounds of the corresponding amines by sulfite–bisulfite mixture or stannous chloride; (I) was prepared in accordance with patent data [10], as follows: 2-nitrophenol → 2-nitrophenoxyacetic acid → 2,2'-carboxymethoxyhydrazobenzene → the dilactam of 4,4'-diaminodiphenyl-3,3'-dihydroxyacetic acid → the dipotassium salt of 4,4'-siaminodiphenyl-3,3'-dihydroxyacetic acid. The characteristics of compounds not described previously, and the method for the preparation of 1-aryl-3-methyl-5-aminopyrazoles, are given below.

1-(3'-sulfamidophenyl)-3-methyl-5-aminopyrazole. To a suspension of 9.35 g of 3-sulfamidophenylhydrazine in 250 ml of water, 3 ml of glacial acetic acid and 4.2 g of diacetonitrile were added, and the mixture was refluxed on a boiling water bath for 1 hour; the turbid solution was then filtered, the filtrate cooled to 0°, and the precipitate which formed was filtered off and dried in a vacuum desiccator over $CaCl_2$. The yield of substance with m.p. 157.5-159.5° was 12.3 g; after recrystallization from water, the m.p. was 159-160° (at 105-107° the substance softens, then hardens again and melts without decomposition); it forms pale yellow, elongated plates with pointed ends (viewed under the microscope).

Found %: C 44.43; H 5.39; N 20.67; H_2O 6.82. $C_{10}H_{12}O_2N_4S \cdot H_2O$. Calculated %: C 44.42; H 5.22; N 20.75; H_2O 6.67.

1-(4'-sulfamidophenyl)-3-methyl-5-aminopyrazole. The preparation was analogous to the above. The crystals were similar in appearance to those of the meta isomer; m.p. 230-231.5°.

Found %: C 47.55; H 4.67; N 22.31. $C_{10}H_{12}O_2N_4S$. Calculated %: C 47.60; H 4.79; N 22.21.

1-(4'-sulfophenyl)-3-methyl-5-aminopyrazole. The crystal form was similar to that of the sulfamide derivatives.

Found %: C 44.3; H 4.68; N 15.19; H_2O 6.75. $C_{10}H_{11}O_3N_3S \cdot H_2O$. Calculated %: C 44.27; H 4.80; N 15.48; H_2O 6.64.

Dye (II). This was a red microcrystalline powder, readily soluble in aqueous alkalies; the crystals were brownish-yellow under the microscope.

Found %: N 19.63. $C_{36}H_{34}O_{10}N_{12}S_2$. Calculated %: N 19.57.

Dye (III). This was similar to (II) in appearance and solubility.

Found %: N 19.55. $C_{36}H_{34}O_{10}N_{12}S_2$. Calculated %: N 19.57.

The copper complexes of the dyes [11] were prepared by the action of tetrammine cupric sulfate on the dyes in an aqueous medium at the boil for 5 hours; they were purified by washing first by dilute aqueous ammonia and then water. The products consisted of small deep red crystals without admixture of brownish-yellow dye crystals (under the microscope).

The SF-2M spectrophotometer was used for determinations of the absorption spectra; $2 \cdot 10^{-5}$ molar solutions of the dyes and their copper complexes in 0.05 N aqueous caustic soda were investigated.

SUMMARY

It was demonstrated, with dyes made from 4,4']diaminodiphenyl-3,3'-dihydroxyacetic acid and 1-(4'- and 3'-sulfamidophenyl, 4'-sulfophenyl, and phenyl)-3-methyl-5-aminopyrazoles, that substituents in the phenyl nucleus of arylmethylaminopyrazole have little influence on dye color. Complex formation of the dyes with copper produces a bathochromic effect, and increases the difference of λ_{max} between sulfo and sulfamide derivatives. Dyes containing sulfamide groups are retained more firmly on the fiber than dyes with sulfo groups.

LITERATURE CITED

[1] T. Ulmann, Enzyclopadie der Technischen Chemie, Munchen-Berlin, Urban Schwarzenberg, 4, 118 (1951).

[2] K. Venkataraman, The Chemistry of Synthetic Dyes, New York, Academic press., 1, 603 (1952).

[3] A. Knight, J. Soc. Dyers and Col., 56, 410 (1950).

[4] P. Diserens, Teintex, 18, 683 (1953).

[5] German Patent 815, 512, Chem. Abs. 46, 7777 (1952); Swiss Patent 250, 817, Chem. Abs. 44, 5602 (1950); Swiss Patent 238, 455, Chem. Abs. 43, 8144 (1949); Swiss Patent 242,492, Chem. Abs. 43, 5964 (1949); U.S. Patent 2,384,419, Chem. Abs. 40, 2633 (1946), etc.

[6] French Patent 842,972; Zbl. 2, 4203 (1939), etc.

[7] German Patent 711,384; Chem. Abs. 37, 4256 (1943).

[8] E. Mohr, J. pr. Ch. 79, 1 (1909).

[9] R. Holtzwart, J. pr. Ch. 39, 230 (1889).

[10] German Patent 55506; Fridl. 2, 455 (1887-1890).

[11] V. I. Mur, J. Gen. Chem. 24, 572 (1954).*

Received December 20, 1956

*Original Russian pagination. See C.B. translation.

STUDY OF THE REACTION OF SOLID p-CARBOMETHOXYSULFANILYL CHLORIDE WITH SOLID 2-AMINOTHIAZOLE AND ITS HYDROCHLORIDE*

M. Kh. Gluzman and I. B. Levitskaia

In the production of norsulfazole, the acylation stage of 2-aminothiazole by p-carbomethoxysulfanilyl chloride (PCSC) in an aqueous medium [1] involves considerable losses of the latter compound owing to the formation of predominant amounts of diacylated aminothiazole (the diacyl derivative, DD) (II)

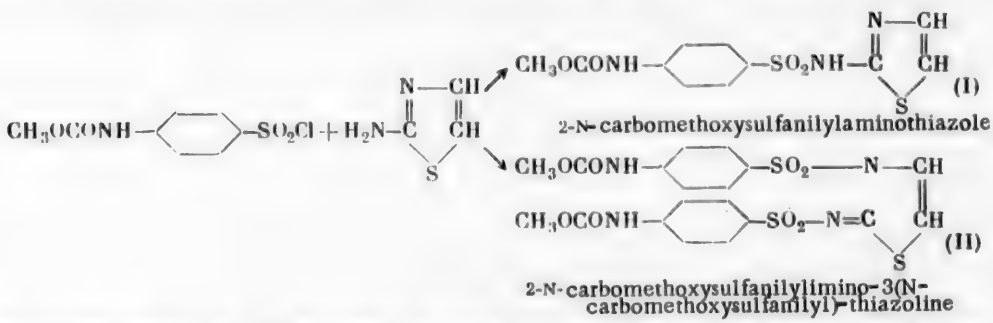

and partial hydrolysis of PCSC. Better results are not obtained if the reaction is carried out in organic solvents [2-6], or by fusion of the components [7].

In a search for reaction conditions which would involve smaller losses of PCSC, we investigated the possibility of the reaction of 2-aminothiazole and PCSC in the solid phase. Comparison of the melting points of the eutectics [8] in the systems 2-aminothazole + PCSC and 2-aminothiazole hydrochloride + PCSC showed that the components of the first system interact in the solid phase, while no reaction occurs in the second system. However, in the presence of solid sodium bicarbonate or carbonate, which aids liberation of aminothiazole from its hydrochloride, the reaction could be effected in the system aminothiazole hydrochloride + PCSC.

To determine the optimum conditions for the reaction between PCSC and aminothiazole or its hydrochloride, the following were studied: 1) stability of PCSC during grinding, heating, and in contact with solid alkali carbonates; 2) the interaction of aminothiazole base with PCSC at various temperatures and component ratios, and in presence of various neutralization agents; 3) the same factors for the system aminothiazole hydrochloride + PCSC; 4) interaction of DD with aminothiazole, for utilization of the second PCSC molecule.

EXPERIMENTAL

The following procedure was used in the kinetic studies of the reaction of solid aminothiazole or its hydrochloride with PCSC in presence or absence of alkaline reagents. The components, taken in definite proportions, were ground together for 15 minutes. A small flask containing the mixture, with a thermometer immersed in it, was placed in a TS-15 thermostat, with the temperature regulated to within ± 0.5°. Samples were taken at intervals and analyzed for the sulfonic chloride. Since the consumption of sulfonic chloride may be unproductive in the sense that part of it is hydrolyzed and is not used for the formation of acylated norsulfazole, from time to

*Communication XVIII in the series on reactions involving solid organic substances.

time the course of the reaction was investigated by experiments on the isolation of crude norsulfazole. A weighed sample of the product, after sintering, was washed with 5% hydrochloric acid to remove unchanged aminothiazole, and then with water until neutral to methyl orange. The residue was heated on a boiling water bath for 1 hour with 9-15% NaOH solution. The mixture was acidified with hydrochloric acid; norsulfazole was isolated, dried, and analyzed by the diazotization method.

DISCUSSION OF RESULTS

The experiments showed that grinding has no influence on the hydrolysis of PCSC; if pure PCSC or its mixture with sodium carbonate or bicarbonate is heated for several hours at 70°, it is hydrolyzed by the action of the moisture present in the air or the components. It was found that unproductive losses of about 5-6% of the PCSC are to be expected in its reaction with aminothiazole in the solid phase.

The course of the reaction of free aminothiazole with PCSC with and without additions of $NaHCO_3$ was studied. The reaction conditions, temperature and time, were varied, and different ratios of aminothiazole and PCSC were used. Moreover, in view of reports in the literature concerning the possible catalytic effects of small amounts of water on reactions between solids [9], we investigated the effects of various amounts of sodium carbonate decahydrate, which loses a considerable part of its water of crystallization at 50-80°, on the reaction yield.

It was found that in the reaction between free aminothiazole and PCSC without alkaline additives the PCSC consumption is about 40%. The amount of reacted PCSC increases with increase of the chloride–aminothiazole ratio from 1:1 to 2:1, and similar changes occur when the temperature is raised from 30 to 70°. The reaction is almost independent of the reaction time.

Acylated norsulfazole is formed in the solid system even at 30°, with a yield of about 20%. In all probability, the reaction is due to the formation of both eutectics, melting at 17 and 24°, in the system aminothiazole + PCSC.

In the experiments on the isolation of crude norsulfazole from samples obtained under these conditions, the yields were in the region of 20-24%. In view of the losses of norsulfazole at the saponification stage, usually estimated at 18% (according to laboratory and plant data), and of the unproductive hydrolysis of the chloride, the kinetic data may be regarded as reliable, and it may be concluded that acylation proceeds with predominant formation of the diacyl derivative. Separate analyses of the samples for mono- and diacylated norsulfazole (the mono derivative being dissolved in NaOH solution) showed that these substances were present in 1:9 ratio.

Equilibrium becomes established in the system at a high content of unchanged PCSC, with a small yield of the diacylated derivative, because of inactivation of the unreacted aminothiazole by addition of the hydrogen chloride liberated in the reaction. Therefore alkaline reagents were introduced into the reaction.

On addition of $NaHCO_3$ to bind the HCl, the consumption of PCSC increased by 7%, and the norsulfazole yield, by 30%. In contrast to the system without additives, the reaction yield was independent of the component ratio.

Addition of Na_2CO_3 produces a much greater effect. The amount of PCSC entering the reaction increases with the amount present and the temperature, but the norsulfazole yield does not always correspond to the analytical data. It is probable that in the ternary system aminothiazole–PCSC–sodium carbonate, the reaction between the amine and the chloride is accompanied by more rapid hydrolysis of PCSC itself, with formation of the sulfonic acid, than is the case in the binary systems PCSC–sodium carbonate and PCSC–aminothiazole, This is possibly the result of the greater activity of the chlorine atom in the sulfonic chloride in presence of sodium carbonate and aminothiazole. This leads to an appreciable increase of the norsulfazole yield, but the activated sulfonic chloride is at the same time hydrolyzed to a greater extent to the acid.

Despite these unfavorable factors, the yield of norsulfazole is nevertheless 60% on the aminothiazole, with the consumption of 2 moles of PCSC. The yield can be raised to 70-72% if the carbonate is introduced by portions, so that is hydrolytic effect is reduced.

The addition of different amounts of crystalline sodium carbonate, in order to utilize the possible catalytic

effect of water, is not justified in practice. In the reaction of 1 mole of aminothiazole, 2 moles of PCSC, 2 moles of Na_2CO_3, and 0.1 to 0.8 mole of $Na_2CO_3 \cdot 10H_2O$, the yield of norsulfazole is 60-65%.

Therefore, consistent yields of about 70% norsulfazole, calculated on aminothiazole, can be obtained by the reaction of solid aminothiazole and PCSC in presence of alkali carbonates, the consumption factor of PCSC being about 3. These results may therefore be significant for norsulfazole production [10], although the easy resinification of solid aminothiazole is a serious difficulty.

The reaction of aminothiazole hydrochloride with PCSC in presence of $NaHCO_3$ and Na_2CO_3 in the solid phase was studied similarly. The maximum yield of the diacyl derivative is obtained when 3 moles of $NaHCO_3$, 2 moles of PCSC, and 1 mole of aminothiazole hydrochloride are heated together for 5 hours. The average yield of norsulfazole is 73.6%. With the losses at the saponification stage (18%) and spontaneous hydrolysis of PCSC (5-6%) taken into account, it may be assumed that this reaction proceeds with the formation of diacylated norsulfazole in quantitative yield.

In view of the fact that the main source of PCSC loss is the formation of diacylated aminothiazole, we studied the reaction of the latter with 2-aminothiazole and its hydrochloride, as it has been reported [11, 12] that a transacylation reaction of this type is possible. The reaction of DD with 2-aminothiazole in the 116-125° range, and with aminothiazole hydrochloride at the same temperatures in presence of sodium, calcium, and ammonium carbonates and of sodium bicarbonate was studied. The maximum norsulfazole yield, 52% on PCSC, was obtained when 1 mole of 2-aminothiazole hydrochloride, 1 mole of DD, and 3 moles of $NaHCO_3$ were heated together for 3 hours at 125°. A somewhat higher yield (55%) is obtained if the free base is used instead of aminothiazole hydrochloride, but considerable resinification of the aminothiazole occurs.

SUMMARY

The reactions of solid p-carbomethoxysulfanilyl chloride with solid 2-aminothiazole and its hydrochloride under various conditions, and of solid 2-N-carbomethoxysulfanilylimino-3-(N-carbomethoxysulfanilyl)-thiazoline (DD) with solid 2-aminothiazole, its hydrochloride, and their melts, were studied; it was shown that the production of norsulfazole may be improved by these procedures, with lower relative consumptions of 2-aminothiazole and p-carbomethoxysulfanilyl chloride.

LITERATURE CITED

[1] Japanese Patent 177,625, August 31, 1948; Chem. Abs. 45, 7153 d (1951).

[2] J. Laudon and B. Sjogren, Svensk. kem. Tid. 52, 64 (1940); cited through Chem. Abs. 34, 4734[8] (1940).

[3] Japanese Patent 2836 (50), September 22; Chem. Abs. 46, 10203d (1952).

[4] British Patent 578,004, June 11, 1946; Chem. Abs. 41, 1704b (1947).

[5] K. Ganapathi, Proc. Indian Acad. Sci. 11A, 298 (1940); cited through Chem. Abs. 34, 6243 (1940).

[6] R. J. Fosbinder and L. A. Walter, J. Am. Chem. Soc. 61, 2032 (1939).

[7] L. F. Shpeier and M. S. Peisakhova, Sci. Mem. Inst. Chem. Kharkov State Univ. 23, 135 (1946).*

[8] M. Kh. Gluzman, Trans. Inst. Chem. Kharkov State Univ. 14 (1955).

[9] F. Taradiore, Zbl. II, 2070 (1938).

[10] M. Kh. Gluzman and I. B. Levitskaia, Authors' Certif. 94014, December 14, 1950.

[11] Indian Patent 39684, May 11, 1949; Chem. Abs. 44, 8371e (1950).

[12] Japanese Patent 175,578, January 31, 1948; Chem. Abs. 45, 178e (1951).

Received November 19, 1956

*In Russian.

CONDENSATION OF XYLENOLS IN PRESENCE OF ALKALINE CATALYSTS*

N. V. Shorygina and G. I. Kurochkina

Methods for the condensation of xylenols in the production of novolac resins were described in the preceding paper [1]. In experiments on the alkaline condensation of xylenols, we studied a) influence of the xylenol–formaldehyde ratio, b) the effects of various catayst, and c) the influence of condensation conditions.

A xylenol–formaldehyde ratio of 1:1.1 is recommended in the literature [2]. The basis for this ratio is that technical xylenols are less active than phenol, and, apart from the 1,3,5 isomer, have only two active points. This view is unjustified, as all the points of the xylenol nucleus react to some extent, because otherwise novolac resins setting in the presence of urotropine could not be obtained from it.

TABLE 1

Effect of Formaldehyde–Xylenol Ratio on Adhesive Quality

Experiment No.	Molar ratio		Content (%)			Viscosity (Ford-Engler degrees)	Cold setting	Hot setting
	xylenol	formaldehyde	free xylenol	free formaldehyde	methylol groups		shear strength** (kg/cm²)	static bend strength (kg/cm²)
12	1	1.1	14	2.7	12.1	50	23	90
13	1	1.1	17	2.9	11.9	40	20	85
22	1	1.5	9	2.4	14.7	27	32	106
11	1	1.5	13.2	3.0	15.0	40	30	85
8	1	2.0	8.5	2.5	21.0	40	35	115
21	1	2.0	6.9	2.08	20.0	53	33	110
9	1	2.2	5	5.5	20.0	50	30	70
16	1	2.2	5.9	6.74	18.0	40	28	60

Our experiments showed (Table 1) that, with increase of the formaldehyde content of the reaction mixture, the free xylenol content of the finished product falls, the methylol-group content rises and the joint strength increases. The best results are obtained with 1:2 ratio of xylenol to formaldehyde.

For determination of the role of the catalyst, a series of experiments was carried out on the condensation of xylenol with formaldehyde taken in 1:2 ratio. It follows from Table 2 that the largest free methylol group content and, accordingly, the highest joint strength, was obtained in experiments in which NaOH was used as the catalyst. Fairly good results were obtained with $Ba(OH)_2$, but in this case the final product had a high content of free xylenol, and the condensation was considerably retarded (twice the time was required). Adhesives of low strength were obtained if even part of the NaOH was replaced by ammonia.

It is known from the literature that water-soluble adhesives, or, more accurately, aqueous emulsion adhesives, are best prepared by two-stage condensation [3]. The reaction is carried out at the first stage with an

*Communication II in the series in xylenol–formaldehyde resins.

**Standard pine blocks were used for the shear strength tests on the set adhesives. The static bend tests were performed on specimens cut from blocks of compressed wood shavings.

TABLE 2

Effects of Various Catalysts on Adhesive Quality, with 1:2 Ratio of Xylenol to Formaldehyde

Experiment No.	Catalyst	Amount of catalyst (%)	Contents (%)			Viscosity (Ford-Engler degrees)	Cold setting	Hot setting
			free xylenol	free formaldehyde	methylol groups		tensile strength (kg/cm²)	static bend strength (kg/cm²)
8	NaOH	3.0	8.5	2.5	21	40	35	115
26	$Ba(OH)_2$	4	15	7.0	14	50	30	106
47	$NaOH + NH_3$	1.5 + 1	8.8	4.1	15—20	30	0	50

TABLE 3

Effects of Condensation Conditions on Adhesive Quality, with 1:2 Ratio of Xylenol to Formaldehyde, in Presence of 3 parts of 100% NaOH

Experiment No.	Contents (%)			Viscosity (Ford-Engler degrees)	Cold setting	Hot setting
	free xylenol	free formaldehyde	methylol groups		tensile strength (kg/cm²)	static bend strength (kg/cm²)
8	8.15	2.50	21	40	35	115
21	6.90	2.08	20	53	33	110
10	8.40	4.06	25	50	50	150
48	8.00	4.00	25	60	40	130

acid catalyst and a deficiency of formaldehyde, and at the second stage an alkaline catalyst is used, with additional formaldehyde. It is clear from Table 3 that the production of xylenol–formaldehyde adhesives by two-stage condensation has a favorable effect on the resin quality and the strength of the adhesive joint. Resins made in one step (Experiments 8 and 21 in Table 3) contained 20-21% of free methylol groups and the tensile strength after cold setting was 33-35 kg/cm². Two-stage resins contained 25% of methylol groups and the tensile strength was 40-50 kg/cm² (Experiments 10 and 48 in Table 3). It seems that at the first stage of the process, with a novolac ratio of phenol to formaldehyde, chains of novolac resin are formed. In the second stage of the process methylol groups become attached to the novolac molecules. Since heat evolution largely ceases at the first stage, when the formation of large molecules is restricted by the formaldehyde deficiency, the second stage proceeds without much heat evolution, and the resin viscosity increases slowly, so that the process may be regulated at will.

TABLE 4

Effect of Degree of Condensation on Adhesive Joint Strength (1) Free Xylenol Content (%)

Free xylenol content (%)	Viscosity (Ford-Engler degrees)	Cold-set; tensile strength (kg/cm²)
8.4	50	50
9.7	107	20
9.5	186	16

The production of high-viscosity adhesives is undesirable, as it has been shown by Müller [4] that the strength of the adhesive joint decreases with increasing molecular weight of the resin used. Our experiments confirmed Müller's findings. Table 4 contains the results of strength tests on joints made with resins with viscosities in the range of 50 to 186 Ford–Engler degrees. The tensile strength falls steadily from 50 to 16 kg/cm² with increase of resin viscosity.

TABLE 5

Improvement of the Water Resistance of KFS-10 Xylenol Adhesive by the Addition of Phenolic B Resin*

% of resin B added to KFS-10 resin	Cold setting	
	tensile strength before soaking (kg/cm^2)	tensile strength after 24 hours of soaking (kg/cm^2)
0.0	50	0
10	70	19
20	52	31
30	60	25
40	60	57
SP-2 adhesive	60	40

Our water-soluble xylenol–formaldehyde resins can be used as hot-hardening adhesives in the production of compressed wood blocks. Tests of these resins as cold-hardening adhesives, with the addition of kerosene "contact"** showed that the xylenol–formaldehyde resins are not water-resistant. However, if 25-40% of phenol–formaldehyde resin is added to the xylenol–formaldehyde resin, adhesive with fairly high mechanical strength and water resistance are obtained, not inferior (with 40% of phenolic resin) to SP-2, one of the best water-soluble phenolic adhesives (Table 5).

A similar improvement of the water resistance of xylenol–formaldehyde glues can be obtained by the joint condensation of xylenol and phenol, taken in ratios of 60-80 to 40-20 respectively.

With the use of crude xylenols for the production of water-soluble hot and cold setting adhesives the consumption of crystalline phenol can be reduced considerably, and the cost of mass-production adhesives can be lowered.

EXPERIMENTAL

Effect of xylenol–formaldehyde ratio on the quality of the resins formed. A round-bottomed flask fitted with a stirrer, reflux condenser, and a thermometer contained xylenol (1 mole), formaldehyde (1 to 2 moles), and 40% NaOH, equivalent to 3.0% of 100% NaOH. The mixture was kept with constant stirring for 1 hour at each of the following temperatures: 40, 50, 60 and 70°, to a viscosity of 40-50 Ford–Engler degrees. The results are summarized in Table 1.

Effects of different catalysts on resin quality. The same flask and the same conditions as before were used for the production of resins, with 1:2 (molar) ratio of xylenol to formaldehyde, in presence of 3.0% NaOH, 4% $Ba(OH)_2$, and a mixture of 1.5% NaOH and 1% NH_3. The results are summarized in Table 2.

The effect of two-stage condensation. For the production of two-stage resins, 100 wt. parts of xylenol, 24.5 parts of 100% formaldehyde, and 2.2 parts of "Petrov's contact"** was put into the flask; the contents were heated to 70° and held at that temperature for 1 hour, when 2.2 more parts of "Petrov's contact" was added and the mixture was kept at the boil for 1 hour 0.43 wt. part of 100% NaOH was then added to neutralize the "contact," the mixture was cooled to 60°, 24.5 wt. parts of 100% formaldehyde was added, and 2.45 wt. parts of 100% NaOH was then added in two portions. The properties of the resins obtained by one-stage condensation (Experiments 8 and 21) and by two-stage condensation (Experiments 10 and 48), with changed catalysts, are given in Table 3. NaOH was added in the form of 40% solution.

SUMMARY

1. The optimum xylenol–formaldehyde ratio for the production of water-soluble xylenol–formaldehyde resins was found to be 1:2.

2. The best quality resins are obtained by two-stage condensation (acid in the first and alkaline in the second). The best alkaline catalyst is NaOH.

LITERATURE CITED

[1] N. V. Shorygina and G. I. Kurochkina, J. Appl. Chem. 31, 1, 144 (1958).***

[2] A. G. Zabrodkin, Chemistry and Technology of Adhesives (State Wood and Paper Press, 1954), p. 98. [In Russian].

*Wood (pine) was used in this series of tests.

**Kerosene "contact", "Petrov's contact" – a sulfonated petroleum mixture – Publisher.

***Original Russian pagination. See C.B. translation.

[3] A. V. Tarasov, Author's Certif. 511, 513, 514 (1914).

[4] H. F. Müller and J. Müller, Kunststoffe, 42, 57 (1952).

Received June 20, 1956

SYNTHESIS OF PHTHALOCYANINE FROM PHTHALONITRILE

V. F. Borodkin

It is believed that, in the reaction of phthalocyanine formation in presence of metallic sodium in benzene solution, the sodium forms a labile addition product of the metallic ketyl type with the phthalonitrile, the nitrile being isomerized into the ketimide form (I), and the latter polymerizes with other phthalonitrile molecules into stable tetrameric ring systems. Thus, the metallic ketimide serves as the reaction nucleus, promoting and interrupting the reaction in the formation of phthalocyanine. As evidence for this course of the reaction, the formation of phthalocyanine by the action of butyl alcohol on boiling benzene solution of phthalonitrile in presence of metallic sodium is cited [1].

In our opinion, this example is not convincing, especially as phthalocyanine is not formed in absence of the alcohol. It seems more likely that in this case sodium butylate reacts with phthalonitrile, forming the unstable addition product (II), which yields phthalocyanine either by interaction with other phthalonitrile molecules, or through an intermediate compound, an isoindolenine derivative (III).

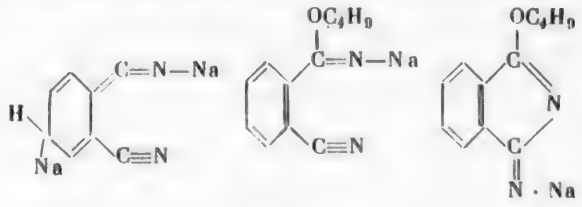

(I) (II) (III)

The possible formation of isoidoline derivatives is noted in the patent literature [2].

It was therefore desired to investigate this reaction, to isolate the reaction products of phthalonitrile with metallic sodium in an alcoholic medium, and to establish their structure.

EXPERIMENTAL

The reaction of phthalonitrile with metallic sodium and sodium methylate in benzene and methyl alcohol was studied.

The reaction in benzene. 5 g of phthalonitrile was dissolved in 50 ml of benzene in a 200 ml flask fitted with a reflux condenser. 0.5 g of metallic sodium was introduced into the solution, and the liquid was boiled for 1 hour; no changes in the solution or the metallic sodium were observed during this time. 5 ml of methyl alcohol was added to the boiling solution through the reflux condenser. The metallic sodium reacted vigorously with the alcohol, and sodium phthalocyanine was immediately formed. Because of the vigorous reaction, it is impossible to detect individual stages in the formation of phthalocyanine or to isolate any intermediate products. It was observed, however, that the benzene solution was colored yellow when the methyl alcohol was added.

When 0.5 g of sodium methylate was taken instead of metallic sodium, and heated with a benzene solution of phthalonitrile at the boil for 3 hours, the solution gradually became yellow-brown in color. When the solution was cooled and the partially unchanged sodium methylate removed, a yellow-brown precipitate was formed on standing.

If this precipitate is boiled in methyl alcohol or in a mixture of methyl alcohol and benzene, phthalocyanine is formed. If the dry precipitate is heated, it forms sodium phthalocyanine without fusion. An aqueous extract of the precipitate has an alkaline reaction.

Quantitative analysis of the substance for carbon, hydrogen, and nitrogen, performed by the combustion method, gave the following results:

0.3462 g substance; 0.7929 g CO_2 and 0.1223 g H_2O.
Found %: C 59.37; H 3.77.
0.1120 g substance; 15.9 ml N_2 (22°, 735 mm).
Found %: N 15.7.

Calculated for the addition compound of sodium methylate and phthalonitrile ($C_9H_7N_2ONa$) Calculated %: C 59.33; H 3.87; N 15.38.

The structure of the addition compound may be represented by Formula (IV)

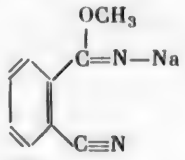

(IV)

The compound (II) of analogous structure is formed when butyl alcohol is added to a benzene solution of phthalonitrile in presence of sodium.

The use of xylene instead of benzene and of higher instead of lower alcohols is mentioned in the patent literature [3, 4, 5]. In such cases, mixtures of sodium phthalocyanine with phthalocyanine, or phthalocyanine alone, are obtained. In our opinion, in such cases the formation of phthalocyanine is preceded by the formation of an addition compound of the alcoholate and phthalonitrile.

The reaction in methanol. 10 g of phthalonitrile was added at 25° into a flask, containing 70 ml of methyl alcohol in which 2 g of metallic sodium was dissolved, fitted with a reflux condenser and stirrer. The phthalonitrile dissolved on stirring, the temperature of the mixture rose, slowly at first and then rapidly, and the solution gradually became yellow, brown, and then green.

Phthalocyanine was formed when the solution was boiled. If the solution temperature did not exceed 40°, rectangular colorless crystals were deposited from the yellow-brown solution. When filtered off, washed with water to remove alkali, and dried in air, they had a characteristic aromatic odor typical of methyl ethers.

The crystals melt at 116-118°, and are sparingly soluble in cold water; an aqueous extract is alkaline. In the air, especially in direct sunlight, the crystals turn blue. When the substance is heated, phthalocyanine is formed.

Combustion analysis for carbon, nitrogen, and hydrogen gave the following results:

0.1832 g substance; 0.3980 g CO_2 and 0.0593 g H_2O.
Found %: C 59.28; H 3.61.
0.0869 g substance; 12.66 ml N_2 (24°, 753 mm).
Found %: N 16.3.

Calculated for the sodium derivative of methoxyiminoisoindolenine (%): C 59.33; H 3.87; N 15.38. The structure of the compound is represented by Formula (V). The sodium content was determined by titration of a weighed sample after it had been boiled with aqueous hydrochloric acid.

Weight taken 0.5000 g 21.4 ml of 0.1 N HCl solution (K = 1.209) was taken for the titration.

Found %: Na 12.0. Calculated %: Na 12.6.

When the substance is heated with alcoholic ammonia in a sealed tube at 100°, 1,3-diiminoisoindoline of m.p. 196° [6] is formed.

DISCUSSION OF RESULTS

The reactions of phthalonitrile in benzene solution in presence of sodium and methanol, or of sodium methylate and methanol, with formation of sodium phthalocyanine (VI), or its mixture with phthalocyanine (VII), may be represented as follows:

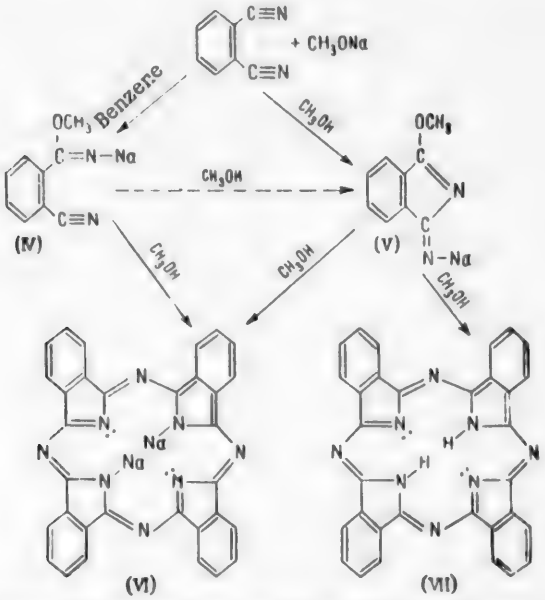

In benzene solution, phthalonitrile and sodium methylate first form the addition compound (IV), which, in an alcoholic medium, gives rise to disodium phthalocyanine (VI) by reacting with other phthalocyanine molecules, or through the intermediate compound (V). Disodium phthalocyanine is not formed in absence of alcohol.

In methyl alcohol, phthalonitrile and sodium methylate first yield the compound (V), which then forms phthalocyanine (VII). It is possible that (V) is formed by way of (IV), which cannot be isolated from the alcoholic solution. The formation of disodium phthalocyanine on addition of methyl alcohol to a benzene solution of phthalonitrile in presence of metallic sodium takes an analogous course.

SUMMARY

1. The reaction of phthalonitrile with sodium methylate in benzene and methanol solutions, leading to the formation of phthalocyanine, was studied.

2. The addition product of sodium methylate to phthalonitrile, and the isoindoline derivative formed from it by ring closure, were isolated and studied.

LITERATURE CITED

[1] A. Sander, Chemia, 55, 225 (1942).

[2] Swiss Patent 291,803; Referat. Zhur. Khim. 4932 (1956).

[3] Swiss Patent 297,412; Referat. Zhur. Khim. 10829 (1956).

[4] British Patent 712,455; Referat. Zhur. Khim. 4931 (1956).

[5] W. Wettstein, U.S. Patent 2,699,441; Referat. Zhur. Khim. 47278 (1955).

[6] J. Elvidge and R. Linstead, J. Chem. Soc. 5009 (1952).

Received July 8, 1956